

Stable isotope-based paleoenvironmental reconstructions of Neogene terrestrial archives

Dissertation
zur Erlangung des Doktorgrades
der Naturwissenschaften

vorgelegt beim Fachbereich 11
der Johann Wolfgang Goethe - Universität
in Frankfurt am Main

von
Tina Lüdecke
aus Bremervörde

Frankfurt, 2015

vom Fachbereich 11 der Johann Wolfgang Goethe - Universität als Dissertation
angenommen.

Dekan: Prof. Dr. Ulrich Achatz

Gutachter: Prof. Dr. Andreas Mulch
Senckenberg Biodiversität und Klima Forschungszentrum,
Frankfurt am Main, Deutschland
und
Goethe-Universität Frankfurt am Main, Deutschland

Prof. Dr. Friedemann Schrenk
Senckenberg Gesellschaft für Naturforschung,
Frankfurt am Main, Deutschland
und
Goethe-Universität Frankfurt am Main, Deutschland

Datum der Disputation:

Contents

List of figures	i
List of tables	ii
Abbreviations	iii
Abstract	1
Chapter 1 Introduction	5
1.1 Motivation and aims of research	5
1.2 Study area (Chiwondo and Chitimwe Beds, Karonga Basin, Malawi)	8
1.3 General introduction to proxy materials and methods	10
1.3.1 $\delta^{13}\text{C}$ and $\delta^{18}\text{O}$ of paleosol and herbivore proxy material	11
1.3.2 $\delta^{13}\text{C}$ and $\delta^{18}\text{O}$ of meteoric water	13
1.4 Structure of this PhD thesis	14
1.5 References	16
Chapter 2 Environmental characteristics of the Plio-Pleistocene Chiwondo and Chitimwe Beds (N-Malawi)	21
2.1 Introduction	22
2.1.1 Geologic and tectonic framework	22
2.1.2 Stratigraphy	25
2.1.3 Palaeosols	25
2.2 Goals and methods	26
2.3 Palaeopedological field observations	27
2.3.1 Mwenirondo	28
2.3.2 Malema	30
2.3.3 Uraha	31
2.4 Synthesis	33
2.5 Acknowledgments	35
2.6 References	35
Chapter 3 Persistent C_3 vegetation accompanied Plio-Pleistocene hominin evolution in the Malawi Rift (Chiwondo Beds, Malawi)	39
3.1 Introduction	40
3.2 Background	42
3.2.1 Stable carbon isotope data in geologic proxy materials	42
3.2.2 Geological context	43
3.2.3 Chiwondo paleosol	44
3.2.4 Age control and correlation of individual sections	45
3.2.5 Vegetation classification system	45
3.2.6 Eastern Rift $\delta^{13}\text{C}$ data	46
3.3 Material and methods	46
3.4 Results	47
3.4.1 $\delta^{13}\text{C}$ values of Plio-Pleistocene (~4.3 Ma to modern) pedogenic carbonate	47
3.2.1 $\delta^{13}\text{C}$ values of Plio-Pleistocene (~4 Ma to modern) suid enamel	49
3.5 Discussion	51
3.6 Conclusion	56
3.7 Acknowledgments	56
3.8 Supplementary material	57
3.9 References	65

Chapter 4	Always walk on the bright side of life? Hominin evolution in a wooded and mesic habitat	71
4.1	Introduction	72
4.2	Background	72
4.2.1	Oxygen stable isotopes in paleosols	72
4.2.2	Karonga Basin modern meteoric water $\delta^{18}\text{O}$ data	73
4.2.3	Eastern Rift pedogenic carbonate $\delta^{13}\text{C}$ data	73
4.3	Material and methods	74
4.4	Results	74
4.4.1	Early Pliocene (ca. 4.3 to 3.75 Ma)	74
4.4.2	3.75 Ma to 2.8 Ma	75
4.4.3	2.8 Ma to 1.8 Ma	76
4.4.4	1.8 Ma to 0.6 Ma	76
4.4.5	<0.6 Ma	76
4.5	Discussion	76
4.5.1	Correlation of $\delta^{18}\text{O}$ values of Karonga Basin paleosol carbonate with modern meteoric water	76
4.5.2	Correlation of $\delta^{18}\text{O}$ values of Karonga Basin paleosol carbonate with Eastern Rift data	77
4.5.3	Co-variance of paleosol carbonate $\delta^{18}\text{O}$ and $\delta^{13}\text{C}$ values	78
4.6	Conclusions	79
4.7	Supplementary material	80
4.8	References	86
Chapter 5	Stable isotope dietary reconstructions of herbivore enamel reveal heterogeneous wooded savanna ecosystems in the Plio-Pleistocene Malawi Rift	89
5.1	Introduction	90
5.2	Background	91
5.2.1	Sampling localities	91
5.2.2	Modern climate and lake hydrology	94
5.2.3	Tooth formation and stable isotopes in enamel	95
5.2.4	$\delta^{18}\text{O}$ values of meteoric water in southeast Africa	96
5.3	Material and methods	97
5.3.1	$\delta^{13}\text{C}$ and $\delta^{18}\text{O}$ of herbivore fossil tooth enamel	97
5.3.2	$\delta^{18}\text{O}$ of meteoric water	97
5.4	Results	98
5.4.1	$\delta^{13}\text{C}$ and $\delta^{18}\text{O}$ of herbivore enamel	98
5.4.2	Intra-tooth $\delta^{13}\text{C}$ and $\delta^{18}\text{O}$ patterns	99
5.4.3	$\delta^{18}\text{O}$ of meteoric water	100
5.5	Discussion	102
5.6	Conclusion	107
5.7	Acknowledgments	107
5.8	Supplementary material	108
5.8.1	Chiwondo Beds Units	108
5.8.2	Material and methods	108
5.8.3	$\delta^{13}\text{C}$ and $\delta^{18}\text{O}$ co-variance	109
5.8.4	$\delta^{13}\text{C}$ and $\delta^{18}\text{O}$ values of analyzed herbivores	110
5.8.5	$\delta^{18}\text{O}$ values of meteoric water	114
5.9	References	117

Chapter 6	Stable isotope-based reconstruction of Oligo-Miocene paleoenvironment and paleohydrology of Central Anatolian lake basins (Turkey)	125
6.1	Introduction	126
6.2	Isotopic compositions of lake sediments	127
6.2.1	Stable oxygen isotope geochemistry	127
6.2.2	Stable carbon isotope geochemistry	128
6.3	Analytical techniques	129
6.3.1	Stable carbon and oxygen isotope geochemistry	129
6.3.2	$^{40}\text{Ar}/^{39}\text{Ar}$ geochronology	129
6.4	Geologic and tectonic framework	130
6.5	Paleoenvironment	130
6.5.1	Oligo-Miocene climatic development	130
6.5.2	Eastern Mediterranean	131
6.5.3	Paleogeography of Turkey	132
6.6	Geologic setting of the studied sections and sampling strategy	133
6.6.1	Timing of deposition and sedimentation rates	133
6.6.2	Ecemiş Corridor	135
6.6.3	Mut Basin	135
6.6.4	Ilgın Basin	136
6.6.5	Ankara region	137
6.7	Results	139
6.7.1	Ecemiş Corridor	139
6.7.2	Mut Basin	140
6.7.3	Ilgın Basin	140
6.7.4	Ankara region	141
6.8	Discussion	141
6.8.1	Fossil and recent $\delta^{18}\text{O}_{\text{mw}}$	142
6.8.2	Oligo-Miocene paleoenvironmental conditions of the CAP	146
6.9	Conclusion	149
6.10	Acknowledgments	150
6.11	Supplementary material	150
6.12	References	156
Chapter 7	Summary and outlook	163
7.1	Summary	163
7.1.1	Karonga Basin	163
7.1.2	Central Anatolian Plateau	166
7.2	Outlook	167
7.2.1	Clumped isotope paleothermometry of pedogenic carb.	167
7.2.2	Stable isotope data of fossil hominin enamel	167
7.2.3	High-resolution and continuous stable isotope analyses	168
7.2.4	Stable isotope data from Lake Malawi drill core material	168
7.2.5	Tooth morphology of Karonga Basin herbivores	168
7.3	References	169
	Zusammenfassung	171
	Acknowledgments	176
	Appendix	177
	Curriculum vitae	193
	Publication and conference abstracts	194

List of Figures

Chapter 1

Figure 1.1	Arial image of Africa with savanna types and hominin localities	5
Figure 1.2	3D schematic diagram of the Rungwe Volcanic Province	9
Figure 1.3	Position and geological map of Karonga Basin study site	10
Figure 1.4	Exemplary Plio-Pleistocene herbivorous mammal teeth	12
Figure 1.5	Typical groundwater pump and precipitation sampling	13

Chapter 2

Figure 2.1	Map of East Africa with the EAR and geology of the study area	23
Figure 2.2	Stratigraphic column of 12-MA-58 (Unit 2)	28
Figure 2.3	Stratigraphic column of 11-MW-04 and 12-MW-19 (Unit 3A)	29
Figure 2.4	Stratigraphic column of 12-MA-08 (Unit 3A)	30
Figure 2.5	Stratigraphic column of 11-UR-99 (Unit 1 and 2)	31
Figure 2.6	Stratigraphic column of 12-UR-47 (Unit 4)	32
Figure 2.7	Key for stratigraphic columns in Fig. 2.2 to 2.6	32

Chapter 3

Figure 3.1	Present-day African vegetation zones and hominin sites	40
Figure 3.2	Eastern Africa with EAR and geological map of Karonga Basin	41
Figure 3.3	Outcrop conditions and field characteristics	44
Figure 3.4	$\delta^{13}\text{C}$ values of pedogenic carbonate in the EAR since 7.5 Ma	48
Figure 3.5	$\delta^{13}\text{C}$ values of suid enamel in the the EAR since 7.5 Ma	50
Figure 3.6	Composite record of paleosol $\delta^{13}\text{C}$ values	53
Figure 3.7	Stratigraphic order of samples pedogenic carbonate	57

Chapter 4

Figure 4.1	$\delta^{18}\text{O}$ values of pedogenic carbonate in the EAR since 7.0 Ma	75
Figure 4.2	Compositoe record of paleosol $\delta^{18}\text{O}$ values	78
Figure 4.3	$\delta^{18}\text{O}$ vs. $\delta^{13}\text{C}$ values of Karonga Basin soil carbonate	79

Chapter 5

Figure 5.1	Atmospheric circulation and vegetational patterns in E Africa	92
Figure 5.2	$\delta^{13}\text{C}$ and $\delta^{18}\text{O}$ values from Karonga Basin herbivore enamel	98
Figure 5.3	Intra-tooth $\delta^{13}\text{C}$ and $\delta^{18}\text{O}$ variation of selected teeth	100
Figure 5.4	$\delta^{18}\text{O}$ values of meteoric water from the Karonga Basin	101
Figure 5.5	Comparison of Karonga Basin and Laetoli enamel data	103
Figure 5.6	Herbivore $\delta^{13}\text{C}$ and $\delta^{18}\text{O}$ data in stratigraphical order	108
Figure 5.7	$\delta^{13}\text{C}$ vs. $\delta^{18}\text{O}$ values of Karonga Basin mammals	109
Figure 5.8	Intra-tooth $\delta^{13}\text{C}$ and $\delta^{18}\text{O}$ variation of all equid and bovid teeth	113

Chapter 6

Figure 6.1	Map of Turkey with elevation, geological features and study sites	127
Figure 6.2	Field characteristics of the studied Oligo-Miocene sediments	134
Figure 6.3	Outcrop conditions of Ilgın Formation	137
Figure 6.4	Outcrop conditions of Gökler sequence	138
Figure 6.5	Stepwise-heating $^{40}\text{Ar}/^{39}\text{Ar}$ degassing spectra with plateau ages	139
Figure 6.6	$\delta^{18}\text{O}$ and $\delta^{13}\text{C}$ values of Ecemiş and Mut Basin carbonate	143
Figure 6.7	$\delta^{18}\text{O}$ and $\delta^{13}\text{C}$ values of Ilgın Basin carbonates	144
Figure 6.8	$\delta^{18}\text{O}$ and $\delta^{13}\text{C}$ values of Ankara region carbonates	145
Figure 6.9	Results of stable oxygen and carbon isotope analysis	147

Chapter 7

Figure 7.1	Summary of paleosol and suid enamel $\delta^{13}\text{C}$ and $\delta^{18}\text{O}$ data	165
------------	--	-----

List of Tables

Chapter 3

Table 3.1	List of ca. 4.3 to 3.75 Ma pedogenic nodules with $\delta^{13}\text{C}$ values	58
Table 3.2	List of 3.75 to 2.8 Ma pedogenic nodules with $\delta^{13}\text{C}$ values	59
Table 3.3	List of 2.8 to 1.8 Ma pedogenic nodules with $\delta^{13}\text{C}$ values	61
Table 3.4	List of <0.6 Ma pedogenic nodules with $\delta^{13}\text{C}$ values	63
Table 3.5	List of all suid samples with $\delta^{13}\text{C}$ values	64

Chapter 4

Table 4.1	List of ca. 4.3 to 3.75 Ma pedogenic nodules with $\delta^{18}\text{O}$ values	80
Table 4.2	List of 3.75 to 2.8 Ma pedogenic nodules with $\delta^{18}\text{O}$ values	81
Table 4.3	List of 2.8 to 1.8 Ma pedogenic nodules with $\delta^{18}\text{O}$ values	83
Table 4.4	List of <0.6 Ma pedogenic nodules with $\delta^{18}\text{O}$ values	85

Chapter 5

Table 5.1	Overview of all analyzed herbivore teeth	94
Table 5.2	$\delta^{13}\text{C}$ and $\delta^{18}\text{O}$ values of <i>Suidae</i>	110
Table 5.3	$\delta^{13}\text{C}$ and $\delta^{18}\text{O}$ values of <i>Hippopotamidae</i>	110
Table 5.4	$\delta^{13}\text{C}$ and $\delta^{18}\text{O}$ values of <i>Elephantidae</i>	110
Table 5.5	$\delta^{13}\text{C}$ and $\delta^{18}\text{O}$ values of <i>Equidae</i>	111
Table 5.6	$\delta^{13}\text{C}$ and $\delta^{18}\text{O}$ values of <i>Bovidae</i>	112
Table 5.7	$\delta^{13}\text{C}$ and $\delta^{18}\text{O}$ values of rainwater	114
Table 5.8	$\delta^{13}\text{C}$ and $\delta^{18}\text{O}$ values of rivers	115
Table 5.9	$\delta^{13}\text{C}$ and $\delta^{18}\text{O}$ values of groundwater	115
Table 5.9	$\delta^{13}\text{C}$ and $\delta^{18}\text{O}$ values of lakes	116

Chapter 6

Table 6.1	Results of $^{40}\text{Ar}/^{39}\text{Ar}$ geochronology	130
Table 6.2	List of each sampled formation	133
Table 6.3	List of stable isotope results for each sampled unit	140
Table 6.4	List of all carbonate samples with $\delta^{13}\text{C}$ and $\delta^{18}\text{O}$ values	150

Appendix

Table A1	List of all Karonga Basin paleosol samples	178
Table A2	List of all Karonga Basin herbivore enamel samples	188

Abbreviations

<i>Alc.</i>	<i>Alcelaphini</i>
<i>Ant.</i>	<i>Antilopini</i>
asl	above sea level
BF	border faults
BiK-F	Senckenberg Biodiversity and Climate Research Centre
cal	calculated
CAP	Central Anatolian Plateau
carb	carbonate
CMT	coldest month Temperature
EAR	East African Rift
EARS	East African Rift System
ER	Eastern Rift
FAD	first appearance date
frag	fragment
GMWL	Global Meteoric Water Line
<i>H.</i>	<i>Homo</i>
HCRP	Hominid Corridor Research Project
<i>Hip.</i>	<i>Hippotragini</i>
HM	heavy minerals
I	incisor
ITCZ	Intertropical Convergence Zone
KB	Karonga Basin
<i>Kol.</i>	<i>Kolpochoerus</i>
L	left
I	lower
LAD	last appearance date
LOEWE	Landes-Offensive zur Entwicklung Wissenschaftlich-ökonomischer Exzellenz
lw	lake water
LWIA	liquid water isotope analyzer
M	molar
<i>Met.</i>	<i>Metridiochoerus</i>
MSA	Middle Stone Age
mw	meteoric waters
<i>Not.</i>	<i>Notochoerus</i>
NOW	Neogene of the Old World Database of Fossil Mammals
<i>Nya.</i>	<i>Nyanzachoerus</i>
<i>P.</i>	<i>Paranthropus</i>
<i>Pha.</i>	<i>Phacochoerus</i>
<i>Pot.</i>	<i>Potamochoerus</i>
R	right
TDIC	total dissolved inorganic carbon
U	Uraha
UNESCO	United Nations Educational, Scientific, and Cultural Organization
u	upper
USGS	United States Geological Survey
VPDB	Vienna Pee Dee Belemnite
VSMOW	Vienna Standard Mean Ocean Water
WMT	warmest month temperature
ZAB	Zaire Air Boundary

Abstract

The stable isotope geochemistry of pedogenic and lacustrine carbonate and fossil herbivore tooth enamel is a powerful tool to study the evolution of terrestrial paleoenvironments. This thesis aims to reconstruct Neogene ecosystems in the **Karonga Basin** in the southern part the East African Rift (EAR) and the **Central Anatolian Plateau** (CAP).

Karonga Basin: Understanding the development of East African savanna biomes is crucial for reconstructing the evolution, migration and dietary behaviors of early hominins. These rift ecosystems range from closed woodland to open grassland savanna and vary widely in fraction of woody cover, providing a wide range of food supply for their associated fauna. This thesis presents Plio-Pleistocene carbon ($\delta^{13}\text{C}$) and oxygen ($\delta^{18}\text{O}$) records from pedogenic carbonate and fossil herbivore tooth enamel collected from the Malawi Rift. These data are the first southern hemisphere long-term record in the East African Rift, a region particularly interesting for reconstructing vegetation patterns and correlating these across the Intertropical Convergence Zone (ITCZ) with data on the evolution and migration of early hominins.

The studied ca. 4.3 Ma to 0.6 Ma paleosol, fluvial, swamp, deltaic, and lacustrine deposits of the Chiwondo Beds (Karonga Basin, northern Malawi) comprise abundant pedogenic carbonates and fossil remains of a diverse fauna, which is dominated by large-bodied terrestrial mammals. The sediments are also home to two hominin fossil finds, a maxillary fragment of *Paranthropus boisei* and a mandible of *Homo rudolfensis*, both dated to ca. 2.4 Ma. These finds mark the earliest co-existence of the two genera. The study site is situated between the well-known hominin-bearing localities of eastern and southern Africa and hence fills an important geographical gap for early hominin research.

The $\delta^{13}\text{C}$ values of pedogenic carbonate ($n = 321$) and of enamel from 14 different large-bodied herbivorous mammal taxa (suid, equid, bovid, elephant and hippopotamus; $n = 122$) permit assessment of the evolutionary history of C_3 and C_4 biomass, which is closely linked to climate patterns in the EAR during the time of early hominin evolution. The reconstruction of C_4 -grassland development offers insights into the retreat of tree cover, seasonality, and the distribution and seasonality of precipitation. $\delta^{18}\text{O}$ values reflect hydrological patterns, and we supplement the data of fossil proxy material with analyses of modern meteoric water to evaluate influences of seasonality and (lake) evaporation.

Consistent $\delta^{13}\text{C}$ values around -9‰ and $\delta^{18}\text{O}$ values of ca. 24‰ of the pedogenic carbonate from 14 sections spanning the last 4.3 Ma indicate a relatively mesic (for subtropical Africa), C_3 -dominated woodland savanna in the Karonga Basin. The results of carbon and oxygen isotope analyses reflect a

persistent climate in the region without any major long- or short-term fluctuations.

The data from tooth enamel of suid (*Notochoerus*, *Metridiochoerus*, *Phacochoerus*), elephant (*Elephantidae*) and hippo (*Hippopotamus amphibius*) taxa complement these findings with constantly low $\delta^{13}\text{C}$ and $\delta^{18}\text{O}$ values, demonstrating intake of mainly C_3 biomass and water from sources which are only very limited affected by evaporation.

In contrast, Karonga Basin equid (*Eurygnathohippus* sp.) and bovid (*Alcelaphini*, *Hippotragini*, *Antilopini*) taxa reflect much more complex dietary patterns, ranging from mixed C_3/C_4 -feeders to strongly (sometimes exclusively) C_4 -influenced diets. Intra-tooth $\delta^{18}\text{O}$ values also show large variations, indicating water intake from resources that differ in their isotopic composition and therefore experienced different hydrological settings.

Overall, the stable isotope data reflect a mostly C_3 -dominated (ca. 60% to 70% woody cover) mesic paleoecosystem, which comprises patches of more open C_4 -grasslands within the range of migrating mammals. These patterns are similar to the Zambezian Savanna environment today. Supplementary analyses of $\delta^{18}\text{O}$ values of modern meteoric water (precipitation, lake, river and groundwater; $n = 111$) show a similar magnitude to the fossil herbivore oxygen isotopic values. Expected $\delta^{18}\text{O}$ values of the drinking water calculated from herbivore enamel of animals with a mixed- or C_3 -diet indicate water intake from barely evaporated sources. Specialized feeders with a high C_4 -consumption, however, reflect reconstructed stable oxygen isotope values of ^{16}O -depleted reservoirs, similar in $\delta^{18}\text{O}$ compositions to modern evaporated lakes.

The absence of long-term trends towards more positive $\delta^{13}\text{C}$ and $\delta^{18}\text{O}$ values in the Karonga Basin contrasts the increasing role of C_4 -grasslands since ca. 2.5 Ma in the Eastern Rift, which is well documented for hominin sites in Tanzania, Kenya and Ethiopia. Our data hence point to regional differences in climate and vegetation dynamics during the Plio-Pleistocene across the ITCZ. Therefore, regions that are home to early hominins such as *H. rudolfensis* and *P. boisei* may have had a different environmental history when compared to the Eastern Rift. This suggests that hominin adaptation is not necessarily directly linked to the emergence of open landscapes.

Central Anatolian Plateau: The development of relief and climate patterns in the Central Anatolian Plateau is another long-standing debate in modern paleoecological studies. This thesis presents long-term $\delta^{13}\text{C}$ and $\delta^{18}\text{O}$ records on five lacustrine successions, which are widely distributed across the CAP. Also, new $^{40}\text{Ar}/^{39}\text{Ar}$ geochronological data from volcanic ashes are established in addition to existing biostratigraphic and paleomagnetic data, to add new age constraints to the depositional ages of the individual sedimentary sequences.

Field relationships combined with stable isotope data of 230 lacustrine carbonates indicate a Late Oligocene environment that was characterized by large, temporally open freshwater lakes in a relatively humid subtropic climate. In the middle Aquitanian (ca. 21 Ma), an increase in lake $\delta^{18}\text{O}$ values reflects more arid settings and an overall increasing dominance of closed saline lakes. This time was probably characterized by frequent climatic fluctuations, recording the influence of seasonality, topography and the waxing and waning of aridity.

Chapter 1 Introduction

1.1 Motivation and aims of research

The reconstruction of paleoenvironments is the focus of numerous interdisciplinary multi-proxy studies. The understanding of ancient landscapes and their link to climate, seasonality, vegetation patterns, evolutionary and dietary behavior of animals, geology and tectonics are essential for the reconstruction of past ecosystems. It has always been of special interest for geoscientists, paleoanthropologists and archeologists to reveal insights into the environment our early ancestors lived in. The focus of this thesis lies on the study of African savanna biomes during the time of early hominin evolution to reconstruct the habitat of the “Cradle of Mankind”.



Figure 1.1: Aerial image of Africa with savanna types after White (1983) and major hominin fossil localities.

One key element in understanding human evolution is deciphering the links and feedbacks between East African paleoclimate and vegetation patterns (e.g., Dart, 1925; Bartholomew and Birdsell, 1953; Potts, 1998; Ségalen et al., 2007; Plummer et al., 2009; Cerling et al., 2011). In subtropical Africa especially, the timing of the appearance of C₄-dominated biomes since the Miocene is important to comprehend large-scale vegetational changes and its impact on hominin evolution (e.g., Ségalen et al., 2007 and references therein). C₄ biomes are associated with open grassland savannas with a high solar radiation and warm temperatures during the growing season. These typical East African savanna floras with their abundant mammal fauna radiated during the course of the Plio-Pleistocene, and C₄ grasses are the dominant component of many subtropical African ecosystems today. The actual timing and evolution of these open landscapes is therefore the focus of many paleoecological studies. Paleoenvironmental research within the East African Rift (EAR) aims at reconstructing ecospace and dietary behaviors of early hominins and other large-bodied herbivores, using traditional ecological features of fauna and flora and/or geochemical proxies (Wesselmann, 1985; Cerling and Hay, 1986; Cerling et al., 1988; Cerling, 1992; Kingston et al., 1994; Morgan et al., 1994; Plummer and Bishop, 1994; Sikes, 1994; deMenocal, 1995; Behrensmeyer et al., 1997; Heinzelin et al., 1999; Plummer et al., 1999; Sikes et al., 1999; Wynn, 2000; Harris and Cerling, 2002; Cerling et al., 2003; Trauth et al., 2003; Levin et al., 2004; Semaw et al., 2005; Trauth et al., 2005; Hopley et al., 2006; White et al., 2006; Quinn et al., 2007; Ségalen et al., 2007; Sikes and Ashley, 2007; Aronson et al., 2008; WoldeGabriel et al., 2009; Bocherens et al., 2011; Cerling et al., 2011; Levin et al., 2011; Cerling et al., 2013a; Cerling et al., 2013b; Feakins et al., 2013; Magill et al., 2013a, b; Wilson et al., 2014). Nearly all these studies, which aim at reconstructing ecospace and diet of early hominins, concentrate on material from hominin sites in the Eastern Branch of the EAR, today's Somali-Masai Endemic Zone in Ethiopia, Kenya and Tanzania (Fig. 1.1).

Therefore, current climate-evolution hypotheses, which include temporal and causal relationships between changes in climate and faunal diversity and adaptation, are based on the ensemble of such paleoclimatic records and fossil discoveries. In general, these hypotheses fall into three groups: (1) One of the oldest and most widely-studied habitat-specific hypotheses, the 'savanna hypothesis', posits that key human traits were consequences of life in the open savanna (e.g., Dart, 1925; Bartholomew and Birdsell, 1953; Klein, 2009). More recent interpretations of the savanna hypothesis link the evolution of hominin fauna to a step-like development of cooler and drier climate regimes in an increasingly open landscape with large aridification shifts around 3.2 Ma to 2.6 Ma (Bonnefille, 1983; deMenocal, 1995; Dupont and Leroy, 1995), or focused bursts of biotic change ('turnovers') near 2.8 Ma, 1.8 Ma and 1.0 Ma (Prentice and Denton, 1988; Vrba et al., 1989; Tiedemann

et al., 1994; deMenocal, 1995; Clemens et al., 1996). (2) Contrasting these habitat-specific hypotheses the ‘variability selection’ hypothesis emphasizes the importance of changes in climate variability on selection, evolution and adaptation (Potts, 1998). A key element here is that many of the large African faunal evolution events occurred during times of high-amplitude paleoclimate variability. (3) The change from a relatively flat, subdued landscape to higher topographic complexity including rift lakes, mountains, and vegetation patterns ranging from desert to cloud forest has also been postulated to influence hominin evolution (Trauth et al., 2005; Maslin et al., 2014; Wilson et al., 2014). Most likely, none of the above hypotheses are mutually exclusive and spatial differences between regional and global forcing parameters may occur, hence the importance to include paleoecological reconstructions of hominin localities outside the Eastern Rift in the discussion.

In contrast to the Eastern Rift, the Southern Rift (Malawi Rift) is poorly studied. Knowledge of the spatial variability in vegetation patterns along the entire EAR may greatly enhance our ability to identify regional from rift-wide characteristics and thus evaluate the role of individual forcing factors. This thesis focuses on Plio-Pleistocene proxy material from the Chiwondo and Chitimwe Beds in the Karonga Basin (Malawi Rift, northern Malawi) in which some of the earliest remains of the genera *Homo* (Schrenk et al., 1993; Bromage et al., 1995, Kullmer et al., 2011) and *Paranthropus* (Kullmer et al. 1999) were found. The locality is located within the large geographical gap between well-studied Eastern Rift hominin fossil sites and southern African ones (Fig. 1.1).

In light of the above, this thesis presents long-term stable isotope geochemistry records of pedogenic carbonate, herbivore tooth enamel and meteoric water on samples from the Karonga Basin in order to address the following main questions:

- How did the Karonga Basin paleoenvironment - particularly paleovegetation and paleoclimate - of savanna ecosystems evolve during time of early hominin evolution?
- How did the landscape in today's Zambezian Savanna (Malawi) differ from the Somali-Masai Endemic Zone (Tanzania, Kenya, Ethiopia) in the last ca. 4.3 Ma?

However, the reconstruction of early hominin paleoenvironments is only one of many long-term stable isotope-based studies that strive the exploration of landscape evolution. The development of relief and climate patterns is another long-standing debate in modern paleoecological studies. The geological history of the Central Anatolian Plateau (CAP) is a prominent example in this context. Climate-tectonics interactions in this region have been complex with respect to its geologic, tectonic and climatic history. The Oligo-Miocene is a critical time interval with major changes in climate and

topography. Numerous studies were carried out to reconstruct these Middle Cenozoic paleoenvironments in the region to deepen our understanding of the patterns of vegetation and climate (e.g., Yağmurlu et al., 1988; İnci, 1990; Akgün, 1993; Whateley and Tuncali, 1995; Akgün and Sözbilir, 1999; Karayığit et al., 1999; Akgün et al., 2002; Ivanov et al., 2002; Böhme, 2003; Akkiraz and Akgün, 2005; Fortelius et al., 2006; Kayseri et al., 2006; Kovar-Eder et al., 2006; Akgün et al., 2007; Bruch et al., 2007; Fauquette et al., 2007; Ivanov et al., 2007a, 2007b; Strömberg et al., 2007; Ivanov et al., 2008; Eronen et al., 2009; Yavuz-Işık and Toprak, 2010; Bruch et al., 2011; Ivanov et al., 2011; Utescher et al., 2011). Most of these studies however are based on micro- and macrofaunal records either addressing spatially extensive coverage, or on sedimentologic analysis, such as tracing the presence of lignite as an indicator of a warm and wet climate. The long-term stable isotope records produced for this thesis demonstrate again that $\delta^{18}\text{O}$ and $\delta^{13}\text{C}$ data of terrestrial proxies are a powerful tool to enlighten the temporal climatic patterns in a complex landscape.

Therefore, stable isotope analyses of lacustrine long-term records have been carried out on Oligo-Miocene lake basins from the Central Anatolian Plateau to address the following question:

- How did the Late Oligocene to Early Miocene paleoenvironmental conditions of the CAP evolve with respect to climate and the absence of orographic barriers?

All crucial information about the CAP research is described in Chapter 6. The focus of this introduction lies therefore on the main body of this thesis, the reconstruction of the Plio-Pleistocene hominin fossil site in the Karonga Basin (Chapter 2 to 5).

1.2 Study area (Chiwondo and Chitimwe Beds, Karonga Basin, Malawi)

The Plio-Pleistocene sediments of the Karonga Basin in northern Malawi are located in the half-graben of the Malawi Rift between the well-studied eastern and southern African hominin localities. This reconstruction fills therefore an important spatial gap for understanding the development of paleolandscapes inhabited by early hominins. The Chiwondo and Chitimwe Beds are exposed in the Karonga Basin in the half-graben of the Malawi Rift Zone. This southern part of the EAR extends over 900 km from the Rungwe Volcanic Province in the north to the Urema Graben in the south. The Karonga Basin is asymmetric and bordered by several sub-parallel eastward-dipping normal faults in the west, and the steep westward dipping Karonga Border Fault in the east (Fig. 1.2). ENE-WSW extension during the Late Miocene formed the block faulting (Ring et al., 1992; Ebinger et al., 1993; Ring and Betzler, 1995; Hamiel et al., 2012) and Permo-Triassic, Jurassic, Cretaceous and the Plio-Pleistocene

sediments are exposed parallel to the NW shore of Lake Malawi in two, narrow NW-SE aligned stripes, which are separated by Proterozoic metamorphic basement ridges (Fig. 1.3b).

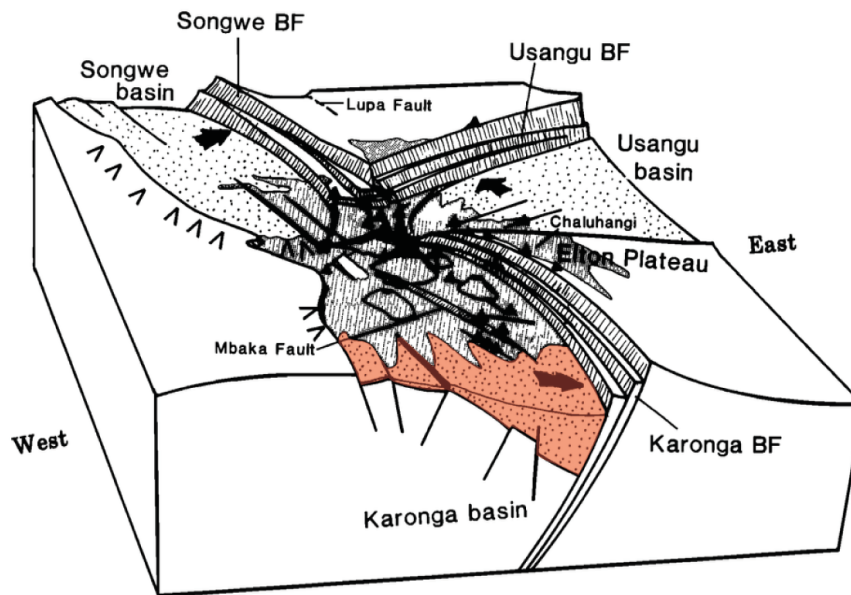


Figure 1.2: Three-dimensional schematic diagram of the Rungwe volcanic province illustrating the morphology of accommodation zones between the Songwe, Usangu, and Karonga Basins after Ebinger et al. (1989) with the Chiwondo and Chitimwe Beds (red), lacustrine sedimentary sequences and alluvium (stipple pattern), border fault (BF) scarps (hatched), Tertiary volcanics (shading), polyphase shield complexes and smaller centers (cones and triangles) and direction of basin asymmetry (bold arrows).

The Chiwondo Beds are divided into Units 1 to 4, followed by the Chitimwe Beds, Unit 5 (Fig. 1.3c; Betzler and Ring, 1995). While pedogenic carbonate is abundant in all units, fossils are only preserved in Units 2 and 3. The anthropologically important Unit 3 (ca. 3.75 to 0.6 Ma) is further subdivided into zones 3A-I, 3A-II and 3B (Fig. 1.3c; Bromage et al., 1995; Sandrock et al., 1999; Kullmer, 2008). The recovered skeletal elements are mostly isolated molars, mandible fragments or high-density limb bones of large-bodied herbivorous mammals (Sandrock et al., 2007).

Material for absolute dating are lacking in the Chiwondo Beds, age determination is done by biostratigraphic correlation (especially suid molars) to well-dated fossil finds in sub-Saharan Africa (Kaufulu and Stern, 1987; Betzler and Ring, 1995; Kullmer, 2008). The shape of present lithic artifacts marks the Chitimwe Beds as Middle Stone Age (Clark et al., 1970).

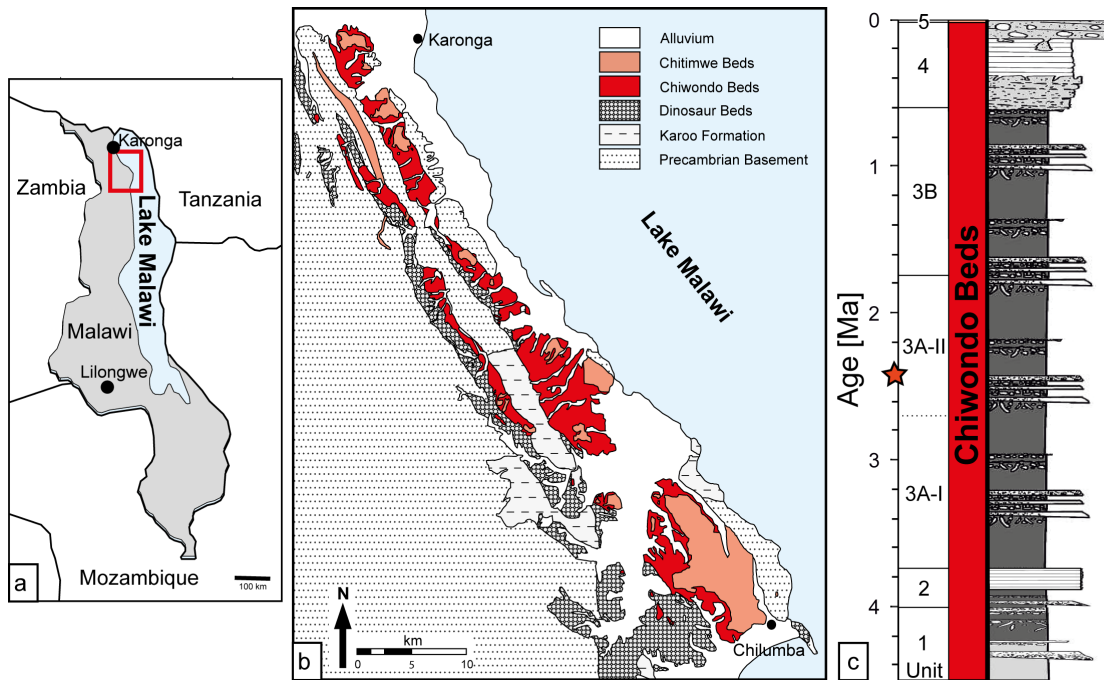


Figure 1.3: Position (a) and geological map (b) of the study site. Star in generalized stratigraphic column (c) after Betzler and Ring (1994) indicates position of hominins (*H. rudolfensis* and *P. boisei*) at ca. 2.4 Ma.

1.3 General Introduction to proxy materials and methods

One of the most powerful tools to reconstruct paleoclimatic and paleoenvironmental conditions, in particular when climate seasonality plays a key role in the evolution of ecosystems, is carbon ($\delta^{13}\text{C}$) and oxygen ($\delta^{18}\text{O}$) isotope geochemistry of multi-proxy archives. This method is well established and widely used in marine and terrestrial environments in virtually all timeframes and regions of this world.

This work emphasizes $\delta^{13}\text{C}$ analyses, which record changes in C_3 vs. C_4 vegetation. The change from C_3 -dominated woodland ecosystems to open C_4 -grasslands is considered the largest vegetational change African ecosystems underwent in the Cenozoic. Interpretation of stable oxygen patterns, however, are more complex. Generally, meteoric water $\delta^{18}\text{O}$ values offer the evaluation of the isotopic composition of today's available (drinking) water. A correlation with fossil proxies allows tracking of possible changes in the climate with empathy on effects of evaporation, seasonality and altitude.

We compare the evolution of Zambezian Savanna biomes in the Karonga Basin with reconstructions of well-studied hominin sites in the Somali-Masai Endemic Zone in the Eastern Rift to enlighten the potential different ecosystems early hominins thrived in.

For this thesis different terrestrial proxy materials that carry the $\delta^{13}\text{C}$ and $\delta^{18}\text{O}$ fingerprint of environmental conditions were used: (1) soil carbonate, ca. 4.3 Ma to today, (2) enamel of fossil (ca. 4.3 Ma to 0.6 Ma) and modern herbivorous mammal teeth, and (3) modern meteoric water (only $\delta^{18}\text{O}$).

1.3.1 $\delta^{13}\text{C}$ and $\delta^{18}\text{O}$ of paleosol and herbivore proxy material

Pedogenic carbonate: All analyzed Chiwondo and Chitimwe paleosol materials were sampled during three field seasons in September to November in 2011, 2012 and 2013. 14 freshly-cut step-sections were trenched to sample - whenever possible - well-consolidated pedogenic carbonate nodules at least 30 cm below paleosols surfaces to eliminate effects of atmospheric CO_2 (Cerling and Quade, 1993). In total 321 pedogenic carbonates were selected for stable isotope analyses from all units (Subunit 3B is missing due to poor outcrop conditions). Outcrop conditions and field characteristics are presented in Chapter 3 (see e.g., Fig. 3.3).

Herbivore enamel: Additionally, 122 enamel samples from 14 different Karonga Basin large-bodied herbivorous mammalian taxa were analyzed for $\delta^{13}\text{C}$ and $\delta^{18}\text{O}$ analyses. These taxa include (1) suids of the extinct genera *Notochoerus* (*Not.*) *jaegeri*, *euilus* and *scotti*, *Metridiochoerus* (*Met.*) *andrewsi* (stage I and III) and *compactus* as well as extant *Phacochoerus* (*Pha.*) *aethiopicus*, (2) bovids of the genus *Hippotragini* sp. (*Hip.*), *Antilopini* sp. (*Ant.*) and *Alcelaphinae* (*Alc.*) *Damaliscus*, *Megalotragus* and *Connochaetes* and one unidentified *Alc.* individual, (3) equids *Eurygnathohippus* sp., (4) elephant *Elephantidae* (*Loxodonta* sp. or *Elephas* sp.?) and (5) hippo *Hippopotamus amphibius*.

During fieldwork, a lower left molar of *Eurygnathohippus* sp. (Hominid Corridor Research Project (HCRP) ID: #1175) and one incisor fragment of *Hippopotamus amphibius* (#1174) were found. Other analyzed teeth were previously collected by the HCRP; typically discovered by systematic surveys along erosional surfaces between 1984 and 2009. Fossils are temporarily stored in Senckenberg Research Institute Frankfurt, Germany and are housed in the collection of the Cultural and Museum Centre Karonga, Malawi. Representative analyzed teeth are displayed in Fig. 1.4.

Different records in proxy material: While $\delta^{13}\text{C}$ and $\delta^{18}\text{O}$ values of tooth enamel record the dietary behavior of an individual animal during the time of tooth development (several month to years) in an area reflecting its migration pattern (see Chapter 5), pedogenic carbonate is stationary and cm-sized nodules reflect isotopic changes in soil over long time periods (up to thousands of years; see Chapter 3; e.g., Birkeland, 1984; Kohn and Cerling, 2002; Pustovoytov, 2003).

The $\delta^{13}\text{C}$ of opportunists (e.g., suids) should reflect major local environmental patterns more accurate than specialized feeders, as they generally ingest biomass they have easy access to, without prioritizing certain plants. Nevertheless, the latter (e.g., *Alcelaphinae* *Connochates*) are also analyzed for this thesis to evaluate the ranges of niche-feeders in a heterogeneous environment. For sampling localities see Chapters 3 and 5.

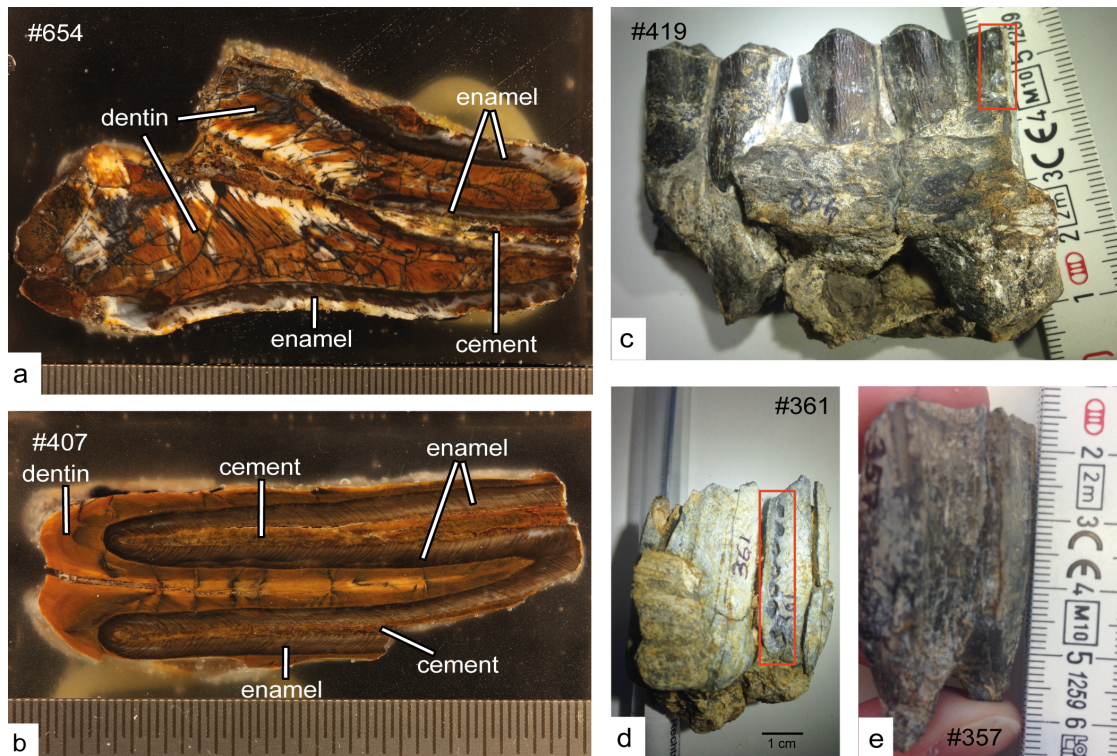


Figure 1.4 Plio-Pleistocene herbivore teeth sampled for $\delta^{13}\text{C}$ and $\delta^{18}\text{O}$ analyses. a) Upper M3 fragment of *Notochoerus euilus* (HRCP #654). b) Lower left M3 of *Metridiochoerus andrewsi* stage I (HCRP #407). c) Upper M of Alcelaphinae *Megalotragus* (HRCP #419). d) Lower right M1 of Alcelaphinae *Megalotragus* (HRCP #361). e) Upper right M1 fragment of equidae *Eurygnathohippus* (HRCP #357). Note holes (c,d) after sampling for stable isotope analyzes (red boxes).

Sample treatment: Pedogenic nodules as well as suid molars were cut laterally (Fig. 1.4a, b) and bulk carbonate powder was extracted with a diamond tip dental drill. Bovid, equid, hippo and elephant enamel samples were generally taken from either drill holes in the outer enamel (Fig. 1.4c, d) or from enamel flakes that chipped from the outer coating. Sampling parallel and across several growth axes of the teeth was necessary to obtain sufficient sample material (2 to 3 mg). Enamel is resistant to isotopic exchange when compared to bone, tooth-cement or dentin (Wang and Cerling, 1994), hence care was taken to avoid these materials in the sampling process. Although the analyzed CO_3 component of the bioapatite is less resistant to diagenetic alteration than the PO_4 component (Kolodny et al., 1983; Shemesh, 1990; Kohn et al., 1999), the large oscillations of $^{16}\text{O}/^{18}\text{O}$ ratios within individual analyzed teeth eliminate an isotopic reset during fossilization.

To remove organic matter and potential diagenetic carbonate, enamel was pretreated with 2% NaOCl solution for 24 hours followed by 1 M Ca-acetate acetic acid buffer solution for another 24 hours and thoroughly rinsed with deionized water (after Spötl and Vennemann, 2003). Typically, enamel pre-treatment resulted in 10% to 60% mass loss. The paleosol material was not pre-treated.

Analysis: Untreated pedogenic carbonate powder (100 to 300 μg) and pretreated enamel (700 to 2050 μg) was reacted with 98% H_3PO_4 for 90 minutes at 70°C in continuous flow mode using a Thermo MAT 253 mass spectrometer interfaced to a Thermo GasBench II. All analyses were performed at the Goethe University-BiK-F Joint Stable Isotope Facility Frankfurt. Final carbon isotopic ratios are reported against VPDB, oxygen isotopic ratios in VSMOW; overall analytical uncertainties are better than 0.03‰ ($\delta^{13}\text{C}$) and 0.04‰ ($\delta^{18}\text{O}$).

1.3.2 $\delta^{18}\text{O}$ of meteoric water

In addition, $\delta^{18}\text{O}$ values of 111 modern meteoric water samples were analyzed. Groundwater ($n = 52$, Fig. 1.5a) and surface water from streams ($n = 9$) and lakes ($n = 5$) in northern Malawi (N of 12°) were sampled in the field seasons during September to November of 2011, 2012 and 2013. In addition, two rainfall collectors (Fig. 1.5b, 1.5c) were positioned in Karonga and Malema; sampling bottles were installed roughly every two weeks during the rainy season (October to May) in 2012/13 and 2013/14 ($n = 45$; for detailed methodology and locality position see Chapter 5).

Analysis: Stable oxygen isotope ratio measurements were made on 1 ml untreated water aliquots using an LGR 24d liquid water isotope analyzer (LWIA). $\delta^{18}\text{O}$ values are calibrated and reported against VSMOW, analytical uncertainties are better than 0.2‰ (2σ). Sampling strategy and analyses followed Schemmel et al. (2013).

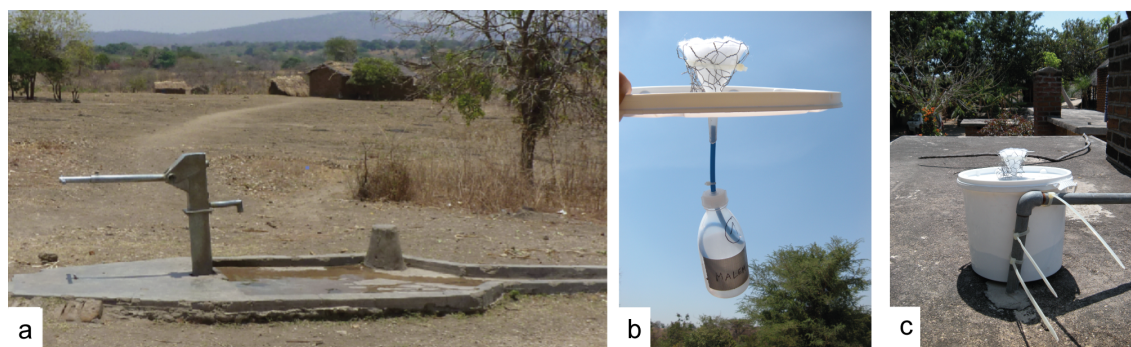


Figure 1.5: a) Typical pump used for groundwater sampling. b) Precipitation was collected in polyethylene plastic containers with a long tube connected to the tip of the funnel, which was additionally filled with polyester to eliminate evaporation. c) On a roof installed rain collector in Malema.

1.4 Structure of this PhD thesis

This thesis includes paleoenvironmental reconstructions of the Plio-Pleistocene Chiwondo and Chitimwe Beds in the Karonga Basin (Chapters 2 to 5) and the Oligo-Miocene lake basins of the Central Anatolian Plateau, Turkey (Chapter 6).

Chapter 2 The manuscript “Palaeoenvironmental Characteristics of the Plio-Pleistocene Chiwondo and Chitimwe Beds (N-Malawi)” by Tina Lüdecke and Heinrich Thiemeyer (Chapter 6 in: Jürgen Runge (Ed.), *New studies on Former and Recent Landscape Changes in Africa: Palaeoecology of Africa Vol. 32* - (2013), pp. 143 - 161) introduces the field relationships and sediment characteristics of the Plio-Pleistocene Chiwondo and Chitimwe Beds in northern Malawi. Here, first conclusions about the paleoenvironment of early hominins were drawn with insight into paleolake phases and lake level changes. Characteristic sedimentological and fossil pedogenic features are described in five exemplary profiles. These indicate a dominance of large river systems and fluctuations of paleolake levels during the last ca. 4.3 Ma.

Chapter 3 The manuscript “Persistent C₃ vegetation accompanied Plio-Pleistocene hominin evolution in the Malawi Rift” by Tina Lüdecke, Friedemann Schrenk, Heinrich Thiemeyer, Ottmar Kullmer, Timothy G. Bromage, Oliver Sandrock, Jens Fiebig and Andreas Mulch (*Journal of Human Evolution* (2016) 90: 163-175) includes first stable carbon isotope long-term records from the Karonga Basin. Here, persistent low $\delta^{13}\text{C}$ values around -9‰ of pedogenic carbonate and suid tooth enamel indicate a C₃-dominated woodland environment in the vicinity of paleolake Malawi during the time of early hominin evolution. This indicates a significantly higher canopy density in this southern part of the East African Rift (EAR) compared to northern EAR localities and therefore implies distinct habitat flexibility of *H. rudolfensis* and *P. boisei*.

Chapter 4 This chapter comprises $\delta^{18}\text{O}$ values from Chiwondo and Chitimwe Bed paleosol carbonate to draw conclusions on the Plio-Pleistocene paleohydrology in the Karonga Basin. $\delta^{18}\text{O}$ data with only small fluctuation and values below 26‰ reflect relatively mesic and persistent climate patterns in this southern part of the EAR during the Plio-Pleistocene. This complements the results of $\delta^{13}\text{C}$ analyses of the same pedogenic proxy material in Chapter 3. The combined data indicate that early hominins at ca. 2.4 Ma lived in a mesic (and wooded) environment in the Karonga Basin. This contrast the ecosystem reconstructed from analysis of Eastern Rift hominin fossil sites, where evolution of our early ancestors is proposed to be linked to changes towards a more open and drier environment during the Pleistocene.

Chapter 5 The manuscript “Stable isotope dietary reconstructions of herbivore enamel reveal heterogeneous wooded savanna ecosystems in the Plio-Pleistocene Malawi Rift” by Tina Lüdecke, Andreas Mulch, Ottmar Kullmer, Heinrich Thiemeyer, Jens Fiebig and Friedemann Schrenk (submitted to *Palaeogeography, Palaeoclimatology, Palaeoecology*) provides foraging strategies of Karonga Basin herbivorous large-bodied mammals which reflect ancient vegetation patterns. Additionally, $\delta^{18}\text{O}$ values of modern meteoric water (precipitation, river, lake and groundwater) were analyzed to compare fossil hydrological parameters with recent ones. The results reflect a relatively mesic environment south of the ITCZ without large fluctuations since the Pliocene, again displaying an increasing discrepancy between the Eastern Rift and the Malawi Rift since ca. 2.5 Ma.

Chapter 6 The manuscript “Stable isotope-based reconstruction of Oligo-Miocene paleoenvironment and paleohydrology of Central Anatolian lake basins (Turkey)” by Tina Lüdecke, Tamás Mikes, F. Bora Rojay, Michael A. Cosca and Andreas Mulch (*Turkish Journal of Earth Sciences* (2013) 22: 793-819) combines stable isotope geochemistry of lacustrine carbonate and field relationships to reconstruct paleoclimatic and paleoenvironmental conditions during the Late Oligocene and Early Miocene in the CAP. The combined data indicate a relatively humid subtropic Chattian (28.4 to 23 Ma) climate with a change to more arid conditions in the middle Aquitanian (ca. 21 Ma) in the central plateau region with frequent climatic fluctuations, probably recording the influence of seasonality, topography, and variations in aridity. Compared to the modern climate these results indicate an absence of orographic barriers at the plateau margins during this time.

Data acquired within this thesis are already published in three manuscripts. Furthermore, Chapter 5 is submitted and Chapter 4 interprets unpublished data.

The author of this thesis is also co-author of the manuscript “Slight pressure imbalances can affect accuracy and precision of dual inlet-based clumped isotope analysis” by Jens Fiebig, Sven Hoffman, Niklas Löffler, Tina Lüdecke, Katharina Methner and Ulrike Wacker (*Isotopes in Environmental and Health Studies* (2015) 16), which is not part of this thesis.

1.5 References

- Aronson, J.L., Hailemichael, M., Savin, S.M., 2008. Hominid Environments at Hadar from Paleosol Studies in a Framework of Ethiopian Climate Change. *Journal of Human Evolution* 55, 532-550.
- Bartholomew, G.A., Birdsell, J.B., 1953. Ecology and the Protohominids. *American Anthropologist* 55, 481-498.
- Behrensmeyer, A.K., Todd, N.E., Potts, R., McBrinn, G.E., 1997. Late Pliocene Faunal Turnover in the Turkana Basin, Kenya and Ethiopia. *Science* 278, 1589-1594.
- Betzler, C., Ring, U., 1995. Sedimentology of the Malawi Rift: Facies and Stratigraphy of the Chiwondo Beds, Northern Malawi. *Journal of Human Evolution* 28, 13.
- Birkeland, P.W., 1984. *Soils and Geomorphology*. Oxford University Press, Oxford, pp. 372.
- Bocherens, H., Sandrock, O., Kullmer, O., Schrenk, F., 2011. Hominin Palaeoecology in Late Pliocene Malawi: First Insights from Isotopes (^{13}C , ^{18}O) in Mammal Teeth. *South African Journal of Science* 107, 6.
- Bonnefille, R., 1983. Evidence for a Cooler and Drier Climate in the Ethiopian Uplands Towards 2.5 Myr Ago. *Nature* 303, 487-491.
- Bromage, T.G., Schrenk, F., Zonneveld, F.W., 1995. Paleoanthropology of the Malawi Rift: An Early Hominid Mandible from the Chiwondo Beds, Northern Malawi. *Journal of Human Evolution* 28, 71-108.
- Cerling, T.E., 1992. Use of Carbon Isotopes in Paleosols as an Indicator of the $p(\text{CO}_2)$ of the Paleatmosphere. *Global Biogeochemical Cycles* 6, 8.
- Cerling, T.E., Bowman, J.R., O'Neil, J.R., 1988. An Isotopic Study of a Fluvial-Lacustrine Sequence: The Plio-Pleistocene Koobi Fora Sequence, East Africa. *Palaeogeography, Palaeoclimatology, Palaeoecology* 63, 22.
- Cerling, T.E., Chritz, K.L., Jablonski, N.G., Leakey, M.G., Kyalo Manthi, F., 2013a. Diet of Theropithecus from 4 to 1 Ma in Kenya. *Proceedings of the National Academy of Sciences* 110, 6.
- Cerling, T.E., Harris, J.M., Leakey, N., 2003. *Stable Isotope Ecology of Northern Kenya, with Emphasis on the Turkana Basin*. In: Leakey, M.G., Harris, J.M. (Eds.), Lothagam: The Dawn of Humanity in Eastern Africa. Columbia University Press, New York, pp. 583-603.
- Cerling, T.E., Hay, R.L., 1986. An Isotopic Study of Paleosol Carbonates from Olduvai Gorge. *Quaternary Research* 25, 16.
- Cerling, T.E., Manthi, F.K., Mbua, E.N., Leakey, L.N., Leakey, M.G., Leakey, R.E., Brown, F.H., Grine, F.E., Hart, J.A., Kaleme, P., Roche, H., Uno, K.T., Wood, B.A., 2013b. Stable Isotope-Based Diet Reconstructions of Turkana Basin Hominins. *Proceedings of the National Academy of Sciences* 110, 10501-10506.
- Cerling, T.E., Mbua, E., Kirera, F.M., Manthi, F.K., Grine, F.E., Leakey, M.G., Sponheimer, M., Uno, K.T., 2011. Diet of Paranthropus Boisei in the Early Pleistocene of East Africa. *Proceedings of the National Academy of Sciences* 108, 9337-9341.
- Cerling, T.E., Quade, J., 1993. Stable Carbon and Oxygen Isotopes in Soil Carbonates. *Geophysical Monograph* 78, 15.
- Cerling, T.E., Wynn, J.G., Andanje, S.A., Bird, M.I., Korir, D.K., Levin, N.E., Mace, W., Macharia, A.N., Quade, J., Remien, C.H., 2011. Woody Cover and Hominin Environments in the Past 6 Million Years. *Nature* 476, 51-56.
- Clark, J.D., Haynes, C.V., Mayby, J.E., Gautier, A., 1970. Interim Report on Palaeoanthropological Investigations in the Lake Malawi Rift. *Quaternaria* 13, 49.
- Clemens, S.C., Murray, D.W., Prell, W.L., 1996. Nonstationary Phase of the Plio-Pleistocene Asian Monsoon. *Science* 274, 943-948.
- Dart, R., 1925. *Australopithecus Africanus*: The Man-Ape of South Africa. *Nature* 115, 195-199.

- deMenocal, P.B., 1995. Plio-Pleistocene African Climate. *Science* (New York, N.Y.) 270, 53-59.
- Dupont, L.M., Leroy, S., 1995. *Steps toward Drier Climatic Conditions in North-Western Africa During the Upper Pliocene*. In: Vrba, E., Partridge, T., Denton, D., Burcle, L. (Eds.), *Palaeoclimate and Evolution, with Emphasis on Human Origins*. Yale University Press, New Haven, CT, pp. 289-298.
- Ebinger, C.J., Deino, A.L., Tesha, A.L., Becker, T., Ring, U., 1993. Tectonic Controls on Rift Basin Morphology: Evolution of the Northern Malawi (Nyasa) Rift. *Journal of Geophysical Research* 98, 17821.
- Feakins, S.J., Levin, N.E., Liddy, H.M., Sieracki, A., Eglinton, T.I., Bonnefille, R., 2013. Northeast African Vegetation Change over 12 M.Y. *Geology* 41, 295-298.
- Fiebig, J., Hoffmann, S., Löffler, N., Lüdecke, T., Methner K., Wacker, U., 2015. Slight pressure imbalances can affect accuracy and precision of dual inlet-based clumped isotope analysis. *Isotopes in Environmental and Health Studies*, 16.
- Hamiel, Y., Baer, G., Kalindekafu, L., Dombola, K., Chindandali, P., 2012. Seismic and Aseismic Slip Evolution and Deformation Associated with the 2009-2010 Northern Malawi Earthquake Swarm, East African Rift. *Geophysical Journal International* 191, 898-908.
- Harris, J.M., Cerling, T.E., 2002. Dietary Adaptations of Extant and Neogene African Suids. *Journal of Zoology* 256, 45-54.
- Heinzelin, J.d., Clark, J.D., White, T., Hart, W., Renne, P., WoldeGabriel, G., Beyene, Y., Vrba, E., 1999. Environment and Behavior of 2.5-Million-Year-Old Bouri Hominids. *Science* 284, 625-629.
- Hopley, P.J., Latham, A.G., Marshall, J.D., 2006. Palaeoenvironments and Palaeodiets of Mid-Pliocene Micromammals from Makapansgat Limeworks, South Africa: A Stable Isotope and Dental Microwear Approach. *Palaeogeography, Palaeoclimatology, Palaeoecology* 233, 235-251.
- Kaufulu, Z.M., Stern, N., 1987. The First Stone Artefacts to Be Found in Situ within the Plio-Pleistocene Chiwondo Beds in Northern Malawi. *Journal of Human Evolution* 16, 12.
- Kingston, J.D., Marino, B.D., Hill, A., 1994. Isotopic Evidence for Neogene Hominid Palaeoenvironments in the Kenya Rift Valley. *Science* 264, 5.
- Klein, R.G., 2009. *The Human Career: Human Biological and Cultural Origins*, Third Edition ed. University Of Chicago Press, Chicago and London, pp. 1024.
- Kohn, M.J., Cerling, T.H., 2002. *Stable Isotope Compositions of Biological Apatite*. In: Kohn, M.J., Rakovan, J., Hughes, J.M. (Eds.), *Phosphates. Geochemical, Geobiological, and Materials Importance*. Mineralogical Society of America, Washington, D.C., pp. 455-488.
- Kohn, M.J., Schoeninger, M.J., Barker, W.W., 1999. Altered States: Effects of Diagenesis on Fossil Tooth Chemistry. *Geochimica et Cosmochimica Acta* 63, 2737-2747.
- Kolodny, Y., Luz, B., Navon, O., 1983. Oxygen Isotope Variations in Phosphate of Biogenic Apatites, I. Fish Bone Apatite—Rechecking the Rules of the Game. *Earth and Planetary Science Letters* 64, 398-404.
- Kullmer, O., 2008. The Fossil Suidae from the Plio-Pleistocene Chiwondo Beds of Northern Malawi, Africa. *Journal of Vertebrate Paleontology* 28, 9.
- Kullmer, O., Sandrock, O., Abel, R., Schrenk, F., Bromage, T.G., Juwayeyi, Y.M., 1999. The first *Paranthropus* from the Malawi Rift. *Journal of Human Evolution* 37, 121-127.
- Kullmer, O., Sandrock, O., Kupczik, K., Frost, S.R., Volpato, V., Bromage, T.G., Schrenk, F., 2011. New primate remains from Mwenirondo, Chiwondo Beds in northern Malawi. *Journal of Human Evolution* 61, 617-623.
- Levin, N.E., Brown, F.H., Behrensmeyer, A.K., Bobe, R., Cerling, T.E., 2011. Paleosol Carbonates from the Omo Group: Isotopic Records of Local and Regional Environmental Change in East Africa. *Palaeogeography, Palaeoclimatology, Palaeoecology* 307, 75-89.

- Levin, N.E., Quade, J., Simpson, S.W., Semaw, S., Rogers, M., 2004. Isotopic Evidence for Plio–Pleistocene Environmental Change at Gona, Ethiopia. *Earth and Planetary Science Letters* 219, 93-110.
- Lüdecke, t., Thiemeyer, H., 2013. *Palaeoenvironmental Characteristics of the Plio-Pleistocene Chiwondo and Chitimwe Beds (N-Malawi)*. In: Runge, J. (Ed.), *New studies on Former and Recent Landscape Changes in Africa: Palaeoecology of Africa*, Vol. 32. (CRC Press, London, pp. 143 - 161.
- Lüdecke, T., Schrenk, F., Thiemeyer, H., Kullmer, O., Bromage, T.G., Sandrock, O., Fiebig, J., Mulch, A., 2016. Persistent C3 vegetation accompanied Plio-Pleistocene hominin evolution in the Malawi Rift. *Journal of Human Evolution* 90, 163-175.
- Magill, C.R., Ashley, G.M., Freeman, K.H., 2013a. Ecosystem Variability and Early Human Habitats in Eastern Africa. *Proceedings of the National Academy of Sciences* 110, 1167-1174.
- Magill, C.R., Ashley, G.M., Freeman, K.H., 2013b. Water, Plants, and Early Human Habitats in Eastern Africa. *Proceedings of the National Academy of Sciences* 110, 1175-1180.
- Maslin, M.A., Brierley, C.M., Milner, A.M., Shultz, S., Trauth, M.H., Wilson, K.E., 2014. East African Climate Pulses and Early Human Evolution. *Quaternary Science Reviews* 101, 1-17.
- Morgan, M.E., Kingston, J.D., Marino, B.D., 1994. Carbon Isotopic Evidence for the Emergence of C4 Plants in the Neogene from Pakistan and Kenya. *Nature* 367, 162-165.
- Plummer, T.W., Bishop, L.C., 1994. Hominid Paleoecology at Olduvai Gorge, Tanzania as Indicated by Antelope Remains. *Journal of Human Evolution* 27, 47-75.
- Plummer, T.W., Bishop, L.C., Ditchfield, P., Hicks, J., 1999. Research on Alte Pliocene Oldowan Sites at Kanjera South, Kenya. *Journal of Human Evolution* 36, 20.
- Plummer, T.W., Ditchfield, P.W., Bishop, L.C., Kingston, J.D., Ferraro, J.V., Braun, D.R., Hertel, F., Potts, R., 2009. Oldest Evidence of Tool Making Hominins in a Grassland-Dominated Ecosystem. *PloS one* 4, e7199.
- Potts, R., 1998. Variability Selection in Hominid Evolution. *Evolutionary Anthropology* 81, 16.
- Prentice, M.L., Denton, G.H., 1988. *The Deep-Sea Oxygen Isotope Record, the Global Ice Sheet System and Hominid Evolution*. In: Grine, F.E. (Ed.), *Evolutionary History of the Robust Australopithecines*. Transaction Publisher, New York, pp. 383-403.
- Pustovoytov, K., 2003. Growth Rates of Pedogenic Carbonate Coatings on Coarse Clasts. *Quaternary International* 106-107, 131-140.
- Quinn, R.L., Lepre, C.J., Wright, J.D., Feibel, C.S., 2007. Paleogeographic Variations of Pedogenic Carbonate Delta13c Values from Koobi Fora, Kenya: Implications for Floral Compositions of Plio-Pleistocene Hominin Environments. *Journal of Human Evolution* 53, 560-573.
- Ring, U., Betzler, C., 1995. Geology of the Malawi Rift: Kinematic and Tectonosedimentary Background to the Chiwondo Beds, Northern Malawi. *Journal of Human Evolution* 28, 15.
- Ring, U., Betzler, C., Delvaux, D., 1992. Normal Vs. Strike-Slip Faulting During Rift Development in East Africa: The Malawi Rift. *Geology* 20, 4.
- Sandrock, O., Dauphin, Y., Kullmer, O., Abel, R., Schrenk, F., Denys, C., 1999. Malema: Preliminary Taphonomic Analysis of an African Hominid Locality. *Earth and Planetary Sciences* 328, 7.
- Sandrock, O., Kullmer, O., Schrenk, F., Juwayeyi, Y.M., Bromage, T.G., 2007. Fauna, Taphonomy, and Ecology of the Plio-Pleistocene Chiwondo Beds, Northern Malawi, in: Bobe, R., Alemseged, Z., Behrensmeyer, A. (Eds.), *Hominin Environments in the East African Pliocene: An Assessment of the Faunal Evidence*. Springer Netherlands, pp. 315-332.

- Schemmel, F., Mikes, T., Rojay, B., Mulch, A., 2013. The Impact of Topography on Isotopes in Precipitation across the Central Anatolian Plateau (Turkey). *American Journal of Science* 313, 61-80.
- Schrenk, F., Bromage, T.G., Betzler, C.G., Ring, U., Juwayeyi, Y.M., 1993. Oldest Homo and Pliocene Biogeography of the Malawi Rift. *Nature* 365, 833-836.
- Ségalen, L., Lee-Thorp, J.A., Cerling, T., 2007. Timing of C₄ Grass Expansion across Sub-Saharan Africa. *Journal of Human Evolution* 53, 549-559.
- Semaw, S., Simpson, S.W., Quade, J., Renne, P.R., Butler, R.F., McIntosh, W.C., Levin, N., Dominguez-Rodrigo, M., Rogers, M.J., 2005. Early Pliocene Hominids from Gona, Ethiopia. *Nature* 433, 301-305.
- Shemesh, A., 1990. Crystallinity and Diagenesis of Sedimentary Apatites. *Geochimica et Cosmochimica Acta* 54, 2433-2438.
- Sikes, N.E., 1994. Early Hominid Habitat Preferences, in East Africa: Paleosol Carbon Isotopic Evidence. *Journal of Human Evolution* 27, 21.
- Sikes, N.E., Ashley, G.M., 2007. Stable Isotopes of Pedogenic Carbonates as Indicators of Paleoecology in the Plio-Pleistocene (Upper Bed I), Western Margin of the Olduvai Basin, Tanzania. *Journal of Human Evolution* 53, 574-594.
- Sikes, N.E., Potts, R., Behrensmeyer, A.K., 1999. Early Pleistocene Habitat in Member 1 Ologesailie Based on Paleosol Stable Isotopes. *Journal of Human Evolution* 37, 26.
- Spötl, C., Vennemann, T.W., 2003. Continuous-Flow Isotope Ratio Mass Spectrometric Analysis of Carbonate Minerals. *Rapid communications in mass spectrometry: RCM* 17, 1004-1006.
- Tiedemann, R., Sarnthein, M., Shackleton, N.J., 1994. Astronomic Timescale for the Pliocene Atlantic $\delta^{18}\text{O}$ and Dust Flux Records of Ocean Drilling Program Site 659. *Paleoceanography* 9, 619-638.
- Trauth, M.H., Deino, A.L., Bergner, A.G.N., Strecker, M.R., 2003. East African Climate Change and Orbital Forcing During the Last 175 Kyr Bp. *Earth and Planetary Science Letters* 206, 297-313.
- Trauth, M.H., Maslin, M.A., Deino, A., Strecker, M.R., 2005. Late Cenozoic Moisture History of East Africa. *Science* 309, 2051-2053.
- Vrba, E.S., Denton, G.H., Prentice, M.L., 1989. Climatic Influences on Early Hominid Behavior. *Ossa* 14, 29.
- Wang, Y., Cerling, T.E., 1994. A Model of Fossil Tooth and Bone Diagenesis: Implications for Paleodiet Reconstruction from Stable Isotopes. *Palaeogeography, Palaeoclimatology, Palaeoecology* 107, 281-289.
- Wesselmann, H.B., 1985. Fossil Micromammals as Indicators of Climatic Change About 2.4 Myr Ago in the Omo Valley, Ethiopia. *South African Journal of Science* 81, 260-261.
- White, T.D., WoldeGabriel, G., Asfaw, B., Ambrose, S., Beyene, Y., Bernor, R.L., Boissarie, J.R., Currie, B., Gilbert, H., Haile-Selassie, Y., Hart, W.K., Hlusko, L.J., Howell, F.C., Kono, R.T., Lehmann, T., Louchart, A., Lovejoy, C.O., Renne, P.R., Saegusa, H., Vrba, E.S., Wesselman, H., Suwa, G., 2006. Asa Issie, Aramis and the Origin of Australopithecus. *Nature* 440, 883-889.
- Wilson, K.E., Maslin, M.A., Leng, M.J., Kingston, J.D., Deino, A.L., Edgar, R.K., Mackay, A.W., 2014. East African Lake Evidence for Pliocene Millennial-Scale Climate Variability. *Geology* 42, 955-958.
- WoldeGabriel, G., Ambrose, S.H., Barboni, D., Bonnefille, R., Bremond, L., Currie, B., DeGusta, D., Hart, W.K., Murray, A.M., Renne, P.R., Jolly-Saad, M.C., Stewart, K.M., White, T.D., 2009. The Geological, Isotopic, Botanical, Invertebrate, and Lower Vertebrate Surroundings of Ardipithecus Ramidus. *Science* 326: 65.
- Wynn, J.G., 2000. Paleosols, Stable Carbon Isotopes, and Paleoenvironmental Interpretation of Kanapoi, Northern Kenya. *Journal of Human Evolution* 39, 411-432.

Chapter 2 Environmental Characteristics of the Plio-Pleistocene Chiwondo and Chitimwe Beds (N-Malawi)

Tina Lüdecke^{1,2}, Heinrich Thiemeyer³

¹ Senckenberg Biodiversity and Climate Research Centre, Frankfurt, Germany

² Institute of Geosciences, Goethe University Frankfurt, Frankfurt, Germany

³ Institute of Physical Geography, Goethe University Frankfurt, Germany

Published in Runge, J. (Ed.), New Studies on Former and Recent Landscape Changes in Africa: Palaeoecology of Africa, Vol. 32 (2013), CRC Press, London, pp. 143-161.

ISSN: 0168-6208

Abstract *Field relationships and sediment characteristics of the Plio-Pleistocene Chiwondo and Chitimwe Beds in Northern Malawi are investigated with the attempt to draw conclusions about the palaeoenvironment in which hominid evolution took place. The objective is to gain information about palaeolake phases of water level transgressions or regressions and to narrow down the geochronological timespan. Widely distributed surface survey was performed to acquire a better understanding of the tectonic relationships and lateral variability of the different lithologies. Here, the descriptions of five exemplary profiles display characteristic features in terms of sediments and palaeosol remnants which indicate the dominance of large river systems and fluctuations of palaeolake levels during the last 4 Ma. The primary fluvial deposits reveal a high rate of pedogenic overprint indicated by abundant carbonate nodules; these erosion-resistant Bk-horizons are well preserved to the contrary to the carbonate depleted upper horizon of the palaeosols in this tectonically active region.*

2.1 Introduction

Reconstruction of the palaeoenvironment in which faunal evolution occurred is a focus of on-going research, with a strong emphasis on the early human history. Numerous studies, applying different methods, have documented the impact of long-term environmental change on the evolution of hominids with a regional focus on East African sites in Ethiopia, Kenya and Tanzania (e.g. Wesselman, 1985; Cerling and Hay, 1986; Cerling et al., 1988; Cerling, 1992; Plummer and Bishop, 1994; Sikes, 1994; Behrensmeyer et al., 1997; de Heinzelin et al., 1999; Sikes et al., 1999; Wynn, 2000; Levin et al., 2004 and 2011; Ségalen et al., 2007; Cerling et al., 2011; Magill et al., 2012a and 2012b; Feakins et al., 2013). Plio-Pleistocene sediments in the Karonga-Chilumba area in northern Malawi are located in the south of the East African Rift System (EARS; see Fig. 2.1) between the 'classical' eastern and southern African hominid localities. Therefore, the study area fills an important spatial gap for understanding the development of our early ancestors in a time during substantial junctures in human evolution. Field relationships, sediment characteristics and heavy minerals (HM) were analyzed to gain information about palaeoecological and palaeoclimatic conditions during deposition of the Chiwondo Beds.

During prior work, vertebrate and invertebrate fossils were recovered from the sediments, including two important hominid fossil finds, a maxillary fragment of *Paranthropus cf. boisei* (Kullmer et al., 1999) and a mandible of *Homo rudolfensis* (Schrenk et al., 1993 and 1995; Bromage et al., 1995b), as well as several cercopithecoid primate cranio-dental remains (Bromage and Schrenk, 1987; Frost and Kullmer, 2008; Kullmer et al., 2011).

2.1.1 Geologic and tectonic framework

The study area is located in the half-graben of the Malawi Rift zone, which is the southern part of the western branch of the EARS and extends over 900 km from the Rungwe Volcanic Province in the north (southern Tanzania) to the Urema Graben in the south (Mozambique). The examined sediments are exposed in the Karonga Basin in the northernmost part, which was formed by block faulting in response to ENE–WSW extension during the Late Miocene (Ebinger *et al.*, 1993; Ring *et al.*, 1992). It is, similar to other rift zones in the area, asymmetric and bordered by a steep westward dipping fault in the east and several sub-parallel eastward-dipping normal faults in the west (Ebinger *et al.*, 1993; Ring and Betzler, 1995; Hamiel *et al.*, 2012). Between the cities of Karonga and Chilumba Permo-Triassic, Jurassic, Cretaceous and the studied Plio-Pleistocene Chiwondo and Chitimwe Beds are exposed in two narrow northwest-southeast aligned stripes separated by Proterozoic metamorphic basement ridges parallel to the western shore of Lake Malawi (Betzler and Ring, 1995), ca. 70 km long (N to S) and 15 km wide (E to W). The focus is on two areas (Fig. 2.1), both located in the eastern strip: i) the Malema and Mwenirondo region in the north, ca. 10 km south of Karonga, here the maxillary

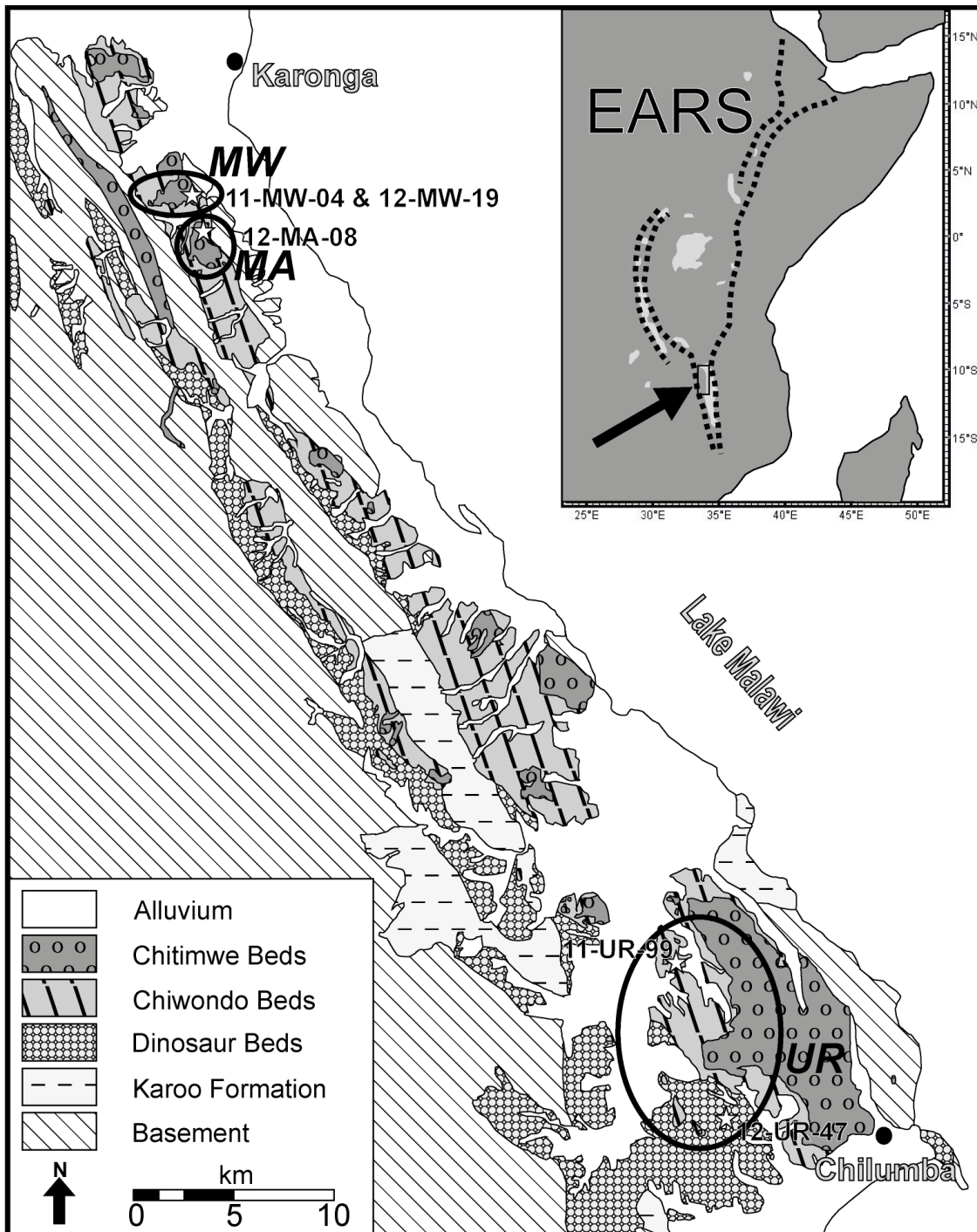


Figure 2.1 Inlet: East Africa with the East African Rift System, EARS (dotted lines) and rift lakes. Box indicates position of large map which shows the geology of the study area with circles around the three sampling localities (MW = Mwenirondo; MA = Malema; UR = Uraha) and logged profiles within (small star).

fragment “RC 911” of *Paranthropus cf. boisei* was recovered in 1996; and ii) the Uraha region, ca. 50 km southeast of Karonga where the mandible “UR 501” of *Homo rudolfensis* was discovered 1991.

The basement and Mesozoic shale- and sandstone-dominated Karoo Supergroup are covered by reddish and grayish sandstones, marls and clays of the Early Cretaceous Dinosaur Beds (Catuneanu et al., 2005; Schlüter, 2008). The Plio-Pleistocene sedimentary group overlies these sediments with a major angular unconformity which is locally pronounced; especially in the western

sediment strip. The formation was first mentioned by Andrew and Bailey (1910) and the grayish sandstone and siltstones were named “Chiwondo” and “Chitimwe Beds” by Dixey in 1927 who interpreted them as lake beds. The lacustrine origin was later confirmed by Stephens, 1966; Charsley, 1972; Kaufulu, 1989; Betzler and Ring, 1995 and others. The depositional facies of these sediments range from alluvial (braided and meandering system deposits, deltaic and fan sediments) to aeolian and lake (high and low energy) deposits (Betzler and Ring, 1995). The sediments are folded, tilted and colluvially translocated due to extreme tectonic uplift and extension in the Malawi Rift area (Ring and Betzler, 1995) which is still ongoing (Hamiel et al., 2012).

Betzler and Ring (1995) and Ring and Betzler (1995) described the tectonics, sedimentology and geology of the Plio-Pleistocene deposits. They divided the Chiwondo Beds into Units 1 to 4, followed by Unit 5, the Chitimwe Beds. The anthropologically important Unit 3 was subdivided into three zones based on faunal remains, mostly suid material (Bromage et al., 1995a; Kullmer, 2008).

After Betzler and Ring (1995) the braided stream deposits of the oldest Unit 1 are reddish coloured due to the partly reworking of the Dinosaur Beds which they overlie with an angular unconformity. After a major calcimorphic palaeosol, lacustrine sediments of Unit 2 with high and low energy fan deposits and abundant calcimorphic palaeosol layers are present. The limestones comprehend pelecypods and gastropods, primary *Bellamyia* freshwater snails. Separated by an angular unconformity, the sediments of Unit 3 are deposited in a mainly fluvial environment, again interrupted by phases of pedogenesis. Due to biostratigraphic data of suid third molar fossils this unit can be differentiated into three zones (Kullmer, 2008). Zone 3A-1 and 3A-2 are made of meandering river deposits which accumulate lakeward in stream-mouth bars of deltas, whereas Subunit 3B is richer in stacked calcimorphic palaeosols than the older zones, some of them are ferruginous. Unit 4 follows after a major angular unconformity. Here aeolian sands and diatom-rich marls and limestones are exposed. Subunit 3B and Unit 4 are restricted to the southern part of the deposal area (Uraha region). Exposures of the up to 15 m thick reddish sands and conglomerates of the Chitimwe Beds (Unit 5) are variable through an overburden of colluvium and overly the Chiwondo Beds with an angular discordance (Betzler and Ring, 1995; Thompson et al., 2012). The grain size of the sub-angular to well-rounded particles ranges from fine sands to large cobbles, which are generally made out of basement or Karoo Supergroup materials. Lithic artifacts with limited indications of post-depositional transport are preserved in this unit (Thompson et al., 2012). The complete Plio-Pleistocene succession has a preserved maximal thickness of 100 m and represents a large-scale transgressive-regressive tectono-sedimentary cycle (Ring and Betzler, 1994). It is to note that due to erosion each of the units can reveal a direct contact to the basement, Karoo Supergroup or Dinosaur Beds.

2.1.2 Stratigraphy

Age determination of the exposed sediments is difficult to evaluate as volcanic layers for absolute dating are lacking in the area (Kaufulu and Stern, 1987; Betzler and Ring, 1994; Kullmer, 2008). Biostratigraphic correlation to well-dated fossil finds elsewhere in sub-Saharan Africa is possible. Here, the documentation of the structural density of enamel bands of suid molars are of importance (Kullmer, 2008). However, vertebrate fossils are only found in Units 2 and 3. Suid material attributed to *Notochoerus jaegeri* was recovered in the south of the study area and suggests an age older than 4.0 Ma for Unit 2 (Kullmer, 2008). With the use of dental fossils of *Not. euilus*, *Not. scotti*, *Metridiochoerus andrewsi* and *Met. compactus* Bromage et al. (1995a) and Kullmer (2008) subdivided Unit 3 into three biozones with ages of 3.75 to 2.7 Ma, 2.7 to 1.8 Ma and 1.74 to 0.6 Ma respectively. The lack of fossils does not allow any biostratigraphical age for Units 1, 4 and 5 (Betzler and Ring, 1995). The maximum age of Unit 1 is restricted by the development of the Malawi Rift about 8.6 Ma ago (Ebinger et al., 1989; Ring et al., 1992). The age of the Chitimwe Beds could be assigned to the Middle and Late Pleistocene due to the presence of lithic artifacts (Clark et al., 1970). The sort and shape of the stone tools recovered classify the unit as Middle Stone Age (MSA; from ca. 0.285 to 0.030 Ma), based on east and central African data (Barham and Smart, 1996; Tryon et al., 2005; Thompson et al., 2012). An unpublished OSL-age of Chitimwe Bed sands near Karonga is reported, having a minimum age of 20 kyrs (S. Stokes, pers. comm. in Betzler and Ring, 1995). However, the Chitimwe Beds exhibit a broad horizontal and vertical variability in clast size. The strong red colour derives from intensive soil development resulting in Chromic Cambisols and Chromic Luvisols on the actual land surface. Soil depth ranges from 0.5 m up to 10 m in some places. The soils are decalcified, the calcic subsoil horizons developed mainly in the underlying Chiwondo sediments.

2.1.3 Palaeosols

Recently, palaeosols have been used to reconstruct palaeoenvironmental conditions of the classical hominid sites in East Africa (e.g. Wynn, 2000; Wynn and Retallack, 2001; Retallack et al., 2002; Wynn, 2004; Aronson et al., 2008; Levin et al., 2011). These studies enhanced the interpretation of environmental conditions of hominid habitation areas where well preserved palaeosols occur within the investigated sections. However, the excellent preservation conditions of the recognized palaeosols play a key role as they are an important prerequisite for proper interpretation.

The siliciclastic parent sediments of palaeosols within the Chiwondo Beds derived mostly from erosion of the hinterland consisting of Proterozoic metamorphic basement rocks and Permo-Triassic Karoo sediments that subsequently accumulated in the Malawi Rift. Due to alternating lake levels with transgression and regression of the shore line, fluvial sediments were partly reworked and sorted under deltaic and lacustrine conditions. Within this setting decalcified B horizons of terrestrial soils are rarely preserved. Moreover,

although the Rungwe Volcanic Province, which had several magmatic pulses during the Plio-Pleistocene represented by tuffaceous sediments and lava flows (Delvaux et al., 1992, Ebinger et al., 1993, Fontijn et al., 2012), is located less than 150 km to the northwest of the study area, no volcanic ash covering older land surfaces (with palaeosols) has been detected in the entire area so far. Crossley (1982) describes a series of pyroclastic deposits overlying the basal lacustrine sediments of the Chiwondo Beds.

The calcimorphic palaeosols mentioned by Betzler and Ring (1995) show horizons with abundant carbonate nodules. They interpret these horizons as remnants of palaeosols which developed during phases of emersion and plant growth. Nonetheless, palaeosols of the Chiwondo and Chitimwe Beds have not been investigated in detail yet.

2.2 Goals and methods

Field relationships, sediment characteristics and heavy minerals (HM) were analyzed to gain information about palaeoecological and palaeoclimatic conditions during deposition of the Chiwondo Beds. With the attempt to narrow down the geochronological timespan of the Plio-Pleistocene units, datable material, namely volcanic tuffs, was searched for within the sediment sequence. Palaeosols were surveyed for the purpose of identifying marker horizons. Widely distributed surface survey was performed to gain a better understanding of the tectonic relationships and lateral variability of the different lithologies.

Reconnaissance field work comprised sediment and soil description of selected sections which were cut into prominently exposed slopes. Five exemplary profiles covering Unit 1, 2, 3A and 4 from three localities (Mwenirondo, Malema and Uraha; see Fig. 2.1) are presented, which display characteristic features in terms of sediments and palaeosol remnants.

Description of sediment characteristics were done according to the standard of the German guidelines for soil and substrate description (Ad-hoc-AG Boden, 2005). For each section, stratification, texture, and soil horizon characteristics were recorded during field survey. Laboratory analyses comprised texture analysis following the German standard DIN ISO 11277 (2002). Determination of soil colour was performed using Munsell Soil Color Chart (2000).

For heavy mineral analyses fine sand (63-200 μm) was fractionized and treated with 5 N Na-dithionite to remove coatings of iron and manganese. Heavy minerals were separated using Na-polytungstenate ($d = 2.85 \text{ g/cm}^3$) and mounted with resin (refraction index $n = 1.66$) on microscope slides. Examination was done using a petrographic microscope; all samples were screened and the heavy mineral suites were recorded qualitatively. Here, a well-weathered sapolite 100 m west of profile 12-MW-58, 8 samples of a section in the Malema region examined by Sandrock (1999) in addition to 38 sediment-samples within profile 11-MW-04 were analysed.

2.3 Palaeopedological field observations

The Chiwondo Beds contain palaeosol horizons which can be described either as Bw-horizons, as oximorphic Cl-horizons or, more often, as Bk-horizons which are rich in carbonate nodules. In the whole sequence no complete palaeosol profile containing A, B and C horizons has been recognized.

The definition of the palaeosol horizons follows FAO (2006), despite the fact that pedofeatures may have changed in comparison with surface soils (Retallack, 1998). The defining properties of the palaeosol horizons in the area are colour, gleyzation, and carbonatization.

The Bw-horizons represent terrestrial palaeosols of Cambisol type. Their matrices generally have brown colour (10 YR to 7.5 YR) and do not contain carbonate unless infiltration from above has formed carbonate nodules subsequently. The parent material is composed of sand, most probably of alluvial or aeolian origin. Locally mottling of a fossil capillary fringe can be recognized.

Other remnants of palaeosols are represented by oximorphic horizons of Gleysols. These horizons developed close to a former surface from where atmospheric air could regularly enter the pore space. It seems that almost no post-burial alteration affected the horizons except later carbonate infiltration from above.

Large parts of the Chiwondo sediments show a light greenish to light greyish colour. This might be an effect of reduction and removal of oxides during times of groundwater influence, most probably directly after deposition of the respective strata. However, horizons with oxidation patterns, i.e. the upper part of Gleysols pointing to former surfaces, have been rarely observed.

Further palaeopedofeatures are Bk-horizons with abundant carbonate nodules. Superficial decalcified horizons as generally expected are absent. Thus, the main question is whether the concretionary carbonates represent genuine palaeosols. The parent material eroded from lime free sources (basement, Karoo Supergroup sediments) and consists of primarily non-calcareous sands and silts. A sedimentary reworking of concretions from elsewhere can be excluded in the dominantly fluvial setting, since their distribution in the respective strata is homogeneous and no placer-like deposits could be observed in the field.

All surface soils, even in the basement areas outside the rift, comprise Bk-horizons in the subsoil. Hence, calcium released by silicate weathering accumulates as carbonate crust in shallow depth and nodules form during pedogenesis. The shape of carbonate glaebules in the palaeosols ranges from diffuse patches of carbonate powder which may be early stages of nodules, to nodules up to 5 cm in diameter. The latter are generally massive with distinct outer boundaries indicating that finely distributed carbonate changed to the present form by subsequent leaching of calcareous phases from overlying soil

horizons. Rarely concentric layers can be observed, which points towards a continuous growth (Retallack, 2011).

Tectonic activity resulted in a complex block pattern dissecting the sediments and correlation of the palaeosols with a small lateral extension is very challenging. The observed palaeosols mentioned by Betzler and Ring (1995) are the most visible ones in the stratigraphy.

2.3.1 Mwenirondo

2.3.1.1 Field aspects

The Mwenirondo region is a flat, plateau area between the rivers of Masapa in the north and Ruasho in the south (Fig. 2.1). Chitimwe deposits overlie the Chiwondo Beds with an unconformity. Due to a normal fault which is exposed on the eastern slope of the plateau, sediments of Unit 2 crop out on the northern slopes and Unit 3A on the southern ones.

2.3.1.2 Unit 2

The 13.2 m long profile 11-MA-58 ($10^{\circ}0.764'S$, $33^{\circ}53.916'E$, 563 m asl), represents a typical sequence of Unit 2, on a steep cut bank of the Masapa river, which is water bearing only in the rainy season.

At the base of the section, saprolitic Precambrian basement gneiss is exposed. Its matrix is non-calcareous but contains detached carbonate-rich patches up to ~3 cm in diameter due to leaching from above.

A thick continuous sequence of Chiwondo Unit 2 sediments follows. The deposits are mainly coarse sand matrix supported fluvial conglomerates with fine to coarse pebbles and well-rounded cobbles (< 15cm). The conglomerates show a general fining up section and are successively enriched in pedogenic carbonate nodules towards the higher part of each layer, until a forming of massive caliche, followed by another conglomerate deposit. Four of those pedogenic cycles are present in the logged profile (Fig. 2.2).

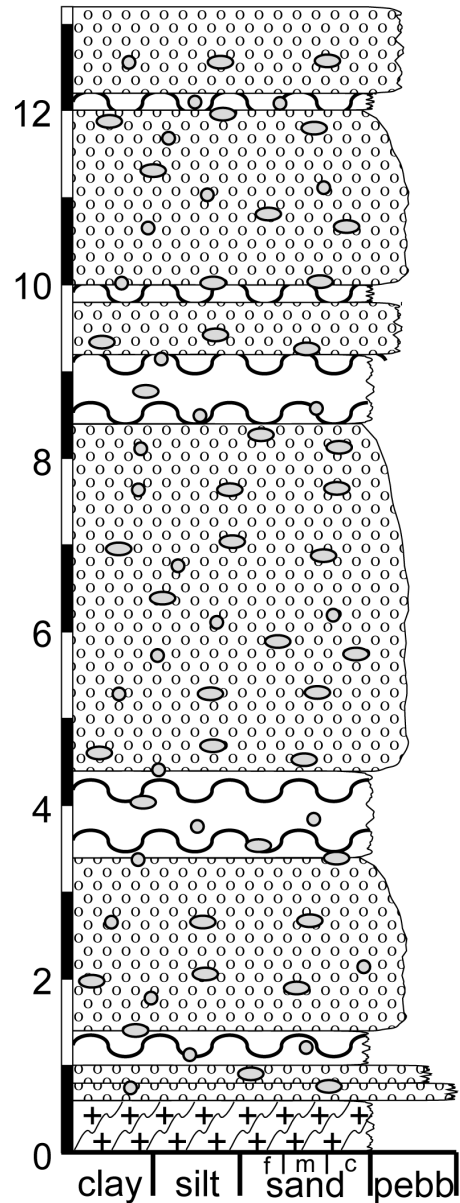


Figure 2.2 Stratigraphic column of profile 12-MA-58 ($10^{\circ}0.764'S$, $33^{\circ}53.916'E$), representing Unit 2 of the Chiwondo Beds in the Mwenirondo region with profile-meter, lithology and grain size. No inner structures are observed. For location see Fig. 2.1, for legend Fig. 2.7

The heavy mineral analysis of the saprolite from approximately 100 m up the valley bottom revealed prevailing green amphibole with little garnet and zircon as accessory minerals.

2.3.1.3 Unit 3A

The section representing a typical Unit 3A sequence in the Mwenirondo region consists of two separate profiles; 11-MW-04 (10° 1.060'S, 33° 55.242'E, 535 m asl) is located 155 m to the north of 12-MW-19 (10° 0.980'S, 33° 55.214'E, 560 m asl) along the southern slope of the plateau. Two step-like profiles with a combined thickness of 19 m were trenched in well exposed slopes and correlated them with a distinct lacustrine bed. The section represents a part of Unit 3A.

The succession consists mainly of fluvial silts and sands with pedogenic overprints (Fig. 2.3). The variation of grain size and bedding structures indicates differences in sedimentation rates, whereas alternations of lacustrine lime represent transgression phases of the nearby palaeolake water level. Nearly the complete alternation comprehends abundant pedogenic carbonate nodules with sizes of 0.5 to 3 cm in diameter. Biogenic activity is reported by animal burrows which are refilled with calcareous silty clay; most seem to have a much younger age than the onset of the original pedogenesis in the sediments. The upper part of the section is calcareous whereas, for the most part, in the lower section the host-deposits around the nodules are non-calcareous.

In order to detect possible reworked volcanic material within the fluvial sediments of the Chiwondo beds heavy mineral analyses have been carried out. All 38 samples taken within Profile 11-MW-04 show a rather uniform composition. Despite some variations, garnet is always

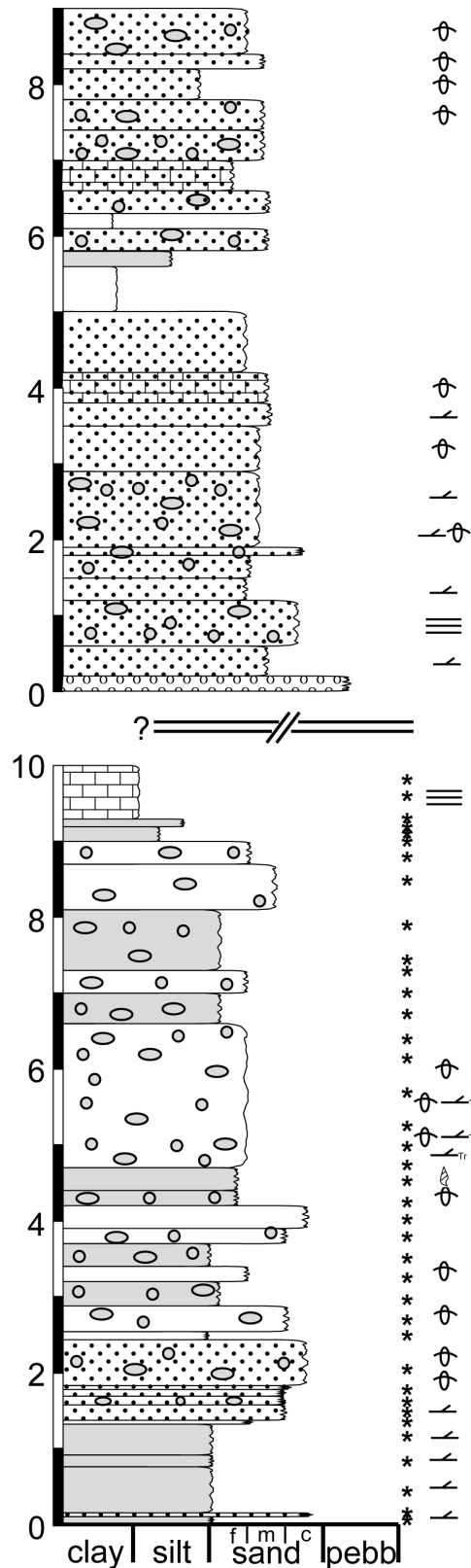


Figure 2.3: Stratigraphic column of profiles 11-MW-04 (10°1.060'S; 33°55.242'E) and 12-MW-19 (10°0.980'S, 33°55.214'E), representing Unit 3A of the Chiwondo Beds in the Mwenirondo region with profile-meter, lithology and grain-size, position of heavy mineral sample, structures and fossils. For location see Fig. 2.1, for legend Fig. 2.7.

dominating, accompanied by epidote/zoisite, zircon, sphene, rutile, anatase, green amphibole, as well as tourmaline, kyanite and sillimanite as accessory minerals. Definite volcanic components, which would represent the basaltic or trachytic character of the Rungwe tuffs, such as olivine, pyroxene, or brown amphibole, however, could not be recognized. Subrounded to rounded components dominate, and grains of euhedral shape are rare.

The weathering status of the heavy minerals differs within each sample. A considerable part of the stable group (zircon, rutile, and tourmaline) shows an advanced degree of corrosion. Also amphiboles are in an advanced stage of corrosion resulting in hacksaw terminations along their preferential crystallographic directions; however, intensive chemical weathering has not taken place.

2.3.2 Malema

2.3.2.1 Field aspects

The sedimentation circumstances of the Malema area south of the Ruasho River are similar to the Mwenirondo area; Chitimwe deposits form the cap sediments of a plateau area, whereas fluvial deposits of Unit 3A with pedogenic signatures are exposed along the slopes. A basement ridge crops out in the east, here Chiwondo or Chitimwe sediments overly the partly saprolitic gneiss with a major unconformity. The region experienced a large degree of tectonic activity which resulted in a complex block pattern; the correlation of palaeosols with a small lateral extension is therefore especially challenging. A bone-bed was excavated in the area; large terrestrial mammals, especially ungulates, dominate the fauna in this delta sequence along palaeolake Malawi (Sandrock, 1999; Sandrock et al., 1999). The occurrence of *Paranthropus cf. boisei* makes Malema the southernmost locality in East Africa yielding this early hominid taxon.

A screening of the heavy mineral assemblages of a 5 m long section close to a basement ridge (10°1.374'S, 33°55.815'E, 533 m asl; see profile S17 in Sandrock, 1999) revealed no volcanic material in the fine sand fraction. The spectra of 8 samples consist of garnet and green amphibole as the main constituents, accompanied by zircon,

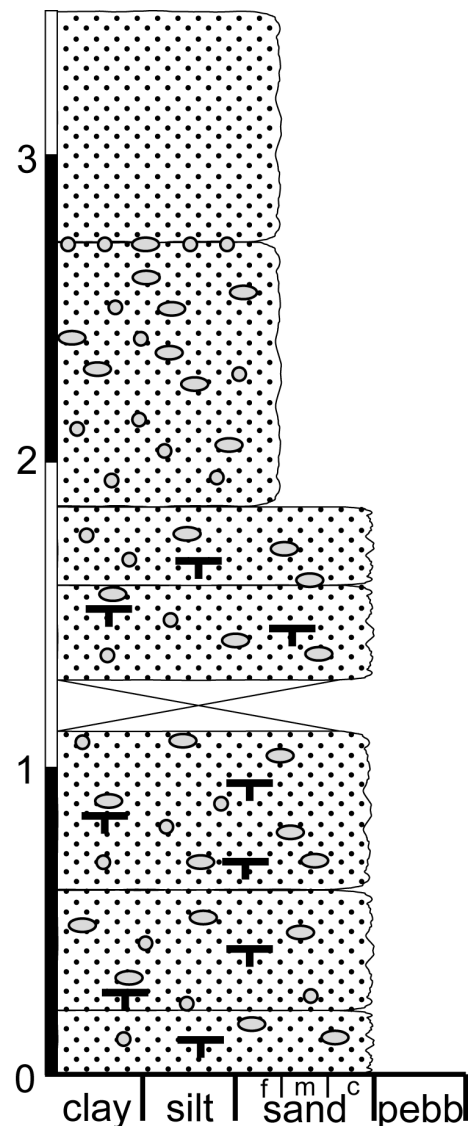


Figure 2.4: Stratigraphic column of Profile 12-MA-08 (10°1.323'S, 33°55.833'E), representing Unit 3A of the Chiwondo Beds in the Malema region with profile-meter lithology and grain-size. No inner structures were observed. For location see Fig. 2.1, for legend Fig. 2.7.

epidote, kyanite, sphene and rutile. The amount of green amphibole is higher than in other examined sediments.

2.3.2.2 Unit 3A

The 3.5 m long profile 12-MA-08 ($10^{\circ}1.323'S$; $33^{\circ}55.833'E$, 538 m asl) is positioned on the northern wall of the archaeological excavation pit. The medium to coarse sands with fine (sub-)angular pebbles are part of Unit 3A (Fig. 2.4). The upper 80 cm are made of Chitimwe fluvial sediments which are non-calcareous and have been subject to pedogenesis until today. The sharp transition to the Bk-horizon of a cut palaeosol within the Chiwondo Beds is marked by a colour-change from dark reddish-brown to beige, an abrupt calcification of the matrix and an appearance of pedogenic carbonate nodules. In the topmost 5 cm of the Chiwondo palaeosol the nodules have a rough surface which indicates modern etching of the fossil carbonate. The sediment is extremely rich in nodules, which are up to 3 cm in diameter and make up 50 to 70 % of the palaeosol material; pebbles are often also coated with carbonate. It is not possible to distinguish different soil horizons.

2.3.3 Uraha

2.3.3.1 Field aspects

Due to the absence of Units 3B and 4 in the northern parts of the study area additional profiles were logged further south in the Uraha region, northwest of Chilumba (Fig. 2.1). On the eastern slope of "Uraha Hill" Unit 1 and 2 are exposed, whereas Unit 4 is best exposed in an abandoned quarry almost 10 km further south.

In the region a mandible of *Homo rudolfensis* was recovered from a ferruginous palaeosol layer of Unit 3A (Bromage et al., 1995b).

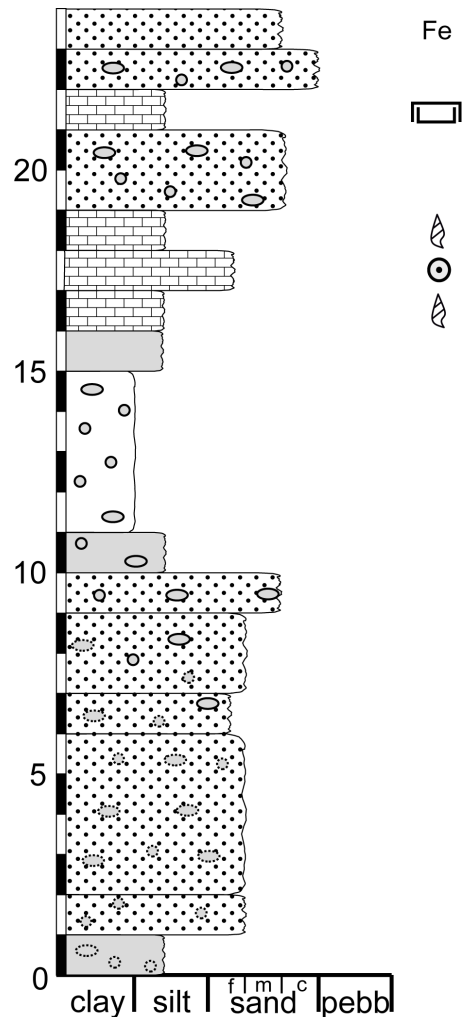


Figure 2.5: Stratigraphic column of profile 11-UR-99 ($10^{\circ}21.323'S$, $34^{\circ}8.483'E$), representing Unit 1 and 2 of the Chiwondo Beds in the Uraha region with profile-meter, lithology and grain-size, structures and fossils. For location see Fig. 2.1, for legend Fig. 2.7.

2.3.3.2 Unit 1 and 2

Poor outcrop conditions on the steep slopes of Uraha Hill do not allow to produce continuous step-sections comparable to the northern parts. The profile 11-UR-99 (10°21.323'S, 34°8.483'E, 556 m asl) has a thickness of 24 m (Fig. 2.5) and was surveyed by excavating holes every meter to log the lithology.

Unit 1 is exposed at the base, whereas the oncoids close to the top characterize Unit 2. The point of transition is most likely the onset of finer sediments at 10 m in the succession.

The fluvial Unit 1 deposits in the lower 10 m of the section range from fine to medium sands and inhabit pedogenic carbonate which is mainly represented in diffuse patches at the base of the section and becomes more and more consolidated to nodules towards the top. The matrix of these stream deposits is for the most parts non-calcareous and varies in colour from gray to reddish brown; latter is probably the result of reworking of the underlying red sands of the Dinosaur Beds (cf. Betzler and Ring, 1995).

The silt and clay deposits in the middle of the section display a general flooding of the area which describes the lower limit of Unit 2. For the most parts these calcareous sediments are also marked by pedogenesis which formed well consolidated nodules. Towards the top the lime content increases until a lacustrine limestone with abundant *Bellamya* gastropods is exposed. As a distinct feature of Unit 2 a layer of oncoids with *Bellamya* shells as nuclei formed is exposed laterally over a few kilometres in the Uraha region.

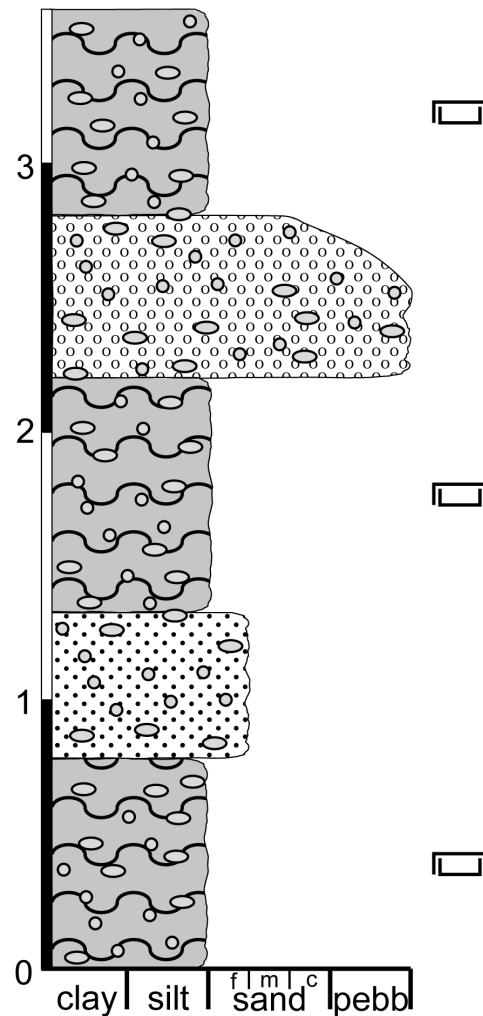


Figure 2.6: Stratigraphic column of profile 12-UR-47 (10°25.215'S, 34°10.996'E), representing Unit 4 of the Chiwondo Beds in the Uraha region with profile-meter, lithology and grain-size and fossils. For location see Fig. 2.1, for legend Fig. 2.7.

The limestone in this upper part of the profile is interrupted by intercalations of sand deposits with carbonate nodules which indicate fluctuations of the water level of palaeolake Malawi during Unit 2.

Legend	
	Carbonate (consolidated)
	Carbonate nodules (diffuse)
	Carbonate-cemented
	Oncoids
	Gastropodes (<i>Bellamya</i>)
	Burrows/Bioturbation
	Diatomite
	Fe Iron-crust
	* Position of HM-sample

Figure 2.7: Key for lithology, structures, fossils and other sedimentary characteristics of the logged profiles displayed in Fig. 2.2 to 2.6.

2.3.3.3 Unit 4

In a valley ca. 8.5 km southeast of Uraha Hill Unit 4 overlies the Dinosaur Beds with a major unconformity. It is not possible to determine if Units 1 to 3 were eroded prior to the sedimentation of Unit 4 or never deposited at all in this area.

The 3.6 m long profile 12-UR-47 (10°25.215'S, 34°10.996'E, 572 m asl) is located along the slope of an isolated hill in the centre of the valley. White diatom-rich marls are interrupted by sand and conglomerates (Fig. 2.6). Pedogenesis is strong in the sediments and the calcareous marls inhabit abundant nodules to the point of the forming of caliche. The fluvial deposits have also pedogenic carbonate nodules.

2.4 Synthesis

The five profiles representing characteristic sections of the Chiwondo Bed consist primarily of fluvial sands with intercalations of silts and lacustrine limestones. Hence, during the last 4 Ma large river systems dominated the northern Malawi region. These probably braided and meandering streams eroded basement and Karoo Supergroup sediments and deposited silts, sands and conglomerates in a medium to high energy environment. Subrounded to rounded components dominate the heavy mineral fraction, which indicates reworking processes over long distances.

The limnic limestones with abundant pelecypods and gastropods (primary *Bellamyia*), which built large portions of Unit 2, as well as the diatomite-rich silts in Unit 4 represent temporary transgressions of palaeolake Malawi. These rises in lake water can either be climatically induced, or present the influence of tectonic activity in the Malawi Rift, or, which is most likely, the result of both.

Nearly all deposits comprehend abundant carbonate nodules, partly to the degree of forming caliche, which indicates a high rate of pedogenic overprint of the sediments. These erosion-resistant Bk-horizons are well preserved to the contrary to the carbonate depleted upper horizon of the palaeosols, which are seldom found in the region. This can be explained by morphodynamic processes such as erosion or fluvial reworking of the loose sediment prior to the next sedimentation cycle. Carbonate nodules form in soils with a net water deficit, generally when precipitation is less than about 1000 mm/a (Jenny, 1980; Birkeland, 1984; Cerling and Quade, 1993), which seems to be the case during the whole timespan of deposition of the Plio-Pleistocene sediments. These circumstances are also given for the modern annual precipitation, which is actually less than 900 mm/a with a rainy season between November and April; subrecent nodules were found in cut banks of rivers. As described in Chapter 3.2.2, pedogenic nodules close to the modern surface can have rough surfaces, which indicate recent etching of the fossil carbonate due to ongoing carbonate solution in the course of actual pedogenic processes. Further down in the soil profile this carbonate can form new coatings around fossil nodules or conglomeratic pebbles.

The stream deposits are composed of unconsolidated sediments, which are only occasionally cemented with carbonate. Post-sedimentary tectonic activity

is difficult to evaluate, and a lateral continuation is often impossible to follow over a long distance. The latter is also hindered by the highly energetic fluvial environment, where sedimentation rates, but also erosion rates, are probably high in a cut-and-fill environment.

After extensive fieldwork and explicit searching for datable minerals, no volcanic layers were found. All heavy mineral samples analyzed for this study display an overall absence of volcanic minerals. As the Rungwe Volcanic Province, which had several magmatic eruptions during the Chiwondo Bed's deposition (Delvaux et al., 1992), is located nearby one would expect tephra minerals as an evidence for the Rungwe volcanic ashes is mostly trachytic (Fontijn et al., 2010). The lack of these could be explained due to the fact that the ashes were relocated from the palaeosurface in the highly erosive fluvial environment, or that they had never been deposited because of an opposite wind direction. The heavy mineral assemblages are dominated by the hinterland source areas and show only little variations; the content of green amphibole is higher in sections close to the basement source area. Grains of euhedral shape are rare. Besides the fact that they appear in all samples, even the sphene grains are generally well rounded, hence, it is unlikely that they sourced from tephra fallout.

There is no evidence on the timespan when palaeosols formed in the sediment sequence before they were covered by younger deposits. Hence, initial soil development in a fluvial environment under Plio-Pleistocene semi-arid conditions in an area of tectonic subsidence may have produced Calcisols with carbonate nodules in the first instance without adequate time to evolve decalcified B horizons.

Intensive in situ weathering of the Chiwondo Beds is unlikely since pH values are generally above pH 7. Thus, the heavy mineral associations throughout the investigated section represent only the input from the source areas into the Chiwondo Beds. The geochronology of the Pleistocene Chitimwe Beds is also still a matter of debate. The broad horizontal and vertical variability in clast size indicate a fluctuation in sedimentation and erosion rates, and topographic energy regime. Complex surficial processes triggered by droughts with dramatic lowering of lake level (c.f. Lyons et al., 2011; Scholz et al., 2011), faulting, tilting, and valley incision during the entire Pleistocene resulted in a highly variable spatial sediment pattern of this Unit 5. The brown to reddish colour of these sediments signifies the long time span of terrestrial soil development. The cover sediments of the plateau-like hills are generally made out of Chitimwe deposits which, in some places, eroded the underlying Chiwondo Beds, also supporting the high relief energy regime. Later, these old surfaces were cut by rivers which formed today's topography.

2.5 Acknowledgements

T.L. acknowledges the support through the LOEWE funding program (Landes Offensive zur Entwicklung Wissenschaftlich ökonomischer Exzellenz) of Hesse's Ministry of Higher Education, Research and Arts. We thank Andreas Mulch, Friedemann Schrenk, Oliver Sandrock and Harrison Simfukwe for logistics and discussion. Two anonymous reviewers helped by additional comments to improve the manuscript.

2.6 References

- Ad-hoc-AG Boden, 2005. *Bodenkundliche Kartieranleitung*. 5th edition, Hannover, Germany, 438 pp.
- Andrew, A.R. and Bailey, T.E.G., 1910. The Geology of Nyasaland. *Quarterly Journal of the Geological Society*, 66, pp. 189-237.
- Aronson, J.L., Hailemichael, M. and Savin, S.M., 2008. Hominid environments at Hadar from paleosol studies in a framework of Ethiopian climate change. *Journal of Human Evolution*, 22, pp. 532-550.
- Barham, L.S. and Smart, P.L., 1996. An early date for the Middle Stone Age of central Zambia. *Journal of Human Evolution*, 30, pp. 287-290.
- Behrensmeyer, A.K., Todd, N.E., Potts, R. and McBrinn, G.E., 1997. Late Pliocene faunal turnover in the Turkana Basin, Kenya and Ethiopia. *Science*, 278, pp. 1589-1594.
- Betzler, C. and Ring, U., 1995. Sedimentology of the Malawi Rift: Facies and stratigraphy of the Chiwondo Beds, northern Malawi. *Journal of Human evolution*, 28, pp. 23-35.
- Birkeland, P.W., 1984. *Soils and Geomorphology*. Oxford University Press, New York, 432 pp.
- Bromage, T.G. and Schrenk, F., 1987. A cercopithecoid tooth from the Pliocene in Malawi. *Journal of Human Evolution*, 15, pp. 497-500.
- Bromage, T.G., Schrenk, F. and Juwayeyi, Y.M., 1995a. Paleogeography of the Malawi Rift: Age and Vertebrate Paleontology of the Chiwondo Beds, Northern Malawi. *Journal of Human Evolution*, 28, pp. 37-57.
- Bromage, T.G., Schrenk, F. and Zonneveld, F.W., 1995b. Paleoanthropology of the Malawi-Rift: An early hominid mandible from the Chiwondo Beds, northern Malawi. *Journal of Human Evolution*, 28, pp. 71-108.
- Catuneanu, O., Wopfner, H., Eriksson, P.G., Cairncross, B., Rubidge, B.S., Smith, R.M.H. and Hancox, P.J., 2005. The Karoo basins of south-central Africa. *Journal of African Earth Sciences*, 43, pp. 211-253.
- Cerling, T.E., 1992. Development of grassland and savannas in East Africa during the Neogene. *Palaeogeography, Palaeoclimatology, Palaeoecology*, 97, pp. 241-247.
- Cerling, T.E. and Hay, 1986. An isotopic study of paleosol carbonates from Olduvai Gorge. *Quaternary Research*, 25, pp. 63-78.
- Cerling, T.E. and Quade, J., 1993. Stable Carbon and Oxygen Isotopes in Soil Carbonates. *Geophysical Monograph*, 78, pp. 217-231.
- Cerling, T.E., Bowmann, J.R. and O'Neil, J.R., 1988. An isotopic study of a fluvial-lacustrine sequence: the Plio-Pleistocene Koobi Fora sequence, East Africa. *Palaeogeography, Palaeoclimatology, Palaeoecology*, 63, pp. 335-356.
- Cerling, T.E., Wynn, J.G., Andanje, S.A., Bird, M.I., Korir, D.K., Levin, N.E., Mace, W., Macharia, A.N. Quade, J. and Remien, C.H., 2011. Woody cover and hominin environments in the past 6 million years. *Nature*, 476, pp. 51-56.

- Charsley, T.J., 1972. *The limestone resources of Malawi*. Geological Survey Department, Zomba, Memoir, 6, pp. 1-128.
- Clark, J.D., Hayners, C.V., Mawby, J.E. and Gautier, A., 1970. Interim report on paleoanthropological investigations in the Lake Malawi Rift, *Quaternario*, 13, pp. 305-354.
- Crossley, R., 1982. Late Cenozoic stratigraphy of the Karonga area in the Malawi rift. *Palaeoecology of Africa*, 15, pp. 139-144.
- Delvaux, D., Levi, K., Kajara, R. and Sarota, J., 1992. Cenozoic paleostress and kinematic evolution of the Rukwa – North Malawi Rift Valley (East African Rift System). *Bulletin des Centres de Recherches Exploration-Production Elf Aquitaine*, 16, pp. 383-406.
- de Heinzelin, J., Clark, J.D., White, T., Hart, W., Renne, P., WoldeGabriel, G., Beyene, Y. and Vrba, E., 1999. Environment and Behavior of 2.5-Million-Year-Old Bouri Hominids. *Science*, 23, pp. 625-629.
- DIN ISO 11277, 2002. Soil quality - *Determination of particle size distribution in mineral soil material - Method by sieving and sedimentation*, Beuth, Berlin, 38 pp.
- Dixey, F., 1927. The Tertiary and Post-Tertiary Lacustrine Sediments of the Nyasan Rift-Valley. *Quarterly Journal of the Geological Society*, 83, pp. 432-442.
- Ebinger, C.J., Deino, A.L., Drake, R.E. and Tesna, A.L., 1989. Chronology of volcanism and rift basin propagation: Rungwe volcanic province, East Africa. *Journal of Geophysical Research*, 94, pp. 15785-15803.
- Ebinger, C.J., Deino, A.L., Tesha, A., Becker, T. and Ring, U., 1993. Tectonic controls on rift basin morphology: Evolution of the northern Malawi (Nyasa) rift. *Journal of Geophysical Research*, 98, pp. 17821-17836.
- Feakins, S.J., Levin, N.E., Liddy, H.M., Sieracki, A., Eglinton, T.I. and Bonnefille, R., 2013. Northeast African vegetation change over 12 m.y. *Geology*, 41, pp. 295-298.
- FAO (Food and Agriculture Organization of the United Nations), 2006. *Guidelines for soil description*. 4th edition, Rome, 97 pp.
- Fontijn, K., Ernst, G.G.J., Elburg, M.A., Williamson, D., Abdallah, E., Kwelwa, S., Mbede, E. and Jacobs, P., 2010. Holocene explosive eruptions in the Rungwe Volcanic Province, Tanzania. *Journal of Volcanology and Geothermal Research*, 196, pp. 91–110.
- Fontijn, K., Williamson D., Mbede E. and Ernst, G.G.J., 2012. The Rungwe Volcanic Province, Tanzania – A volcanological review. *Journal of African Earth Sciences*, 63, pp. 12–31.
- Frost, S.R. and Kullmer, O., 2008. Cercopithecidae from the Pliocene Chiwondo Beds, Malawi-Rift. *Geobios*, 41, pp. 743-749.
- Hamiel, Y., Baer, G., Kalindekafu, L., Dombola, K. and Chindandali, P., 2012. Seismic and aseismic slip evolution and deformation associated with the 2009-2010 northern Malawi earthquake swarm, East African Rift. *Geophysical Journal International*, 191, pp. 898-908.
- Jenny, H., 1980. *The Soil Resource*. Springer, New York, 377 pp.
- Kaufulu, Z.M., 1989. Sedimentary conditions within a Plio-Pleistocene graben at Karonga, northern Malawi and their implications for the prehistoric record of the area. *Paleoecology of Africa*, 20, pp. 99-108.
- Kaufulu, Z.M. and Stern, N., 1987. The first stone artifacts to be found in situ within the Plio-Pleistocene Chiwondo Beds in northern Malawi. *Journal of Human Evolution*, 16, pp. 729-740.
- Kullmer, O., 2008. The fossil *Suidea* from the Plio-Pleistocene Chiwondo Beds of Northern Malawi, Africa. *Journal of Vertebrate Paleontology*, 28, pp. 208-216.

- Kullmer, O., Sandrock, O., Abel, R., Schrenk, F., Bromage, T.G. and Juwayeyi, 1999. The first Paranthropus from the Malawi Rift. *Journal of Human Evolution*, 37, pp. 121-127.
- Kullmer, O., Sandrock, O., Kupczik, K., Frost, S.R., Volpato, V., Bromage, T.G. and Schrenk, F., 2011. New primate remains from Mwenirondo, Chiwondo Beds in northern Malawi. *Journal of Human Evolution*, 61, pp. 617-623.
- Levin, N.E., Quade J., Simpson S.W., Semaw S. and Rogers, M., 2004. Isotopic evidence for Plio-Pleistocene environmental change at Gona, Ethiopia. *Earth and Planetary Science Letters*, 219, 93-110.
- Levin, N.E., Brown F.H., Behrensmeyer A.K., Bobe R. and Cerling, T.E., 2011. Paleosol carbonates from the Omo Group: Isotopic records of local and regional environmental change in East Africa. *Palaeogeography, Palaeoclimatology, Palaeoecology*, 307, pp. 75–89.
- Lyons, R.P., Scholz C.A., Buoniconti M.R. and Martin, M.R., 2011. Late Quaternary stratigraphic analysis of the Lake Malawi Rift, East Africa: An integration of drill-core and seismic-reflection data. *Palaeogeography, Palaeoclimatology, Palaeoecology*, 303, pp. 20–37.
- Magill, C.R., Ashley, G.M. and Freemann, K.H., 2012a. Ecosystem variability and early human habitats in eastern Africa. *Proceedings of the National Academy of Science of the United States of America*, 110, pp. 1167-1174.
- Magill, C.R., Ashley, G.M. and Freemann, K.H., 2012b. Water, plants, and early human habitats in eastern Africa. *Proceedings of the National Academy of Science of the United States of America*, 110, pp. 1175-1180.
- Munsell Color Company, 2000. *Standard soil color charts*, Baltimore.
- Plummer, T.W. and Bishop, L.C., 1994. Hominid paleoecology at Olduvai Gorge, Tanzania as indicated by antelope remains. *Journal of Human Evolution*, 27, pp. 47-75.
- Retallack, G.J., 1998. Adapting Soil Taxonomy for use with Paleosols. *Quaternary International*, 51/52, pp. 55-60.
- Retallack, G.I., 2011. *Soils of the past, 2nd edition*. Wiley-Blackwell, pp. 512.
- Retallack, G.J., Wynn, J.G., Benefit, B.R. and McCrossin, M.L., 2002. Paleosols and paleoenvironments of the middle Miocene, Maboko Formation, Kenya. *Journal of Human Evolution*, 42, pp. 659–703.
- Ring, U., Betzler, C. and Devaux, D., 1992. Normal vs. strike-slip faulting during rift development in East Africa: The Malawi Rift. *Geology*, 20, pp. 1015-1018.
- Ring, U. and Betzler, C., 1995. Geology of the Malawi Rift: kinematic and tectonosedimentary background to the Chiwondo Beds, northern Malawi. *Journal of Human Evolution*, 28, pp. 7-21.
- Sandrock, O., 1999. *Taphonomy and Paleoecology of the Malema Hominid Site, Northern Malawi*. PhD Thesis, University of Mainz, 277 pp.
- Sandrock, O., Dauphin, Y., Kullmer, O., Abel, E., Schrenk, F. and Denys, C., 1999. Malema: Preliminary taphonomic analysis of an African hominid locality. *Human Palaeontology*, 328, pp. 133-139.
- Schlüter, T., 2008. *Geological Atlas of Africa: With Notes on Stratigraphy, Tectonics, Economic Geology, Geohazards and Geosites of Each Country – 2nd edition*. Springer, Berlin, pp. 1-308.

- Scholz, C.A., Cohen A.S., Johnson T.C., King J., Talbot M.R. and Brown, E.T., 2011. Scientific drilling in the Great Rift Valley: The 2005 Lake Malawi Scientific Drilling Project - An overview of the past 145,000 years of climate variability in Southern Hemisphere East Africa. *Palaeogeography, Palaeoclimatology, Palaeoecology*, 303, pp. 3–19.
- Schrenk, F., Bromage, T.G., Betzler, C.G., Ring, U., Juwayeyi, Y.M., 1993. Oldest homo and Pliocene biography of the Malawi Rift. *Nature*, 365, pp. 833-836.
- Schrenk, F., Bromage, T.G., Gorthner, A. and Sandroock, O., 1995. Paleoeecology of the Malawi Rift: Vertebrate and invertebrate faunal contexts of the Chiwondo Beds, northern Malawi. *Journal of Human Evolution*, 28, pp. 59-70.
- Ségalen, L., Lee-Thorp, J. and Cerling, T., 2007. Timing of C4 grass expansion across sub-Saharan Africa. *Journal of Human Evolution*, 53, pp. 549-559.
- Sikes, N.E., 1994. Early hominid habitat preferences in East Africa: Paleosol carbon isotopic evidence. *Journal of Human Evolution*, 27, pp. 25-45.
- Sikes, N.E., Potts, R. and Behrensmeyer, A.K., 1999. Early Pleistocene habitat in Member 1 Olorgesailie based on paleosol stable isotopes. *Journal of Human Evolution*, 37, pp. 721-746.
- Stephens, E.A., 1966. Geological account of the Northwest coast of Lake Malawi between Karonga and Lion Point, Malawi. *American Anthropological Association*, Special Publication, 68, pp. 50-58.
- Thompson, J.C., Mackay, A., Wright, D.K., Welling, M., Greaves, A., Gomani-Chindebvu, E. and Simengwa, D., 2012. Renewed investigations into the Middle Stone Age of Northern Malawi. *Quaternary International*, 270, pp. 129-139.
- Tryon, C.A., McBrearty, S. and Texier, P.-J., 2005. Levallois lithic technology from the Kapthurin formation, Kenya: Acheulian origin and Middle Stone Age diversity. *African Archaeological Review*, 22, pp. 199-229.
- Wesselman, H.B., 1985. Fossil micromammals as indicators of climatic change about 2.4 Myr ago in the Omo Valley, Ethiopia. *South African Journal of Science*, 81, pp. 260-261.
- Wynn, J.G., 2000. Paleosols, stable carbon isotopes, and paleoenvironmental inter-pretations of Kanapoi, Northern Kenya. *Journal of Human Evolution*, 39, pp. 411-432.
- Wynn, J.G., 2004. Influence of Plio-Pleistocene Aridification on Human Evolution: Evidence From Paleosols of the Turkana Basin, Kenya. *American Journal of Physical Anthropology*, 123, pp. 106–118.
- Wynn, J.G. and Retallack, G.J., 2001. Paleoenvironmental reconstruction of middle Miocene paleosols bearing Kenyapithecus and Victoriapithecus, Nyakach Formation, southwestern Kenya. *Journal of Human Evolution*, 40, pp. 263–288.

Chapter 3

Persistent C₃ vegetation accompanied Plio-Pleistocene hominin evolution in the Malawi Rift (Chiwondo Beds, Malawi)

Tina Lüdecke^{a,b,*}, Friedemann Schrenk^{a,c}, Heinrich Thiemeyer^d, Ottmar Kullmer^e, Timothy G. Bromage^{e,f,g}, Oliver Sandrock^h, Jens Fiebig^{a,b}, Andreas Mulch^{a,b}

^aSenckenberg Biodiversity and Climate Research Centre, Frankfurt, Germany

^bInstitute of Geosciences, Goethe University Frankfurt, Germany

^cInstitute for Ecology, Evolution, and Diversity, Goethe University Frankfurt, Germany

^dInstitute of Physical Geography, Goethe University Frankfurt, Germany

^eDepartment of Paleoanthropology and Messel Research, Senckenberg Research Institute, Frankfurt, Germany

^fDepartment of Biomaterials and Biomimetics, New York University College of Dentistry, USA

^gDepartment of Basic Science and Craniofacial Biology, New York University College of Dentistry, USA

^hEarth- and Life History, Hessisches Landesmuseum Darmstadt, Germany

Published in *Journal of Human Evolution* (2016), 90: 163-175.

doi: 10.1016/j.jhevol.2015.10.014

Abstract The development of East African savannas is crucial for the origin and evolution of early hominins. These ecosystems, however, vary widely in their fraction of woody cover and today range from closed woodland to open grassland savanna. Here, we present the first Plio-Pleistocene long-term carbon isotope ($\delta^{13}\text{C}$) record from pedogenic carbonate and Suidae teeth in the southern East African Rift (EAR). These $\delta^{13}\text{C}$ data from the Chiwondo and Chitimwe Beds (Karonga Basin, Northern Malawi) represent a southern hemisphere record in the EAR, a key region for reconstructing vegetation patterns in today's Zambezian Savanna, and permit correlation with data on the evolution and migration of early hominins in today's Somali-Masai Endemic Zone. The sediments along the northwestern shore of Lake Malawi contain fossils attributed to *Homo rudolfensis* and *Paranthropus boisei*. The associated hominin localities (Uraha, Malema) are situated between the well-known hominin bearing sites of the Somali-Masai Endemic Zone in the Eastern Rift and the Highveld Grassland in southern Africa, and fill an important geographical gap for hominin research. Persistent $\delta^{13}\text{C}$ values around -9‰ from pedogenic carbonate and suid enamel covering the last ~4.3 Ma indicate a C₃-dominated closed environment with regional patches of C₄-grasslands in the Karonga Basin. The overall fraction of woody cover of 60-70% reflects significantly higher canopy density in the Malawi Rift than the Eastern Rift through time. The discrepancy between the two savanna types originated in the Late Pliocene, when the Somali-Masai ecosystem started to show increasing evidence for open, C₄-dominated landscapes. Based on the Malawi $\delta^{13}\text{C}$ data,

the evolution of savanna ecosystems in Eastern Africa followed different patterns along the north-south extent of the EAR. The appearance of C₄-grasses is considered a driver of evolutionary faunal shifts, but despite the difference of ecosystem evolution in the north, similar hominins and suids occurred in both landscapes, pointing to distinct habitat flexibility and also nutritional versatility.

Keywords Carbon isotopes, paleosol carbonate, tooth enamel, hominin evolution, East African Rift, C₄ expansion.

3.1 Introduction

Deciphering the links and feedback between East African paleoclimate, vegetation, and faunal patterns is a key element in understanding human evolution (e.g., Dart, 1925; Bartholomew and Bridsell, 1953; Vrba, 1988; Potts, 1998; Ségalen et al., 2007; Plummer et al., 2009; Cerling et al., 2011b). In particular, the influence of subtropical African climate variability on faunal evolution during the last 5 to 6 millions of years ago (Ma) has been at the center of a long-standing debate (see e.g., deMenocal, 2004 and references therein). As a result, numerous paleoenvironmental studies on the East African Rift (EAR) aim to reconstruct the ecospace and diets of early hominins, using traditional ecological features of fauna and flora and/or geochemical proxies (e.g., Wesselman, 1985; Cerling and Hay, 1986; Cerling et al., 1988, 2003,



Figure 3.1: Present-day African vegetation zones and hominin sites. a) Main African vegetation zones (White, 1983) and the East African Rift (EAR; orange). Highlighted are today's Somali-Masai Endemic Zone (yellow) and the Zambeزيan Savanna (green). b) Major early hominin fossil sites in the EAR. Note that the Chiwondo Beds (Karonga Basin, Malawi) is the only site located in the Zambeزيan Savanna. All other sites in the EAR occur in the Somali-Masai Endemic Zone.

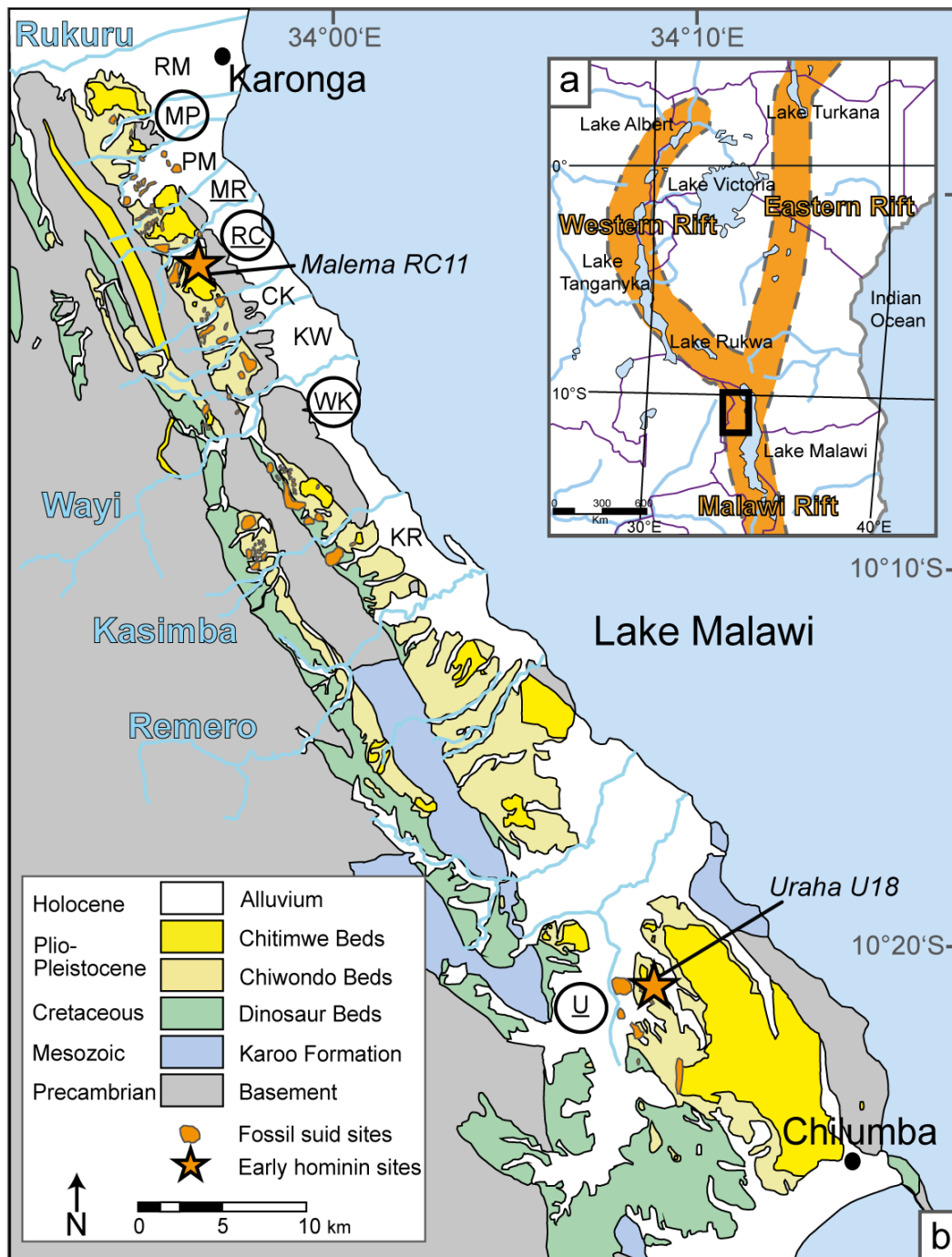


Figure 3.2: a) Overview of eastern Africa and the EAR (orange). b) Geological map of the Karonga Basin showing Plio-Pleistocene Chiwondo and Chitimwe Beds with suid fossil localities. Nine survey areas are named after the initials of bounding major streams: Rukuru, Mwangwabila, Phapa, Masapa, Ruasho, Chomolo, Kanyolola, Wayi, Kasimba, and Remero (first letter = stream to the north, second letter = stream to the south). U = Uraha. Circled and underlined survey areas indicate fossil suid molars (pedogenic carbonate) used as proxy materials and analyzed for this study. Malema and Uraha hominin sites are marked with stars.

2011a, b, 2013; Cerling, 1992; Kingston, 1992; Kingston et al., 1994; Morgan et al., 1994; Plummer and Bishop, 1994; Sikes, 1994; deMenocal, 1995; Behrensmeyer et al., 1997; de Heinzelin et al., 1999; Plummer et al., 2009; Sikes et al., 1999; Wynn, 2000; Harris and Cerling, 2002; Trauth et al., 2003; Levin et al., 2004; Semaw et al., 2005; Trauth et al., 2005; Hopley et al., 2006; White et al., 2006; Quinn et al., 2007; Ségalen et al., 2007; Sikes and Ashley, 2007; Aronson et al., 2008; WoldeGabriel et al., 2009; Bocherens et al., 2011;

Levin et al., 2011; Magill et al., 2012a, b; Feakins et al., 2013; Wilson et al., 2014). Current climate evolution hypotheses include temporal and causal relationships between changes in climate, faunal diversity, and adaptation based on the ensemble of paleoclimatic records and fossil discoveries, most of them established within the Eastern Rift in Ethiopia, Kenya, and Tanzania (Fig. 3.1). In general, these hypotheses link the evolution of early hominin fauna either to a constant or step-wise change in climate (e.g., Dart, 1925; Vrba et al., 1989; deMenocal, 1995), to high-amplitude paleoclimate variability (e.g., Potts, 1998), and/or to changes in topography (e.g., Trauth et al., 2005; Maslin et al., 2014). Most likely, none of the many hypotheses are mutually exclusive, and spatial differences between regional and global forcing parameters may occur. However, knowledge of the spatial variability in vegetation patterns along the entire EAR is a prerequisite of enhancing our ability to identify regional from rift-wide characteristics, and thus evaluating the role of individual forcing factors.

Whereas most published vegetation reconstructions rely on data derived from the Eastern Rift in the northern part of the EAR, this study presents the first long-term stable carbon isotope ($\delta^{13}\text{C}$) record from pedogenic carbonate and fossil suid enamel from the southern EAR, the Malawi Rift (Fig. 3.1). We compare $\delta^{13}\text{C}$ values of pedogenic and tooth enamel carbonate from the Malawi Rift with the evolution of $\delta^{13}\text{C}$ values in the Eastern Rift. Further, the Karonga Basin (Malawi, Fig. 3.2) is the only studied locality in the EAR that is located in today's Zambezian Savanna, whereas all other East African hominin localities are located in the Somali-Masai Endemic Zone (Fig. 3.1). We present a compiled $\delta^{13}\text{C}$ record of 321 pedogenic carbonate and 18 suid enamel samples that collectively show persistently low $\delta^{13}\text{C}$ values ranging from -11.2 to -5.8‰, with an average of -9.1‰ (pedogenic carbonate), and -13.1 to -4.5‰, with an average of -9.3‰ (suid enamel). Collectively, these data point towards the protracted presence of a patchy, yet largely C₃-dominated vegetation pattern in the Malawi Rift with increasingly marked differences in landscape openness over the past <2.6 Ma when compared to other key sites of early hominin evolution in eastern Africa.

3.2 Background

3.2.1 Stable carbon isotope ratios in geologic proxy materials

On a continental scale, different biomes are distinguishable through the $\delta^{13}\text{C}$ values of associated biomass. Tropical dicots (trees, bushes, herbs) are primarily C₃ plants, whereas tropical grasses and sedges use the C₄ photosynthetic pathway and differ in their discrimination against $^{13}\text{CO}_2$ (e.g., Pearcy and Ehleringer, 1984; Cerling et al., 2011a). C₄ photosynthesis is typically prevalent in warm and seasonally dry, open conditions with high light intensity, whereas the C₃ pathway is advantageous under lower water stress and at high-pCO₂ conditions. As a result, C₃ grasses typically have $\delta^{13}\text{C}$ values ca. 14‰ more negative than C₄ plants. $\delta^{13}\text{C}$ values of C₃ plants typically range from ca. -20 to -33‰, whereas C₄ grasses range from ca. -10 to -16‰ (Cerling et al., 1997).

Pedogenic carbonate formed in equilibrium with soil-respired CO₂ is typically enriched in ¹³C by 13.5 to 17.0‰ compared to CO₂ respired from plants, as well as the CO₂ released during decomposition of soil organic carbon and related soil organic matter (Cerling, 1984; Cerling et al., 1989; Cerling and Quade, 1993). A carbon isotope fractionation of similar size (ca. 14‰; Cerling et al., 1997) occurs between consumed plant material and tooth enamel in a wide range of herbivores, resulting in δ¹³C values of tooth enamel <-8‰ for pure browsers and >-1‰ for pure grazers (e.g., Lee-Thorp and van der Merwe, 1987; Lee-Thorp et al., 1989; Cerling and Harris, 1999; Passey et al., 2005). As a result, δ¹³C values of geologic proxy materials that reliably record δ¹³C values of vegetation may be used as tracers of the vegetation patterns and fraction of woody cover in (sub-)tropical environments (e.g., Lloyd et al., 2008; Wynn and Bird, 2008; Cerling et al., 2010, 2011b; Uno et al., 2011; Bibi et al., 2013).

3.2.2 Geological context

Among the multiple sites that have provided stable isotope information about past hominin environments in the EAR (Fig. 3.1), the Karonga Basin is the first rift valley site located in today's Zambezian Savanna (Miombo Woodlands), whereas all other sites are situated in the Somali-Masai semi-desert grassland and scrubland (White, 1983). The Plio-Pleistocene Chiwondo and Chitimwe Beds are located in the Malawi Rift half-graben, which forms the southern part of the western branch of the EAR. The examined sediments are exposed in the Karonga Basin that formed by block faulting in response to Late Miocene east-northeast to west-northwest extension (Ring et al., 1992; Ebinger et al., 1993). Permo-Triassic, Jurassic, Cretaceous, and Plio-Pleistocene sedimentary sequences are exposed along the western shore of Lake Malawi (Fig. 3.2a). We studied the Chiwondo and Chitimwe Beds between Karonga and Chilumba in two ca. 70 km long (north to south) and 15 km wide (east to west) northwest-southeast segments that are separated by Proterozoic metamorphic basement ridges.

At these sites, metamorphic basement and Mesozoic shale- and sandstone-dominated Karoo Supergroup sediments are covered by reddish and grayish sandstones, marls, and clays of the Early Cretaceous Dinosaur Beds (Catuneanu et al., 2005; Schlüter, 2008). Plio-Pleistocene sediments overlie these deposits with a major angular unconformity (Andrew and Bailey, 1910; Dixey, 1927; Betzler and Ring, 1995). The depositional facies of these sediments range from alluvial (braided and meandering system deposits, deltaic and fan sediments) to aeolian and lake deposits (Betzler and Ring, 1995). The sediments are locally folded, tilted, and colluvially translocated due to tectonic uplift and extension in the Malawi Rift (Ring and Betzler, 1995), which is still ongoing (Hamiel et al., 2012). Due to a lack of directly datable volcanic markers (Kaufulu and Stern, 1987; Betzler and Ring, 1995), we rely on internal and external biostratigraphic correlations of mammal remains. Suid molars (Kullmer, 2008) have led to a subdivision into Units 1 to 4 (Chiwondo Beds) that are overlain by Unit 5 (Chitimwe Beds; Betzler and Ring, 1995; Ring and Betzler, 1995). The anthropologically important Unit 3 (ca. 3.75 to 0.6 Ma) was further

subdivided into three biozones (3A-I, 3A-II, and 3B; Bromage et al., 1995a; Sandrock et al., 1999; Kullmer, 2008). Pedogenic carbonate is abundant and found in all units (Lüdecke and Thiemeyer, 2013).

Pedogenic carbonate and suid molar enamel analyzed here were sampled in five areas throughout the Chiwondo Beds covering the regions of Masapa (PM), Mwenirondo (MR), Malema (RC), and Mwimbi (WK) in the north and Uraha (U) in the south (Fig. 3.2b). The Chiwondo Beds are home to a large suite of mammal fossils, including Cercopithecidae (Bromage and Schrenk, 1986; Schrenk et al., 1995; Bromage et al., 1995a; Sandrock et al., 1999, 2007; Frost and Kullmer, 2008; Kullmer, 2008; Kullmer et al., 2011), and are key archives for important hominin fossil remains (Schrenk et al., 1993; Bromage et al., 1995b; Kullmer et al., 1999), including a mandible of *Homo rudolfensis* (Uraha) and a maxillary fragment of *Paranthropus boisei* (Malema), both biostratigraphically dated to ca. 2.4 Ma (Bromage et al., 1995b; Kullmer et al., 1999). They hence document the earliest co-existence of these two hominin genera so far discovered. In addition, a hominin molar fragment of similar age

and tentatively assigned to *H. rudolfensis* was recently reported from Mwenirondo (Kullmer et al., 2011). Oxygen and carbon isotope analysis of dental enamel of different mammals (e.g., equids, bovids, elephants) is the subject of a concurrent study with the goal of a more comprehensive paleo-environmental reconstruction of the Karonga Basin.

3.2.3 Chiwondo paleosols

The siliciclastic parent material of the Chiwondo paleosols is derived mostly from Proterozoic metamorphic basement and Permo-Triassic Karoo sediments in the hinterland of the Karonga Basin. In contrast to the carbonate depleted upper horizons or decalcified B-horizons, erosion resistant Bk-horizons are well-preserved in the tectonically active fluvial, swamp, and deltaic settings. Paleosols are typically brown, locally mottled cambisols or oximorphic horizons of Gleysols



Figure 3.3: Outcrop conditions and field characteristics of the Plio-Pleistocene Chiwondo and Chitimwe Beds. A) Section 12-MR-19, step section sampling profile. Only pedogenic carbonate was sampled. B) Chitimwe and Chiwondo Beds, upper part of Profile 12-RC-08, sampled at the wall of the excavation pit of *Paranthropus boisei*. The deltaic sediments are rich in well-consolidated carbonate due to pedogenic overprint. C) Pedogenic carbonate can occur in patches and nodules or in D) carbonate filled root casts. E) Close up of pedogenic carbonate in a carbonate-free matrix.

containing mm- to cm-sized carbonate nodules in a usually carbonate-free matrix (Fig. 3.3). The parent material is composed of sand, most probably of alluvial or aeolian origin.

3.2.4 Age control and correlation of individual sections

A precise age assignment of the exposed Chiwondo and Chitimwe sediments is hampered by the absence of datable volcanic material (Kaufulu and Stern, 1987; Betzler and Ring, 1995; Kullmer, 2008). Biostratigraphic age constraints based mostly on surface finds of fossil suid molars were established for sediments with an age range of ca. 4.3 Ma (*Notochoerus jaegeri*) to 0.7 Ma (*Metridiochoerus compactus*; White, 1995; Kullmer, 2008; Bishop, 2010). The age of the overlying Chitimwe Beds is assigned to the Middle and Late Pleistocene due to the presence of lithic artifacts (Clark et al., 1970).

Correlation of the fluvial, lacustrine, and swamp successions is based on field relationships established during three field campaigns in 2011, 2012, and 2013, structural mapping, and mammal fossil occurrences that are supported by $\delta^{13}\text{C}$ and $\delta^{18}\text{O}$ patterns within individual sections. It is not possible to assign an absolute age to each profile and nodule, but we were able to divide them into five intervals (± 0.2 Ma): ca. 4.3 to 3.75 Ma (Units 1 and 2), 3.75 to 2.8 Ma (Unit 3A-1), 2.8 to 1.8 Ma (Unit 3A-2), 1.8 to 0.6 Ma (Unit 3B), and <0.6 Ma (Units 4 and 5), after Betzler and Ring (1995), Bromage et al. (1995a), Sandrock et al. (1999), and Kullmer (2008). Suid fossils occur in Unit 2, 3A, and 3B. Unit 2 contains *Not. jaegeri*. Unit 3A was subdivided in two biozones by *Notochoerus euilus* (3A-1), *Notochoerus scotti*, and *Metridiochoerus andrewsi* stage I (3A-2). Unit 3B contains *Met. andrewsi* stage III and *Met. compactus* (Kullmer, 2008).

Based on the observed field relationships, the stratigraphic order of each profile within these intervals is accurate; however, it is difficult to ascertain sediment accumulation rates in these erosional, mostly high-energy deposits that usually only stretch over small lateral distances. When compared to the total stratigraphic thickness of each unit, the data presented here typically cover most of the unit and we tentatively assign the oldest (and youngest) age of the unit to the stratigraphical lowest (and highest) sample. Within each unit we assume constant accumulation rates (that range from 25 to 60 m/Ma); however, we would like to highlight that the general conclusions being drawn here are largely independent of this assumption. For further information see Appendix 3.8, especially Figure 3.7.

3.2.5 Vegetation classification system

We adopt the vegetation classification system (White, 1983), which is primarily based on woody cover after The United Nations Educational, Scientific, and Cultural Organization (UNESCO) classification of African vegetation, where forest has interlocking crowns, woodland/bushland/thicket/shrubland has a woody cover $>40\%$, wooded grassland between 10 and 40% , and grassland $<10\%$. We further assign 80% woody cover as the forest-woodland boundary (Cerling et al., 2011b).

Today, the Eastern Rift (Somali-Masai Endemic Zone) and the Malawi Rift (Zambeziyan Savanna) belong to two savanna ecosystems that differ strongly in woody cover and type of biomass. The Miombo woodlands are a moist/dystrophic savanna and tree cover is typically limited by disturbances such as fire and herbivory, rather than climate (van Wilgen, 1997; Sankaran et al., 2005). It hosts a diverse tree community dominated by the Leguminosae subfamily Caesalpinioideae (Coates Palgrave et al., 2002), with a high fraction of woody cover that provides shade, shelter, and food resources. In contrast, today's Somali-Masai Endemic Zone is dominated by open grassland savanna with only sparse tree cover.

3.2.6 Eastern Rift $\delta^{13}\text{C}$ data

3.2.6.1 *Pedogenic carbonate*

$\delta^{13}\text{C}$ values of pedogenic carbonate from fossil hominin localities in the Eastern Rift Valley since 7.5 Ma exist from Hadar and Busidima in the Lower Awash and Sagantole and Adu-Asa in the Middle Awash Valley (WoldeGabriel et al., 1994, 2009; Levin et al., 2004; Quade et al., 2004; Semaw et al., 2005; White et al., 2006; Aronson et al., 2008; Passey et al., 2010; Cerling et al., 2011a), Omo-Turkana (Cerling et al., 1988, 2003; Wynn, 2004; Quinn et al., 2007; Levin et al., 2011), Tugen Hills (Cerling, 1992; Kingston, 1992; Kingston et al., 2002), Kanjera (Plummer et al., 2009), Olororgesailie (Sikes et al., 1999), Olduvai (Cerling and Hay, 1986; Sikes, 1994; Sikes and Ashley, 2007), and Laetoli (Cerling, 1992). A compilation of the data is available at EarthChem Library (Levin, 2013).

3.2.6.2 *Suid enamel*

$\delta^{13}\text{C}$ values samples of suid enamel from fossil hominid localities in the Eastern Rift since 7.5 Ma come from the Awash Valley (Gona; Semaw et al., 2005), Omo-Turkana (Lothagam, Mursi, Koobi Fora, Kanapoi; Harris and Cerling, 2002; Cerling et al., 2003; Uno et al., 2011; Bibi et al., 2013; Drapeau et al., 2014), Tugen Hills (Morgan et al., 1994), and Laetoli (Kingston, 2011).

3.3 Material and methods

The stable carbon isotope geochemistry of pedogenic carbonate and fossil suid enamel is a robust tool to reconstruct continental paleoenvironmental conditions, in particular when climate change plays a key role in the evolution of ecosystems. While $\delta^{13}\text{C}$ values of cm-sized pedogenic carbonates record the time-averaged effects of changes in C₃ versus C₄ vegetation on carbon isotope ratios in soils, $\delta^{13}\text{C}$ values in enamel reflect the diet of the individual during the time of tooth development (several month to years) in an area reflecting the migration pattern of the animal (e.g., Birkeland, 1984; Kohn and Cerling, 2002; Pustovoytov, 2003). In total, 321 pedogenic carbonates were selected from 14 freshly-cut step-sections (Fig. 3.3a) in the Chiwondo Beds, one sample from the Chitimwe Beds, and four (sub)recent pedogenic carbonate nodules. Whenever possible, well-consolidated nodules were sampled at least 30 cm below paleosol surfaces (Fig. 3.3b). Nodules were cut in half and bulk carbonate

powder was extracted with a diamond tip dental drill. Untreated carbonate (100-300 mg) were reacted with 98% H₃PO₄ for 90 min at 70°C in continuous flow mode using a Thermo MAT 253 mass spectrometer interfaced to a Thermo GasBench II.

$\delta^{13}\text{C}$ values of fossil enamel have shown to be rather insensitive to the influence of diagenesis (Koch et al., 1997). We focus here on Suidae as mixed feeders, as their enamel $\delta^{13}\text{C}$ values should reflect local environment more accurately than specialized feeders. Eighteen samples from ten suid molars were analyzed. These include the extinct *Not. jaegeri*, *Not. euilus*, and *Not. scottii*; *Met. andrewsi* stage I and III and *Met. compactus*, plus the extant *Phacochoerus aethiopicus*. Suid molars were cut laterally and enamel was sampled either with a hand-held diamond tip dental drill or a micromilling device (Merchantek Micromill). Sampling parallel and across several growth axes of the teeth was necessary to obtain sufficient sample material (2e3 mg). Bulk samples, therefore, represent $\delta^{13}\text{C}$ values averaged over the time of tooth formation, likely encompassing several months to years (Kohn, 2004), depending on species and wear pattern. Only if a tooth provided enough enamel, several (up to four) measurements per tooth could be realized. To remove organic and potential diagenetic carbonate, enamel was pretreated with 2% NaOCl solution for 24 h followed by 1 M Ca-acetate acetic acid buffer solution for another 24 h (Kohn, 2004). Typically, enamel pre-treatment resulted in 20 to 40% mass loss. 830 to 2030 mg of pretreated enamel material was reacted with 98% H₃PO₄ for 90 min at 70°C in continuous flow mode using a Thermo MAT 253 mass spectrometer interfaced to a Thermo GasBench II. All analyses were performed at the Goethe University-BiK-F Joint Stable Isotope Facility Frankfurt. Analytical procedures followed Spötl and Vennemann (2003). Final isotopic ratios are reported against VPDB; overall analytical uncertainties are better than 0.03‰.

3.4 Results

3.4.1 $\delta^{13}\text{C}$ values of Plio-Pleistocene (~4.3 Ma to modern) pedogenic carbonate

Based on correlation of individual sections, we provide a composite pedogenic carbonate $\delta^{13}\text{C}$ record that encompasses the fluvial, deltaic, lacustrine, and swamp deposits of northern Malawi (Fig. 3.4). Throughout the Plio-Pleistocene, $\delta^{13}\text{C}$ values range between -5.8 and -11.2‰, with a mean of -9.1‰ ($\sigma = 1.1\%$; $n = 321$). Age constraints for the individual units are based on biostratigraphic correlation (in particular suid molars; Kullmer, 2008) with well-dated sites in the Eastern Rift Valley, observed and measured field relationships (Betzler and Ring, 1995) that are supported by patterns in $\delta^{13}\text{C}$ and $\delta^{18}\text{O}$ of the individual analyzed paleosol sections (for further description see Appendix 3.8). The results can be divided into five time intervals.

3.4.1.1 Early Pliocene (ca. 4.3 Ma to 3.75 Ma)

$\delta^{13}\text{C}$ values from the Karonga Basin show only little variation and range between -10.6 and -8.1‰ with a mean of -9.6‰ ($\sigma = -0.7\text{‰}$; $n = 27$). Comparison of these results to ^{13}C values from the Eastern Rift in the age interval of 7.5 Ma to 3.75 Ma (mean = -6.1‰; $\sigma = -2.3$; $n = 126$; Levin, 2013) documents generally lower $\delta^{13}\text{C}$ values in the Karonga Basin, forming a statistically distinct data-population of $\delta^{13}\text{C}$ (t-test, $t = 14.420$; $df = 143$; $p < 0.05$). The difference of the averages in $\delta^{13}\text{C}$ values between the Karonga Basin and the Eastern Rift, $\Delta(\delta^{13}\text{C})_{\text{KB-ER}}$, equals 3.5‰.

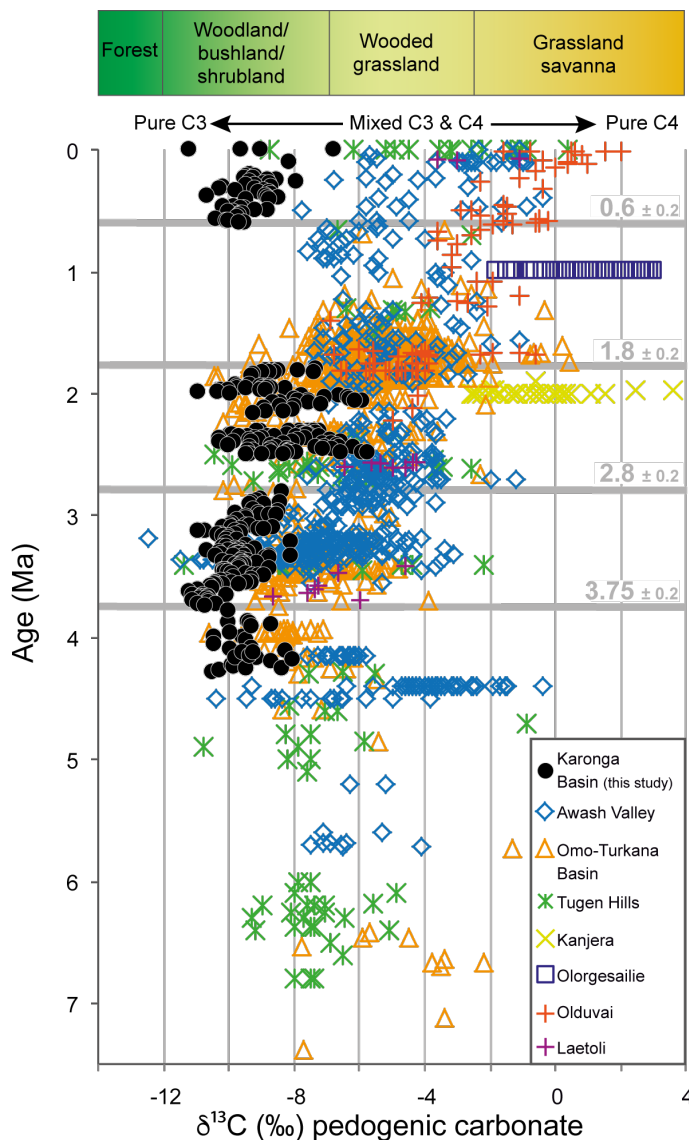


Figure 3.4: $\delta^{13}\text{C}$ values of pedogenic carbonate in the EAR since 7.5 Ma. Filled circles show $\delta^{13}\text{C}$ data from the Karonga Basin (Malawi Rift), open symbols represent the Eastern Rift including Middle and Lower Awash (WoldeGabriel et al., 1994, 2009; Levin et al., 2004; Quade et al., 2004; Semaw et al., 2005; White et al., 2006; Aronson et al., 2008; Passey et al., 2010; Cerling et al., 2011a), Omo-Turkana (Cerling et al., 1988, 2003; Wynn, 2004; Quinn et al., 2007; Levin et al., 2011), Tugen Hills (Cerling, 1992; Kingston et al., 1994, 2002), Kanjera (Plummer et al., 2009), Olorgesailie (Sikes et al., 1999), Olduvai (Cerling and Hay, 1986; Sikes, 1994; Sikes and Ashley, 2007), and Laetoli sites (Cerling, 1992). Note that age assignment for the Karonga Basin is based on the relative position of the sampled intervals within the different unit boundaries (for further information see Supplementary Material 3.8).

3.4.1.2 3.75 Ma to 2.8 Ma

Despite the high sample density, $\delta^{13}\text{C}$ values of pedogenic carbonate from the Karonga Basin only occupy a narrow range with $\delta^{13}\text{C}$ values between -11.2 and -8.1‰. The mean of -9.8‰ ($\sigma = 0.7$; $n = 123$) is, within error, identical to the mean of -9.6‰ ($\sigma = 0.7\text{‰}$; $n = 27$) during the 4.3 Ma to 3.75 Ma time interval. Compared to the Eastern Rift ($\delta^{13}\text{C}$ mean = -7.4‰; $\sigma = 1.6\text{‰}$; $n = 349$; Levin, 2013), $\delta^{13}\text{C}$ values of the Karonga basin form a clearly distinct data-population ($t = 22.483$; $df = 458$; $p < 0.05$) and $\Delta(\delta^{13}\text{C})_{\text{KB-ER}} = 2.4\text{‰}$.

3.4.1.3 2.8 Ma to 1.8 Ma

During this important time interval for early hominin evolution in Eastern Africa, pedogenic carbonate $\delta^{13}\text{C}$ values in the Karonga Basin range from -11.0 to -5.8‰ ($\sigma = 1.1\text{‰}$; $n = 126$), with a mean of -8.3‰. Compared to the previous time intervals, $\delta^{13}\text{C}$ values increase by ca. 1.0-1.5‰ and further display slightly larger variability.

Whereas the most negative $\delta^{13}\text{C}$ values persistently remain at around -11‰ , we observe the first occurrence of more positive $\delta^{13}\text{C}$ values attaining -6‰ . At the same time the mean $\delta^{13}\text{C}$ value from pedogenic carbonates in the Eastern Rift increases to -5.6‰ ($\sigma = 2.1\text{‰}$; $n = 331$; Levin, 2013). The difference between the two datasets with $\Delta(\delta^{13}\text{C})_{\text{KB-ER}} = 2.7\text{‰}$ is still pronounced ($t = 18.480$; $df = 405$; $p < 0.05$).

3.4.1.4 1.8 to 0.6 Ma

No data from this time interval could be collected in the Karonga Basin. $\delta^{13}\text{C}$ values from Eastern Rift sites continue their trend towards more positive values with a mean $\delta^{13}\text{C}$ value of -4.0‰ ($\sigma = 2.7\text{‰}$; $n = 395$; Levin, 2013).

3.4.1.5 <0.6 Ma

During the Upper Pleistocene and Holocene, Karonga Basin pedogenic carbonate $\delta^{13}\text{C}$ values remain consistent with those observed in the older time intervals. $\delta^{13}\text{C}$ values range between -11.2 and -6.8‰ , with a mean of -9.3‰ ($\sigma = 0.7\text{‰}$; $n = 52$). Pedogenic carbonate $\delta^{13}\text{C}$ values from the Eastern Rift show much more positive values (mean = -2.4‰ ; $\sigma = 2.2\text{‰}$; $n = 90$; Levin, 2013) and therefore document the largest difference in $\delta^{13}\text{C}$ values when compared to the Karonga Basin, with $\Delta(\delta^{13}\text{C})_{\text{KB-ER}} = 6.9\text{‰}$. Consequently, the statistical difference between $\delta^{13}\text{C}$ datasets from the Eastern Rift and Karonga Basin datasets is strongest during this youngest evaluated time interval ($t = 27.509$; $df = 188$; $p < 0.05$). The overall pattern of $\delta^{13}\text{C}$ values in different parts of the EAR terminates with $\delta^{13}\text{C}$ values of modern pedogenic carbonate that attain mean $\delta^{13}\text{C}$ values of -9.2‰ in the Karonga Basin ($\sigma = 1.8\text{‰}$; $n = 4$) and 2.0‰ within the Eastern Rift (Awash Valley, Tugen Hills, and Olduvai; $\sigma = 2.6\text{‰}$; $n = 23$), resulting in $\Delta(\delta^{13}\text{C})_{\text{KB-ER}} = 7.2\text{‰}$.

3.4.2 $\delta^{13}\text{C}$ values of Plio-Pleistocene (~4 Ma to modern) suid enamel

We complement our long-term pedogenic carbonate $\delta^{13}\text{C}$ record from the Karonga Basin by a ca. 4 Ma $\delta^{13}\text{C}$ record of enamel from suid teeth (Fig. 3.5). These data comprise molars from 10 individuals of three genera found in the Chiwondo Beds. Up to four replicate analyses of third molars from the extinct *Not. jaegeri* ($n = 3$), *Not. euilus* ($n = 2$), *Not. scotti* ($n = 2$), *Met. andrewsi* stage I ($n = 4$) and III ($n = 1$) and *Met. compactus* ($n = 1$), plus the extant *Pha. aethiopicus* ($n = 4$) show $\delta^{13}\text{C}$ values that range between -13.1 and -4.5‰ (mean = -9.3‰ , $\sigma = 2.6\text{‰}$, $n = 18$). Similar to the pedogenic carbonate $\delta^{13}\text{C}$ data, these values are much more negative when compared to $\delta^{13}\text{C}$ values from suids within the Eastern Rift Valley at Middle Awash, Omo-Turkana, Tugen Hills, and Laetoli (<7 Ma; mean = -2.4‰ ; $\sigma = 2.6\text{‰}$; $n = 249$; for references see Fig. 3.5) and form a statistically different data-population ($t = 11.010$; $df = 20$; $p < 0.05$). In the following section, we separate the Karonga Basin data according to the same time intervals as our pedogenic $\delta^{13}\text{C}$ record; the suid data (Fig. 3.5) is plotted between their first (FAD) and last appearance date (LAD), following White (1995), Kullmer (2008), and Bishop (2010).

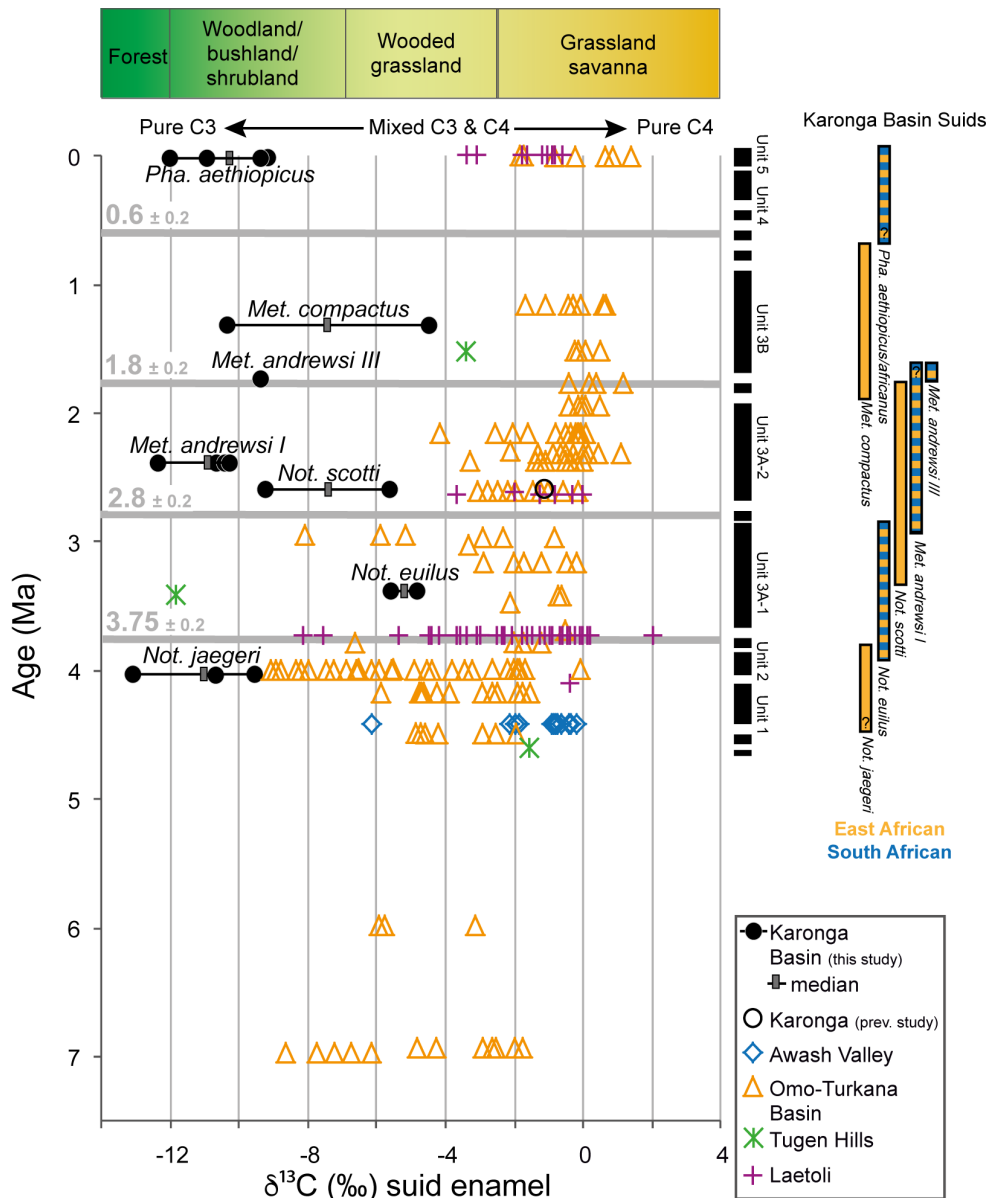


Figure 3.5: $\delta^{13}\text{C}$ values of suid enamel in the EAR since 7.5 Ma. Filled circles show $\delta^{13}\text{C}$ data from the Karonga Basin (Malawi Rift), open circle from Bocherens et al. (2011), samples from the same species are connected by black lines with the median marked as a gray oblong. Other symbols represent: Middle Awash (Gona; Semaw et al., 2005), Omo-Turkana (Lothagam, Mursi, Koobi Fora, Kanapoi; Harris and Cerling, 2002; Cerling et al., 2003; Uno et al., 2011; Bibi et al., 2013; Drapeau et al., 2014), Tugen Hills (Morgan et al., 1994), and Laetoli (Kingston, 2011). The Chiwondo Beds in the Malawi Rift are divided into Units 1 to 4; Unit 5 is the Chitimwe Beds (Betzler and Ring, 1995; Bromage et al., 1995a; Kullmer, 2008). Suidae genera age distribution after White (1995), Kullmer (2008), and Bishop (2010). Pha. = Phacochoerus, Met. = Metridiochoerus, Not. = Notochoerus.

3.4.2.1 Early Pliocene (ca. 4.3 Ma to 3.75 Ma)

Teeth from *Not. jaegeri* (FAD \approx 4.3 Ma; LAD \approx 3.75 Ma) from the Karonga Basin show $\delta^{13}\text{C}$ values between -9.5 and -13.1‰ (mean = -11.1‰; σ = 1.8‰, n = 3), and are ca. 1.5‰ more negative than $\delta^{13}\text{C}$ values from pedogenic carbonate in the Karonga Basin. *Not. jaegeri*, *Nyanzachoerus pattersoni*, *Nyanzachoerus kanamensis*, and *Nyaustralis australis* from the Eastern Rift in the age interval of 7.0 Ma to 3.75 Ma generally show less negative values, with a mean of -4.2‰ (σ = 2.8‰; n = 90). The difference of the averages in $\delta^{13}\text{C}$ between the Karonga Basin and the Eastern Rift, $\Delta(\delta^{13}\text{C})_{\text{KB-ER}}$, equals 6.9‰.

3.4.2.2 3.75 Ma to 2.8 Ma

The two individuals of the Upper Pliocene *Not. euilus* (FAD \approx 3.9 Ma; LAD \approx 2.85 Ma) from the Karonga Basin show values of -5.5 and -4.8‰. Samples of *Not. euilus*, *Nya. pattersoni*, *Potamochoerus porcus*, and *Kolpochoerus limnetes* from the Eastern Rift display a mean $\delta^{13}\text{C}$ value of -2.2‰ ($\sigma = 2.1\%$; $n = 58$). One individual from the Tugen Hills, shows exceptionally low $\delta^{13}\text{C}$ values of -11.8‰ (Morgan et al., 1994). $\Delta(\delta^{13}\text{C})_{\text{KB-ER}} = 3.0\%$ (excluding the Tugen Hills sample) represents the smallest Karonga Basin-Eastern Rift difference in the suid enamel data through time.

3.4.2.3 2.8 Ma to 1.8 Ma

With $\delta^{13}\text{C} = -9.8$ and -5.6% , the Karonga Basin samples of *Not. scotti* (FAD \approx 3.36; LAD \approx 1.8 Ma) are less negative than comparable analyses of enamel from *Met. andrewsi* stage I (FAD \approx 2.95; LAD \approx 1.8 Ma), which show an average of -10.9% ($\sigma = 1.0\%$; $n = 4$). Again, the $\delta^{13}\text{C}$ values of co-existing Suidae *Not. scotti*, *Met. andrewsi*, and *Kol. limnetes* from the Eastern Rift show more positive values with a mean of -0.9% ($\sigma = 1.1\%$; $n = 65$). $\Delta(\delta^{13}\text{C})_{\text{KB-ER}}$ between suids from the Karonga Basin and the Eastern Rift equals 10.0% . Enamel from a tooth of *Not. scotti* from the Chiwondo Beds shows a $\delta^{13}\text{C}$ value of -1.1% (Bocherens et al., 2011).

3.4.2.4 1.8 Ma to 0.6 Ma

The $\delta^{13}\text{C}$ value of *Met. andrewsi* stage III (FAD \approx 1.8 Ma; LAD \approx 1.7 Ma) attains -9.3% and is slightly more positive than the values of the stage I individual. Analyses of two enamel samples from different localities of an M3 sample of *Met. compactus* (FAD \approx 1.9 Ma; LAD \approx 0.7 Ma) spread widely with $\delta^{13}\text{C}$ values of -10.3 and -4.5% . $\delta^{13}\text{C}$ data of *Met. andrewsi*, *Metridiochoerus hopwoodi*, *Met. compactus*, *Kol. limnetes*, and *Kolpochoerus olduvaiensis* from the Eastern Rift show much more positive $\delta^{13}\text{C}$ values (mean = -0.3% ; $\sigma = 1.0\%$; $n = 17$) resulting in $\Delta(\delta^{13}\text{C})_{\text{KB-ER}} = 7.7\%$.

3.4.2.5 <0.6 Ma

The recent individual of *Pha. aethiopicus* (FAD \approx 0.8 Ma) from the Karonga Basin shows a mean $\delta^{13}\text{C}$ value of -10.3% ($\sigma = 1.4$; $n = 4$) and, therefore, differs significantly from *Pha. aethiopicus* and *Pha. africanus* from Omo-Turkana (mean = -1.1% , $\sigma = 1.1\%$; $n = 18$). $\Delta(\delta^{13}\text{C})_{\text{KB-ER}} = 9.2\%$.

3.5 Discussion

$\delta^{13}\text{C}$ data of pedogenic carbonate (Fig. 3.4) and suid enamel (Fig. 3.5) from fluvio-lacustrine deposits in the Eastern Rift at Awash Valley, Omo-Turkana Basin, Tugen Hills, Kanjera, Olorgesailie, Olduvai, and Laetoli have provided a cornerstone for reconstructing hominin environments in the EAR (for references see captions in Figs. 3.4 and 3.5). In the Eastern Rift, pedogenic and biogenic carbonate $\delta^{13}\text{C}$ values suggest the dominance of C₃ biomass until the Late Pliocene and Early Pleistocene with an increasing dominance of C₄ grasses, which radiated during the last 2 Ma in today's Somali-Masai Endemic Zone. The Malawi Rift at more southerly latitudes contrasts with this pattern. The long-term

$\delta^{13}\text{C}$ data from the Malawi Rift that was home to early (ca. 2.4 Ma) hominins indicate a mesic habitat with a strongly different vegetation and climate history when compared to the majority of hominin sites in today's drier parts of the EAR. The combined Plio-Pleistocene paleosol and enamel $\delta^{13}\text{C}$ data from the Malawi Rift therefore provide a foundation for reconstructing the long-term ecological context of hominin evolution in the Malawi Rift, and allow a debut for the comparison with similar records covering the same time frame in the Eastern Rift. We are fully aware that a comparison of numerous sites in the Eastern Rift with a spatially restricted set of sites in the Karonga Basin underestimates the complexity of habitats likely to be encountered in the Malawi Rift. Collectively, pedogenic carbonate and tooth enamel data from Malawi, however, provide compelling evidence for the long-term persistence of a C₃-dominated ecosystem in the Karonga Basin, which is strikingly different from the majority of paleoenvironments reconstructed for the EAR so far (Figs. 3.4-3.6). Calculated differences in $\delta^{13}\text{C}$ between the Karonga Basin (Malawi Rift) and the entirety of the Eastern Rift data, $\Delta(\delta^{13}\text{C})_{\text{KB-ER}}$, consequently serve as a guide in documenting regional long-term differences in vegetation type and biome structure rather than representing precise predictors of differences in local vegetation patterns. $\Delta(\delta^{13}\text{C})_{\text{KB-ER}}$ values analyzed in five time intervals (Fig. 3.6c) range from 2.7 to 7.2‰ (pedogenic carbonate) and 3.0 and 10.0‰ (suid enamel). $\delta^{13}\text{C}$ values of pedogenic carbonate in the Malawi Rift never exceed -5.8‰ during the last 4.3 Ma and attain a long-term mean of -9.1‰. Such low $\delta^{13}\text{C}$ values are typical for a C₃-dominated ecosystem characterized by a woodland, bushland, shrubland, or wooded grassland environment (following the vegetation classification of White [1983]) with a woody cover of at least 38% (calculated for the most positive $\delta^{13}\text{C}$ value of -5.8‰), but on average in excess of ca. 66% (for the average $\delta^{13}\text{C}$ value of -9.1‰) using the 'paleo-shade' proxy (Cerling et al., 2011b).

The suid enamel $\delta^{13}\text{C}$ data support this model (see Fig. 3.5). $\delta^{13}\text{C}$ values of all analyzed suids from the Karonga Basin as low as -13.1‰ reflect wooded grassland to dominantly C₃ forest environments. Collectively, the $\delta^{13}\text{C}$ values of pedogenic carbonate as well as suid enamel indicate a less open environment in the Malawi Rift than in the Eastern Rift over the past ca. 4.3 million years, with 50-70% woody cover in a woodland, shrubland, or bushland environment in the Karonga Basin. *Notochoerus jaegeri* from the Malawi Rift selectively consumed C₃ biomass, indicating browsing in a closed bushland or forest prior to 3.75 Ma, whereas Suidae from the same genera and time interval in the Awash Valley and the Omo-Turkana Basin all show a mixed C₃-C₄ diet characteristic of more open paleoenvironments (Morgan et al., 1994; Harris and Cerling, 2002; Cerling et al., 2003; Semaw et al., 2005; Kingston, 2011; Uno et al., 2011; Drapeau et al., 2014). Data from Late Pliocene pedogenic carbonate nodules from the Chiwondo Beds confirm a persistent woodland environment in the Malawi Rift, whereas $\delta^{13}\text{C}$ values from soil carbonate in the Eastern Rift generally indicate increasingly open wooded grassland environments with only

sparse occurrence of woodlands. The two *Not. euilus* individuals from the Karonga Basin ($\delta^{13}\text{C} = -5.5\text{‰}$ and -4.8‰), however, point to a mixed diet with roughly balanced C₃ and C₄ consumption, requiring (at least) temporary access to C₄ vegetation elements. This offset, when compared to the other time intervals, could either indicate a selection of C₄ grasses in the suid diet in a mostly C₃ dominated environment and/or the effect of a patchy ecosystem structure with e.g., gallery forest along the shoreline of paleolake Malawi and its contributing rivers. The Chiwondo deltaic, fluvial, and swamp deposits comprising the pedogenic carbonate were accumulated close to lakes or rivers, whereas the suids were able to migrate and roam larger areas. Although diet reconstruction of the Late Pliocene *Not. euilus* from Malawi shows the strongest C₄ influence, individuals from the Eastern Rift still reflect feeding in a much more open environment (Fig. 3.6b, c).

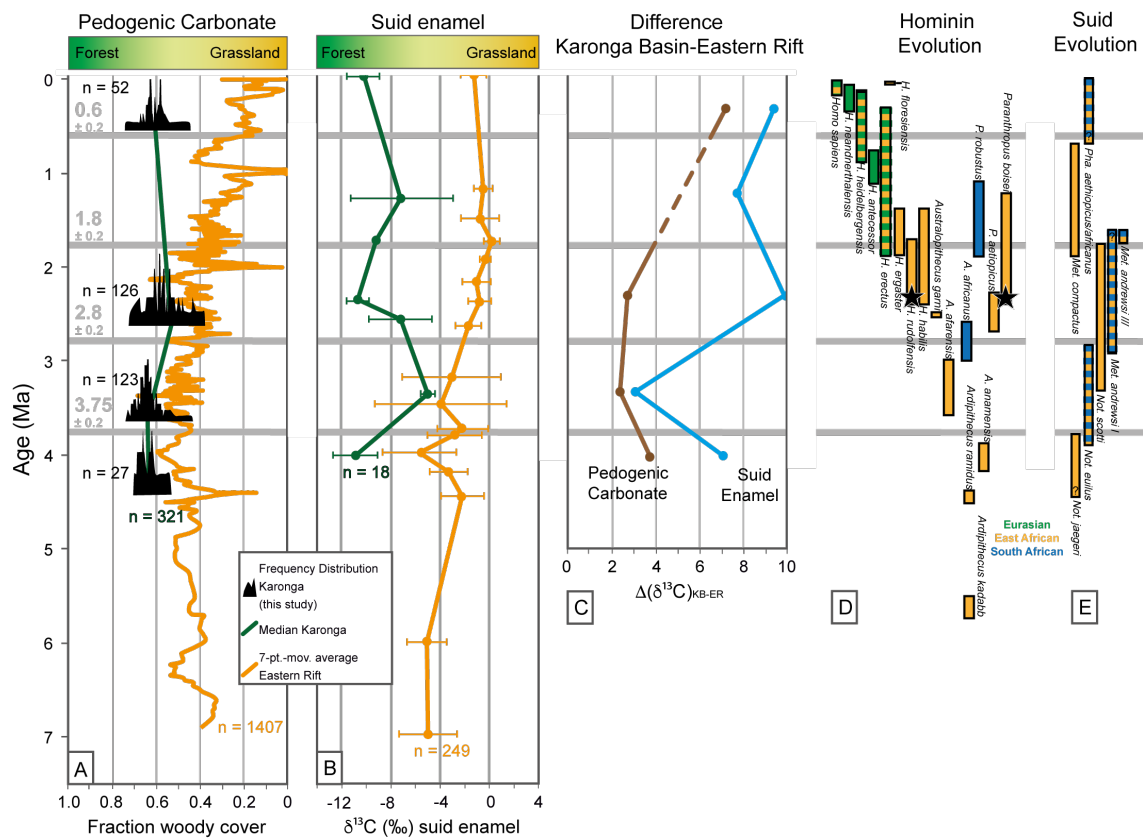


Figure 3.6: Composite record of paleosol $\delta^{13}\text{C}$ values from the Karonga Basin in the Malawi Rift (marked in black) presented as normalized probability density function of predicted woody cover. Lines represent the overall median of $\delta^{13}\text{C}$ values of Malawi Rift samples per interval (green) and the 7-point running average for pedogenic carbonate from the Eastern Rift (orange). B) Median $\delta^{13}\text{C}$ values for suid data of the Malawi Rift (green) and the Eastern Rift (orange) with 1σ standard deviation. C) Differences of average $\delta^{13}\text{C}$ between Karonga Basin and Eastern Rift for pedogenic carbonate (brown) and suid enamel (blue). Although absolute $\delta^{13}\text{C}$ values cover a large range especially in the Eastern Rift, the difference in $\delta^{13}\text{C}$ between the Eastern Rift and the Malawi Rift is distinct throughout time and becomes more pronounced during the last ca. 2.6 Ma in both proxy materials. D) Hominin evolution transitions after Shultz et al. (2012) and references therein. Stars indicate Karonga Basin fossils. E) Suidae genera age distribution after White (1995), Kullmer (2008), and Bishop (2010).

In the Early Pleistocene (~2.6 Ma), the Eastern Rift started to change towards increasingly open grasslands with a large fraction of C₄ biomass (e.g., Harris and Cerling, 2002; Ségalen et al., 2007; Cerling et al., 2011b). The Malawi Rift data on the other hand reflect a primary woodland environment with some areas of wooded grassland represented in the pedogenic carbonate, as well as *Not. scotti* and *Met. andrewsi* stage I enamel. The variability of $\delta^{13}\text{C}$ values is largest during this important time of early hominin evolution. The relatively large variability in $\delta^{13}\text{C}$ values probably hints at the existence of local microhabitats, characterized by restricted areas of woodland and bushland adjacent to grassland environments with reduced canopy and up to 60% C₄ plants. At the same time, the $\delta^{13}\text{C}$ data from pedogenic and enamel carbonate proxy materials from Eastern Rift hominin localities indicate a persistent trend towards a C₄-dominated grassland savanna. There is increasing evidence, however, that some regions deviate from this overall pattern where average pedogenic carbonate and suid enamel $\delta^{13}\text{C}$ values remained rather low (e.g., Shungura Formation, Omo Valley with $\delta^{13}\text{C}$ values of almost -9‰; Levin et al., 2011; Drapeau et al., 2014).

Karonga Basin soil carbonate $\delta^{13}\text{C}$ data are lacking for the Middle Pleistocene, but $\delta^{13}\text{C}$ values from *Met. andrewsi* stage III and *Met. compactus* enamel point to the persistence of C₃-dominated environments (Fig. 3.5). $\delta^{13}\text{C}$ values of Late Pleistocene to recent pedogenic carbonates support the model of a persistent long-term (ca. 4.3 Ma) ecosystem structure in the Karonga Basin with a continuously increasing difference to more open environments in the Eastern Rift. The recent warthog individual (Appendix 3.8; Table S3.5, sample #129) with $\delta^{13}\text{C}$ values ~10‰ more negative than equivalent proxy data in the Eastern Rift also demonstrates a clear distinction from co-existing suids in the Omo-Turkana Basin.

Collectively, the $\delta^{13}\text{C}$ results are supported by carbon isotope ratios of primary C₃ biomass in today's Zambebian Savanna when compared to open C₄ savanna biomass characteristic for the Somali-Masai Endemic Zone (White, 1983). Today, the Eastern Rift (Somali-Masai Endemic Zone) and the Malawi Rift (Zambebian Savanna) belong to distinct savanna ecosystems that differ strongly in terms of woody cover and type of biomass. The Miombo woodlands in the southern part of the EAR are a moist/dystrophic savanna, and tree cover is typically limited, influenced by disturbances through bush fire and herbivory rather than climate (van Wilgen, 1997; Sankaran et al., 2005). They are home to a diverse tree community with a high fraction of woody cover that provides shade, shelter, and food resources. Today's Somali-Masai Endemic Zone, on the contrary, is dominated by open grassland savanna with only sparse tree cover except for gallery forests along rivers and in the vicinity of lakes. Both ecosystems, however, can be very diverse on smaller spatial scales as a response to local variations in amount and seasonality of precipitation and/or temperature, which ultimately results in different vegetation patterns.

Paleoenvironmental reconstructions of hominin localities in the Plio-Pleistocene Eastern Rift also show increasing evidence for local deviations in vegetation biomes, with reconstructed C₃ biomass proportions almost as high as in the Karonga Basin (e.g., Omo Mursi; Drapeau et al., 2014) to almost pure C₄ vegetation (e.g., Olorgesailie; Sikes et al., 1999). Here, we aggregate the Plio-Pleistocene Eastern Rift $\delta^{13}\text{C}$ data to interpret first-order, long-term evolutionary changes between the Malawi Rift and the Eastern Rift. As a result of this analysis, the Karonga Basin $\delta^{13}\text{C}$ data consistently present the lowest $\delta^{13}\text{C}$ values in the entire EAR over protracted periods of time, indicating robust and persistent vegetation with a low C₄ component.

The radiation of C₄ grasses is considered as a major driver of evolutionary faunal shifts, since variation in woody cover and accompanied effects of heat and shade distribution may have been significant triggers for hominin physiological and behavioral adaptations (e.g., Vrba, 1983, 1988; Passey et al., 2010). The Karonga Basin $\delta^{13}\text{C}$ data indicate only regional patches of open landscape with C₄ vegetation interspersed in a C₃-dominated, closed habitat throughout the time of hominin evolution and the appearance of the genus *Homo* in Malawi at around 2.4 Ma ago (Schrenk et al., 1993). The Malawi Rift-Eastern Rift difference in ecosystem evolution is striking, considering that early *Homo* (*H. rudolfensis*) and *Paranthropus* (*P. boisei*) occurred in both landscapes. Our Malawi geochemical data suggest that two different types of savannas covered Eastern Africa from the Late Pliocene onwards that increasingly differed in vegetation type and fraction of woody cover. The boundary between these savanna types might have shifted through time, but remained within ca. 3°S and 10°S (between the Chiwondo Beds and Laetoli, the southernmost hominin locality in today's Somali-Masai Endemic Zone, see Fig. 3.1). Based on the $\delta^{13}\text{C}$ values, both savanna types are statistically distinguishable in each of the analyzed time intervals (<3.7 Ma, older data is not available from Laetoli) with a difference in woody cover of at least 15%.

The paleobiogeographic distribution of the large mammal fauna from the Malawi Rift is dominated by Eastern African endemics (Bromage et al., 1995a). The fauna includes *H. rudolfensis* and *P. boisei*, which suggests that these and other similar taxa may be characterized as eurybiomic insofar as their habitat preferences are supportable within an environmental matrix that includes a variety of open, marginal, and closed habitats. Understanding to what extent the Malawi Rift data presented here are representative for the entire southern EAR will benefit from analysis of additional sites and proxy materials.

Today the Zambezian Savanna ecozone is considered a large mammal barrier (Klein, 1984) owing to the dry season winter belt that originates at its southern margin, becoming dryer toward the Tropic of Capricorn. Interestingly, large mammals of the Malawi Rift that are not endemic to Eastern or Southern Africa are predominantly adapted to open floodplain habitats (cf. Table 3 in Bromage et al., [1995a]), which is a habitat preference that is easily transgressed. However, *H. rudolfensis* and *P. boisei* as eastern African endemics within the

Zambeziian Savanna show that open conditions are not exclusive to models of hominin evolution. This indicates habitat versatility in these two coexisting species as both were able to exist in predominantly closed (Malawi) and open (Eastern Rift) savanna settings.

3.6 Conclusions

Two different types of savanna were present in the East African Rift system at least since the Pliocene. The Malawi Rift, with a mean of >65% fraction of woody cover, has had persistently more canopy than the Eastern Rift (changing the fraction of woody cover from around 50% in the Pliocene to less than 20% since the Late Pleistocene). Overall, during the last ~4.3 Ma, constant $\delta^{13}\text{C}$ values of ca. -9‰ in pedogenic carbonate and mixed-feeding suids show no considerable changes in vegetation patterns compared to today's Zambeziian Savanna environment. Throughout the Plio-Pleistocene until today the Karonga Basin is characterized by a C₃-dominated patchy C₃/C₄ ecosystem with presumably gallery forests along (paleo-)Lake Malawi and its contributing rivers. Based on the compiled $\delta^{13}\text{C}$ data, the boundary between the Somali-Masai Endemic Zone and the Zambeziian Savanna never moved as far south as the northern shore of Lake Malawi. Therefore, regions that are home to early hominins such as *H. rudolfensis* and the coexisting *P. boisei* may have had a different environmental history when compared to the Eastern Rift, resulting in a large difference in fraction of woody cover. This suggests that hominin adaptation is not necessarily directly linked to the emergence of open landscapes.

3.7 Acknowledgments

We are grateful to our local Malawian field crew in Karonga, the Cultural Museum Centre Karonga (CMCK), and the Malawi Government for the long-term cooperation with the Hominid Corridor Research Project (HCRP). We want to thank in particular Mr. Harrison Simfukwe for assistance and hospitality. We acknowledge support through the LOEWE funding program (Landes-Offensive zur Entwicklung wissenschaftlich-ökonomischer Exzellenz) of Hesse's Ministry of Higher Education, Research, and the Arts. We thank N. Thiemeyer for field assistance and U. Treffert and S. Hoffmann for laboratory support. Support was also provided to TGB by the 2010 Max Planck Research Award (Human Paleobiomics) through the German Federal Ministry of Education and Research and the Alexander von Humboldt Foundation and to AM through the A. Cox Visiting Professor program at Stanford University (USA). The manuscript was greatly improved by the thoughtful comments of K. Uno and two anonymous journal reviewers.

3.8 Supplementary material

Precise age assignments in the Chiwondo and Chitimwe sediments suffer from absence of datable volcanic material (e.g., Kaufulu and Stern, 1987, Betzler and Ring, 1994; Kullmer, 2008). Here we present the stratigraphic relationships of the individual (sub-)sections that comprise the long-term $\delta^{13}\text{C}$ record in the Karonga Basin. Note that accurate age assignments are hampered by the lack of knowledge of the duration of sedimentation for the individual sections. The depositional order within the units, however, (Figs. 3.4 and 3.7) is accurate. Sample IDs of pedogenic carbonate nodules are composed of survey area initial (see Fig. 2b), profile number, and individual sample number.

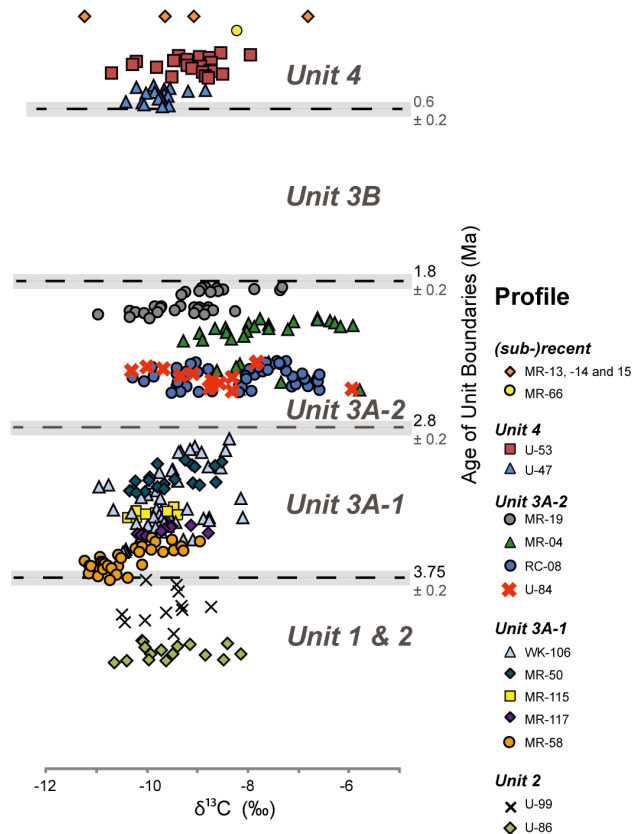


Figure 3.7: Stratigraphic order of all sampled pedogenic carbonates from the Karonga basin ordered by individual units. Synthetic lithological column after Betzler and Ring (1995). Depositional order of individual (sub-)sections is accurate within the respective units, however, ages of individual samples are only extrapolated from assumed total stratigraphic thickness. Due to uncertainties in sedimentation rates common in fluvo-lacustrine depositional settings, absolute ages of individual samples should not be extrapolated.

$\delta^{13}\text{C}$ values of Plio-Pleistocene (~4.3 Ma to modern) pedogenic carbonate

Early Pliocene to 3.75 Ma

This succession is merged from two sections sampled on the slope of “Uraha Hill”, U-99 (10°21'19.38"S; 34° 8'28.97"E) and U-86 (10°21'26.05"S; 34° 8'30.72"E). The sections describe Unit 1 and Unit 2 of the Chiwondo Beds. While it is possible that the lowest layers of Unit 1 were not sampled, the top of Unit 2 is marked by an oncoïd layer followed by an angular unconformity that forms the top of Profile U-99. With a combined total of 33.2 m thickness, the largest part of the units should be recorded. The calculated average sedimentation rate is ~60 m/Ma. A schematic stratigraphic column of U-99 is shown in Figure 5 in Lüdecke and Thiemeyer (2013).

Table 3.1: List of ca. 4.3 to 3.75 Ma (Unit 1 and 2) pedogenic nodules from Uraha (U) with sample ID, section-meter, and $\delta^{13}\text{C}$ values.

Sample ID	Profile meter	$\delta^{13}\text{C}$ (‰) PDB	Sample ID	Profile meter	$\delta^{13}\text{C}$ (‰) PDB
U-99-23	33.20	-10	U-86-14	7.35	-9.1
U-99-21	31.20	-9.4	U-86-13	6.80	-9.4
U-99-20	28.20	-9.4	U-86-12	6.00	-10
U-99-15	23.20	-9.3	U-86-11	4.80	-9.7
U-99-14	22.20	-8.7	U-86-10	3.90	-9.5
U-99-13	21.20	-9.3	U-86-09	3.70	-9.9
U-99-12	20.20	-9.6	U-86-08	3.50	-8.1
U-99-11	19.20	-10.5	U-86-07	3.00	-8.8
U-99-09	17.20	-10	U-86-05	1.20	-8.5
U-99-08	16.20	-10.4	U-86-04	1.00	-9.9
U-99-03	11.20	-9.5	U-86-03	0.80	-10.4
U-86-18	9.20	-10.1	U-86-02	0.60	-9.6
U-86-17	8.70	-10.1	U-86-01	0.15	-10.6
U-86-15	7.75	-8.4			

3.75 to 2.8 Ma

This Upper Pliocene sequence is composed of one section from the area of Mwimbi (13-WK-106; 10°7.033'S; 33°57.957'E) and four well-correlated profiles near Masapa River in Mwenirondo (MR-50 [10°0'46.43"S, 33°54'0.65"E], MR-115 [10°0.785'S, 33°53.928'E], MR-117 [10°0.767'S, 33°53.987'E], and MR-58 [10°0'19.90"S, 33°53'57.42"E]). For the most part, the Mwimbi and the Mwenirondo sections overlap (correlated with $\delta^{13}\text{C}$ values and field relationships) and form Unit 3A-1 with a total thickness of 33.8 m. Again, absolute dating is not possible, but field relationships supported by stable isotopic results convincingly point towards filling the gap between 3.75 Ma and the hominin sites with an age of ca. 2.4 Ma. Profile MR-58 is shown in Figure 2 in Lüdecke and Thiemeyer (2013). The calculated average sedimentation rate is ca. 36 m/Ma.

Table 3.2: List of 3.75 to 2.8 Ma (Unit 3A-1) pedogenic nodules from Mwimbi (WK) and Mwenirondo (MR) with sample ID, section-meter, and $\delta^{13}\text{C}$ values. Note that these profiles chronologically overlap.

Sample ID	Profile meter	$\delta^{13}\text{C}$ (‰) PDB	Sample ID	Profile meter	$\delta^{13}\text{C}$ (‰) PDB
WK-106-71	33.80	-8.4	MR-50-11	28.55	-9.1
WK-106-68	31.50	-9	MR-50-10	28.40	-9.6
WK-106-67	30.60	-9.1	MR-50-09	28.20	-9
WK-106-66	30.40	-8.4	MR-50-08	26.95	-9.8
WK-106-65	30.20	-9.3	MR-50-07	27.55	-9.7
WK-106-64	29.80	-9.4	MR-50-04	26.75	-10.3
WK-106-63	29.70	-8.9	MR-50-03	26.45	-10.3
WK-106-60	25.40	-8.8	MR-50-02	26.05	-10
WK-106-59	25.30	-8.5	MR-50-01	25.75	-10.2
WK-106-58	24.80	-9.5	MR-115-01	23	-10.1
WK-106-57	24.50	-9.5	MR-115-02	22.6	-9.5
WK-106-56	23.70	-9.7	MR-115-03	22.2	-10.2
WK-106-54	21.40	-9.4	MR-115-04	21.8	-10.1
WK-106-53	20.80	-9.9	MR-115-05	21.4	-9.7
WK-106-52	20.00	-10.8	MR-115-06	21	-9.8
WK-106-51	19.60	-10.9	MR-115-07	20.6	-10
WK-106-50	18.40	-9.8	MR-115-08	20.2	-9.8
WK-106-47	17.20	-10	MR-115-09	19.8	-9.4
WK-106-43	16.40	-10.1	MR-115-10	19.4	-9.6
WK-106-41	16.20	-9.7	MR-115-11	19	-10.2
WK-106-40	16.10	-8.1	MR-115-12	18.6	-10.4
WK-106-37	13.05	-9.2	MR-117-01	16.3	-9.1
WK-106-36	12.90	-9.8	MR-117-02	16	-9.5
WK-106-35	12.70	-10.7	MR-117-03	15.7	-9.5
WK-106-34	12.50	-9.7	MR-117-05	15.1	-9.6
WK-106-33	12.20	-9.6	MR-117-07	14.5	-9.7
WK-106-32	11.80	-10.3	MR-117-09	13.9	-8.8
WK-106-31	11.40	-9.7	MR-117-10	13.6	-10.2
WK-106-30	11.10	-9.7	MR-117-11	13.3	-10.1
WK-106-29	10.90	-9.5	MR-117-12	13	-10
WK-106-28	10.75	-9.8	MR-58-31	12.15	-9.9
WK-106-27	10.50	-8.8	MR-58-30	12.05	-9.5

Table 3.2 (continued)

Sample ID	Profile meter	δ¹³C (‰) PDB	Sample ID	Profile meter	δ¹³C (‰) PDB
WK-106-26	10.50	-8.4	MR-58-29	11.50	-8.9
WK-106-23	9.70	-8.7	MR-58-27	9.95	-9.3
WK-106-22	9.30	-9.6	MR-58-26	9.85	-10.1
WK-106-21	9.00	-9.4	MR-58-25	9.50	-10.2
WK-106-20	8.90	-9.7	MR-58-24	9.10	-9.9
WK-106-19	8.80	-10.2	MR-58-23	8.90	-9.3
WK-106-18	8.00	-10	MR-58-22	8.70	-9.5
WK-106-17	8.10	-9.6	MR-58-21	8.50	-10.2
WK-106-16	7.90	-9.6	MR-58-20	8.20	-9.7
WK-106-15	7.50	-9.8	MR-58-19	7.40	-10.6
WK-106-14	6.30	-9.7	MR-58-18	6.90	-10.5
WK-106-13	5.50	-10.1	MR-58-17	6.40	-10.9
WK-106-12	5.00	-10.1	MR-58-16	5.60	-11.2
WK-106-11	3.80	-9.3	MR-58-15	4.60	-10.1
WK-106-10	3.80	-9.1	MR-58-14	4.39	-11.1
WK-106-03	1.10	-10.4	MR-58-13	4.20	-10.8
WK-106-02	0.50	-10.4	MR-58-12	4.00	-10.8
WK-106-01	0.10	-10.5	MR-58-11	3.80	-10.7
MR-50-28	35.40	-9.2	MR-58-10	3.60	-10.6
MR-50-28	34.90	-8.5	MR-58-09	3.20	-10.9
MR-50-26	34.50	-9.8	MR-58-08	2.80	-10.7
MR-50-25	34.15	-9.1	MR-58-07	2.40	-11.1
MR-50-24	33.85	-8.7	MR-58-06	2.10	-10.6
MR-50-23	33.55	-9	MR-58-05	1.90	-10.6
MR-50-17	30.35	-9.9	MR-58-04	1.35	-11
MR-50-15	29.75	-9.4	MR-58-03	1.20	-10.4
MR-50-14	29.45	-10	MR-58-02	1.05	-10.4
MR-50-13	29.15	-10.2	MR-58-01	0.40	-10.7
MR-50-12	28.95	-8.6			

2.8 to 1.8 Ma

This Lower Pleistocene time interval covers sediments of the hominin bearing sites up to ca. 1.75 Ma. Three profiles in Mwenirondo (12-MR-06 [10°0'55.20"S, 33°55'12.11"E], 11-MR-04 [10°1'3.62"S, 33°55'14.50"E], and 12-MR-19 [10°1'6.98"S, 33°54'48.50"E]) with a total combined thickness of 18.5 m cover large parts of the Unit. Additionally, one section was sampled near the excavation site of *Homo rudolfensis* UR 501 in Uraha (U-84; 10°21'0.20"S, 34°9'22.84"E) and one from the excavation pit of *Paranthropus boisei* RC 911 in Malema (RC-08; 10°0'57.78"S, 33°55'9.46"E). Both sections are correlated to the same age of ca. 2.5 to 2.3 Ma based on fossil evidence (Bromage et al., 1995; Kullmer et al., 1999). The hominin sites in Uraha and Malema are the oldest parts sampled of this unit. No sound correlation of additional profiles that cover the oldest part (ca. 0.3 Ma) of the unit was possible. Calculated average sedimentation rate is ca. 31 m/Ma in this dominantly meandering river and lagoonal system that includes several erosional surfaces and hiatuses (Betzler and Ring, 1995). Profiles RC-08, MR-19, and MR-04 are shown in Figure 3 in Lüdecke and Thiemeyer (2013).

Table 3.3: List of 2.8 to 1.8 Ma (Unit 3A-2) pedogenic nodules from Mwenirondo (MR), Malema (RC), and Uraha (U) with sample ID, section-meter, and $\delta^{13}\text{C}$ values.

Sample ID	Profile meter	$\delta^{13}\text{C}$ (‰) PDB	Sample ID	Profile meter	$\delta^{13}\text{C}$ (‰) PDB
MR-19-01	18.50	-7.3	MR-06-01	1.90	-6.7
MR-19-03	18.30	-8.8	MR-06-02	1.60	-7.3
MR-19-05	18.20	-8.6	MR-06-04	1.00	-8.2
MR-19-07	18.10	-8.5	MR-06-05	0.60	-8.2
MR-19-09	18.00	-7.9	MR-06-06	0.30	-5.8
MR-19-11	17.90	-8.9	MR-06-07	0.00	-7.6
MR-19-13	17.80	-7.4	RC-08-01	2.70	-7.2
MR-19-15	17.70	-8.6	RC-08-02	2.68	-9.1
MR-19-19	17.50	-8.7	RC-08-03	2.65	-7.4
MR-19-21	17.40	-9	RC-08-04	2.60	-9.1
MR-19-23	17.30	-9.3	RC-08-05	2.55	-7.6
MR-19-25	16.90	-9.3	RC-08-06	2.50	-7.4
MR-19-26	16.70	-9.3	RC-08-07	2.45	-7.7
MR-19-37	13.70	-9.4	RC-08-08	2.40	-7.8
MR-19-38	13.60	-9.8	RC-08-09	2.35	-7.6
MR-19-39	13.50	-8.9	RC-08-10	2.30	-7.7
MR-19-40	13.40	-9.7	RC-08-11	2.25	-7.6
MR-19-41	13.30	-9	RC-08-12	2.20	-9.9
MR-19-42	13.20	-8.7	RC-08-13	2.15	-9.4
MR-19-43	13.10	-9.7	RC-08-14	2.10	-8.8
MR-19-44	13.00	-9	RC-08-15	2.05	-8
MR-19-45	12.90	-8.2	RC-08-16	2.00	-7.3
MR-19-46	12.80	-8.7	RC-08-17	1.95	-7.7
MR-19-47	12.70	-8.8	RC-08-18	1.90	-9
MR-19-48	12.60	-9.8	RC-08-19	1.85	-9.2
MR-19-49	12.50	-9.4	RC-08-20	1.80	-9.4
MR-19-50	12.40	-10.3	RC-08-22	1.70	-6.9
MR-19-51	12.30	-10.2	RC-08-23	1.65	-7.9

Table 3.3 (continued)

Sample ID	Profile meter	$\delta^{13}\text{C}$ (‰) PDB	Sample ID	Profile meter	$\delta^{13}\text{C}$ (‰) PDB
MR-19-52	12.20	-9.1	RC-08-24	1.60	-6.6
MR-19-53	12.10	-8.9	RC-08-26	1.50	-9.9
MR-19-54	12.00	-10	RC-08-27	1.45	-10.3
MR-19-55	11.90	-11	RC-08-28	1.40	-8
MR-19-56	11.50	-10.3	RC-08-29	1.35	-7.1
MR-19-57	11.00	-9.9	RC-08-30	1.30	-6.9
MR-04-96	10.85	-6.6	RC-08-31	1.25	-10
MR-04-95	10.55	-7.8	RC-08-32	0.95	-6.6
MR-04-94	10.40	-6.6	RC-08-33	0.90	-9.4
MR-04-93	10.25	-6.4	RC-08-34	0.85	-6.2
MR-04-92	9.90	-7.1	RC-08-35	0.80	-7.1
MR-04-91	9.70	-6.3	RC-08-36	0.75	-6.8
MR-04-90	9.50	-8	RC-08-39	0.60	-7.1
MR-04-89	9.20	-7.6	RC-08-40	0.55	-9.3
MR-04-88	9.10	-5.9	RC-08-41	0.50	-8.2
MR-04-87	8.85	-6.2	RC-08-42	0.45	-8.1
MR-04-86	8.75	-7.9	RC-08-43	0.40	-9.4
MR-04-85	8.50	-8.4	RC-08-44	0.35	-6.6
MR-04-84	8.40	-8.6	RC-08-45	0.30	-8.7
MR-04-83	8.20	-7.6	RC-08-46	0.25	-7.9
MR-04-82	7.95	-7.2	RC-08-47	0.20	-8.2
MR-04-81	7.60	-8	RC-08-48	0.15	-9.3
MR-04-80	7.40	-8.4	RC-08-49	0.10	-9
MR-04-79	7.05	-8.9	RC-08-50	0.05	-9.5
MR-04-77	6.30	-8.1	RC-08-51	0.00	-6.7
MR-04-76	5.80	-8.3	U-84-14	2.70	-7.8
MR-04-75	5.55	-8.9	U-84-13	2.60	-7.8
MR-04-74	5.10	-9.3	U-84-12	2.30	-10
MR-04-72	4.65	-8.1	U-84-11	2.10	-9.7
MR-04-71	4.10	-8.2	U-84-10	1.90	-10.3
MR-04-70	3.60	-8.6	U-84-09	1.70	-9.1
			U-84-08	1.50	-9.3
			U-84-07	1.30	-8.3
			U-84-06	1.10	-8.7
			U-84-05	0.85	-8.5
			U-84-04	0.55	-8.7
			U-84-03	0.40	-8.8
			U-84-02	0.25	-5.9
			U-84-01	0.10	-8.3

<0.6 Ma

This youngest part of the succession is constructed from two sections from Uraha (12-UR-47 [10°0'58.42"S, 33°54'8.20"E] and 12-UR-53 [10°0'44.24"S, 33°53'48.23"E]) with a combined total thickness of 8 m forming Unit 4; correlation due to field relationships is supported by stable isotopic values. The sort and shape of lithic artifacts (Clark et al., 1970) in the overlying Chitimwe Beds suggests a maximum age of the Chiwondo Beds at the onset of the Middle Stone Age (~0.285 Ma; Barham and Smart, 1996; Tryon et al., 2005; Thompson et al., 2012). The average calculated sedimentation rate is ca. 25 m/Ma.

One Chitimwe carbonate nodule was sampled (MR-66 [10°0'30.08"S, 33°53'58.08"E]), in addition to four (sub-)recent nodules from two locations in a river (Ruascho) cut bank (MR-13 [10°1'15.68"S, 33°55'12.59"E] and MR-14 [10°1'2.85"S, 33°55'10.83"E]). Here the position below the recent ground level is given (m). Profile U-47 is shown in Figure 6 in Lüdecke and Thiemeyer (2013).

Table 3.4: List of <0.6 Ma (Unit 4 and Chitimwe Beds) pedogenic nodules from Uraha (U) with sample ID, profile-meter, and $\delta^{13}\text{C}$ values.

Sample ID	Profile meter	$\delta^{13}\text{C}$ (‰) PDB	Sample ID	Profile meter	$\delta^{13}\text{C}$ (‰) PDB
U-53-22	9.30	-11.2	U-47-18	3.60	-9.9
U-53-21	9.00	-9.1	U-47-17	3.40	-10.2
U-53-20	8.80	-6.8	U-47-16	3.20	-9.5
U-53-19	8.60	-9.6	U-47-15	3.00	-9.6
U-53-18	8.40	-8.2	U-47-14	2.80	-8.8
U-53-17	8.20	-9.5	U-47-13	2.60	-9.2
U-53-16	8.00	-10.2	U-47-12	2.45	-9.8
U-53-15	7.80	-8.7	U-47-11	2.30	-10.0
U-53-14	7.60	-10.3	U-47-10	2.10	-9.6
U-53-13	7.40	-9.2	U-47-09	1.90	-9.6
U-53-12	7.20	-8.9	U-47-08	1.70	-9.7
U-53-11	7.00	-9.8	U-47-07	1.50	-9.7
U-53-10	6.80	-9.1	U-47-06	1.30	-9.8
U-53-09	6.60	-8.7	U-47-05	0.80	-10.4
U-53-08	6.40	-8.7	U-47-04	0.60	-10.1
U-53-07	6.20	-8.9	U-47-03	0.40	-10.0
U-53-06	6.00	-10.7	U-47-02	0.20	-9.5
U-53-05	5.80	-8.5	U-47-01	0.00	-9.7
U-53-04	5.60	-8.8	MR-66-1	1.00	-8.2
U-53-03	5.40	-9.5	MR-13-01	0.00	-11.2
U-53-02	5.20	-8.8	MR-13-02	0.40	-9.1
U-53-01	5.00	-11.2	MR-14-01	2.00	-6.8
			MR-15-01	3.00	-9.6

$\delta^{13}\text{C}$ of Plio-Pleistocene (ca. 4 Ma to modern) suid enamel

Table 3.5: List of all suid enamel samples analyzed in this study with Hominid Corridor Research Project (HCRP) catalogue number, $\delta^{13}\text{C}$ values, genera, species, locality (see Fig. 2), FAD, and LAD, using the stratigraphy of White (1995), Kullmer (2008), and Bishop (2010).

Genera	Species	Locality	FAD (Ma)	LAD (Ma)	HCRP catalogue	$\delta^{13}\text{C}_{\text{PDB}}$ (‰)
					129-01	-12.0
<i>Phacochoerus</i>	<i>aethiopicus</i>	RC 1	0.8	Extant	129-02	-9.3
					129-03	-9.1
					129-04	-10.9
<i>Metridiochoerus</i>	<i>compactus</i>	U 25	1.9	0.7	429-01	-10.3
					429-02	-4.4
<i>Metridiochoerus</i>	<i>andrewsi stage III</i>	U 23	1.8	1.7	423-01	-9.3
<i>Metridiochoerus</i>	<i>andrewsi stage I</i>	U 19	2.95	1.8	407-01	-10.3
					407-03	-10.2
					407-04	-10.6
					407-05	-12.3
<i>Notochoerus</i>	<i>scotti</i>	MP 1	3.36	1.8	118-01	-9.2
<i>Notochoerus</i>	<i>scotti</i>	WK 18			253-01	-5.6
<i>Notochoerus</i>	<i>euilus</i>	WK 36	3.9	2.85	498-01	-4.8
<i>Notochoerus</i>	<i>euilus</i>	WK			654-01	-5.5
<i>Notochoerus</i>	<i>jaegeri</i>	U 6	4.3	3.75	457-01	-9.5
<i>Notochoerus</i>	<i>jaegeri</i>	WK 38			546-02	-13.1
					546-01	-10.6

3.9 References

- Andrew, A.R., Bailey, T.E.G., 1910. The Geology of Nyasaland. *J. Geol. Soc.* 66, 189-237.
- Aronson, J.J., Hailemichael, M., Savin, S.M., 2008. Hominid environments at Hadar from paleosol studies in a framework of Ethiopian climate change. *J. Hum. Evol.* 44, 532-550.
- Barham, L.S., Smart, P.L., 1996. An early date for the Middle Stone Age of central Zambia. *J. Hum. Evol.* 30, 287-290.
- Bartholomew, G.A., Bridsell, J.B., 1953. Ecology and the protohominids. *Am. Anthropol.* 55, 481-498.
- Behrensmeyer, A.K., Todd, N.E., Potts, R., McBrinn, G.E., 1997. Late Pliocene faunal turnover in the Turkana Basin, Kenya and Ethiopia. *Science* 278, 1589-1594.
- Betzler, C., Ring, U., 1995. Sedimentology of the Malawi rift: Facies and stratigraphy of the Chiwondo Beds, northern Malawi. *J. Hum. Evol.* 30, 287-290.
- Bibi, F., Souron, A., Bocherens, H., Uno, K., Boisserie, J.-R., 2013. Ecological change in the lower Omo Valley around 2.8 Ma. *Biol. Lett.* 9, 20120890.
- Birkeland, P.W., 1984. *Soils and Geomorphology*. Oxford University Press, New York.
- Bishop, L.C., 2010. *Suoidea*. In: Werdelin, L., Sanders, W.J. (Eds.), *Cenozoic mammals of Africa*. University of California Press, Berkeley, pp. 821-842.
- Bocherens, H., Sandrock, O., Kullmer, O., Schrenk, F., 2011. Hominin paleoecology in Late Pliocene Malawi: First insights from isotopes (¹³C, ¹⁸O) in mammal teeth. *S. Afr. J. Sci.* 107, 1-6.
- Bromage, T.G., Schrenk, F., 1986. A Cercopithecoid Tooth from the Pliocene of Malawi. *J. Hum. Evol.* 15, 497-500.
- Bromage, T.G., Schrenk, F., Juwayeyi, Y.M., 1995a. Paleogeography of the Malawi Rift: age and Vertebrate Paleontology of the Chiwondo Beds, northern Malawi. *J. Hum. Evol.* 28, 37-57.
- Bromage, T.G., Schrenk, F., Zonneveld, F.W., 1995b. Paleoanthropology of the Malawi Rift: an early hominid mandible from the Chiwondo Beds, northern Malawi. *J. Hum. Evol.* 28, 71-108.
- Catuneanu, O., Wopfner, H., Eriksson, P.G., Cairncross, B., Rubidge, B.S., Smith, R.M.H., Hancox, P.J., 2005. The Karoo basins of south-central Africa. *J. Afr. Earth Sci.* 43, 211-253.
- Cerling, T.E., 1984. The stable isotopic composition of modern soil carbonate and its relationship to climate. *Earth Planet. Sci. Lett.* 71, 229-240.
- Cerling, T.E., 1992. Development of grassland and savannas in East Africa during the Neogene. *Palaeogeogr. Palaeoclimatol. Palaeoecol.* 97, 241-247.
- Cerling, T.E., Harris, J.M., 1999. Carbon isotope fractionation between diet and bioapatite in ungulate mammals and implications for ecological and paleoecological studies. *Oecologia* 120, 347-363.
- Cerling, T.E., Hay, R.L., 1986. An isotopic study of paleosol carbonates from Olduvai Gorge. *Quatern. Res.* 25, 63-78.
- Cerling, T.E., Quade, J., 1993. *Stable Carbon and Oxygen Isotopes in Soil Carbonates*. In: Swart, P.K., Lohmann, K.C., McKenzie, J., Savin, S. (Eds.), *Climate Change in Continental Records*. Geoph. Monog. Series 78. American Geophysical Union, Washington, D.C., pp. 217-231
- Cerling, T.E., Bowman, J.R., O'Neil, J.R., 1988. An isotopic study of a fluviallacustrine sequence: the Plio-Pleistocene Koobi Fora sequence, East Africa. *Palaeogeogr. Palaeoclimat. Palaeoecol.* 63, 335-356.
- Cerling, T.E., Harris, J.M., MacFadden, B.J., Leakey, M.G., Quade, J., Eisenmann, V., Ehleringer, J.R., 1997. Global vegetation change through the Miocene/Pliocene boundary. *Nature* 389, 153-159.
- Cerling, T.E., Quade, J., Wang, Y., Bowman, J.R., 1989. Carbon isotopes in soils and paleosols as ecology and paleoecology indicators. *Nature* 341, 138-139.

- Cerling, T.E., Harris, J.M., Leakey, M.G., 2003. *Isotope paleoecology of the Nawata and Nachukui Formations at Lothagam, Turkana Basin, Kenya*. In: Leakey, M.G., Harris, J.M. (Eds.), *Lothagam: The Dawn of Humanity in Eastern Africa*. Columbia University Press, New York, pp. 605-614.
- Cerling, T.E., Levin, N.E., Quade, J., Wynn, J.G., Fox, D.L., Kingston, J.D., Klein, R.G., Brown, F.H., 2010. Comment on the Paleoenvironment of *Ardipithecus ramidus*. *Science* 328, 1105.
- Cerling, T.E., Levin, N.E., Passey, B.H., 2011a. Stable Isotope Ecology in the Omo-Turkana Basin. *Evol. Anthro.* 20, 228-237.
- Cerling, T.E., Wynn, J.G., Andanje, S.A., Bird, M.I., Korir, D.K., Levin, N.E., Mace, W., Macharia, A.N., Quade, J., Remien, C.H., 2011b. Woody cover and hominin environments in the past 6 million years. *Nature* 476, 51-56.
- Cerling, T.E., Manthi, F.K., Mbbua, E.N., Leakey, L.N., Leakey, M.G., Leakey, R.E., Brown, F.H., Grine, F.E., Hart, J.A., Kaleme, P., Roche, H., Uno, K.T., Wood, B.A., 2013. Stable isotope-based reconstructions of Turkana Basin hominins. *Proc. Natl. Acad. Sci. USA* 110, 10501-10506.
- Clark, J.D., Haynes, C.V., Mawby, J.E., Gautier, A., 1970. Interim report on palaeoanthropological investigations in the Lake Malawi Rift. *Quaternaria* 13, 305-354.
- Coates Palgrave, K., Drummond, R.B., Moll, E.J., Coates Palgrave, M., 2002. *Trees of southern Africa*. Struik Publishers, Cape Town.
- Dart, R.A., 1925. *Australopithecus africanus*: The man ape of South Africa. *Nature* 115, 195-199.
- de Heinzelin, J., Clark, J.D., White, T., Hart, W., Renne, P., WoldeGabriel, G., Beyene, Y., Vrba, E., 1999. Environment and Behavior of 2.5-Million-Year-Old Bouri Hominids. *Science* 23, 625-629.
- deMenocal, P.B., 1995. Plio-Pleistocene African climate. *Science* 270, 53-59.
- deMenocal, P.B., 2004. African climate change and faunal evolution during the Pliocene-Pleistocene. *Earth Planet. Sci. Lett.* 220, 3-24.
- Dixey, F., 1927. The Tertiary and Post-Tertiary Lacustrine Sediments of the Nyasan Rift-Valley. *J. Geol. Soc.* 83, 432-442.
- Drapeau, M.S.M., Bobe, R., Wynn, J.G., Campisano, C.J., Dumouchel, L., Geraads, D., 2014. The Omo Mursi Formation: A window into the East African Pliocene. *J. Hum. Evol.* 75, 64-79.
- Ebinger, C.J., Deino, A.L., Tesha, A., Becker, T., Ring, U., 1993. Tectonic controls on rift basin morphology: Evolution of the northern Malawi (Nyasa) rift. *J. Geophys. Res.* 98, 17821-17836.
- Feakins, S.J., Levin, N.E., Liddy, H.M., Sieracki, A., Eglinton, T.I., Bonnefille, R., 2013. Northeast African vegetation change over 12 m.y. *Geol.* 41, 295-298.
- Frost, S.R., Kullmer, O., 2008. Cercopithecidae from the Pliocene Chiwondo beds, Malawi-rift. Cercopithecidae des couches pliocènes de Chiwondo, rift de Malawi. *Geobios* 41, 743-749.
- Hamiel, Y., Baer, G., Kalindekafe, L., Dombola, K., Chindandali, P., 2012. Seismic and aseismic slip evolution and deformation associated with the 2009-2010 northern Malawi earthquake swarm, East African Rift. *Geophys. J. Int.* 191, 898-908.
- Harris, J.M., Cerling, T.E., 2002. Dietary adaptations of extant and Neogene African suids. *J. Zool.* 256, 45-54.
- Hopley, P.J., Latham, A.G., Marshall, J.D., 2006. Paleoenvironments and palaeodiets of mid-Pliocene micromammals from Makapansgat Limeworks, South Africa: a stable isotope and dental microwear approach. *Palaeogeogr. Palaeoclimatol. Palaeoecol.* 233, 235-251.
- Kaufulu, Z.M., Stern, N., 1987. The first stone artifacts to be found in situ within the Plio-Pleistocene Chiwondo Beds in northern Malawi. *J. Hum. Evol.* 16, 729-740.
- Kingston, J.D., 1992. *Stable isotopic evidence for hominid paleoenvironments in East Africa*. Ph.D. Dissertation, Harvard University.

- Kingston, J.D., 2011. *Stable Isotopic Analyses of Laetoli Fossil Herbivores*. In: Harrison, T. (Ed.), *Paleontology and Geology of Laetoli: Human Evolution in Contest, Geology, Geochronology, Paleocology, and Paleoenvironments*, Volume 1. Springer, Dordrecht, pp. 293-328.
- Kingston, J.D., Marino, B.D., Hill, A., 1994. Isotopic Evidence for Neogene Hominid Paleoenvironments in the Kenya Rift Valley. *Science* 264, 955-959.
- Kingston, J.D., Fine Jacobs, B., Hill, A., Deino, A., 2002. Stratigraphy, age and environments of the late Miocene Mpesida Beds, Tugen Hills, Kenya. *J. Hum. Evol.* 42, 95-116.
- Klein, R.G., 1984. *The large mammals of southern Africa: late Pliocene to Recent*. In: Klein, R.G. (Ed.), *South African prehistory and Paleoenvironments*. A.A. Balkema, Rotterdam, pp. 107-146.
- Koch, P.L., Tuross, N., Fogel, M.L., 1997. The Effects of Sample Treatment and Diagenesis on the Isotopic Integrity of Carbonate in Biogenic Hydroxyapatite. *J. Archaeol. Sci.* 24, 417-429.
- Kohn, M.J., 2004. Comment: Tooth enamel mineralization in ungulates: Implications for recovering a primary isotopic time-series, by B.H. Passey and T.E. Cerling 2002. *Geochim. Cosmochim. Acta* 68, 403-405.
- Kohn, M.J., Cerling, T.E., 2002. Stable Isotope Compositions of Biological Apatite. *Rev. Mineral. Geochem.* 48, 455-488.
- Kullmer, O., 2008. The fossil Suidea from the Plio-Pleistocene Chiwondo Beds of Northern Malawi, Africa. *J. Vert. Paleontol.* 28, 208-216.
- Kullmer, O., Sandrock, O., Abel, R., Schrenk, F., Bromage, T.G., Juwayeyi, M., 1999. The first Paranthropus from the Malawi Rift. *J. Hum. Evol.* 37, 121-127.
- Kullmer, O., Sandrock, O., Kupczik, K., Frost, S.R., Volpato, V., Bromage, T.G., Schrenk, F., 2011. New Primate Remains from Mwenirondo, Chiwondo Beds in northern Malawi. *J. Hum. Evol.* 61, 617-623.
- Lee-Thorp, J.A., van der Merwe, N.J., 1987. Carbon isotope analysis of fossil bone apatite. *S. Afr. J. Sci.* 83, 712-715.
- Lee-Thorp, J.A., Sealy, J.C., van der Merwe, N.J., 1989. Stable carbon isotope ratio differences between bone collagen and bone apatite, and their relationship to diet. *J. Archaeol. Sci.* 16, 585-599.
- Levin, N.E., 2013. Compilation of East Africa Soil Carbonate Stable Isotope Data. *EarthChem Library*. <http://dx.doi.org/10.1594/IEDA/100231>.
- Levin, N.E., Quade, J., Simpson, S.W., Semaw, S., Rogers, M., 2004. Isotopic evidence for Plio-Pleistocene environmental change at Gona, Ethiopia. *Earth Planet. Sci. Lett.* 219, 93-110.
- Levin, N.E., Brown, F.H., Behrensmeyer, A.K., Bobe, R., Cerling, T.E., 2011. Paleosol carbonates from the Omo Group: Isotopic records of local and regional environmental change in East Africa. *Palaeogeogr. Palaeoclimatol. Palaeoecol.* 307, 75-89.
- Lloyd, J., Bird, M.I., Vellen, L., Miranda, A.C., Veenendaal, E.M., Djybletey, G., Miranda, H.S., Cook, G., Farquhar, G.D., 2008. Contributions of woody and herbaceous vegetation to tropical savanna ecosystem productivity: a quasi-global estimate. *Tree. Physiol.* 28, 451-468.
- Lüdecke, T., Thiemeyer, H., 2013. *Palaeoenvironmental Characteristics of the Plio-Pleistocene Chiwondo and Chitimwe Beds (N-Malawi)*. In: Runge, J. (Ed.), *New Studies on Former and Recent Landscape Changes in Africa: Palaeoecology of Africa*, Vol. 32. CRC Press, London, pp. 143-161.
- Magill, C.R., Ashley, G.M., Freemann, K.H., 2012a. Ecosystem variability and early human habitats in eastern Africa. *Proc. Natl. Acad. Sci. USA* 110, 1167-1174.
- Magill, C.R., Ashley, G.M., Freemann, K.H., 2012b. Water, plants, and early human habitats in eastern Africa. *Proc. Natl. Acad. Sci. USA* 110, 1175-1180.
- Maslin, M.A., Brierley, C.M., Milner, A.M., Shultz, S., Trauth, M., Wilson, K.E., 2014. East African climate pulses and early human evolution. *Quat. Sci. Rev.* 101, 1-17.

- Morgan, M.E., Kingston, J.D., Marino, B.D., 1994. Carbon isotopic evidence for the emergence of C₄ plants in the Neogene from Pakistan and Kenya. *Nature* 367, 162-165.
- Passey, B.H., Robinson, T.F., Ayliffe, L.K., Cerling, T.E., Sponheimer, M., Dearing, D.M., Roeder, B.L., Ehleringer, J.R., 2005. Carbon isotope fractionation between diet, breath CO₂ and bioapatite in different mammal. *J. Archaeol. Sci.* 32, 1459-1470.
- Passey, B.H., Levin, N.E., Cerling, T.E., Brown, F.H., Eiler, J.M., 2010. High-temperature environments of human evolution in East Africa based on bond ordering in paleosol carbonates. *Proc. Natl. Acad. Sci. USA* 107, 11245-11249.
- Pearcy, R.W., Ehleringer, J.R., 1984. Comparative ecophysiology of C₃ and C₄ plants. *Plant Cell. Environ.* 7, 1-13.
- Plummer, T.W., Bishop, L.C., 1994. Hominid paleoecology at Olduvai Gorge, Tanzania as indicated by antelope remains. *J. Hum. Evol.* 27, 47-75.
- Plummer, T.W., Ditchfield, P.W., Bishop, L.C., Kingston, J.D., Ferraro, J.V., Braun, D.R., Hertel, F., Potts, R., 2009. Oldest evidence of Toolmaking Hominins in a Grassland Dominated Ecosystem. *PLoS One* 4, e7199.
- Potts, R., 1998. Environmental Hypotheses of Hominin Evolution. *Yearb. Phys. Anthropol.* 41, 93-136.
- Pustovoytov, K., 2003. Growth rates of pedogenic carbonates on coarse clasts. *Quatern. Int.* 106-107, 131-140.
- Quade, J., Levin, N., Sileshi, S., Stout, D., Penne, P., Rogers, M., Simpson, S., 2004. Paleoenvironments of the earliest stone toolmakers, Gona, Ethiopia. *Geol. Soc. Am. Bull.* 116, 1529-1544.
- Quinn, R.L., Lepre, C.J., Wright, J.D., Feibel, C.S., 2007. Paleogeographic variations of pedogenic carbonate $\delta^{13}\text{C}$ values from Koobi Fora, Kenya: implications for floral compositions of Plio-Pleistocene hominin environments. *J. Hum. Evol.* 53, 560-573.
- Ring, U., Betzler, C., 1995. Geology of the Malawi Rift: kinematic and tectonosedimentary background to the Chiwondo Beds, northern Malawi. *J. Hum. Evol.* 28, 7-21.
- Ring, U., Betzler, C., Devaux, D., 1992. Normal vs. strike-slip faulting during rift development in East Africa: The Malawi Rift. *Geol.* 20, 1015-1018.
- Sandrock, O., Dauphin, Y., Kullmer, O., Abel, R., Schrenk, F., Denys, C., 1999. Malema: preliminary taphonomic analysis of an African hominid locality. *C.R. Acad. Sci. Paris* 328, 133-139.
- Sandrock, O., Kullmer, O., Schrenk, F., Yuwayeyi, Y.M., Bromage, T.G., 2007. Fauna, taphonomy and ecology of the Plio-Pleistocene Chiwondo Beds, northern Malawi. In: Bobe, R., Alemseged, Z., Behrensmeyer, A.K. (Eds.), *Hominin Environments in the East African Pliocene: an Assessment of the Faunal Evidence*. Springer, Dordrecht, pp. 315-332.
- Sankaran, M., Hanan, N.P., Scholes, R.J., Ratnam, J., Augustine, D.J., Cade, B.S., Gignoux, J., Higgins, S.I., Le Roux, X., Ludwig, F., Ardo, J., Banyikwa, F., Bronn, A., Bucini, G., Caylor, K.K., Coughenour, M.B., Diouf, A., Ekaya, W., Feral, C.J., February, E.C., Frost, P.G.H., Hiernaux, P., Hrabar, H., Metzger, K.L., Prins, H.H.T., Ringrose, S., Sea, W., Tews, J., Worden, J., Zambatis, N., 2005. Determinants of woody cover in African savannas. *Nature* 438, 846-849.
- Schlüter, T., 2008. *Geological Atlas of Africa: With Notes on Stratigraphy, Tectonics, Economic Geology, Geohazards and Geosites of Each Country* 2nd edition. Springer, Berlin.
- Schrenk, F., Bromage, T.G., Betzler, C.G., Ring, U., Juwayeyi, Y.M., 1993. Oldest Homo and Pliocene biogeography of the Malawi Rift. *Nature* 365, 833-836.
- Schrenk, F., Bromage, T.G., Gorthner, A., Sandrock, O., 1995. Paleoecology of the Malawi Rift: vertebrate and invertebrate faunal contexts of the Chiwondo Beds, northern Malawi. *J. Hum. Evol.* 28, 59-70.
- Ségalen, L., Lee-Thorp, J., Cerling, T., 2007. Timing of C₄ grass expansion across sub-Saharan Africa. *J. Hum. Evol.* 53, 549-559.

- Semaw, S., Simpson, S.W., Quade, J., Renne, P.R., Butler, R.F., McIntosh, W.C., Levin, N., Dominguez-Rodrigo, M., Rogers, M.J., 2005. Early Pliocene Hominids from Gona, Ethiopia. *Nature* 433, 301-305.
- Shultz, S., Nelson, E., Dunbar, R.I.M., 2012. Hominin cognitive evolution: identifying patterns and processes in the fossil and archaeological record. *Philos. Trans. R. Soc. B: Biol. Sci.* 367, 2130-2140.
- Sikes, N.E., 1994. Early hominid habitat preferences in East Africa: Paleosol carbon isotopic evidence. *J. Hum. Evol.* 27, 25-45.
- Sikes, N.E., Ashley, G.M., 2007. Stable isotopes of pedogenic carbonates as indicators of paleoecology in the Plio-Pleistocene (upper Bed I), western margin of the Olduvai Basin, Tanzania. *J. Hum. Evol.* 53, 574-594.
- Sikes, N.E., Potts, R., Behrensmeier, A.K., 1999. Early Pleistocene habitat in Member 1 Ologesailie based on paleosol stable isotopes. *J. Hum. Evol.* 37, 721-746.
- Spötl, C., Vennemann, T.W., 2003. Continuous-flow isotope ratio mass spectroscopic analysis of carbon minerals. *Rapid Commun. Mass Spectrom.* 17, 1004-1006.
- Thompson, J.C., Mackay, A., Wright, D.K., Welling, M., Greaves, A., Gomani-Chindebvu, E., Simengwa, D., 2012. Renewed investigations into the Middle Stone Age of Northern Malawi. *Quat. Int.* 270, 129-139.
- Trauth, M.H., Deino, A.L., Bergner, G.N., Strecker, M.R., 2003. East African climate change and orbital forcing during the last 175 kyr BP. *Earth Planet. Sci. Lett.* 206, 297-313.
- Trauth, M.H., Maslin, M.A., Deino, A.L., Strecker, M.R., 2005. Late Cenozoic moisture history of East Africa. *Science* 309, 2051-2053.
- Tryon, C.A., McBrearty, S., Texier, P.-J., 2005. Levallois lithic technology from the Kapthurin formation, Kenya: Acheulian origin and Middle Stone Age diversity. *Afr. Archaeol. Rev.* 22, 199-229.
- Uno, K.T., Cerling, T.E., Harris, J.M., Kunimatsu, Y., Leakey, M.G., Nakatsukasa, M., Nakaya, H., 2011. Late Miocene to Pliocene carbon isotope record of differential diet change among East African herbivores. *Proc. Natl. Acad. Sci.* 108, 6509-6512.
- van Wilgen, B.W., 1997. *Fire in southern African savannas: ecological and atmospheric perspectives*. Witwatersrand University Press, Johannesburg.
- Vrba, E.S., 1983. Turnover-pulses, the Red Queen, and related topics. *Am. J. Sci.* 293, 418-452.
- Vrba, E.S., 1988. *Late Pliocene Climatic Events and Hominid Evolution*. In: Grine, F.E. (Ed.), *Evolutionary history of the "robust" australopithecines*. Aldine Press, New York, pp. 405-426.
- Vrba, E.S., Denton, G.H., Prentice, M.L., 1989. Climatic influences on early hominid behavior. *Ossa* 14, 127-156.
- Wesselman, H.B., 1985. Fossil micromammals as indicators of climatic change about 2.4 Myr ago in the Omo Valley, Ethiopia. *S. Afr. J. Sci.* 81, 260-601.
- White, F., 1983. *The vegetation of Africa Vol. 20: a descriptive memoir to accompany the Unesco/AETFAT/UNSO vegetation map of Africa*. Unesco Natural Resources Research, Paris.
- White, T.D., 1995. *African omnivores: global climatic change and Plio-Pleistocene hominids and suids*. In: Vrba, E.S., Denton, G.H., Partridge, T.C., Burchle, L.H. (Eds.), *Paleoclimate and Evolution, with Emphasis on Human Origins*. Yale University Press, New Haven, pp. 369-384.
- White, T.D., WoldeGabrial, G., Asfaw, B., Ambrose, S., Beyene, Y., Bernor, R.L., Biosserie, J.-R., Currie, B., Gilbert, H., Haile-Selassie, Y., Hart, W.K., Hlusko, L.J., Howell, F.C., Kono, R.T., Lehmann, T., Louchart, A., Lovejoy, C.O., Renne, P.R., Saegusa, H., Vrba, E.S., Wesselman, H., Suwa, G., 2006. Asa Issie, Aramis and the Origin of Australopithecus. *Nature* 440, 883-889.
- Wilson, K.E., Maslin, M.A., Leng, M.L., Kingston, J.D., Deino, A.L., Edgar, R.K., Macky, A.W., 2014. East African lake evidence for Pliocene millennial-scale Climate variability. *Geol.* 42, 955-958.

- WoldeGabriel, G., White, T.D., Suwa, G., Renne, P., de Heinzelin, J., Hart, W.K., Heiken, H., 1994. Ecological and temporal placement of early Pliocene hominids at Aramis, Ethiopia. *Nature* 371, 330-333.
- WoldeGabriel, G., Ambrose, S.H., Baroni, D., Bonnefille, R., Bremond, L., Currie, B., DeGusta, D., Hart, W.K., Murray, A.M., Renne, P.R., Jolly-Saad, M.C., Stewart, K.M., White, T.D., 2009. The Geological, Isotopic, Botanical, Invertebrate, and Lower Vertebrate Surroundings of *Ardipithecus ramidus*. *Science* 326: 65.
- Wynn, J.G., 2000. Paleosols, stable carbon isotopes, and paleoenvironmental interpretations of Kanapoi, Northern Kenya. *J. Hum. Evol.* 39, 411-432.
- Wynn, J.G., 2004. Influence of Plio-Pleistocene aridification on human evolution: evidence from paleosols of the Turkana Basin, Kenya. *Am. J. Phys. Anthropol.* 123, 106-118.
- Wynn, J.G., Bird, M.I., 2008. Environmental controls on the stable carbon isotopic composition of soil organic carbon: Implications for modeling the distribution of C₃ and C₄ plants, *Australia. Tellus B* 60, 604-621.

Chapter 4

Always walk on the bright side of life? Hominin evolution in a wooded and mesic habitat

Abstract *Determining the development of ecosystems is critical for understanding the evolution of their associated fauna. We focus on the Chiwondo and Chitimwe Beds in the Karonga Basin (Malawi Rift), a region inhabited by early hominins (*Homo rudolfensis* and *Paranthropus boisei*) at ca. 2.4 Ma. This was a time of major environmental changes in Eastern Africa and therefore critical for human evolution. In the Eastern Rift, a change from woodlands to open savanna grasslands (Somali-Masai Endemic Zone) was introduced ca. 2.5 Ma ago. In the Malawi Rift (Zambeziyan Savanna) however, closed to open woodland environments remain dominant since at least ca. 4.3 Ma.*

We examine long-term variations in climatic conditions in the Karonga Basin since the Pliocene, using stable oxygen isotope composition ($\delta^{18}\text{O}$) from over 300 soil carbonate samples. $\delta^{18}\text{O}$ of pedogenic carbonate is controlled by soil temperature and $\delta^{18}\text{O}$ values of soil water, which in turn reflect climatic features such as evaporation or seasonality and amount of rainfall. Compared to the Eastern Rift, the analyzed Karonga Basin carbonates show low $\delta^{18}\text{O}$ values between 22‰ and 26‰ with only little variation and no significant long-term trend, indicating overall persistent, relatively mesic climatic patterns since ca. 4.3 Ma. These findings complement the stable carbon isotope ($\delta^{13}\text{C}$) values analyzed from the same material, which reflect persistent C_3 woodland vegetation in this time interval.

The Karonga Basin environmental interpretations differ strongly from paleoecological reconstructions in the Eastern Rift area (Tanzania, Kenya, Ethiopia), where open savanna biomes became dominant since the Early Pleistocene. The appearance of open savanna grasslands is considered a driver of hominin evolution, but despite the differences of ecosystem developments in the Malawi Rift and the Eastern Rift, similar hominins and other large-bodied mammals occurred in both landscapes, pointing to distinct habitat flexibility of this fauna.

4.1 Introduction

Interpretations of habitats occupied by early hominins have always played a key role in the analysis of human evolution patterns. In comparison to carbon isotope systematics, $\delta^{18}\text{O}$ records of pedogenic carbonate have received considerably less attention in East Africa. However, when approached systematically, pedogenic carbonate oxygen isotope data can yield valuable information on climate. Especially if rainfall patterns are the largest influence on climate and vegetation, as it is the case in Eastern Africa, climatic changes are reflected in pedogenic carbonate (Hély et al., 2006). The oxygen isotopic composition of soil carbonates is sensitive to both, soil temperature and the isotopic composition of soil water, and is hence a potential source of paleoclimatic information.

Vegetation reconstructions from pedogenic carbonates in the Karonga Basin (Malawi Rift) show persistent C_3 vegetation during the Plio-Pleistocene in the vicinity of paleolake Malawi during early hominin evolution (see Chapter 3). Here we evaluate the $\delta^{18}\text{O}$ values of these soil carbonates.

4.2 Background

Information about the geologic context of the Chiwondo paleosols, including images of the outcrop conditions, as well as age control and correlation of individual sections can be found in Sections 2.1, 3.2 and 3.8 of this thesis.

4.2.1 *Oxygen isotope ratios in paleosols*

Pedogenic carbonate forms in oxygen isotope equilibrium with soil water (Cerling and Quade, 1993). The $\delta^{18}\text{O}$ value of soil carbonate is a function of soil water composition (Friedman and O'Neil, 1977) and temperature, which is, at shallow depths, similar to air temperature (Brady and Weil, 2007). Soil water is derived from meteoric water, but can differ from local meteoric water due to enrichment through evaporation from the soil surface, mixing with evaporatively ^{18}O -enriched infiltrating water, and addition of isotopically distinct water from overland and vadose zone flow (Cerling and Quade, 1993; Hsieh et al., 1998). Nevertheless, $\delta^{18}\text{O}$ values of modern pedogenic carbonate have a strong positive correlation with the composition of meteoric water, which in turn has a positive correlation with local air temperature (Rozanski et al., 1993). Collectively, this makes paleosol carbonate an important paleoclimate proxy. However, without constraints on paleotemperature or ancient soil water $\delta^{18}\text{O}$ composition, temporal and geographic variations in fossil soil carbonate $\delta^{18}\text{O}$ values can only be used to identify qualitative changes in climatic patterns.

The temperature during pedogenic carbonate growth affects the isotopic composition with ca. $-0.24\text{‰}/^\circ\text{C}$ (Craig, 1965). Here, we assume a soil temperature of 26°C , referring to preliminary clumped isotope data we measured from the same pedogenic carbonate material used for the stable

oxygen and carbon isotope analyses. At this temperature, fractionation between soil water and soil carbonate of ca. 28‰ occurs (after Kim and O'Neil, 1997).

However, in hot and often (semi)arid East African environments, temperature is not the most important factor when comparing EAR climate patterns, which are highly sensitive to changes in precipitation and seasonality. Today, rainfall amount and seasonality exert the major controls on the local vegetation and climate. Hence, variations in $\delta^{18}\text{O}$ values of sampled pedogenic carbonate are primarily the result of fluctuating precipitation amounts, which in turn regulate evaporation of surface water. Evaporation increases $\delta^{18}\text{O}$ values of soil water with respect to $\delta^{18}\text{O}$ values of local precipitation; in semiarid settings akin to much of Eastern Africa, enrichment in ^{18}O of soil water has been widely demonstrated (Hsieh et al., 1998; Quade et al., 2007).

Nevertheless, the composition of local meteoric water has a large influence on $\delta^{18}\text{O}$ of soil water and hence pedogenic carbonate $\delta^{18}\text{O}$. Today, East African climate is a result of interactions between the African Monsoon, the Intertropical Convergence Zone (ITCZ) and the Zaire Air Boundary (ZAB; White et al., 1983; Nicholson, 1996; Leroux, 2001; Hély et al., 2006). These complex patterns complicate the comparison of absolute $\delta^{18}\text{O}$ values of distant localities, due to possibly different isotopic composition of local precipitation. Therefore, we primarily compare general trends in $\delta^{18}\text{O}$ values of the Malawi Rift and Eastern Rift.

Additionally, we correlate stable oxygen isotope values of modern local meteoric water (see Chapter 5) to the values of the fossil soil carbonate to place Plio-Pleistocene climate conditions in the context of recent ones. $\delta^{18}\text{O}$ values in Malawi decrease with ca. -2.8‰/km of elevation (see Section 5.4.3), which reflects the Global Meteoric Water Line (GMWL; Rowley and Garzzone, 2007). However, the sampled pedogenic carbonate is derived from the vicinity of paleolake Malawi at present-day elevations of 537 to 593 m asl and these sediments were already in a similar altitude during the deposition of the Chiwondo and Chitimwe Beds. Therefore the analyzed carbonates all formed at a comparable elevation, which makes a consideration of the altitude effect insignificant when correlating the results through time.

4.2.2 Karonga Basin modern meteoric waters $\delta^{18}\text{O}$ data

$\delta^{18}\text{O}$ of different meteoric water reservoirs (precipitation, river, lake and groundwater) are presented in Chapter 5 and reflect the dependence of $\delta^{18}\text{O}$ values on seasonality, altitude and climate (evaporation).

4.2.3 Eastern Rift pedogenic carbonate $\delta^{18}\text{O}$ data

$\delta^{18}\text{O}$ values of pedogenic carbonate from fossil hominin localities in the Eastern Rift since 7 Ma exist from Hadar and Busidima in the Lower Awash

and Sagantole and Adu-Asa in the Middle Awash Valley (WoldeGabriel et al., 1994; Levin et al., 2004; Quade et al., 2004; Semaw et al., 2005; White et al., 2006; Aronson et al., 2008; WoldeGabriel et al., 2009; Passey et al., 2010; Cerling et al., 2011), Omo-Turkana (Cerling et al., 1988; Cerling et al., 2003; Wynn, 2004; Quinn et al., 2007; Levin et al., 2011), Tugen Hills (Cerling, 1992; Kingston, 1992; Kingston et al., 2002), Kanjera (Plummer et al., 2009), Olorgesailie (Sikes et al., 1999), Olduvai (Cerling and Hay, 1986; Sikes and Ashley, 2007) and Laetoli (Cerling, 1992). A compilation of the data is available at EarthChem Library (Levin, 2013).

4.3 Material and methods

The stable oxygen isotope geochemistry of pedogenic carbonate is a robust tool to deepen our understanding of climatic and hydrological patterns of past environments, in particular when evaporation and precipitation seasonality play a key role in the evolution of the region. $\delta^{18}\text{O}$ values record the long-term, time-averaged pattern of soil water changes, which in turn reflect changes in meteoric water composition. In total, 321 pedogenic carbonates from all units of the Plio-Pleistocene deposits were analyzed, the same proxy material used for $\delta^{13}\text{C}$ analyzes in Chapter 3. For profile and sample position, treatment and analytical procedure see Section 3.3 and 3.9. All analyses were performed at the Goethe University-BiK-F Joint Stable Isotope Facility Frankfurt. Final oxygen isotopic ratios are reported against VSMOW; overall analytical uncertainties are better than 0.04‰.

4.4 Results

We provide a composite pedogenic carbonate $\delta^{18}\text{O}$ record that encompasses the fluvial, deltaic, lacustrine and swamp deposits of northern Malawi based on correlations of individual sections (Fig. 4.1). Age constraints for the individual sections follow Chapter 3.

Throughout the Plio-Pleistocene, the $\delta^{18}\text{O}$ values range between 22.0‰ and 25.8‰ (mean = 24.0‰; σ = 0.8‰; n = 321), indicating no variation or overall trend through time. Generally, the $\delta^{18}\text{O}$ values of soil carbonate are more negative than values derived from Eastern Rift carbonate, which have a mean $\delta^{18}\text{O}$ value of 26.5‰ (σ = 2.7‰; n = 1186; Levin, 2013) and show a trend towards higher values since the Early Pleistocene (see Fig. 4.1). Low isotopic values with only little variation are as well characteristic for the stable carbon isotope record described in Chapter 3; however, the co-variance of the entire dataset is weak (R^2 = 0.14).

4.4.1 Early Pliocene (ca. 4.3 Ma to 3.75 Ma)

$\delta^{18}\text{O}$ values from the Karonga Basin show generally little variations and range between 22.8‰ and 25.1‰ (mean = 24.1‰; σ = 0.5‰; n = 27). Eastern Rift data from a time period of 7.0 Ma to 3.75 Ma document with $\delta^{18}\text{O}$ mean values of 25.5‰ (σ = 2.8‰; n = 157; Levin, 2013) to some extent higher $\delta^{18}\text{O}$

values (see Fig. 4.1; t-test, $t = 6.000$; $df = 182$; $p < 0.05$). The difference of the averages in the stable oxygen isotope record between the Karonga Basin and Eastern Rift, $\Delta(\delta^{18}\text{O})_{\text{KB-ER}}$, equals 1.5‰ (Fig. 4.2b).

4.4.2 3.75 Ma to 2.8 Ma

$\delta^{18}\text{O}$ values of Middle to Late Pliocene pedogenic carbonate from the Karonga Basin occupy a range between 22.0‰ and 25.5‰ with a mean value of 23.5‰ ($\sigma = 0.8\text{‰}$; $n = 27$), indicating a general decrease compared to the older time interval. The Eastern Rift data show a distinct trend towards lower $\delta^{18}\text{O}$ values in the course of this time interval (Fig. 4.2a). However, the average value increases compared to the Late Miocene/Early Pliocene record (mean $\delta^{18}\text{O} = 26.8\text{‰}$; $\sigma = 2.0$; $n = 349$; $t = 16.143$; $df = 465$; $p < 0.05$) The difference between the two datasets is therefore pronounced with $\Delta(\delta^{18}\text{O})_{\text{KB-ER}} = 2.1\text{‰}$.

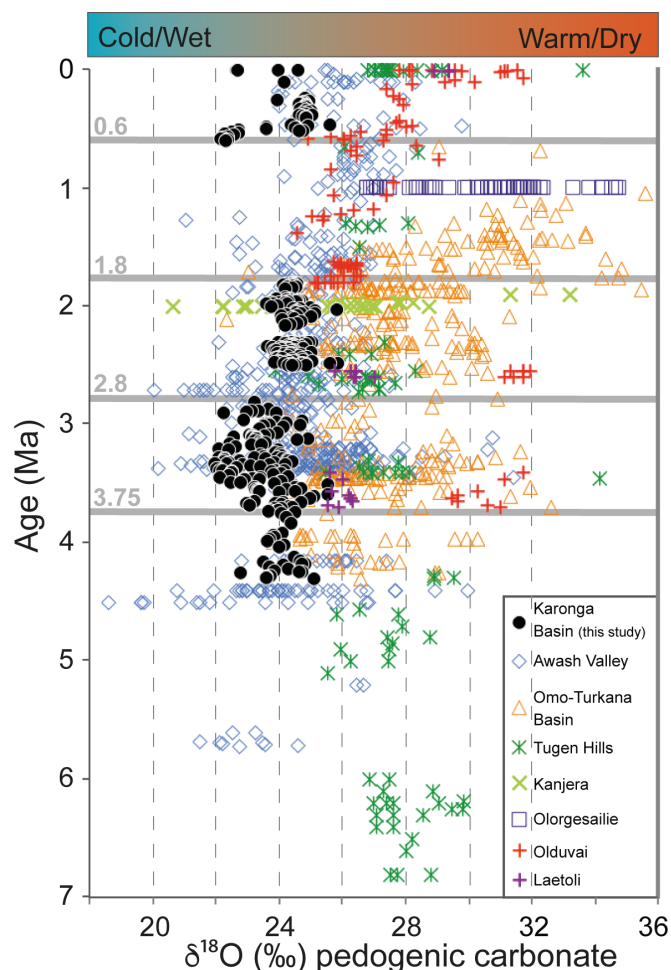


Figure 4.1: $\delta^{18}\text{O}$ values of pedogenic carbonate in the EAR since 7.0 Ma. Filled circles show $\delta^{18}\text{O}$ data from the Karonga Basin (Malawi Rift), open symbols represent the Eastern Rift including Middle and Lower Awash (WoldeGabriel et al., 1994, 2009; Levin et al., 2004; Quade et al., 2004; Semaw et al., 2005; White et al., 2006; Aronson et al., 2008; Passey et al., 2010; Cerling et al., 2011a), Omo-Turkana (Cerling et al., 1988, 2003; Wynn, 2004; Quinn et al., 2007; Levin et al., 2011), Tugen Hills (Cerling, 1992; Kingston et al., 1994, 2002), Kanjera (Plummer et al., 2009), Olorgesailie (Sikes et al., 1999), Olduvai (Cerling and Hay, 1986; Sikes, 1994; Sikes and Ashley, 2007), and Laetoli sites (Cerling, 1992). Note that age assignment for the Karonga Basin is based on the relative position of the sampled intervals within the different unit boundaries (for further information see Section 3.8).

4.4.3 2.8 Ma to 1.8 Ma

During this important time interval for human evolution, pedogenic carbonate $\delta^{18}\text{O}$ values in the Karonga Basin fall again with small fluctuations between 23.6‰ and 25.8‰ (mean = 24.4‰; $\sigma = 0.4\%$; $n = 126$), which is striking considering the high sample density. The Karonga Basin values remain generally lower than stable oxygen isotopic values from the Eastern Rift, which however indicate a slight decrease in $\delta^{18}\text{O}$ with a mean of 26.1‰ ($\sigma = 2.1\%$; $n = 157$; Levin, 2013). The statistical difference between the two datasets is less distinct than in the previous dataset ($t = 13.864$; $df = 382$; $p < 0.05$) with $\Delta(\delta^{18}\text{O})_{\text{KB-ER}} = 1.7\%$.

4.4.4 1.8 Ma to 0.6 Ma

No data from this time interval could be collected in the Karonga Basin. $\delta^{18}\text{O}$ values from Eastern Rift sites generally increase with a mean $\delta^{18}\text{O}$ value of 28.3‰ ($\sigma = 2.9\%$; $n = 259$; Levin, 2013).

4.4.5 <0.6 Ma

Since the Upper Pleistocene, Karonga Basin pedogenic carbonate $\delta^{18}\text{O}$ values remain consistent with those observed in the older time intervals. $\delta^{18}\text{O}$ values range between 22.2‰ and 25.6‰ (mean = 24.1‰; $\sigma = 1.0\%$; $n = 45$). While the mean $\delta^{18}\text{O}$ value of 27.9‰ ($\sigma = 2.3\%$; $n = 90$; Levin, 2013) of pedogenic carbonate from the Eastern Rift is slightly lower than the mean in the older time interval, it remains higher than the overall average. Again, the difference between the two datasets is distinct ($t = 13.249$; $df = 132$; $p < 0.05$) and $\Delta(\delta^{18}\text{O})_{\text{KB-ER}} = 3.9\%$, which documents the largest difference in $\delta^{18}\text{O}$ values when compared to the Karonga Basin (Fig. 4.2b).

4.5 Discussion

Stable carbon isotope data of pedogenic carbonate and mammal enamel from the Karonga Basin (Malawi Rift) allow first reconstructions of Plio-Pleistocene hominin habitats in this southern part of the EAR (see Chapter 3 and Chapter 5). The data suggest persistent C_3 vegetation without large changes in the last ca. 4.3 Ma. The new stable oxygen isotopic evidence supports this interpretation. The small scatter in $\delta^{18}\text{O}$ values indicates little variation in both, precipitation and local evaporative regime, while the overall low values indicate a mesic environment with only little influence of evaporation on soil water.

4.5.1 Correlation of $\delta^{18}\text{O}$ values of Karonga Basin paleosol carbonate with modern meteoric waters

To evaluate aridity and hence evaporative influences during the Plio-Pleistocene in the Karonga Basin, we compare the stable isotope ratios of fossil soil carbonate to the ones of modern meteoric waters displayed in Chapter 5. Precipitation from Karonga Basin shows an average monthly $\delta^{18}\text{O}$

value of -3.4‰ ($\sigma = 2.2\text{‰}$; $n = 45$; Chapter 5). Samples from evaporatively enriched sources are ca. 6‰ more positive, such as near-surface waters of Lake Malawi, which loses about 90% of its annual water budget via evaporation (Drayton, 1984) and has $\delta^{18}\text{O}$ values of $>+2\text{‰}$. Assuming shallow soil temperatures of ca. 26°C (unpublished clumped isotope data), a fractionation between water and carbonate of ca. 28‰ occurs (Kim and O'Neil, 1997), resulting in expected $\delta^{18}\text{O}$ values of $<26\text{‰}$ for carbonates in soils that are only little influenced by evaporation and $>30\text{‰}$ for samples that form in a strongly evaporated environment. Stable oxygen isotope records of pedogenic carbonate from the Chiwondo Beds have constant low values of ca. 24‰ with the most positive $\delta^{18}\text{O}$ values yet lower than 26‰ . These results therefore indicate only very limited influence of evaporation in a mesic habitat in the Karonga Basin during the time of carbonate formation in the Plio-Pleistocene.

However, this approach ignores possible variations in the stable isotope composition of rainwater. Yet, modern pedogenic carbonate also shows low $\delta^{18}\text{O}$ values between 22.7‰ and 24.6‰ (see Section 4.7.5), indicating a similar moisture regime today and during Plio-Pleistocene carbonate formation. These interpretations complement the published stable carbon isotope based vegetation reconstructions which reflect a dominantly C_3 -woodland environment in the vicinity of paleolake Malawi, indicating a relatively humid environment (Chapter 3).

4.5.2 Correlation of $\delta^{18}\text{O}$ values of Karonga Basin paleosol carbonate with Eastern Rift data

$\delta^{18}\text{O}$ values of soil carbonate from the Eastern Rift are in all analyzed time intervals in terms of their mean values at least 1.4‰ more positive than the respective $\delta^{18}\text{O}$ values from the Karonga Basin. This discrepancy is generally larger in younger time intervals (Fig. 4.2b).

While the $\delta^{18}\text{O}$ values of Chiwondo Bed carbonate remain persistent in the last ca. 4.3 Ma, the Eastern Rift values generally increase through time, resulting in their overall largest values in modern times (Fig. 4.2b). This indicates an environment that became more arid and reflects increasing evaporation of soil water, which supports the evolution from woodland environments in the Pliocene to open C_4 -grassland savannas during the Pleistocene in the Somali-Masai ecosystems (see e.g., Ségalen et al., 2007 and references therein). The Malawi Rift environments south of the ITCZ, in contrast, remain wooded with a balanced water regime similar to today.

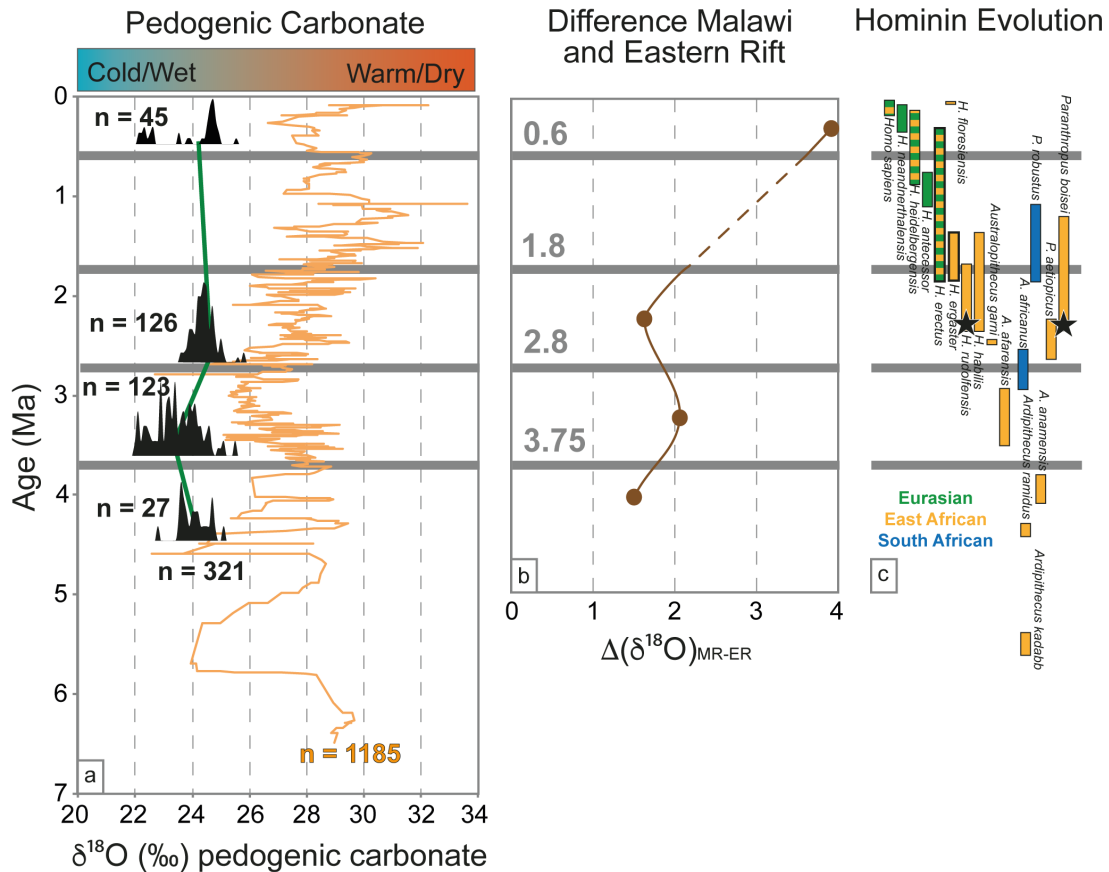


Figure 4.2: a) Composite record of paleosol $\delta^{18}\text{O}$ values from the Karonga Basin in the Malawi Rift (marked in black) presented as normalized probability density function. Lines present overall median of Malawi Rift samples (green) and the 7-point running average for pedogenic carbonate from the Eastern Rift (orange). b) Differences of average $\delta^{18}\text{O}$ values between Karonga Basin and Eastern Rift carbonate. Although the difference is generally not as large as in the carbon stable isotope data (see Fig. 3.6), it is still distinct and becomes more pronounced during the last ca. 2.6 Ma, following the trend of $\delta^{13}\text{C}$ values. c) Hominin evolution transitions after Schultz et al. (2012) and references therein. Stars indicate Karonga Basin hominin fossils.

4.5.3 Co-variance of paleosol carbonate $\delta^{18}\text{O}$ and $\delta^{13}\text{C}$ values

Oxygen and carbon isotopic records should be strongly correlated, if the C_3/C_4 ratio of Karonga Basin vegetation is related to long-term patterns of climate change (Fox and Koch, 2004). While low $\delta^{18}\text{O}$ values correspond to low $\delta^{13}\text{C}$ values, indicating a relatively mesic environment with dominantly C_3 vegetation, the small variations within the two datasets however do not exhibit a co-variance (Fig. 4.3), and the correlation for the entire dataset is weak, although statistically significant ($R^2 = 0.14$). This supports the theory of a persistent climate. The overall relatively little fluctuations within a limited range of $\delta^{18}\text{O}$ and $\delta^{13}\text{C}$ values in both data sets are not the reflection of overall climatic changes, but can be the result of local influences as groundwater composition, soil type or other locality-specific parameters. The $\delta^{18}\text{O}$ - $\delta^{13}\text{C}$ co-variance of pedogenic carbonate of individual Eastern Rift localities is generally significant in the Eastern Rift (e.g., $R^2 = 0.77$ (Olduvai Gorge) and $R^2 = 0.43$ (Laetoli), the two closest hominin study sites; see Levin, 2013).

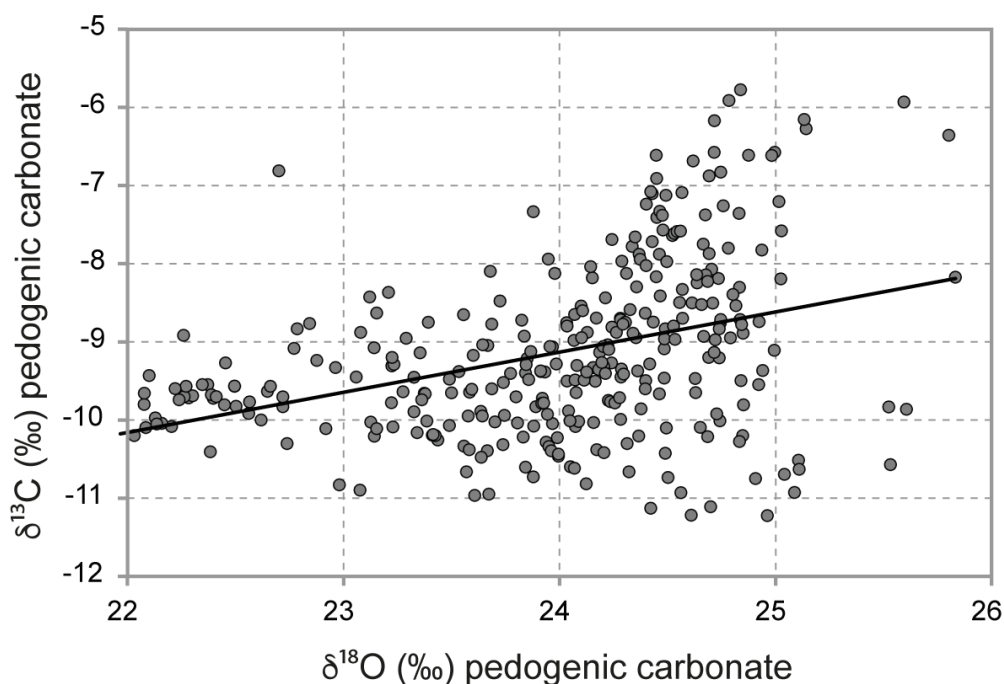


Figure 4.3: $\delta^{18}\text{O}$ vs. $\delta^{13}\text{C}$ values of Karonga Basin soil carbonate show only a weak co-variation ($R^2 = 0.14$) in the generally low values.

4.6 Conclusion

The Karonga Basin in the Malawi Rift had a persistent mesic environment in the Plio-Pleistocene. Soil water was less influenced by evaporation in this southern part of the EAR than the Eastern Rift, probably a consequence of a more humid climate and a higher fraction of woody cover in the Malawi Rift woodland savannas providing more shade. The flora underwent no significant changes and was similar to today's Zambezian Savanna environments, indicating that hominin adaptation is not necessarily linked to the emergence of open landscapes. Since the Plio-Pleistocene, the Karonga Basin is characterized by a C_3 -dominated patchy C_3/C_4 ecosystem. This shows that early hominins (*H. rudolfensis* and *P. boisei*) in the Karonga Basin probably had easier access to freshwater and shelter than in the Eastern Rift throughout the year.

4.7 Supplementary Material

Early Pliocene to 3.75 Ma

This succession is merged from two profiles sampled on the slope of “Uraha Hill”, U-99 (10°21'19.38"S; 34°8'28.97"E) and U-86 (10°21'26.05"S; 34°8'30.72"E). The profiles cover Unit 1 and Unit 2 of the Chiwondo Beds. A schematic stratigraphic column of U-99 is shown in Fig. 2.5 in Chapter 2.

Tab. 4.1: List of ca. 4.3 to 3.75 Ma pedogenic nodules from Uraha (U) with sample ID, profile-meter and $\delta^{18}\text{O}$ values in PDB and SMOW.

Sample ID	Profile meter	$\delta^{18}\text{O}_{\text{PDB}}$ (‰)	$\delta^{18}\text{O}_{\text{SMOW}}$ (‰)	Sample ID	Profile meter	$\delta^{18}\text{O}_{\text{PDB}}$ (‰)	$\delta^{18}\text{O}_{\text{SMOW}}$ (‰)
U-99-23	33.20	-6.6	24.0	U-86-14	7.35	-6.0	24.7
U-99-21	31.20	-6.5	24.2	U-86-13	6.80	-6.6	24.1
U-99-20	28.20	-6.3	24.4	U-86-12	6.00	-7.0	23.7
U-99-15	23.20	-6.6	24.1	U-86-11	4.80	-6.4	24.3
U-99-14	22.20	-6.9	23.8	U-86-10	3.90	-6.8	23.9
U-99-13	21.20	-6.8	23.8	U-86-09	3.70	-6.0	24.7
U-99-12	20.20	-7.0	23.7	U-86-08	3.50	-6.1	24.6
U-99-11	19.20	-7.0	23.6	U-86-07	3.00	-7.9	22.8
U-99-09	17.20	-6.5	24.2	U-86-05	1.20	-7.0	23.7
U-99-08	16.20	-6.7	24.0	U-86-04	1.00	-7.1	23.6
U-99-03	11.20	-6.2	24.5	U-86-03	0.80	-7.1	23.6
U-86-18	9.20	-6.1	24.7	U-86-02	0.60	-7.1	23.6
U-86-17	8.70	-7.2	23.5	U-86-01	0.15	-5.6	25.1
U-86-15	7.75	-5.9	24.8				

3.75 – 2.8 Ma

This upper Pliocene sequence is composed of one profile from the area of Mwimbi (13-WK-106; 10°7.033'S; 33°57.957'E) and four well-correlated profiles near the river Masapa in Mwenirondo (MR-50 [10°0'46.43"S, 33°54'0.65"E], MR-115 [10°0.785'S, 33°53.928'E], MR-117 [10°0.767'S, 33°53.987'E], and MR-58 [10°0'19.90"S, 33°53'57.42"E]). For the most part the Mwimbi and the Mwenirondo sections overlap (correlated with $\delta^{13}\text{C}$ values and field relationships). Again, absolute dating is not possible, but field relationships and the stable isotopic values are strongly pointing towards a filling of the gap between the older group and the hominin sites with an age of ca. 2.4 Ma. Profile MR-58 is shown in Fig. 2.2 in Chapter 2.

Tab. 4.2: List of ca. 3.75 to 2.8 Ma pedogenic nodules from Uraha (U) with sample ID, profile-meter and $\delta^{18}\text{O}$ values in PDB and SMOW.

Sample ID	Profile meter	$\delta^{18}\text{O}_{\text{PDB}}$ (‰)	$\delta^{18}\text{O}_{\text{SMOW}}$ (‰)	Sample ID	Profile meter	$\delta^{18}\text{O}_{\text{PDB}}$ (‰)	$\delta^{18}\text{O}_{\text{SMOW}}$ (‰)
WK-106-71	33.80	-7.5	23.2	MR-50-11	28.55	-7.5	23.1
WK-106-68	31.50	-7.0	23.6	MR-50-10	28.40	-7.4	23.3
WK-106-67	30.60	-7.3	23.4	MR-50-09	28.20	-7.4	23.3
WK-106-66	30.40	-7.5	23.1	MR-50-08	26.95	-7.3	23.4
WK-106-65	30.20	-7.7	23.0	MR-50-07	27.55	-7.4	23.2
WK-106-64	29.80	-6.8	23.9	MR-50-04	26.75	-7.2	23.4
WK-106-63	29.70	-8.4	22.3	MR-50-03	26.45	-7.1	23.6
WK-106-60	25.40	-7.0	23.7	MR-50-02	26.05	-7.5	23.1
WK-106-59	25.30	-6.0	24.7	MR-50-01	25.75	-7.2	23.4
WK-106-58	24.80	-7.2	23.5	MR-115-12	18.60	-6.5	24.2
WK-106-57	24.50	-6.6	24.1	MR-115-11	19.00	-6.8	23.8
WK-106-56	23.70	-7.3	23.4	MR-115-10	19.40	-6.3	24.4
WK-106-54	21.40	-7.1	23.5	MR-115-09	19.80	-6.4	24.3
WK-106-53	20.80	-8.1	22.6	MR-115-08	20.20	-6.4	24.3
WK-106-52	20.00	-5.8	24.9	MR-115-07	20.60	-6.6	24.1
WK-106-51	19.60	-6.1	24.6	MR-115-06	21.00	-6.8	23.9
WK-106-50	18.40	-8.2	22.4	MR-115-05	21.40	-7.2	23.5
WK-106-47	17.20	-8.0	22.6	MR-115-04	21.80	-6.6	24.1
WK-106-43	16.40	-8.5	22.1	MR-115-03	22.20	-7.3	23.4
WK-106-41	16.20	-8.2	22.4	MR-115-02	22.60	-6.6	24.0
WK-106-40	16.10	-6.7	24.0	MR-115-01	23.00	-6.8	23.9
WK-106-37	13.05	-7.4	23.2	MR-117-12	13.00	-7.3	23.4
WK-106-36	12.90	-8.5	22.1	MR-117-11	13.30	-7.5	23.2
WK-106-35	12.70	-7.1	23.6	MR-117-10	13.60	-7.3	23.4
WK-106-34	12.50	-8.4	22.3	MR-117-09	13.90	-6.4	24.3
WK-106-33	12.20	-8.4	22.3	MR-117-07	14.50	-6.9	23.8
WK-106-32	11.80	-7.9	22.7	MR-117-05	15.10	-6.6	24.1
WK-106-31	11.40	-8.4	22.2	MR-117-03	15.70	-6.9	23.7
WK-106-30	11.10	-8.2	22.4	MR-117-02	16.00	-6.5	24.2
WK-106-29	10.90	-8.3	22.3	MR-117-01	16.30	-6.8	23.9
WK-106-28	10.75	-8.7	22.0	MR-58-31	12.15	-6.6	24.0
WK-106-27	10.50	-7.0	23.7	MR-58-30	12.05	-6.6	24.1

Table 4.2 (continued)

Sample ID	Profile meter	$\delta^{18}\text{O}_{\text{PDB}}$ (‰)	$\delta^{18}\text{O}_{\text{SMOW}}$ (‰)	Sample ID	Profile meter	$\delta^{18}\text{O}_{\text{PDB}}$ (‰)	$\delta^{18}\text{O}_{\text{SMOW}}$ (‰)
WK-106-26	10.50	-7.8	22.8	MR-58-29	11.50	-6.8	23.8
WK-106-25	10.20	-7.6	23.1	MR-58-28	11.00	-5.2	25.5
WK-106-23	9.70	-7.3	23.4	MR-58-27	9.95	-7.4	23.2
WK-106-22	9.30	-8.0	22.7	MR-58-26	9.85	-6.2	24.5
WK-106-21	9.00	-8.5	22.1	MR-58-25	9.50	-6.0	24.7
WK-106-20	8.90	-8.5	22.1	MR-58-24	9.10	-7.3	23.3
WK-106-19	8.80	-8.6	22.0	MR-58-23	8.90	-7.4	23.2
WK-106-18	8.00	-8.4	22.2	MR-58-22	8.70	-7.3	23.3
WK-106-17	8.10	-8.5	22.1	MR-58-21	8.50	-7.3	23.3
WK-106-16	7.90	-8.1	22.5	MR-58-20	8.20	-7.3	23.4
WK-106-15	7.50	-8.1	22.5	MR-58-19	7.40	-5.2	25.5
WK-106-14	6.30	-8.2	22.4	MR-58-18	6.90	-5.6	25.1
WK-106-13	5.50	-8.5	22.1	MR-58-17	6.40	-5.6	25.1
WK-106-12	5.00	-7.7	22.9	MR-58-16	5.60	-5.8	25.0
WK-106-11	3.80	-7.9	22.8	MR-58-15	4.60	-7.4	23.2
WK-106-10	3.80	-8.2	22.5	MR-58-14	4.39	-6.0	24.7
WK-106-03	1.10	-6.5	24.2	MR-58-13	4.20	-6.6	24.1
WK-106-02	0.50	-6.2	24.5	MR-58-12	4.00	-7.7	23.0
WK-106-01	0.10	-6.7	24.0	MR-58-11	3.80	-6.8	23.9
MR-50-28	35.40	-7.8	22.9	MR-58-10	3.60	-6.6	24.0
MR-50-28	34.90	-6.0	24.7	MR-58-09	3.20	-7.6	23.1
MR-50-26	34.50	-6.8	23.9	MR-58-08	2.80	-6.4	24.3
MR-50-25	34.15	-6.5	24.2	MR-58-07	2.40	-6.3	24.4
MR-50-24	33.85	-7.1	23.6	MR-58-06	2.10	-6.6	24.1
MR-50-23	33.55	-7.0	23.7	MR-58-05	1.90	-6.8	23.8
MR-50-17	30.35	-6.7	23.9	MR-58-04	1.35	-7.0	23.7
MR-50-15	29.75	-7.6	23.1	MR-58-03	1.20	-6.7	24.0
MR-50-14	29.45	-7.0	23.6	MR-58-02	1.05	-7.0	23.7
MR-50-13	29.15	-7.5	23.1	MR-58-01	0.40	-6.2	24.5
MR-50-12	28.95	-7.5	23.2				

2.8 to 1.8 Ma

This Lower Pleistocene timespan covers the sediments of the hominin bearing sites up to ca. 1.75 Ma. Three profiles in Mwenirondo (12-MR-06 [10°0'55.20"S, 33°55'12.11"E], 11-MR-04 [10°1'3.62"S, 33°55'14.50"E] and 12-MR-19 [10°1'6.98"S, 33°54'48.50"E]) probably cover the whole timespan of this interval. Additionally, a profile was sampled near the excavation site of *homo rudolfensis* UR 501 in Uraha (U-84; 10°21'0.20"S, 34° 9'22.84"E) and one from excavation pit of *Paranthropus boisei* RC 911 in Malema (RC-08; 10°0'57.78"S, 33°55'9.46"E). Both sections are correlated to the same age of ca. 2.5 to 2.3 Ma due to fossil finds (Bromage et al., 1995b; Kullmer et al., 1999). Profile RC-08, MR-19 and MR-04 are shown in Fig. 2.3 in Chapter 2.

Tab. 4.3: List of ca. 2.8 to 1.8 Ma pedogenic nodules from Uraha (U) with sample ID, profile-meter and $\delta^{18}\text{O}$ values in PDB and SMOW.

Sample ID	Profile meter	$\delta^{18}\text{O}_{\text{PDB}}$ (‰)	$\delta^{18}\text{O}_{\text{SMOW}}$ w (‰)	Sample ID	Profile meter	$\delta^{18}\text{O}_{\text{PDB}}$ (‰)	$\delta^{18}\text{O}_{\text{SMOW}}$ (‰)
MR-19-01	18.50	-6.2	24.5	MR-06-01	1.90	-6.1	24.6
MR-19-03	18.30	-6.4	24.2	MR-06-02	1.60	-6.8	23.9
MR-19-05	18.20	-6.3	24.4	MR-06-04	1.00	-5.7	25.0
MR-19-07	18.10	-6.1	24.6	MR-06-05	0.60	-4.9	25.8
MR-19-09	18.00	-6.2	24.5	MR-06-06	0.30	-5.9	24.8
MR-19-11	17.90	-6.6	24.1	MR-06-07	0.00	-5.7	25.0
MR-19-13	17.80	-6.2	24.5	RC-08-01	2.70	-6.2	24.5
MR-19-15	17.70	-6.4	24.3	RC-08-02	2.68	-6.3	24.4
MR-19-19	17.50	-6.3	24.4	RC-08-03	2.65	-6.7	24.0
MR-19-21	17.40	-6.2	24.5	RC-08-04	2.60	-6.0	24.7
MR-19-23	17.30	-6.4	24.2	RC-08-05	2.55	-6.5	24.2
MR-19-25	16.90	-6.3	24.4	RC-08-06	2.50	-6.2	24.5
MR-19-26	16.70	-6.5	24.2	RC-08-07	2.45	-5.9	24.8
MR-19-37	13.70	-6.5	24.2	RC-08-08	2.40	-6.3	24.4
MR-19-38	13.60	-6.8	23.9	RC-08-09	2.35	-6.4	24.3
MR-19-39	13.50	-6.3	24.4	RC-08-10	2.30	-6.2	24.5
MR-19-40	13.40	-6.8	23.9	RC-08-11	2.25	-6.3	24.3
MR-19-41	13.30	-6.5	24.2	RC-08-12	2.20	-6.2	24.5
MR-19-42	13.20	-6.4	24.3	RC-08-13	2.15	-7.0	23.6
MR-19-43	13.10	-6.5	24.2	RC-08-14	2.10	-6.9	23.8
MR-19-44	13.00	-6.0	24.7	RC-08-15	2.05	-6.7	24.0
MR-19-45	12.90	-6.1	24.6	RC-08-16	2.00	-6.4	24.3
MR-19-46	12.80	-6.1	24.6	RC-08-17	1.95	-5.9	24.8
MR-19-47	12.70	-6.2	24.5	RC-08-18	1.90	-6.4	24.2
MR-19-48	12.60	-6.5	24.2	RC-08-19	1.85	-6.6	24.1
MR-19-49	12.50	-6.4	24.3	RC-08-20	1.80	-6.8	23.9
MR-19-50	12.40	-6.9	23.7	RC-08-22	1.70	-6.8	23.9
MR-19-51	12.30	-6.7	24.0	RC-08-23	1.65	-6.2	24.4
MR-19-52	12.20	-6.5	24.2	RC-08-24	1.60	-6.3	24.4
MR-19-53	12.10	-6.4	24.3	RC-08-26	1.50	-5.7	25.0
MR-19-54	12.00	-6.9	23.8	RC-08-27	1.45	-6.3	24.4
MR-19-55	11.90	-7.1	23.6	RC-08-28	1.40	-6.7	23.9

Table 4.3 (continued)

Sample ID	Profile meter	$\delta^{18}\text{O}_{\text{PDB}}$ (‰)	$\delta^{18}\text{O}_{\text{SMOW}}$ (‰)	Sample ID	Profile meter	$\delta^{18}\text{O}_{\text{PDB}}$ (‰)	$\delta^{18}\text{O}_{\text{SMOW}}$ (‰)
MR-19-56	11.50	-6.7	24.0	RC-08-29	1.35	-6.5	24.1
MR-19-57	11.00	-6.9	23.7	RC-08-30	1.30	-6.3	24.4
MR-04-95	10.55	-6.0	24.7	RC-08-32	0.95	-6.7	24.0
MR-04-94	10.40	-6.2	24.4	RC-08-33	0.90	-5.8	24.9
MR-04-93	10.25	-4.9	25.8	RC-08-34	0.85	-6.7	23.9
MR-04-92	9.90	-6.1	24.6	RC-08-35	0.80	-6.0	24.7
MR-04-91	9.70	-5.6	25.1	RC-08-36	0.75	-6.3	24.4
MR-04-90	9.50	-6.2	24.5	RC-08-39	0.60	-6.0	24.7
MR-04-89	9.20	-6.2	24.5	RC-08-40	0.55	-6.2	24.5
MR-04-88	9.10	-5.9	24.8	RC-08-41	0.50	-6.7	24.0
MR-04-87	8.85	-5.6	25.1	RC-08-42	0.45	-6.2	24.4
MR-04-86	8.75	-6.0	24.7	RC-08-43	0.40	-6.4	24.3
MR-04-85	8.50	-6.5	24.2	RC-08-44	0.35	-6.8	23.8
MR-04-84	8.40	-6.6	24.1	RC-08-45	0.30	-6.0	24.7
MR-04-83	8.20	-6.1	24.6	RC-08-46	0.25	-6.5	24.2
MR-04-82	7.95	-5.7	25.0	RC-08-47	0.20	-6.3	24.4
MR-04-81	7.60	-6.3	24.4	RC-08-48	0.15	-6.0	24.7
MR-04-80	7.40	-6.2	24.5	RC-08-49	0.10	-6.4	24.3
MR-04-79	7.05	-6.6	24.1	RC-08-50	0.05	-6.2	24.5
MR-04-77	6.30	-6.0	24.7	RC-08-51	0.00	-6.3	24.4
MR-04-76	5.80	-6.1	24.6	U-84-14	2.70	-5.9	24.8
MR-04-75	5.55	-6.4	24.3	U-84-13	2.60	-5.8	24.9
MR-04-74	5.10	-6.5	24.2	U-84-12	2.30	-6.4	24.3
MR-04-72	4.65	-6.0	24.7	U-84-11	2.10	-6.2	24.5
MR-04-71	4.10	-6.0	24.7	U-84-10	1.90	-6.4	24.3
MR-04-70	3.60	-6.6	24.1	U-84-09	1.70	-6.2	24.5
				U-84-08	1.50	-6.5	24.2
				U-84-07	1.30	-6.3	24.4
				U-84-06	1.10	-6.4	24.3
				U-84-05	0.85	-6.6	24.1
				U-84-04	0.55	-6.4	24.3
				U-84-03	0.40	-6.7	24.0
				U-84-02	0.25	-5.1	25.6
				U-84-01	0.10	-5.9	24.8

<0.6 Ma

This youngest part of the succession is constructed from two profile from Uraha (12-UR-47 [10°0'58.42"S, 33°54'8.20"E] and 12-UR-53 [10°0'44.24"S, 33°53'48.23"E]); correlation due to field relationships and stable isotopic values. One sample of Chitimwe nodule was sampled (MR-66 [10°0'30.08"S, 33°53'58.08"E]) in addition to four (sub-)recent nodules from two locations in the cut bank of Ruasho (MR-13 [10°1'15.68"S, 33°55'12.59"E], MR-14 [10°1'2.85"S, 33°55'10.83"E]). Here the position below the recent ground level is given (m). Profile U-47 is shown in Fig. 2.6 in Chapter 2.

Tab. 4.4: List of <0.6 Ma pedogenic nodules from Uraha (U) with sample ID, profile-meter and $\delta^{18}\text{O}$ values in PDB and SMOW.

Sample ID	Profile meter	$\delta^{18}\text{O}_{\text{PDB}}$ (‰)	$\delta^{18}\text{O}_{\text{SMOW}}$ (‰)	Sample ID	Profile meter	$\delta^{18}\text{O}_{\text{PDB}}$ (‰)	$\delta^{18}\text{O}_{\text{SMOW}}$ (‰)
U-53-22	9.30	-5.9	24.8	U-47-18	3.60	-5.1	25.6
U-53-21	9.00	-6.7	23.9	U-47-17	3.40	-6.3	24.4
U-53-20	8.80	-5.8	24.9	U-47-16	3.20	-5.8	24.9
U-53-19	8.60	-5.9	24.8	U-47-15	3.00	-7.1	23.6
U-53-18	8.40	-6.0	24.7	U-47-14	2.80	-6.2	24.5
U-53-17	8.20	-6.0	24.7	U-47-13	2.60	-7.1	23.6
U-53-16	8.00	-6.1	24.6	U-47-12	2.45	-7.9	22.7
U-53-15	7.80	-5.9	24.8	U-47-11	2.30	-6.0	24.7
U-53-14	7.60	-5.9	24.8	U-47-10	2.10	-6.1	24.6
U-53-13	7.40	-5.9	24.8	U-47-09	1.90	-8.1	22.5
U-53-12	7.20	-6.0	24.7	U-47-08	1.70	-7.9	22.7
U-53-11	7.00	-6.0	24.7	U-47-07	1.50	-8.3	22.3
U-53-10	6.80	-5.9	24.9	U-47-06	1.30	-8.1	22.6
U-53-09	6.60	-5.7	25.0	U-47-05	0.80	-8.3	22.4
U-53-08	6.40	-5.8	24.9	U-47-04	0.60	-8.4	22.2
U-53-07	6.20	-6.0	24.7	U-47-03	0.40	-8.5	22.2
U-53-06	6.00	-5.9	24.8	U-47-02	0.20	-8.3	22.4
U-53-05	5.80	-5.7	25.0	U-47-01	0.00	-8.3	22.3
U-53-04	5.60	-6.1	24.6	MR-66-1	1.00	-6.5	24.2
U-53-03	5.40	-6.0	24.7	MR-13-01	0.00	-6.1	24.6
U-53-02	5.20	-5.9	24.8	MR-13-02	0.40	-6.7	24.0
U-53-01	5.00	-5.9	24.8	MR-14-01	2.00	-7.9	22.7
				MR-15-01	3.00	-8.0	22.6

4.8 References

- Aronson, J.L., Hailemichael, M., Savin, S.M., 2008. Hominid Environments at Hadar from Paleosol Studies in a Framework of Ethiopian Climate Change. *Journal of Human Evolution* 55, 532-550.
- Betzler, C., Ring, U., 1995. Sedimentology of the Malawi Rift: Facies and Stratigraphy of the Chiwondo Beds, Northern Malawi. *Journal of Human Evolution* 28, 13.
- Brady, N.C., Weil, R.R., 2007. *The Nature and Properties of Soils*, 14 ed. Prentice Hall, Upper Saddle River, NJ.
- Bromage, T.G., Schrenk, F., Zonneveld, F.W., 1995. Paleoanthropology of the Malawi Rift: An Early Hominid Mandible from the Chiwondo Beds, Northern Malawi. *Journal of Human Evolution* 28, 71-108.
- Cerling, T.E., 1992. Use of Carbon Isotopes in Paleosols as an Indicator of the p(CO₂) of the Paleatmosphere. *Global Biogeochemical Cycles* 6, 8.
- Cerling, T.E., Bowman, J.R., O'Neil, J.R., 1988. An Isotopic Study of a Fluvial-Lacustrine Sequence: The Plio-Pleistocene Koobi Fora Sequence, East Africa. *Palaeogeography, Palaeoclimatology, Palaeoecology* 63, 22.
- Cerling, T.E., Harris, J.M., Leakey, M.G., 2003. *Isotope Paleocology of the Nawata and Nachukui Formations at Lothagam, Turkana Basin, Kenya*. In: Leakey, M.G and Harris, J.M. (Eds.), *Lothagam: The Dawn of Humanity in Eastern Africa*. Columbia University Press, New York, 583-604.
- Cerling, T.E., Hay, R.L., 1986. An Isotopic Study of Paleosol Carbonates from Olduvai Gorge. *Quaternary Research* 25, 16.
- Cerling, T.E., Levin, N.E., Passey, B.H., 2011. Stable Isotope Ecology in the Omo-Turkana Basin. *Evolutionary anthropology* 20, 228-237.
- Cerling, T.E., Quade, J., 1993. Stable Carbon and Oxygen Isotopes in Soil Carbonates. *Geophysical Monograph* 78, 15.
- Clark, J.D., Haynes, C.V., Mayby, J.E., Gautier, A., 1970. Interim Report on Palaeoanthropological Investigations in the Lake Malawi Rift. *Quaternaria* 13, 49.
- Craig, H., 1965. *The Measurements of Oxygen Isotope Paleotemperatures*. In: Tongiorgi, E. (Ed.), *Stable Isotopes in Oceanographic Studies and Paleotemperatures*. Consiglio Nazionale delle Ricerche, Laboratorio di Geologia Nucleare, Pisa, Italy, pp. 3-24.
- Drayton, R.S., 1984. Variations in the Level of Lake Malawi. *Hydrological Sciences Journal* 29, 1-12.
- Fox, D.L., Koch, P.L., 2004. Carbon and Oxygen Isotopic Variability in Neogene Paleosol Carbonates: Constraints on the Evolution of the C4-Grasslands of the Great Plains, USA. *Palaeogeography, Palaeoclimatology, Palaeoecology* 207, 305-329.
- Friedman, I., O'Neil, J.R., 1977. *Compilation of Stable Isotope Fractionation Factors of Geochemical Interest*. Professional Paper, pp. 1-11.
- Hély, C., Bremond, L., Alleaume, S., Smith, B., Sykes, M.T., Guiot, J., 2006. Sensitivity of African Biomes to Changes in the Precipitation Regime. *Global Ecology and Biogeography* 15, 258-270.
- Hsieh, J.C.C., Chadwick, O.A., Kelly, E.F., Savin, S.M., 1998. Oxygen Isotopic Composition of Soil Water: Quantifying Evaporation and Transpiration. *Geoderma* 82, 269-293.
- Kaufulu, Z.M., Stern, N., 1987. The First Stone Artefacts to Be Found in Situ within the Plio-Pleistocene Chiwondo Beds in Northern Malawi. *Journal of Human Evolution* 16, 12.
- Kim, S.-T., O'Neil, J.R., 1997. Equilibrium and Nonequilibrium Oxygen Isotope Effects in Synthetic Carbonates. *Geochimica et Cosmochimica Acta* 61, 3461-3475.
- Kingston, J.D., 1992. *Stable Isotopic Evidence for Hominid Paleoenvironments in East Africa*. Dissertation, Harvard University.

- Kingston, J.D., Fine Jacobs, B., Hill, A., Deino, A., 2002. Stratigraphy, Age and Environments of the Late Miocene Mpesida Beds, Tugen Hills, Kenya. *Journal of Human Evolution* 42, 95-116.
- Kullmer, O., 2008. The Fossil Suidae from the Plio-Pleistocene Chiwondo Beds of Northern Malawi, Africa. *Journal of Vertebrate Paleontology* 28, 9.
- Leroux, M., 2001. The Meteorology and Climate of Tropical Africa. Springer, Praxis Publishing, London.
- Levin, N.E., 2013. *Compilation of East Africa Soil Carbonate Stable Isotope Data*. EarthChem Library.
- Levin, N.E., Brown, F.H., Behrensmeyer, A.K., Bobe, R., Cerling, T.E., 2011. Paleosol Carbonates from the Omo Group: Isotopic Records of Local and Regional Environmental Change in East Africa. *Palaeogeography, Palaeoclimatology, Palaeoecology* 307, 75-89.
- Levin, N.E., Quade, J., Simpson, S.W., Semaw, S., Rogers, M., 2004. Isotopic Evidence for Plio-Pleistocene Environmental Change at Gona, Ethiopia. *Earth and Planetary Science Letters* 219, 93-110.
- Nicholson, S.E., 1996. *A Review of Climate Dynamics and Climate Variability in Eastern Africa*. In: Johnson, T.C., Odada, E.O. (Eds.), *The Limnology, Climatology and Paleoclimatology of the East African Lakes*. Gordon and Breach, Amsterdam, pp. 22-56.
- Passey, B.H., Levin, N.E., Cerling, T.E., Brown, F.H., Eiler, J.M., 2010. High-Temperature Environments of Human Evolution in East Africa Based on Bond Ordering in Paleosol Carbonates. *Proceedings of the National Academy of Sciences of the United States of America* 107, 11245-11249.
- Plummer, T.W., Ditchfield, P.W., Bishop, L.C., Kingston, J.D., Ferraro, J.V., Braun, D.R., Hertel, F., Potts, R., 2009. Oldest Evidence of Tool Making Hominins in a Grassland-Dominated Ecosystem. *PloS one* 4, e7199.
- Quade, J., Garzzone, C., Eiler, J., 2007. Paleoelevation Reconstruction Using Pedogenic Carbonates. *Reviews in Mineralogy and Geochemistry* 66, 53-87.
- Quade, J., Levin, N., Semaw, S., Stout, D., Renne, P., Rogers, M., Simpson, S., 2004. Paleoenvironments of the Earliest Stone Toolmakers, Gona, Ethiopia. *Geological Society of America Bulletin* 116, 1529.
- Quinn, R.L., Lepre, C.J., Wright, J.D., Feibel, C.S., 2007. Paleogeographic Variations of Pedogenic Carbonate $\Delta^{13}C$ Values from Koobi Fora, Kenya: Implications for Floral Compositions of Plio-Pleistocene Hominin Environments. *Journal of Human Evolution* 53, 560-573.
- Rowley, D.B., Garzzone, C.N., 2007. Stable Isotope-Based Paleoelevation. *Annual Review of Earth and Planetary Sciences* 35, 463-508.
- Rozanski, K., Araguás-Araguás, L., Gonfiantini, R., 1993. Isotopic Patterns in Modern Global Precipitation, Climate Change in Continental Isotopic Records. *American Geophysical Union*, pp. 1-36.
- Sandrock, O., Dauphin, Y., Kullmer, O., Abel, R., Schrenk, F., Denys, C., 1999. Malema: Preliminary Taphonomic Analysis of an African Hominid Locality. *Earth and Planetary Sciences* 328, 7.
- Segalen, L., Lee-Thorp, J.A., Cerling, T., 2007. Timing of C_4 Grass Expansion across Sub-Saharan Africa. *Journal of Human Evolution* 53, 549-559.
- Semaw, S., Simpson, S.W., Quade, J., Renne, P.R., Butler, R.F., McIntosh, W.C., Levin, N., Dominguez-Rodrigo, M., Rogers, M.J., 2005. Early Pliocene Hominids from Gona, Ethiopia. *Nature* 433, 301-305.
- Sikes, N.E., Ashley, G.M., 2007. Stable Isotopes of Pedogenic Carbonates as Indicators of Paleoecology in the Plio-Pleistocene (Upper Bed I), Western Margin of the Olduvai Basin, Tanzania. *Journal of Human Evolution* 53, 574-594.

- Sikes, N.E., Potts, R., Behrensmeyer, A.K., 1999. Early Pleistocene Habitat in Member 1 Ologesailie Based on Paleosol Stable Isotopes. *Journal of Human Evolution* 37, 26.
- White, F., 1983. *The Vegetation of Africa: A Descriptive Memoir to Accompany the Unesco/Aetfat/Unso Vegetation Map of Africa*. Unesco.
- White, T.D., WoldeGabriel, G., Asfaw, B., Ambrose, S., Beyene, Y., Bernor, R.L., Boisserie, J.R., Currie, B., Gilbert, H., Haile-Selassie, Y., Hart, W.K., Hlusko, L.J., Howell, F.C., Kono, R.T., Lehmann, T., Louchart, A., Lovejoy, C.O., Renne, P.R., Saegusa, H., Vrba, E.S., Wesselman, H., Suwa, G., 2006. Asa Issie, Aramis and the Origin of Australopithecus. *Nature* 440, 883-889.
- WoldeGabriel, G., Ambrose, S.H., Barboni, D., Bonnefille, R., Bremond, L., Currie, B., DeGusta, D., Hart, W.K., Murray, A.M., Renne, P.R., Jolly-Saad, M.C., Stewart, K.M., White, T.D., 2009. The Geological, Isotopic, Botanical, Invertebrate, and Lower Vertebrate Surroundings of Ardipithecus Ramidus. *Science* 326, 65-65, 65e61-65e65.
- WoldeGabriel, G., White, T.D., Suwa, G., Renne, P., de Heinzelin, J., Hart, W.K., Heiken, G., 1994. Ecological and Temporal Placement of Early Pliocene Hominids at Aramis, Ethiopia. *Nature* 371, 330-333.
- Wynn, J.G., 2004. Influence of Plio-Pleistocene Aridification on Human Evolution: Evidence from Paleosols of the Turkana Basin, Kenya. *American Journal of Physical Anthropology* 123, 106-118.

Chapter 5

Stable isotope dietary reconstructions of herbivore enamel reveal heterogeneous wooded savanna ecosystems in the Plio-Pleistocene Malawi Rift

Tina Lüdecke^{a,b,*}, Andreas Mulch^{a,b}, Ottmar Kullmer^c, Oliver Sandrock^d
Heinrich Thiemeyer^e, , Jens Fiebig^{a,b}, Friedemann Schrenk^{c,f},

^aSenckenberg Biodiversity and Climate Research Centre, Frankfurt, Germany

^bInstitute of Geosciences, Goethe University Frankfurt, Germany

^cSenckenberg Research Institute and Natural History Museum Frankfurt, Senckenberganlage 25, 60325 Frankfurt, Germany

^dEarth- and Life History, Hessisches Landesmuseum Darmstadt, Germany

^eInstitute of Physical Geography, Goethe University Frankfurt, Germany

^fInstitute for Ecology, Evolution, and Diversity, Goethe University Frankfurt, Germany

Submitted to Palaeogeography, Palaeoclimatology, Palaeoecology.

Manuscript number: PALAEO9150

Abstract *The Plio-Pleistocene expansion of Eastern Africa savanna ecosystems was a major driver for morphological and behavioral innovations in hominin evolution. Most evidence for hominin ecosystem reconstructions originates from the Eastern Rift in today's Somali-Masai Endemic Zone. Here, we provide stable carbon ($\delta^{13}\text{C}$) and oxygen ($\delta^{18}\text{O}$) isotope data from bovids, equids, suids, hippopotamids and elephants of the southern part of the East African Rift supplemented by $\delta^{18}\text{O}$ values of meteoric water. The Karonga Basin in Malawi hosts remains of *Homo rudolfensis* and *Paranthropus boisei*. It is situated between the hominin-bearing sites of Eastern and Southern Africa and therefore fills an important geographical gap for hominin evolution.*

Tooth enamel $\delta^{13}\text{C}$ and $\delta^{18}\text{O}$ data of 14 large-bodied mammalian herbivore genera from Units 2 and 3 (ca. 4.3 to 0.6 Ma) in the Chiwondo Beds provide information about foraging strategies and vegetation patterns. Our stable isotope data are consistent with extensive C_3 -dominated ecosystems that permitted access to open C_4 -environments for migratory mammals. Many analyzed taxa show evidence for mixed diets with high abundances of C_3 biomass consumption; only select bovids were specialized grazers.

$\delta^{18}\text{O}$ of present-day meteoric water reflects seasonality, altitude and lake evaporation. $\delta^{18}\text{O}$ values of Karonga Basin herbivore enamel are generally low and cover values similar to present-day drinking water, indicating both, evaporated as well as freshwater sources. Comparison of $\delta^{13}\text{C}$ values from the Karonga Basin with other Eastern African herbivore communities reveals significant differences in dietary patterns with much more generalized mixed

C₃/C₄, and pure C₃ feeding behaviors in the Malawi Rift. Similarly, enamel $\delta^{18}\text{O}$ values are lower than in most Plio-Pleistocene Eastern African herbivores, suggesting more humid conditions. Collectively, our data support models in which early hominin foraging activity included access to forest and woodland biomes, complicating traditional interpretations linking early human evolutionary innovations to a shift towards savanna habitats.

Keywords *East Africa, Paleoecology, Hominin evolution, Herbivore diet, Plio-Pleistocene, Malawi.*

5.1 Introduction

Africa's present-day ecosystems are very diverse ranging from tropical rainforests to hyper-arid subtropical deserts. Reconstructing the disparate and highly dynamic evolutionary history of these environments since the Pliocene is a key element in understanding the impact of climatic and faunal change on early hominin evolution (e.g., Ségalen et al., 2007; Cerling et al., 2011b). Of particular importance in this context are the emergence of open grassland savannas and the development of C₄ grass biomes.

Today, the East African Rift (EAR), a key region of early hominin evolution, comprises two savanna vegetation zones: the Somali-Masai Endemic Zone in the Eastern Rift (Ethiopia, Kenya and Tanzania) and the Zambezian Savanna in the Malawi Rift (Malawi and Mozambique), the southernmost part of the EAR (White et al., 1983). The environmental history of Eastern Rift ecosystems is intensely studied, using traditional ecological features of fauna and flora and/or geochemical proxies with a strong regional focus on early hominin sites in Ethiopia, Kenya and Tanzania (e.g., Wessellmann, 1985; Cerling and Hay, 1986; Cerling et al., 1988; Cerling, 1992; Kingston et al., 1994; Morgan et al., 1994; Plummer and Bishop, 1994; Sikes, 1994; deMenocal, 1995; Behrensmeyer et al., 1997; Kappelman et al., 1997; Heinzelin et al., 1999; Plummer et al., 1999; Sikes et al., 1999; Wynn, 2000; Harris and Cerling, 2002; Cerling et al., 2003; Trauth et al., 2003; deMenocal, 2004; Levin et al., 2004; Semaw et al., 2005; Trauth et al., 2005; White et al., 2006; Quinn et al., 2007; Ségalen et al., 2007; Sikes and Ashley, 2007; Aronson et al., 2008; WoldeGabriel et al., 2009; Cerling et al., 2011a; Cerling et al., 2011b; Kingston, 2011; Levin et al., 2011; Uno et al., 2011; Bibi et al., 2013; Cerling et al., 2013; Feakins et al., 2013; Magill et al., 2013a, b; Wilson et al., 2014; Bibi and Kiessling, 2015). Collectively, these studies indicate high variability and recurrent shifts in climate state, which resulted in the transition from a C₃-dominated ecosystem to C₄-dominated open grassland savannas with woody cover typically below 50%, at some important hominin localities even less than 10% (Cerling et al., 2011b). This expansion of C₄-dominated environments started in the Late Pliocene and Early Pleistocene and resulted in the open grassland environment typical of the Somali-Masai Endemic Zone today (Fig. 5.1a). Many of the modern climate-evolution hypotheses on human evolution are based on the ensemble of these paleoclimatic records and fossil

discoveries and include temporal and causal relationships among changes in climate, faunal diversity and adaptation.

In contrast, there is increasing evidence that the southern part of the EAR, which inhabits some of the earliest remains of the genera *Homo* (Schrenk et al., 1993; Bromage et al., 1995; Kullmer et al., 2011) and *Paranthropus* (Kullmer et al., 1999) differed significantly in ecosystem composition when compared to the Eastern Branch of the rift (Lüdecke et al., 2016). Consistently low carbon isotope ($\delta^{13}\text{C}$) values from pedogenic carbonate and suid enamel indicate a C_3 -dominated woody environment in the Zambezian Savanna of the Northern Malawi Rift over the last ca. 4.3 Ma. With 60% to 70%, the reconstructed overall fraction of woody cover based on $\delta^{13}\text{C}$ values of pedogenic carbonates points to a significantly higher canopy cover in the Karonga Basin (Malawi Rift) than in the Eastern Rift throughout the Plio-Pleistocene (Lüdecke et al., 2016). This discrepancy between the two savanna types has been amplified since ca. 2.5 Ma when the Somali-Masai ecosystem started to show clear evidence for open grassland environments (e.g., Ségalen et al., 2007).

Here we investigate the evolution of the C_3 -dominated ecosystem in the Karonga Basin (southern Rift, Northern Malawi) with respect to mammalian feeding strategies and the homogeneity of the ecosystem through comparison of browsers and grazers by using stable carbon ($\delta^{13}\text{C}$) and oxygen ($\delta^{18}\text{O}$) isotope values of dental enamel from suids, equids and bovids.

Mixed-feeding omnivores (*Suidae sp.*) in the Southern Rift show $\delta^{13}\text{C}$ values characteristic of strongly C_3 -dominated biomass consumption, well in line with the results of $\delta^{13}\text{C}$ data of pedogenic carbonate (Lüdecke et al., 2016). The fossil vertebrate faunal assemblage from the Chiwondo Beds, however, is heavily biased towards large-bodied terrestrial mammals, the majority being ungulates known to rely on short-grass plains (Sandrock et al., 2007). Based on modern bovid representation in African game parks, the Plio-Pleistocene Karonga Basin faunal assemblage shows a taxon composition similar to today's Somali-Masai and Zambezian ecozones (Sandrock et al., 2007). Among the different faunal groups equids are also well represented (~15%). They are the earliest mammals to fully exploit the C_4 dietary resource, attaining predominantly C_4 -grazing diet by 7 Ma and therefore are typical inhabitants of C_4 -grassland savannas (Uno et al., 2011; Cerling et al., 2015). The large number of C_4 -specialized grazers in a C_3 -dominated ecosystem is striking and seems contradictory to a model of a C_3 -dominated woody ecosystem. The new enamel $\delta^{13}\text{C}$ and $\delta^{18}\text{O}$ data presented here show that a) C_4 resources were present within the herbivore grazing ranges and b) that these herbivores had mixed feeding dietary preferences in the Southern Rift with a higher fraction of C_3 -consumption compared to other parts of Africa.

5.2 Background

5.2.1 Sampling localities

The analyzed fossil mammal teeth originate from the Plio-Pleistocene Chiwondo Beds, in the southern part of the western branch of the EAR (Karonga Basin, Malawi Rift; Fig. 5.1). These locally folded, tilted and colluvially translocated sediments range from lake and aeolian to alluvial deposits (Betzler and Ring, 1995; Hamiel et al., 2012). Absence of directly datable volcanic markers (Kaufulu and Stern, 1987; Betzler and Ring, 1995) requires internal and external biostratigraphic correlations. Suid molars (Kullmer, 2008) allow a subdivision of the Chiwondo Beds into Units 1 to 4 (Betzler and Ring, 1995; Ring and Betzler, 1995). The anthropologically important Unit 3 (ca. 3.75 to 0.6 Ma) was further subdivided into zones 3A-I, 3A-II and 3B (Bromage et al., 1995; Sandrock et al., 1999; Kullmer, 2008). While pedogenic carbonate is present in all units (Lüdecke and Thiemeyer, 2013; Lüdecke et al., 2016), fossils are only preserved in Units 2 and 3. The recovered skeletal elements are mostly isolated molars, mandible fragments or high-density limb bones (Sandrock et al., 2007).

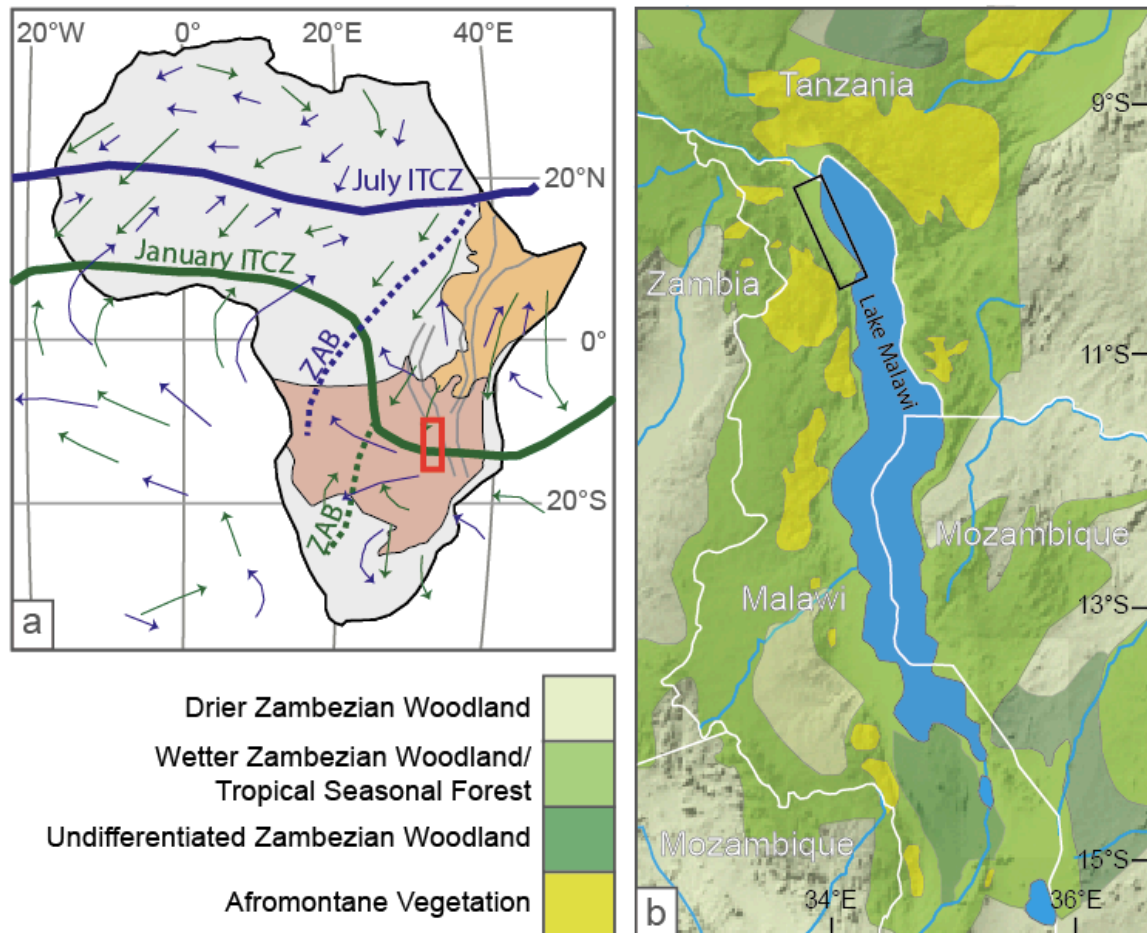


Figure 5.1: Atmospheric circulation and vegetation patterns in Eastern Africa. a) General wind patterns and major air boundaries over Africa in January (green) and July (blue) (Nicholson, 2000; Nicholson, 1996). Note that the Karonga Basin is located east of the Zaire Air Boundary (ZAB) at all times, while the Intertropical Convergence Zone (ITCZ) crosses Northern Malawi in the austral summer. Red: Zambebian Savanna; orange: Somali-Masai Endemic Zone (White et al., 1983). b) Vegetation map of the Lake Malawi region (adapted from White et al., 1983 and Ivory et al., 2012) with position of Chiwondo Beds (black box) and main rivers. The Wetter Zambebian Woodland has a dominantly C_3 vegetation, the Drier Zambebian Woodland inhabits a mixed C_3/C_4 vegetation and the Afromontane Vegetation in the highlands can have a high fraction of C_4 biomass.

5.2.1.1 Faunal composition of the Chiwondo Beds

Fossil teeth analyzed here are temporarily stored in Senckenberg Research Institute Frankfurt, Germany and are housed in the collection of the Cultural and Museum Centre Karonga, Malawi; all samples are listed in the Hominid Corridor Research Project (HCRP) catalogue (for ID and data see Supplementary Material S4, Tab. 5.2 to 5.6). Typically, the fossil specimens have been collected by systematic surveys along erosional surfaces between 1984 and 2009. Bovids are the dominant faunal element in the Chiwondo Beds (~50% of fossil collection material) followed by equids, suids and hippopotamids (Sandrock et al., 1999; Sandrock et al., 2007). Seven bovid tribes are represented: *Alcelaphini*, *Reduncini*, *Hippotragini*, *Bovini*, *Antilopini*, *Aepycerotini*, *Tragelaphini*. These include genera with different body sizes that prefer different ecosystems (closed wet to open arid). All these tribes are also present in the Eastern Rift (e.g., Bedaso et al., 2013). With the ultimate aim to analyze members of both, C₃ and C₄ feeders, we target tooth samples of *Alcelaphini* and *Hippotragini*, which are best adapted to open arid grassland savannas to establish the dietary variability for animals with a high C₄ consumption (Cerling et al., 2003; Codron et al., 2007) in addition to samples of *Antilopini* which mostly have a higher fraction of C₃-biomass in their diet (Cerling et al., 2003). The analyzed horses (*Eurygnathohippus* sp.; Sandrock et al., 2007) commonly occur in C₄-dominated or even exclusively C₄-grass environments in tropical and sub-tropical Africa (Morgan et al., 1994; Bocherens et al., 1996; Cerling et al., 1997; Kingston, 1999; Cerling et al., 2003; Cerling et al., 2003; Zazzo et al., 2005). Suids (*Notochoerus* and *Metridiochoerus*) represent ca. 12% of the recovered fossil mammal assemblage whereas almost 10% of the Chiwondo Beds fauna is composed of hippopotamids. Oxygen isotope ratios of the latter are particularly interesting in these obligate drinkers since $\delta^{18}\text{O}$ of tooth enamel primarily depends on the $\delta^{18}\text{O}$ of drinking water, minimizing the evaporative enrichment of ^{18}O which occurs in plant leaf water (Kohn et al., 1996; Kingston and Harrison, 2007). Elephants (about 5% of the mammal assemblage) were analyzed to compare individuals from the southern EAR to other parts of the world where elephants are known to have shifted their diet from C₃ to C₄ and back within the last 8 Ma (Cerling et al., 1999).

Biostratigraphic age constraints were established for the time interval between ca. 4.3 Ma (*Notochoerus jaegeri*) to 0.7 Ma (*Metridiochoerus compactus*; Kullmer, 2008). Based on the biostratigraphic constraints it is not possible to assign an absolute age for each fossil, but we were able to a) divide the fossil assemblage into four intervals: ca. 4.3 to 3.75 Ma (Unit 1 and 2), 3.75 to 2.8 Ma (Unit 3A-1), 2.8 to 1.8 Ma (Unit 3A-2), 1.8 to 0.6 Ma (Unit 3B; after Betzler and Ring, 1995; Bromage et al., 1995; Sandrock et al., 1999; Kullmer, 2008) and b) analyze bovids, equids and suids from every fossil bearing unit (Tab. 5.1, Fig. 5.6).

Table 5.1: Overview of all analyzed herbivore teeth.

Taxa	HRCP Cat. #	$\delta^{18}\text{O}/\delta^{13}\text{C}$ analyses	Unit	Locality
<i>Bovidae Alcelaphini Connochaetes sp.</i>	154	21	3A	RC1
<i>Bovidae Alcelaphini Megalotragus sp.</i>	361; 373; 419	15	3A; 3B	U11; U13; U21
<i>Bovidae Alcelaphini Damaliscus sp.</i>	187	9	3A	WK11
<i>Bovidae Hippotragini gen. indet.</i>	348	3	2	U6
<i>Bovidae Antilopini gen. indet.</i>	547	5	2	WK38
<i>Equidae Eurygnathohippus sp.</i>	351; 357; 600; 1173	40	2 & 3A	U8; U8; WK, MR/RC?
<i>Hippopotamidae Hippopotamus amphibius</i>	1174	2	3A	WK?
<i>Elephantidae Loxodonta sp.? or Elephas sp.?</i>	1175	9	3A-2	U?
<i>Suidae Notochoerus euilus</i>	498; 654	2	3A-1	WK36; WK?
<i>Suidae Notochoerus scotti</i>	118; 253	2	3A-2	MP1; WK18
<i>Suidae Notochoerus jaegeri</i>	457; 546	3	2	U6; WK38
<i>Suidae Metridiochoerus compactus</i>	429	2	3B	U25
<i>Suidae Metridiochoerus andrewsi I & III</i>	407; 423	5	3A-2; 3B	U19; U23
<i>Suidae Phacochoerus aethiopicus</i>	129	4	Modern	RC1

5.2.2 Modern climate and lake hydrology

Southeast African vegetation primarily depends on regional hydrology. It is highly sensitive to changes in precipitation and seasonality and past climate changes frequently resulted in biome reorganization (Gajewski et al., 2002; Hély et al., 2006; Gasse et al., 2008). Today, rainfall amount and seasonality exert the major controls on the distribution of tropical African vegetation (Hély et al., 2006). The enhanced sensitivity of southeast African vegetation to changes in precipitation and rainfall seasonality is due to the complex interactions among the African Monsoon, the Intertropical Convergence Zone (ITCZ) and the Zaire Air Boundary (ZAB; Fig. 5.1a; White et al., 1983; Nicholson, 1996; Leroux, 2001; Hély et al., 2006). While the dry season (May to October) is dominated by SE trade winds, a single rainy season marks the passage of the ITCZ in November to April with prevailing NE surface winds (Fig. 5.1a, Ivory et al., 2012). Today's mean annual precipitation ranges from 800 mm/a in the lowlands to 2400 mm/a on the slopes of Rungwe Highlands (DeBusk, 1994; Ivory et al., 2012). Rainfall variability is broadly linked to Indian Ocean sea surface temperatures, while moisture is derived from both the Atlantic and the Indian Oceans. This climate pattern results in a moist/dystrophic savanna with limited tree cover (Zambeziian Savanna, Miambo woodlands), which is influenced by disturbance through bush fire and herbivory rather than climate (Van Wilgen, 1997; Sankaran et al., 2005). Shade, shelter and food resources are provided due to a diverse tree community and a high fraction of woody cover. Today, vegetation in the Karonga Basin includes lowland (<1500 m asl elevation) elements that are comprised of Wetter Zambeziian Woodlands with

abundant C₃ plants (Fig. 5.1b), while above 1500 m asl Afromontane Grasslands dominate and are locally interrupted by patches of Afromontane Forest (White et al., 1983; Ivory et al., 2012). Drier Zambebian woodlands, which have a higher percentage of (C₄-)grasses and a more open canopy than the Wetter Zambebian Savanna, are present >70 km away of the modern Lake Malawi outside of the Karonga Basin (Fig. 5.1b).

Lake Malawi is currently the most important freshwater and moisture source in the region and moderates local and regional climate (Goddard and Graham, 1999; Marchant et al., 2007). The Malawi Rift basin started to develop ca. 8 Ma ago, but deep water conditions were attained only by ~4 Ma (Delvaux, 1995). Lake Malawi (478 m asl) today is up to 700 m deep and is bordered by the rift flanks with elevations of up to 3000 m asl in the Rungwe Highlands to the north and the Nyika Plateau to the west (Malawi Government, 1983). The modern lake is hydrologically open and stratified, but with the Shire River as only outlet ca. 90% of the annual water budget is lost via evaporation (Drayton, 1984). Seismic surveys reveal the presence of outflow stands in Lake Malawi, indicating that since the beginning of lake formation fluctuations in water level of 250 to 400 m have occurred (Delvaux, 1995; Finney et al., 1996).

5.2.3 Tooth formation and stable isotopes in enamel

The stable carbon and oxygen isotope geochemistry of fossil herbivore enamel is a robust and well-established tool to reconstruct continental paleo-environmental conditions in particular when climate change plays a key role in the evolution of ecosystems (e.g., Cerling et al., 1997; Kingston and Harrison, 2007; Ségalen et al., 2007; Uno et al., 2011; Roche et al., 2013). In general, the diet of individual species is reflected in the carbon, oxygen and nitrogen isotopic composition of their biomass (e.g., DeNiro and Epstein, 1978). $\delta^{18}\text{O}$ and $\delta^{13}\text{C}$ values in tooth enamel record nutrition (including food and drinking water) in an area reflecting the migration pattern of the animal during the weeks and years of enamel formation (Birkeland, 1984; Pustovoytov, 2003; Kohn and Cerling, 2002). Over this time interval food intake is sequentially recorded in the tooth enamel. Horses (modern and fossil), for example display total mineralization times for individual molars between ca. 1.5 and 2.8 years (Hoppe et al., 2004).

5.2.3.1 $\delta^{13}\text{C}$ isotopes in herbivore enamel

Based on different photosynthetic pathways, plants can be divided into two main ecophysiological groups: Tropical grasses, typically savanna plants in Eastern Africa, use the C₄ photosynthetic pathway, while most brushes and trees in Africa use the globally dominant C₃ pathway. C₄ plants are more tolerant to high water stress and light intensity compared to C₃ plants which are in advantage under moderate climates (Sage and Sage, 2013). Due to a difference in their discrimination against ¹³C during photosynthesis (Percy and Ehleringer, 1984), $\delta^{13}\text{C}$ values of most C₄ plants range from -19‰ to -9‰, while $\delta^{13}\text{C}$ values of C₃ plants lie between -25‰ and -29‰, resulting in ¹³C/¹⁴C ratios of savanna grasses ca. 14‰ higher than most woody and forest plants (Cerling et al., 1997). The comparably small variability of $\delta^{13}\text{C}$ in C₄ plants can be

attributed to three different C₄ photosynthetic subpathways (Cerling et al., 2003), while the variation in $\delta^{13}\text{C}$ among C₃ plants is affected by a variety of environmental factors including temperature, drought, canopy density, salinity, light intensity, nutrient levels, and partial pressure of CO₂ (Medina and Minchin, 1980; Medina et al., 1986; Farquhar et al., 1989; Ehleringer and Monson, 1993). Collectively, however, these effects on $\delta^{13}\text{C}$ of C₃ plants are still considerably small compared to the differences between C₃ and C₄ biomass. During biomineralization a fractionation of ca. 14‰ occurs between the consumed biomass and herbivore bioapatite (Cerling and Harris, 1999; Passey et al., 2005). As a consequence, modern East African grazing herbivores have a ca. 14‰ higher ¹³C/¹²C ratio than modern East African C₃-browsers and forest feeding herbivores.

5.2.3.2 $\delta^{18}\text{O}$ values in herbivore enamel

The oxygen isotope composition of mammalian tooth enamel is directly linked to the $\delta^{18}\text{O}$ values of body water and is therefore a complex function of paleohabitat, climate, diet and physiology (Longinelli, 1984; Kohn et al., 1996; Sponheimer and Lee-Thorp, 1999; Kohn and Cerling, 2002). In principle, $\delta^{18}\text{O}$ values of obligate-drinker taxa, e.g., hippopotamids, primarily depend on the $\delta^{18}\text{O}$ values of drinking water, whereas drought-tolerant non-obligate drinkers usually have higher $\delta^{18}\text{O}$ values, reflecting evaporative enrichment of ¹⁸O which occurs in plant leaf water (Ayliffe and Chivas, 1990; Kohn et al., 1996; Levin et al., 2006). Different factors influence the $\delta^{18}\text{O}$ values of body water: (1) drinking water composition (Longinelli, 1984; Luz et al., 1984; Luz and Kolodny, 1985), (2) climate (humidity) and (3) C₃ vs. C₄ consumption ($\delta^{18}\text{O}$ values typically decrease with increasing fraction of C₃ diet since C₃ plants have lower $\delta^{18}\text{O}$ values than coexisting C₄ plants; Sternberg et al., 1984; Bocherens et al., 1996). For mammals, there is a constant offset (~26‰) between $\delta^{18}\text{O}$ of body water (reflecting drinking water in large mammals; Bryant and Froelich, 1995) and the CO₃ component of bioapatite (Bryant et al., 1996; Iacumin et al., 1996; Kohn and Cerling, 2002). $\delta^{18}\text{O}$ values of fossil enamel therefore can reflect climate habitat and dietary preferences of an animal.

5.2.4 $\delta^{18}\text{O}$ values of meteoric water in southeast Africa

$\delta^{18}\text{O}$ values of meteoric water in Eastern Africa are largely controlled by oscillations of the ITCZ, the convergence and interactions between the zonal ZAB and the meridional southeastern trade winds and monsoonal northeastern wind (Fig. 5.1a). During the austral winter (July/August), high pressure systems prevail over southern Africa (Nicholson, 2000) suppressing precipitation in Northern Malawi. The wet season (November-April) starts when the ITCZ moves southward over the Karonga Basin (Fig. 5.1a; Nicholson et al., 2014). At current there are no systematic surveys of $\delta^{18}\text{O}$ in precipitation for Malawi; the closest GNIP stations are located at >650 km from our sampling sites (Ndola in Zambia, Dar es Salaam in Tanzania and Harare in Zimbabwe; IAEA/WMO, 2015).

5.3 Material and methods

5.3.1 $\delta^{13}\text{C}$ and $\delta^{18}\text{O}$ of herbivore fossil tooth enamel

We analyzed a total of 122 samples from 14 different mammalian taxa from Unit 2 and 3 of the Chiwondo Beds. These include: a) 18 samples from ten Suidae molars (Tab. 5.2) of the extinct *Notochoerus* (*Not.*) *jaegeri* (two individuals, $n = 3$), *Not. euilus* (two individuals, $n = 2$) and *Not. scotti* (two individuals, $n = 2$); *Metridiochoerus* (*Met.*) *andrewsi* stage I and III (two individuals, $n = 5$) and *Met. compactus* (one individual, $n = 2$), plus an extant *Phacochoerus* (*Pha.*) *aethiopicus* (one individual, $n = 4$) ($\delta^{13}\text{C}$ data from Lüdecke et al., 2016); b.) two samples of one tooth of *Hippopotamus amphibius* (Tab. 5.3); c) Nine enamel samples of one individual of *Elephantidae gen. and sp. indet.* (*Loxodonta* or *Elephas*; Tab. 5.4); d) 40 samples of four individuals of the Equidae (Tab. 5.5); e) 53 samples from three Bovidae genera (Tab. 5.6) including *Alcelaphini* (*Alc.*) *Connochaetes* (one individual, $n = 21$), *Alc. Megalotragus sp.* (three individuals, $n=15$) and *Alc. Damaliscus sp.* (one individual, $n = 9$). We preferentially analyzed molars and premolars to avoid juvenile dietary signals, however, the *Hippopotamus amphibius* tooth is an incisor and the origin of the piece of enamel from the elephant is not allocated. For sampling and pretreatment methods of the enamel samples see Section 4.8.

400 to 2030 μg of pretreated enamel material were reacted with 98% H_3PO_4 for 90 minutes at 70°C in continuous flow mode using a Thermo MAT 253 mass spectrometer interfaced with a Thermo GasBench II. All analyses were performed at the Goethe University-BiK-F Joint Stable Isotope Facility Frankfurt, Germany. Analytical procedures followed Spötl and Vennemann (2003). Final isotopic ratios are reported against VPDB ($\delta^{13}\text{C}$) and VSMOW ($\delta^{18}\text{O}$); overall analytical uncertainties are better than 0.02 ‰ ($\delta^{13}\text{C}$) and 0.04 ‰ ($\delta^{18}\text{O}$).

5.3.2 $\delta^{18}\text{O}$ of meteoric water

We sampled precipitation during the rainy seasons (October to May) 2012/13 and 2013/14. Two rainfall collectors were installed in Karonga and Malema (position and data see Supplementary Material S5, Tab. 5.7 to 5.10) and sampling bottles were installed roughly every two weeks ($n = 45$). Additionally, we sampled natural water ($n = 66$) from different sources in Northern Malawi (N of 12°S , see Fig. 5.4c). Field campaigns took place during the months of September, October and November from 2011 to 2013. Surface water was sampled from rivers contributing to Lake Malawi ($n = 9$), Lake Malawi ($n = 3$) and from artificially dammed lakes on the Nyika Plateau ($n = 2$); groundwater was sampled from water pumps ($n = 52$). Stable oxygen isotope ratio measurements were made on 1 ml aliquots using an LGR 24d liquid isotope water analyzer. $\delta^{18}\text{O}$ values are calibrated and reported against VSMOW, with an analytical precision <0.2 ‰ (2σ). Sampling strategy and analyses follow Schemmel et al. (2013).

5.4 Results

5.4.1 $\delta^{13}\text{C}$ and $\delta^{18}\text{O}$ of herbivore enamel

The complete range of C_3 - C_4 dietary adaptations is represented in the Plio-Pleistocene Chiwondo fauna with $\delta^{13}\text{C}$ enamel values ranging from -13.1‰ to $+1.6\text{‰}$ ($n = 122$, Fig. 5.2a, complete data see Supplementary Material S4, Tab. 5.2 to 5.6). Based on their $\delta^{13}\text{C}$ values we define three groups: (a) primary C_3 consumers with $\delta^{13}\text{C}$ values of $<-8\text{‰}$, (b) animals with a mixed C_3/C_4 diet with $\delta^{13}\text{C}$ values from -8‰ to -1‰ and (c) browsers with $\delta^{13}\text{C}$ values of $>-1\text{‰}$ reflecting a pure C_4 diet (Lee-Thorp and Van der Merwe, 1987; Lee-Thorp et al., 1989; Cerling and Harris, 1999; Passey et al., 2005). The associated $\delta^{18}\text{O}$ values range from 22.4‰ to 30.2‰ (Fig. 5.2b), reflecting $\delta^{18}\text{O}$ of drinking water from different water reservoirs available in the region. Within the fossiliferous Units 2 and 3 no distinct trend in the $\delta^{13}\text{C}$ and $\delta^{18}\text{O}$ data is visible for any herbivore taxa (see Fig. 5.S2).

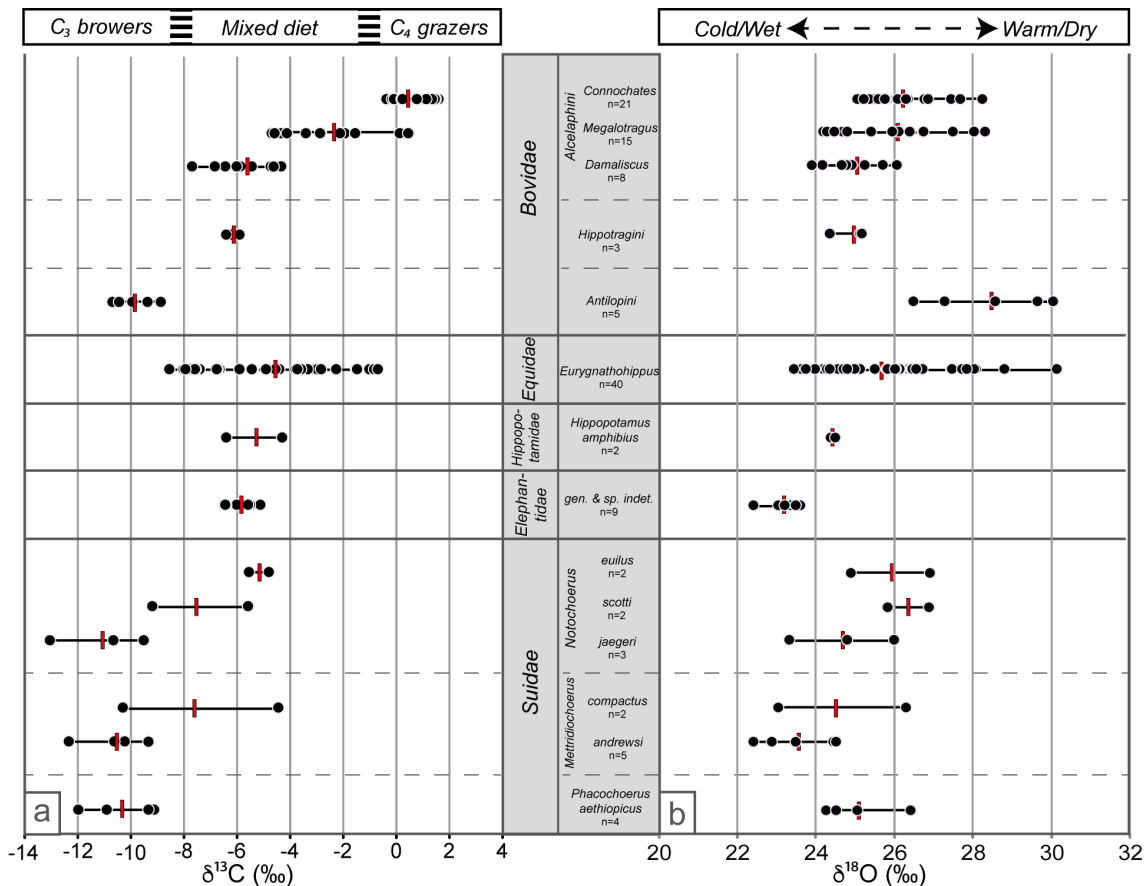


Figure 5.2: $\delta^{13}\text{C}$ and $\delta^{18}\text{O}$ values from Karonga Basin herbivore enamel. Stable carbon (a) and oxygen (b) isotope data of herbivore taxa from the Chiwondo Beds in the Malawi Rift show a large variation in foraging behaviors. For data see Supplementary Material 5.8.4 (Tab. 5.2 to 5.6).

Suidae: Ten third molars from the recent *Phacochoerus* and fossil *Notochoerus* and *Metridiochoerus* from Units 2, 3A and 3B ($n=18$) show $\delta^{13}\text{C}$ values between -13.1‰ and -4.5‰ (mean = -9.3‰ , $\sigma = 2.6\text{‰}$) and $\delta^{18}\text{O}$ values from 22.4‰ to 26.9‰ (mean = 24.8‰ , $\sigma = 1.4\text{‰}$) (Lüdecke et al., 2016). The stable isotope data indicate a pure browsing to mixed feeding diet with water intake from freshwater sources with only limited influence of evaporation (Fig. 5.2).

Elephantidae: A small piece of enamel of one individual of *Loxodonta* or *Elephas* ($n = 9$) from Unit 3A-2 shows $\delta^{13}\text{C}$ values between -5.1‰ and -6.5‰ (mean = -5.8‰ , $\sigma = 0.5\text{‰}$, Fig. 5.2). This small range in $\delta^{13}\text{C}$ values reflects a mixed C_3/C_4 diet. Variation in $\delta^{18}\text{O}$ is also very low with values between 22.4‰ and 23.6‰ (mean = 23.3‰ , $\sigma = 0.4\text{‰}$), indicative of drinking from an ^{18}O -depleted source.

Hippopotamidae: The two analyses of an upper incisor from *Hippopotamus* from Unit 3A show $\delta^{13}\text{C}$ values of -6.4‰ and -4.3‰ (Fig. 5.2), reflecting a mixed C_3/C_4 diet. The $\delta^{18}\text{O}$ values of 24.4‰ and 24.5‰ are low with very little spread, which is typical for water-dependent animals.

Equidae: We sampled enamel of four individual *Eurygnathohippus* sp. molars ($n = 40$) from Unit 2 and 3A. The $\delta^{13}\text{C}$ values cover a very large range from -8.5‰ to -0.7‰ (mean = -4.6‰ , $\sigma = 2.4\text{‰}$; Fig. 5.2), reflecting a mixed C_3/C_4 diet, with the most negative values indicative of an almost exclusively C_3 diet while the most positive $\delta^{13}\text{C}$ values indicate an almost pure C_4 diet. The variation in $\delta^{18}\text{O}$ is also large (23.4‰ to 30.2‰ ; mean = 25.8‰ , $\sigma = 1.6\text{‰}$) covering almost the entire range of the analyzed herbivore samples, indicating water intake from isotopically different sources. $\delta^{13}\text{C}$ and $\delta^{18}\text{O}$ values generally show an overall positive co-variance (see Fig. 5.7). Samples derived from one *Eurygnathohippus* sp. individual of Unit 3A ($n = 3$) plot within the range of samples of older Unit 2 ($n = 37$); however, the $\delta^{13}\text{C}$ values in the younger Unit 3A occupy the positive end of the spectrum in Unit 2 (see Fig. 5.6), suggesting a dietary change to higher C_4 consumption.

Bovidae: Seven teeth from *Alcelaphini*, *Antilopini* and *Hippotragini* ($n = 53$) from Units 2, 3A and 3B have $\delta^{13}\text{C}$ values ranging from -10.7‰ to $+1.6\text{‰}$ (mean = -2.7‰ , $\sigma = 3.6\text{‰}$). $\delta^{18}\text{O}$ values vary between 24.1‰ and 30.0‰ (mean = 26.1‰ , $\sigma = 1.4\text{‰}$). The different species can be grouped according to their $\delta^{13}\text{C}$ values. Most of them reflect a mixed C_3/C_4 diet; only *Antilopini* (browser) and *Alc. Connochates* (grazer) and an individual of *Alc. Megalotragus* (#373) from Unit 3A (grazer) indicate a specialized behavior (Fig. 5.2a). $\delta^{13}\text{C}$ and $\delta^{18}\text{O}$ values show mostly positive co-variance (Fig. 5.7), with the exception of *Antilopini*. Here low $\delta^{13}\text{C}$ values correspond to high $\delta^{18}\text{O}$ values (Fig. 5.2b and 5.7). Only *Alc. Megalotragus* individuals were sampled from different units, here a slight decrease in $\delta^{13}\text{C}$ and $\delta^{18}\text{O}$ values is visible from Unit 3A to the younger Unit 3B (see Fig. 5.6).

5.4.2 Intra-tooth $\delta^{13}\text{C}$ and $\delta^{18}\text{O}$ patterns

Intra-tooth $\delta^{13}\text{C}$ and $\delta^{18}\text{O}$ patterns provide insight into the migrational behavior of individual animals and seasonality. We present selected equid and bovid teeth data in Fig. 5.3, for all patterns see Supplementary Material S4, Fig. 5.8.

Equidae: Different stable isotope patterns characterize intra-tooth stable isotope values of equid *Eurygnathohippus* sp. teeth (Fig. 5.3a): low $\delta^{13}\text{C}$ and $\delta^{18}\text{O}$ values with a small to medium variability (range of $\delta^{13}\text{C}$ values = 2.6‰ ;

$\delta^{18}\text{O} = 1.5\text{‰}$) with some co-variance of ($R^2 = 0.29$; #1173); and medium $\delta^{13}\text{C}$ and $\delta^{18}\text{O}$ with either small variability in $\delta^{13}\text{C}$ (1.5‰) but a significantly larger variability in $\delta^{18}\text{O}$ (2.8‰; $R^2 = 0.15$; #351) or large fluctuations in $\delta^{13}\text{C}$ (6.9‰) and $\delta^{18}\text{O}$ (6.8‰) with a strong co-variance ($R^2 = 0.96$), covering some of the most positive and most negative $\delta^{13}\text{C}$ and $\delta^{18}\text{O}$ values of all equids (#357).

Bovidae: Individual *Alcelaphini* teeth (#154, #187, #361; Fig. 5.3b) display different ranges in values with hardly any overlap with a medium range of ca. 2‰ to 3‰. $\delta^{18}\text{O}$ values however overlap significantly within a large range of up to 3.2‰ within one tooth, reflecting similar drinking sources with distinctly different diets of the individual genera. The co-variance varies and is positive for *Alc. Damaliscus* ($R^2 = 0.64$; #187) and *Alc. Megalotragus* ($R^2 = 0.17$, #361) while negative for *Alc. Connochaetes* ($R^2 = 0.28$; #154). *Antilopini* (#547) $\delta^{13}\text{C}$ values are very low with a range of 1.8‰, while displaying a wide range (3.5‰) of very high $\delta^{18}\text{O}$ values with a negative co-variance ($R^2 = 0.57$).

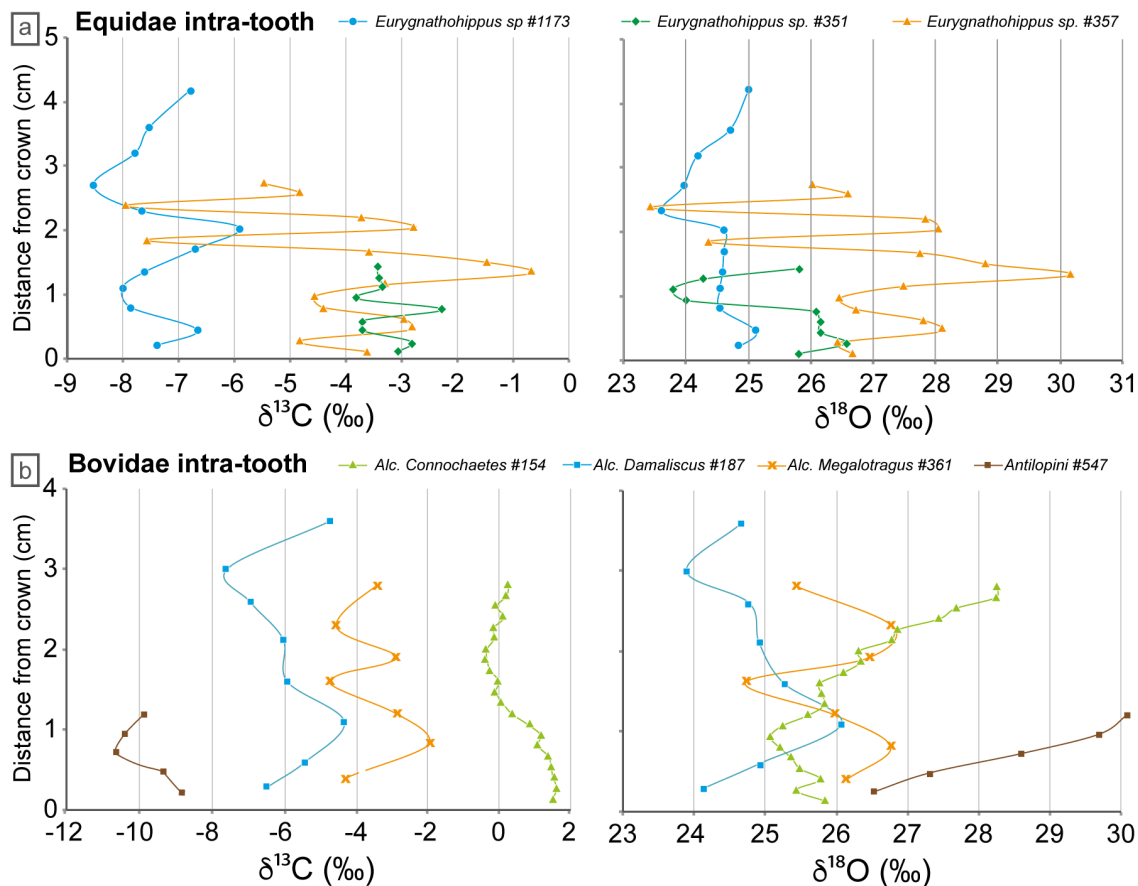


Figure 5.3: Intra-tooth $\delta^{13}\text{C}$ and $\delta^{18}\text{O}$ variation of representative equid (a) and bovid (b) teeth. Different patterns indicate different migratory behavior of the individuals. For results of all equids and bovinds see Supplementary Material S4 (Fig. 5.8; data Tab. 5.2 to 5.6).

5.4.3 $\delta^{18}\text{O}$ of meteoric water

The different meteoric water sampled here (rainwater, river and lake water as well as groundwater; Fig. 5.4, data: Tab. 5.7 to 5.10) reflects the dependence of $\delta^{18}\text{O}$ values on seasonality, altitude and climate (evaporation): a) Seasonality: average monthly rainfall $\delta^{18}\text{O}$ values (-4.9‰ to +0.3‰; Fig. 5.4b) display the most positive values at the beginning and the end of the rainy season

(November and April/May) and lowest $\delta^{18}\text{O}$ values during the summit of the rainy season with increasing values during the dry season. b) Altitude: There is a good correlation ($R^2 = 0.68$) of $\delta^{18}\text{O}$ values of river- and rainwater with elevation. Including the average rainfall data from Karonga and Malema, the oxygen isotope lapse rate is ca. $-2.8\text{‰}/\text{km}$ (Fig. 5.4c). $\delta^{18}\text{O}$ values of rivers within the catchment of Lake Malawi fall between -7.0‰ and -3.4‰ . $\delta^{18}\text{O}$ values from groundwater cover between -6.9‰ and -3.7‰ (Fig. 5.4c). c) Evaporation: lake water, which is subject to lake evaporation, shows more positive values than stream water (Fig. 5.4c): dammed lakes on the Niyka Plateau ($\delta^{18}\text{O} = -5.6\text{‰} \pm 0.1\text{‰}$ at >2250 m asl) have about 1.5‰ more positive $\delta^{18}\text{O}$ values than rivers in the same area. Lake Malawi ($\delta^{18}\text{O} = +2.0\text{‰}$ to $+2.4\text{‰}$) loses ca. 90% of the annual water via evaporation (Drayton, 1984) and is about 6‰ more positive than river water feeding the lake (Fig. 5.4c).

$\delta^{18}\text{O}$ values of the analyzed present-day meteoric water show a range of 9.7‰ that is similar in magnitude to the variation measured in fossil herbivore $\delta^{18}\text{O}$ ($\sim 7.9\text{‰}$) of tooth enamel.

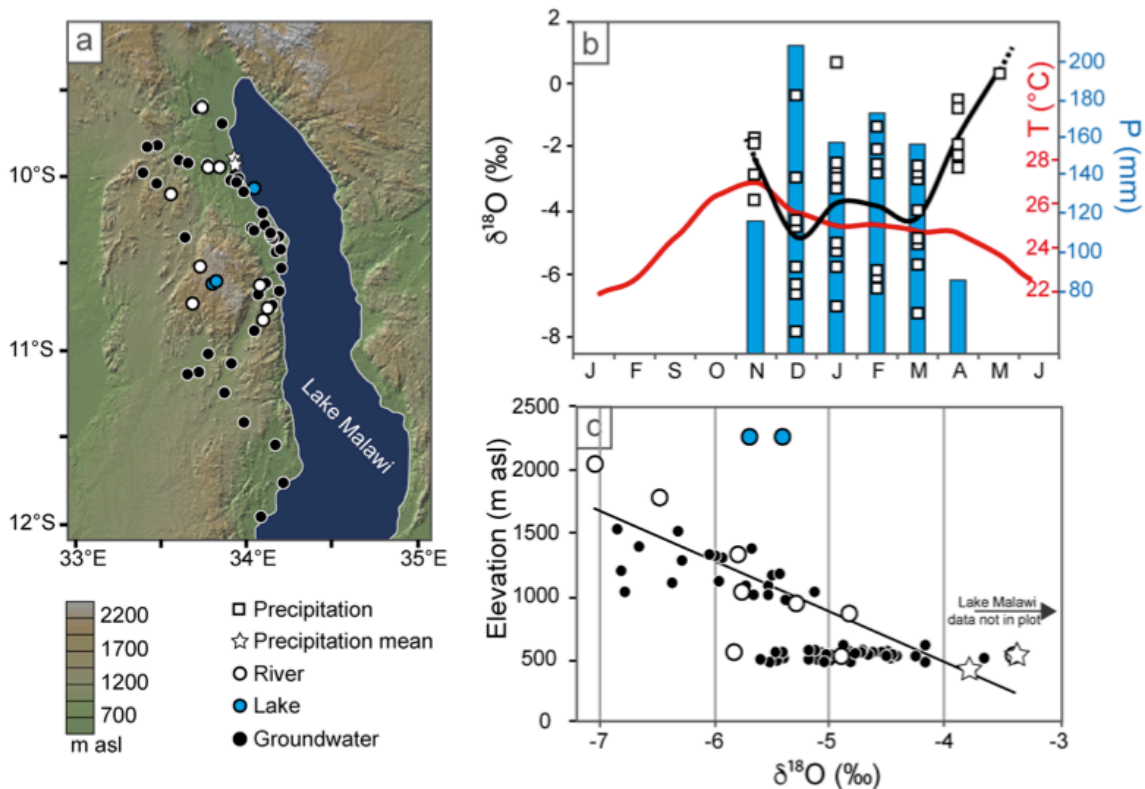


Figure 5.4: $\delta^{18}\text{O}$ values of meteoric water from the Karonga Basin. a) Sample localities of meteoric water, topography from GeomapApp database (<http://www.geomapapp.org>). For coordinates and data see Supplementary Material S4 (Tab. 5.7 to 5.10). b) $\delta^{18}\text{O}$ values of rainwater (open squares) collected in Karonga ($S9^{\circ}55.887'$; $E33^{\circ}56.570'$) and Malema ($S10^{\circ}01.199'$; $E33^{\circ}55.639'$) in the rainy season 2012/13 and 2013/14 with mean monthly values (black line). Climate chart of Karonga with temperature (red line) and precipitation (blue columns; source: National Oceanic and Atmospheric Administration). Results of Lake Malawi water is not on plot, $\delta^{18}\text{O}$ values are between 2.0‰ and 2.5‰ (lake surface elevation at ca. 500 m asl). c) $\delta^{18}\text{O}$ values of meteoric water from rivers and lakes and groundwater vs. elevation. Note the strong correlation ($R^2 = 0.68$) of $\delta^{18}\text{O}$ with elevation (rivers and precipitation mean) and evaporation (lakes).

5.5 Discussion

Plio-Pleistocene herbivore $\delta^{13}\text{C}$ and $\delta^{18}\text{O}$ data from the Karonga Basin (Malawi Rift) indicate a wide range of foraging strategies, characterized by highly variable diets ranging from specialized C_3 to C_4 feeders with a majority of mixed-feeders (Fig. 5.2). A high variation in $\delta^{13}\text{C}$ and $\delta^{18}\text{O}$ values indicates presence of a wide range of ecosystems over time and space: dryland environments in the Drier Zambezian Woodlands (Fig. 5.1b), accessible for migrating herbivores and (closed to open) woodlands in the water-rich near-shore environments with a majority of C_3 vegetation as reflected by $\delta^{13}\text{C}$ values of pedogenic carbonate (Lüdecke et al., 2016). A similar magnitude in $\delta^{18}\text{O}$ values of recent meteoric water and fossil herbivore enamel indicates Plio-Pleistocene paleoenvironments that were comparable in seasonality, altitude and evaporation to today.

Generally low $\delta^{13}\text{C}$ values in enamel from suids, hippopotamus, elephants, select equids and bovids reflect the intake of either (aquatic) C_3 biomass and/or parts of plants that are not affected by evaporation such as stems, roots, bark and fruits in mesic environments (e.g., Drapeau et al., 2014). Low $\delta^{13}\text{C}$ values in the Karonga Basin fauna are often accompanied by low $\delta^{18}\text{O}$ values (Fig. 5.7), which indicates drinking from a freshwater source that has experienced only limited evaporation. Such animals probably browsed in the abundant woodlands with access to rivers along the flanks of the rift valley. Some of the equids and bovids have more positive $\delta^{13}\text{C}$ and $\delta^{18}\text{O}$ values than other taxa. These more specialized feeders probably migrated to the Drier Zambezian Woodlands or to elevated areas on the rift flanks where C_4 grasses were available and drinking water was more evaporative. Only *Antilopini* show a negative correlation between $\delta^{13}\text{C}$ and $\delta^{18}\text{O}$ ratios (Fig. 5.3): low $\delta^{13}\text{C}$ values accompanied by high $\delta^{18}\text{O}$ values indicate a mixed, C_3 rich diet with water intake from ^{18}O enriched sources, reflecting e.g., a habitat with lakes surrounded by gallery forests. The opposite trend, high $\delta^{13}\text{C}$ values with low $\delta^{18}\text{O}$ values (e.g., *Alc. Connochaetes* #154) indicates a C_4 -rich diet with water supply from rivers. In the last case, however, the $\delta^{18}\text{O}$ values shift to more positive values as the individual gets older, indicating more arid conditions, which could be an indicator for seasonality or migration patterns. Seasonality and/or migration are also supported by the very large variability in $\delta^{13}\text{C}$ and $\delta^{18}\text{O}$ in some individual teeth (e.g., *Eurygnathohippus* #357).

Compared to other parts of the EAR, the herbivore $\delta^{13}\text{C}$ and $\delta^{18}\text{O}$ data from the Karonga Basin are generally more negative than in equivalent Plio-Pleistocene taxa in the Eastern Rift or in their modern counterparts (e.g., Cerling et al., 2003; Kingston and Harrison, 2007; Kingston, 2011). Also, a mixed C_3/C_4 diet with $\delta^{13}\text{C}$ values between -8‰ and -3‰ is rare in modern East African herbivores, yet this range is common in the Plio-Pleistocene Karonga data as well as some other African fossil sites (e.g., Kingston, 2011). This could indicate that many herbivores were generalists and may have occupied different feeding niches or inhabited ecosystems in the past for which there are no modern

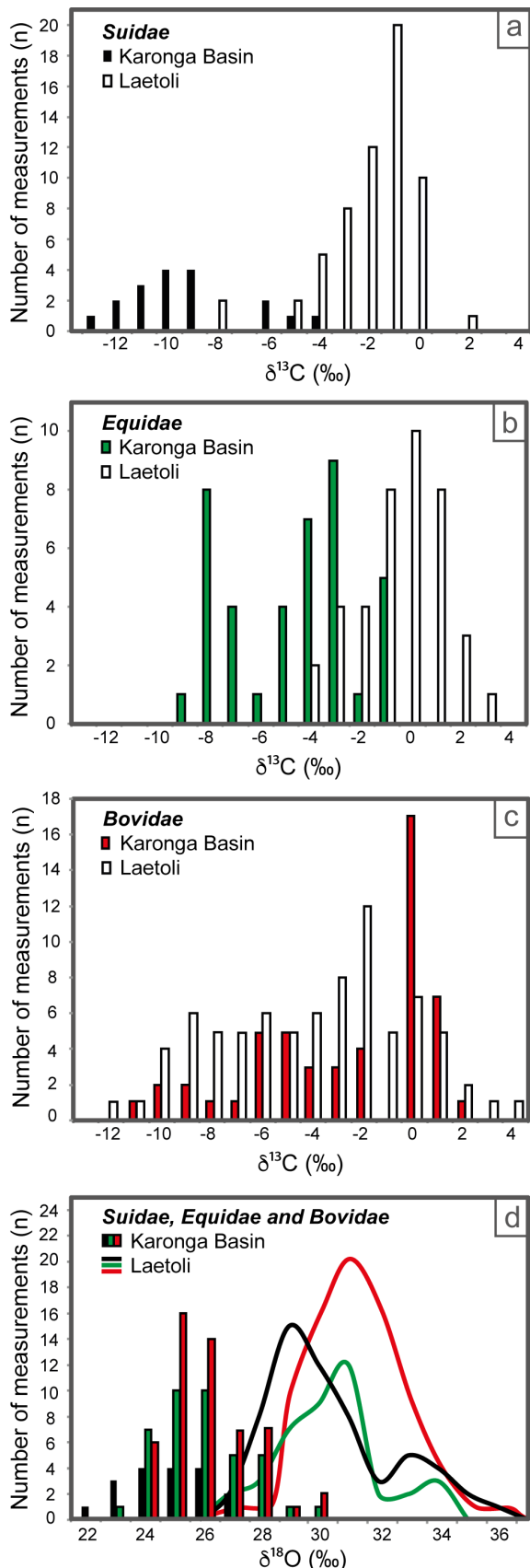


Figure 5.5: Comparison of Karonga Basin and Laetoli herbivore enamel data. $\delta^{13}\text{C}$ data from Suidae (a), Equidae (b) and Bovidae (c) and $\delta^{18}\text{O}$ data of all taxa (d) with columns (Karonga Basin) and lines (Laetoli data; Kingston, 2011) display a large offset in feeding strategies of Suidae and Equidae while specialized bovids plot in a similar range. Note that Karonga Basin taxa include Notochoerus, Metridiochoerus, Phacochoerus (suid), and Hipparion (equid) while Laetoli data is comprised of Notochoerus, Kolpochoerus, Potamochoerus, Phacochoerus (suid) and Eurygnathohippus (equid). The analyzed bovid taxa are the same (Alcelaphini, Hippotragini, Antilopini).

analogs in Eastern Africa. A comparison of the Karonga Basin data with herbivore $\delta^{13}\text{C}$ values from the closest hominin site in the Eastern Rift (Laetoli) reveals a distinct offset between the suid and equid $\delta^{13}\text{C}$ data, while specialized bovids show similar dietary preferences (Fig. 5.5). Apparently, no large-scale ecological sorting of species among the wide pool of Eastern African vertebrates in the diverse environments occurred, but grazers found their niches in a regional patchy ecosystem in the Karonga Basin. Studies of extinct herbivores suggest that morphological adaptations (e.g., hypsodonty) generally interpreted as specialization into a grazing niche, may in fact reflect a widening of the niche breadth that allowed grazing as well as browsing (Pérez-Barbeía et al., 2001; Feranec, 2003). Earliest representatives of lineages with grazing adaptations may have been intermediate feeders with a preference for browsing (Kingston and Harrison, 2007), in the Karonga Basin no major dietary changes within Unit 2 and 3 are observed.

Different herbivores provide complementary information about the overall composition of the ecosystem:

Suids are large-bodied omnivores (Hillson, 2005), which are thought to represent a potentially useful proxy for generating hypotheses about hominin paleoecology. Most features

(enlarged 3rd and 4th premolar, elongated molars, increase in both occlusal area and hyposodonty particular of third molars, enlarged tusk and body size) of suids are interpreted as adaptations to an abrasive grazing diet (Cooke and Wilkinson, 1978; Harris, 1983; Pickford, 1986; Kullmer, 2008). Their preferred habitat in Eastern Africa is interpreted as savannas or grassland biomes, feeding mostly on C₄ plants since the Upper Pliocene (e.g., Kingston et al., 1994; Harris and Cerling, 2002; Bibi et al., 2013). Only *Notochoerus euilus* from Unit 3A-1 is associated with a woodland habitat indicated by ecomorphological analysis of the postcranial and might have shared a more similar mode of life to the forest-dwelling modern giant forest hog (*Hylochoerus meinertzhageni*) rather than to the more commonly associated modern warthogs (*Phacochoerus*; Bishop et al., 1999; Kullmer, 2008). The analyzed fossil suids from the Karonga Basin (Unit 2 and 3) are mixed feeders with a high C₃ intake (*Not. euilus*, *Not. scotti* and *Met. compactus*) to pure browsers (*Not. jaegeri*, *Met. andrewsi* and *Pha. aethiopicus*), indicating easy access to C₃ plants for these dietary opportunists from the Plio-Pleistocene to today. The eclectic and flexible foraging behavior indicates a more mesic and wooded environment in the Malawi Rift than the Eastern Rift branch in the last 3 Ma (e.g., Laetoli, see Fig. 5.5a).

Elephantidae and their diet underwent many changes over the course of their evolutionary history. Around 8 Ma, elephants changed their diet from browsing to grazing. The high crowned cheek teeth represent an adaptation to abrasive grazing diet between 5 and 1 Ma (time of the Chiwondo Bed fauna) in East Africa, which is complimented by stable isotope data after the middle Pleistocene (~1 Ma) however, *Loxodonta* as well as *Elephas* abandoned this diet and became browsers again, resulting in a largely C₃ diet today (Cerling et al., 1999). The fossil enamel $\delta^{13}\text{C}$ values from Karonga Basin elephants (Unit 3A-2) are more negative than $\delta^{13}\text{C}$ data from East African (Cerling et al., 1999; Cerling et al., 2003; Kingston, 2011) and other (e.g, Chad; Zazzo et al., 2000) regions. The most negative $\delta^{13}\text{C}$ values found so far are from Laetoli, showing a mixed diet (mean $\delta^{13}\text{C}$ value = -3.8‰; $n = 13$; Kingston, 2011) and still reflecting a much higher C₄ intake compared to the Karonga Basin dataset. The Karonga Basin $\delta^{13}\text{C}$ elephant data complement the suid data and collectively suggest that the Karonga Basin was more wooded than the Somali-Masai ecozones in Eastern Africa. Additionally, Karonga Basin elephant $\delta^{18}\text{O}$ values are much more negative than modern and fossil and $\delta^{18}\text{O}$ values from Eastern Africa. This indicates water intake from sources less influenced by evaporation in this southern part of the EAR.

Hippopotamus is commonly assumed to be a pure browser, but recent stable isotope data show that they have no distinct dietary preferences and hippos in Africa can have diets ranging from a pure C₄ to pure C₃ diet (Zazzo et al., 2000; Franz-Odenaal et al., 2002; Boissarie et al., 2005; Cerling et al., 2008; Harris et al., 2008; Brachert et al., 2010). Therefore, these territorial, water-dependent mammals are particularly useful for paleoenvironmental studies. $\delta^{13}\text{C}$ values of

the Karonga Basin *Hippopotamus* (Unit 3A) range from -6.4‰ to -4.3‰ , reflecting a mixed C_3/C_4 diet, complementing the results from other Karonga Basin omnivores. The $\delta^{18}\text{O}$ values of the Karonga individual are low compared to other hippos from Eastern Africa, indicating a drinking source of these water-dependent animals that is less enriched in ^{18}O and therefore probably less influenced by evaporation.

Equidae in Eastern Africa adapted their diet from C_3 -dominant to C_4 -dominant as a response to the global expansion of C_4 biomass during the late Miocene (Cerling et al., 1997). Except at Langebaanweg (South Africa), where C_4 grasses were not established by 5 Ma (Franz-Odenaal et al., 2002), equid enamel younger than ca. 7 Ma in tropical and sub-tropical Africa, including all modern samples, yields $\delta^{13}\text{C}$ values in the range of -4‰ to $+3\text{‰}$, indicating C_4 dominated to exclusive C_4 grass diets (Morgan et al., 1994; Bocherens et al., 1996; Cerling et al., 1997; Kingston, 1999; Zazzo et al., 2000; Cerling et al., 2003; Cerling et al., 2003; Kingston, 2011). However, the Karonga Basin $\delta^{13}\text{C}$ data indicate a much broader dietary range for *Eurygnathohippus* sp. between ca. 4 and 2 Ma (Fig. 5.3 and Fig. 5.5b). This could reflect dietary adaptation associated with an inhomogeneous environment with abundant regions of C_3 woodlands. *Eurygnathohippus* individuals adjusted to different diets and therefore different Plio-Pleistocene environments. There is no change in diet between the units and already the earliest individuals of Unit 2 had excess to C_4 vegetation (Fig. 5.6). The large spread in $\delta^{18}\text{O}$ values indicates water intake from different sources ranging from rivers to evaporated lakes/paleolake Malawi, which are generally less influenced by evaporation than Eastern Rift fossil sites (e.g., Laetoli, see Fig. 5.5d).

Bovidae form a speciose and ubiquitous group, adapted to diverse habitats and diets in the Karonga Basin. We compare stable isotope data from *Antilopini*, *Alcelaphini* and *Hippotragini* from the Karonga Basin to the same genera from Laetoli in Fig. 5.5c and 5.5d (Kingston, 2011).

Modern *Antilopini* are adapted to arid grassland habitat with limbs specialized for cursoriality, and physiological and dietary adaptations to drought (Kingdon, 1982; Plummer and Bishop, 1994). They inhabit desert, grassland, savanna and open woodland with a diet ranging from grazers and mixed feeders to variable browsers (Gentry, 1992; Gagnon and Chew, 2000). Very negative $\delta^{13}\text{C}$ values of the Karonga Basin individual (Unit 2) document a pure browsing diet. Higher, more variable $\delta^{18}\text{O}$ values, however, reflect drinking from an evaporative source. Therefore, ca. 4 Ma stable isotope data of *Antilopini* from the Malawi Rift indicates C_3 feeding e.g., in a gallery forest around paleolake Malawi with its very positive $\delta^{18}\text{O}$ values mixed with more ^{18}O -depleted water from the contributing rivers.

Ecological, dietary and social patterns of *Hippotragini* have been interpreted as adaptations to an ancestral 'desert ordeal' during the Early Pliocene (Kingdon, 2016). Modern oryx, roan and sable antelopes dominate the larger-scale desert bovid niches, with well-developed adaptations to heat, drought, and desert

pastures. All species younger than 2.5 Ma are primarily obligate grazers (Cerling et al., 2015), associated with habitats ranging from desert grasslands to open woodlands. The radiation of other bovid tribes, such as *Alcelaphini* probably declined the *Hippotragini* diversity during the Plio-Pleistocene as a consequence of being forced into increasingly more marginal environments (Kingston and Harrison, 2007). The fossil Karonga Basin *Hippotragini* (Unit 2) indicate a mixed C₃/C₄ diet with a large fraction of C₃ browsing, contrasting with their modern counterparts (van der Merwe et al., 2003; Harrison, 2011; Cerling et al., 2015). This results in pressure to rely more on browsing, especially since *Alcelaphini* make the majority of the Karonga Basin bovid fauna (Sandrock et al., 2007). The range of niches available to browsers at this time accommodated a greater taxonomic diversity with less competition for access to grasses from obligate specialist grazers.

Today, most *Alcelaphini* are variable to obligate grazers and inhabit open woodlands or secondary grassland (Gagnon and Chew, 2000; Estes, 2012). In fossil enamel isotopic data East African Rift *Alcelaphini* reflect also diets dominated by C₄ grasses (e.g., Kenya and Uganda, Cerling et al., 2003) and mixed diet with a significant amount of C₃ browsing (e.g., Laetoli, Tanzania, Kingston and Harrison, 2007; Kingston, 2011). The large range in $\delta^{13}\text{C}$ of the Karonga Basin *Alcelaphini* indicate a mixed diet (with high influence of C₃ biomass) to pure C₄ grazer, similar to Eastern Rift individuals (Fig. 5.5d), which suggest that some early lineages or individual taxa of *Alcelaphini* may not have been as committed to as their modern-day counterparts. Enamel of East African *Alcelaphini* has high $\delta^{18}\text{O}$ values compared to most of the other Karonga taxa analyzed (Fig. 5.3 and 5.5d). This could partly be explained with the effect of water intake through C₄ plants (Kohn et al., 1996). Interestingly, *Alc. Damaliscus*, *Megalotragus* and *Connochaetes* are considered to have an almost exclusively grazing diet (van der Merwe et al., 2003; Codron et al., 2007), but in the Karonga Basin assemblage (Unit 3A and 3B), they inhabit very different niches with mixed feeders, such as *Alc. Damaliscus* (high C₃ intake) and *Alc. Megalotragus* (high C₄ intake) and pure grazers like *Alc. Connochaetes* (Fig. 5.3). This again reflects a high diversity of the landscape with different food-supplies during the Plio-Pleistocene in the Malawi Rift and in its vicinity.

The intra-tooth stable isotopes values of equids and bovids reflect seasonal diet and drinking water variations: different patterns indicate different migrational and dietary behavior of individual animals. a) Some equid and bovid individuals have nourishment that is relatively constant in its isotopic composition for a long timespan (>1 yr), which could indicate food and water supplies that are similar throughout the year with only small seasonal fluctuations. A migration (with resources) over large distances is unlikely because the $\delta^{18}\text{O}$ ratios remain largely constant, indicating a continuous water source that is little influenced by evaporation and local meteoric water $\delta^{18}\text{O}$ ratios fluctuations. b) Small variations in $\delta^{13}\text{C}$, but large ones in $\delta^{18}\text{O}$ could indicate a seasonal migration of the herbivores with the favored food source (e.g., specialized grazers) with

changing drinking sources. The signal could also come from the same drinking source, but it changes its $\delta^{18}\text{O}$ composition due to climate (evaporation and different precipitation sources). c) A large fluctuation in both, $\delta^{13}\text{C}$ and $\delta^{18}\text{O}$, reflect changes in the diet (food and water). Individuals could stay in one region where the biomasses changed seasonally and the water source was largely influenced by climate (evaporation) and could have a different source in different periods of the year. C_4 consumption can shift $\delta^{18}\text{O}$ values in teeth towards more positive values resulting in a good co-variance (Fig. 5.7).

5.6 Conclusion

Oxygen and carbon isotope ratios of mammalian taxa including multiple samples of herbivores representing five families permit a consensus reconstruction of the habitat types in the Plio-Pleistocene Chiwondo Beds (Karonga Basin, Northern Malawi) by identification of foraging strategies. Over the past ca. 4 Ma the majority of herbivores, including suids, elephants, hippos, most equids and some bovids, had an eclectic, mixed C_3/C_4 diet with a large amount of C_3 biomass. Some specialized feeders reflect a dominant browsing C_3 diet (*Antilopini* and some suids), while *Alcelaphini* *Connochates* was a pure grazer. Herbivores living around paleolake Malawi had access to C_4 biomass already in the Late Pliocene. The limited representation of obligate grazers and the abundance of mixed feeders and browsers, in combination with large variability in the generally low $\delta^{18}\text{O}$ values of herbivore enamel suggest a regional heterogeneous environment. Water-rich woodlands border patches of C_4 -savanna with evaporatively ^{18}O -enriched water sources. Over the entire time of deposition of the Chiwondo Beds, both environments lie within the migratorial ranges of large bodied herbivores. These ecosystem patterns are strikingly different to the majority of reconstructed environments further north in the Eastern Rift, where open grassland-savannas dominate since ca. 2.5 Ma. Collectively, these stable isotope based reconstructions situate the Karonga Basin hominins *Homo rudolfensis* and *Paranthropus boisei* in a woodland-forest mosaic, which has important implications for developing explanations for evolutionary innovations such as dietary and behavioral versatility, encephalization, bipedalism and tool use, all of which have traditionally been linked to selective pressures encountered by early hominins foraging in grassland-savannas.

5.7 Acknowledgments

We are grateful to our local Malawian field crew in Karonga, the Cultural Museum Centre Karonga, and the Malawi Government for the long-term cooperation with the Hominid Corridor Research Project (HCRP). We want to thank in particular H. Simfukwe for assistance and hospitality. We acknowledge support through the LOEWE funding program (Landes-Offensive zur Entwicklung wissenschaftlich-ökonomischer Exzellenz) of Hesse's Ministry of Higher Education, Research, and the Arts and thank U. Treffert and S. Hoffmann for laboratory support.

5.8 Supplementary material

5.8.1 Chiwondo Beds Units

Precise age assignments in the Chiwondo and Chitimwe fossil material suffer from absence of datable volcanic material. Biostratigraphic constrains, mostly based on suid teeth divide the fossil assemblage into four intervals: ca. 4.3 to 3.75 Ma (Unit 1 and 2), 3.75 to 1.8 Ma (Unit 3A) and 1.8 to 0.6 Ma (Unit 3B; after Betzler and Ring, 1995; Bromage et al., 1995; Kullmer, 2008; Sandrock et al., 1999).

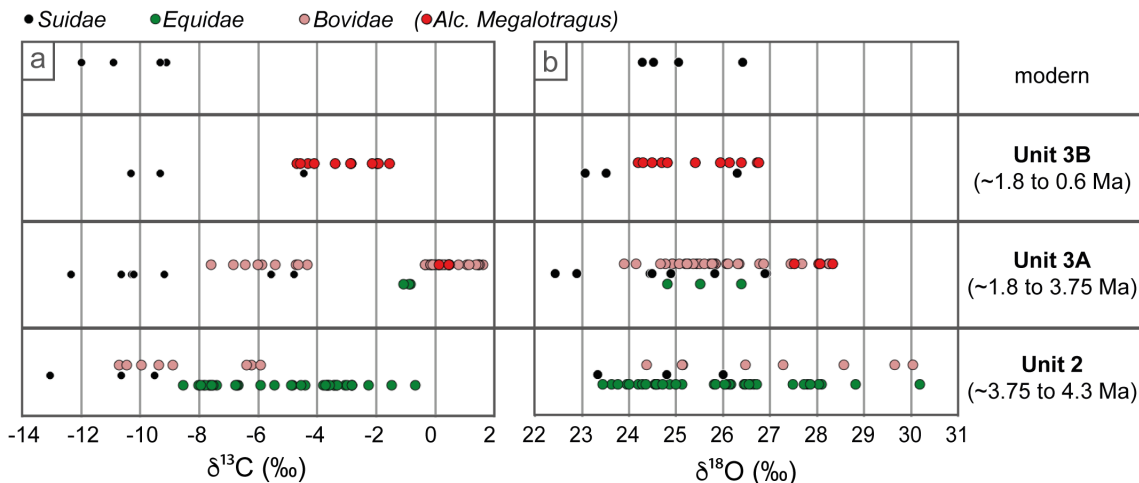


Figure 5.6: Suid, equid and bovid $\delta^{13}\text{C}$ (a) and $\delta^{18}\text{O}$ (b) data in stratigraphical order in the Chiwondo Beds. Note that *Alcelaphini Megalotragus* is the only bovidae genus sampled across two units (3A and 3B).

5.8.2 Material and methods

Suidae molars were laterally cut in half and enamel was sampled either with a hand-held diamond tip dental drill or a Merchantec micromill device. One equid molar (#1173) was also cut in half; the remaining enamel sample material is derived from either drill holes from the outer enamel or from enamel flakes that chipped from the outer coating. Sampling parallel and across several growth axes of the teeth was necessary to obtain sufficient sample material (2 to 3 mg). $\delta^{13}\text{C}$ and $\delta^{18}\text{O}$ values of bulk enamel samples, therefore, represent averages over the time of tooth formation and the dietary signal of bulk samples is attenuated over weeks or months, depending on species and wear pattern (Fisher and Fox, 1998; Passey and Cerling, 2002). Enamel is resistant to isotopic exchange (Wang and Cerling, 1994; Koch et al., 1997) when compared to bone or tooth-cement and dentine, hence care was taken to avoid these materials in the sample powder. Although the CO_3 component of bioapatite can be less resistant to diagenetic alteration of $\delta^{18}\text{O}$ values than the oxygen in the PO_4 component (Kolodny et al., 1983; Shemesh, 1990; Kohn et al., 1999), we feel that the large magnitude, systematic intra-tooth $\delta^{18}\text{O}$ variability within individual teeth very strongly points to primary $\delta^{18}\text{O}$ values that were not isotopically reset during fossilization. To remove organic matter and potential diagenetic carbonate, enamel was pretreated with 2% NaOCl solution for 24 hours followed by 1 M Ca-acetate acetic acid buffer solution for another 24

hours and thoroughly rinsed with deionized water (Spötl and Vennemann, 2003). Typically, enamel pre-treatment resulted in 10% to 60% mass loss.

5.8.3 $\delta^{13}\text{C}$ and $\delta^{18}\text{O}$ co-variance

Generally, low $\delta^{13}\text{C}$ values are associated with low $\delta^{18}\text{O}$ values, which holds true within the patterns of most teeth (Fig. 5.8), as well as in comparison of individual animals or even taxa (Fig. 5.2). This indicates that a consumption of mainly C_3 biomass is accompanied by water intake from sources that are only little influenced by evaporation (e.g., *Metridiochoerus*), which complements our ecosystem reconstructions. Therefore, animals that migrate farther away from freshwater rivers to drier parts of the ecosystem have access to open C_4 -grasslands and ^{18}O enriched drinking water (e.g., *Alc. Connochates*). The stable oxygen isotope composition of C_4 plants can also shift $\delta^{18}\text{O}$ values in teeth towards more positive values, especially for animals that have some of their water intake through plants.

However, *Antilopini* displays the opposite trend with displaying extremely low $\delta^{13}\text{C}$ values and high $\delta^{18}\text{O}$ values. A possible explanation for this individual is browsing in C_3 woodland at the margin of paleolake Malawi and drinking from the depleted lake water (see Fig. 5.4c).

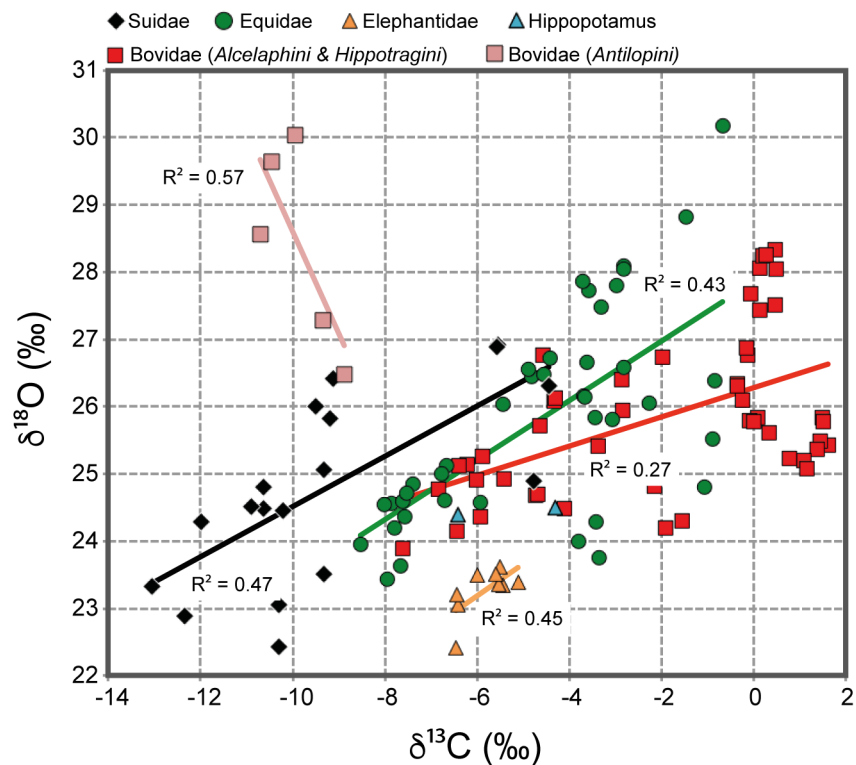


Figure 5.7: $\delta^{13}\text{C}$ vs. $\delta^{18}\text{O}$ values of mammals analyzed from the Karonga Basin. A general positive co-variance is observed with the exception of *Antilopini*, which displays a negative co-variance.

5.8.4 $\delta^{13}\text{C}$ and $\delta^{18}\text{O}$ values of analyzed herbivores

List of fossil Chiwondo herbivore enamel $\delta^{13}\text{C}$ and $\delta^{18}\text{O}$ with Hominid Corridor Research Project (HRCP) catalogue ID, sample ID, taxon, element, locality, unit within the Chiwondo Beds and position within tooth.

Table 5.2: Family Suidae

HRC P Cat.#	Sample #	Taxon	Element	Local- ity	Unit	cm from crown	$\delta^{13}\text{C}$ PDB (‰)	$\delta^{18}\text{O}$ SMOW (‰)
498	498-01	<i>Notochoerus euilus</i>	M	WK36	3A-1	0.5	-4.8	24.9
654	654-01	<i>Notochoerus euilus</i>	u M3	WK?	3A-1	3.5	-5.5	26.9
118	118-01	<i>Notochoerus scotti</i>	u M3	MP1	3A-2	0.2	-9.2	25.8
253	253-01	<i>Notochoerus scotti</i>	M3	WK18	3A-2	2.5	-5.6	26.9
457	457-01	<i>Notochoerus jaegeri</i>	M3	U6	2	1.2	-9.5	26.0
546	546-01	<i>Notochoerus jaegeri</i>	u M3	WK38	2	1.8	-13.1	23.3
546	546-02	<i>Notochoerus jaegeri</i>	u M3	WK38	2	0.5	-10.6	24.8
429	429-01	<i>Metridiochoerus compactus</i>	u M3	U25	3B	0.7	-10.3	23.1
429	429-02	<i>Metridiochoerus compactus</i>	M3	U25	3B	2.6	-4.4	26.3
407	407-01	<i>Metridiochoerus andrewsi stage I</i>	L I M3	U19	3A-2	0.8	-10.3	22.4
407	407-03	<i>Metridiochoerus andrewsi stage I</i>	L I M3	U19	3A-2	2.3	-10.2	24.5
407	407-04	<i>Metridiochoerus andrewsi stage I</i>	L I M3	U19	3A-2	2.7	-10.6	24.5
407	407-05	<i>Metridiochoerus andrewsi stage I</i>	L I M3	U19	3A-2	0.8	-12.3	22.9
423	423-01	<i>Metridiochoerus andrewsi stage III</i>	M3	U23	3B	0.5	-9.3	23.5
129	129-01	<i>Phacochoerus aethiopicus</i>	L I M3	RC1	mod	4	-12	24.3
129	129-01w	<i>Phacochoerus aethiopicus</i>	L I M3	RC1	mod	4	-10.9	24.5
129	129-02	<i>Phacochoerus aethiopicus</i>	L I M3	RC1	mod	4.7	-9.3	25.1
129	129-03	<i>Phacochoerus aethiopicus</i>	L I M3	RC1	mod	1.9	-9.1	26.4

Table 5.3: Family Hippopotamidae

HRCP Cat.#	Sample#	Taxon	Element	Locality	Unit	cm from crown	$\delta^{13}\text{C}$ PDB (‰)	$\delta^{18}\text{O}$ SMOW (‰)
1174	1174-01	<i>Hippopotamus amphibius</i>	u I1 or I2	WK	3A	2.50	-6.4	24.4
1174	1174-02	<i>Hippopotamus amphibius</i>	u I1 or I2	WK	3A	1.50	-4.3	24.5

Table 5.4: Family Elephantidae

HRCP Cat.#	Sample#	Taxon	Element	Locality	Unit	cm from break	$\delta^{13}\text{C}_{\text{VPDB}}$ (‰)	$\delta^{18}\text{O}_{\text{VSMOW}}$ (‰)
1175	1175-01	<i>Loxodonta</i> or <i>Elephas</i>	?	U	3A-2	0.10	-6.0	23.5
1175	1175-02	<i>Loxodonta</i> or <i>Elephas</i>	?	U	3A-2	0.40	-5.4	23.3
1175	1175-03	<i>Loxodonta</i> or <i>Elephas</i>	?	U	3A-2	0.70	-5.5	23.6
1175	1175-04	<i>Loxodonta</i> or <i>Elephas</i>	?	U	3A-2	0.95	-6.4	23.0
1175	1175-05	<i>Loxodonta</i> or <i>Elephas</i>	?	U	3A-2	1.30	-6.5	22.4
1175	1175-06	<i>Loxodonta</i> or <i>Elephas</i>	?	U	3A-2	1.70	-5.1	23.4
1175	1175-07	<i>Loxodonta</i> or <i>Elephas</i>	?	U	3A-2	2.05	-5.5	23.4
1175	1175-08	<i>Loxodonta</i> or <i>Elephas</i>	?	U	3A-2	2.60	-5.6	23.5
1175	1175-09	<i>Loxodonta</i> or <i>Elephas</i>	?	U	3A-2	2.80	-6.4	23.2

Table 5.5: Family Equidae

HRCP Cat.#	Sample#	Taxon	Element	Locality	Unit	cm from crown	$\delta^{13}\text{C}_{\text{VPDB}}$ (‰)	$\delta^{18}\text{O}_{\text{VSMOW}}$ (‰)
351	351-01	<i>Eurygnathohippus</i> sp.	R u M1	U8	2	0.10	-3.1	25.8
351	351-02	<i>Eurygnathohippus</i> sp.	R u M1	U8	2	0.27	-2.8	26.6
351	351-03	<i>Eurygnathohippus</i> sp.	R u M1	U8	2	0.43	-3.7	26.2
351	351-04	<i>Eurygnathohippus</i> sp.	R u M1	U8	2	0.60	-3.7	26.1
351	351-05	<i>Eurygnathohippus</i> sp.	R u M1	U8	2	0.77	-2.3	26.1
351	351-06	<i>Eurygnathohippus</i> sp.	R u M1	U8	2	0.93	-3.8	24.0
351	351-07	<i>Eurygnathohippus</i> sp.	R u M1	U8	2	1.10	-3.4	23.8
351	351-08	<i>Eurygnathohippus</i> sp.	R u M1	U8	2	1.27	-3.4	24.3
351	351-09	<i>Eurygnathohippus</i> sp.	R u M1	U8	2	1.43	-3.4	25.8
357	357-01	<i>Eurygnathohippus</i> sp.	R u M1	U8	2	0.10	-3.6	26.7
357	357-02	<i>Eurygnathohippus</i> sp.	R u M1	U8	2	0.28	-4.8	26.4
357	357-03	<i>Eurygnathohippus</i> sp.	R u M1	U8	2	0.45	-2.8	28.1
357	357-04	<i>Eurygnathohippus</i> sp.	R u M1	U8	2	0.63	-3.0	27.8
357	357-05	<i>Eurygnathohippus</i> sp.	R u M1	U8	2	0.80	-4.4	26.7
357	357-06	<i>Eurygnathohippus</i> sp.	R u M1	U8	2	0.98	-4.6	26.5
357	357-07	<i>Eurygnathohippus</i> sp.	R u M1	U8	2	1.15	-3.3	27.5
357	357-08	<i>Eurygnathohippus</i> sp.	R u M1	U8	2	1.33	-0.7	30.2
357	357-09	<i>Eurygnathohippus</i> sp.	R u M1	U8	2	1.50	-1.5	28.8
357	357-10	<i>Eurygnathohippus</i> sp.	R u M1	U8	2	1.68	-3.6	27.7
357	357-11	<i>Eurygnathohippus</i> sp.	R u M1	U8	2	1.85	-7.6	24.4
357	357-12	<i>Eurygnathohippus</i> sp.	R u M1	U8	2	2.03	-2.8	28.0
357	357-13	<i>Eurygnathohippus</i> sp.	R u M1	U8	2	2.20	-3.7	27.9
357	357-14	<i>Eurygnathohippus</i> sp.	R u M1	U8	2	2.38	-8.0	23.4
357	357-15	<i>Eurygnathohippus</i> sp.	R u M1	U8	2	2.55	-4.9	26.6
357	357-16	<i>Eurygnathohippus</i> sp.	R u M1	U8	2	2.73	-5.4	26.0
600	600-01	<i>Eurygnathohippus</i> sp.	PreM	WK	3A	0.00	-0.8	26.4
600	600-02	<i>Eurygnathohippus</i> sp.	PreM	WK	3A	0.45	-0.9	25.5
600	600-03	<i>Eurygnathohippus</i> sp.	PreM	WK	3A	0.90	-1.1	24.8
1173	1173-01	<i>Eurygnathohippus</i> sp.	L I M	MR/RC	2	0.20	-7.4	24.9
1173	1173-02	<i>Eurygnathohippus</i> sp.	L I M	MR/RC	2	0.45	-6.7	25.1
1173	1173-03	<i>Eurygnathohippus</i> sp.	L I M	MR/RC	2	0.80	-7.9	24.6
1173	1173-04	<i>Eurygnathohippus</i> sp.	L I M	MR/RC	2	1.10	-8.0	24.5
1173	1173-05	<i>Eurygnathohippus</i> sp.	L I M	MR/RC	2	1.35	-7.6	24.6
1173	1173-06	<i>Eurygnathohippus</i> sp.	L I M	MR/RC	2	1.70	-6.7	24.6
1173	1173-07	<i>Eurygnathohippus</i> sp.	L I M	MR/RC	2	2.05	-5.9	24.6
1173	1173-08	<i>Eurygnathohippus</i> sp.	L I M	MR/RC	2	2.30	-7.7	23.6
1173	1173-09	<i>Eurygnathohippus</i> sp.	L I M	MR/RC	2	2.70	-8.5	24.0
1173	1173-10	<i>Eurygnathohippus</i> sp.	L I M	MR/RC	2	3.20	-7.8	24.2
1173	1173-11	<i>Eurygnathohippus</i> sp.	L I M	MR/RC	2	3.60	-7.5	24.7
1173	1173-12	<i>Eurygnathohippus</i> sp.	L I M	MR/RC	2	4.20	-6.8	25.0

Table 5.6: Family Bovidae

HRC P Cat.#	Sample #	Taxon	Element	Locality	Unit	cm from crown	$\delta^{13}\text{C}$ VPDB (‰)	$\delta^{18}\text{O}$ VSMOW (‰)
154	154-01	<i>Alc. Connochaetes sp.</i>	u L M3	RC1	3A	0.13	1.5	25.8
154	154-02	<i>Alc. Connochaetes sp.</i>	u L M3	RC1	3A	0.27	1.6	25.4
154	154-03	<i>Alc. Connochaetes sp.</i>	u L M3	RC1	3A	0.40	1.5	25.8
154	154-04	<i>Alc. Connochaetes sp.</i>	u L M3	RC1	3A	0.53	1.4	25.5
154	154-05	<i>Alc. Connochaetes sp.</i>	u L M3	RC1	3A	0.67	1.4	25.4
154	154-06	<i>Alc. Connochaetes sp.</i>	u L M3	RC1	3A	0.80	1.1	25.2
154	154-07	<i>Alc. Connochaetes sp.</i>	u L M3	RC1	3A	0.93	1.1	25.1
154	154-08	<i>Alc. Connochaetes sp.</i>	u L M3	RC1	3A	1.07	0.8	25.2
154	154-09	<i>Alc. Connochaetes sp.</i>	u L M3	RC1	3A	1.20	0.3	25.6
154	154-10	<i>Alc. Connochaetes sp.</i>	u L M3	RC1	3A	1.33	0.1	25.8
154	154-11	<i>Alc. Connochaetes sp.</i>	u L M3	RC1	3A	1.47	-0.1	25.8
154	154-12	<i>Alc. Connochaetes sp.</i>	u L M3	RC1	3A	1.60	0.0	25.8
154	154-13	<i>Alc. Connochaetes sp.</i>	u L M3	RC1	3A	1.73	-0.3	26.1
154	154-14	<i>Alc. Connochaetes sp.</i>	u L M3	RC1	3A	1.87	-0.4	26.3
154	154-15	<i>Alc. Connochaetes sp.</i>	u L M3	RC1	3A	2.00	-0.3	26.3
154	154-16	<i>Alc. Connochaetes sp.</i>	u L M3	RC1	3A	2.13	-0.1	26.8
154	154-17	<i>Alc. Connochaetes sp.</i>	u L M3	RC1	3A	2.27	-0.2	26.9
154	154-18	<i>Alc. Connochaetes sp.</i>	u L M3	RC1	3A	2.40	0.1	27.4
154	154-19	<i>Alc. Connochaetes sp.</i>	u L M3	RC1	3A	2.53	-0.1	27.7
154	154-20	<i>Alc. Connochaetes sp.</i>	u L M3	RC1	3A	2.67	0.2	28.2
154	154-21	<i>Alc. Connochaetes sp.</i>	u L M3	RC1	3A	2.80	0.3	28.3
361	361-02	<i>Alc. Megalotragus sp.</i>	I M	U11	3B	0.40	-4.3	26.1
361	361-03	<i>Alc. Megalotragus sp.</i>	I M	U11	3B	0.80	-2.0	26.7
361	361-04	<i>Alc. Megalotragus sp.</i>	I M	U11	3B	1.20	-2.8	25.9
361	361-06	<i>Alc. Megalotragus sp.</i>	I M	U11	3B	1.60	-4.7	24.7
361	361-07	<i>Alc. Megalotragus sp.</i>	I M	U11	3B	1.90	-2.9	26.4
361	361-08	<i>Alc. Megalotragus sp.</i>	I M	U11	3B	2.30	-4.6	26.8
361	361-08	<i>Alc. Megalotragus sp.</i>	I M	U11	3B	2.80	-3.4	25.4
373	373-01	<i>Alc. Megalotragus sp.</i>	u M	U13	3A	0.00	0.5	28.0
373	373-02	<i>Alc. Megalotragus sp.</i>	u M	U13	3A	0.43	0.1	28.1
373	373-03	<i>Alc. Megalotragus sp.</i>	u M	U13	3A	0.87	0.5	28.3
373	373-04	<i>Alc. Megalotragus sp.</i>	u M	U13	3A	1.30	0.5	27.5
419	419-01	<i>Alc. Megalotragus sp.</i>	L I M3	U21	3B	0.30	-1.9	24.2
419	419-02	<i>Alc. Megalotragus sp.</i>	L I M3	U21	3B	0.50	-1.6	24.3
419	419-03	<i>Alc. Megalotragus sp.</i>	L I M3	U21	3B	0.90	-2.1	24.8
419	419-04	<i>Alc. Megalotragus sp.</i>	L I M3	U21	3B	1.10	-4.1	24.5
187	187-01	<i>Alc. Damaliscus sp.</i>	I M3	WK11	3A	0.30	-6.4	24.1
187	187-02	<i>Alc. Damaliscus sp.</i>	I M3	WK11	3A	0.60	-5.4	24.9
187	187-03	<i>Alc. Damaliscus sp.</i>	I M3	WK11	3A	1.10	-4.3	26.1
187	187-04	<i>Alc. Damaliscus sp.</i>	I M3	WK11	3A	1.60	-5.9	25.3
187	187-05	<i>Alc. Damaliscus sp.</i>	I M3	WK11	3A	2.10	-6.0	24.9
187	187-06	<i>Alc. Damaliscus sp.</i>	I M3	WK11	3A	2.60	-6.8	24.8
187	187-07	<i>Alc. Damaliscus sp.</i>	I M3	WK11	3A	3.00	-7.6	23.9
187	187-08	<i>Alc. Damaliscus sp.</i>	I M3	WK11	3A	3.60	-4.7	24.7
187	187-09	<i>Alc. Damaliscus sp.</i>	I M3	WK11	3A	no info	-4.6	25.7
348	348-01	<i>Hippotragini</i>	u M	U6	2	3.10	-6.2	25.1
348	348-02	<i>Hippotragini</i>	u M	U6	2	3.10	-6.4	25.1
348	348-03	<i>Hippotragini</i>	u M	U6	2	3.10	-5.9	24.4
547a	547-01	<i>Antilopini</i>	I M	WK 38	2	0.24	-8.9	26.5
547a	547-02	<i>Antilopini</i>	I M	WK 38	2	0.48	-9.4	27.3
547a	547-03	<i>Antilopini</i>	I M	WK 38	2	0.72	-10.7	28.6
547a	547-04	<i>Antilopini</i>	I M	WK 38	2	0.96	-10.5	29.6
547a	547-05	<i>Antilopini</i>	I M	WK 38	2	1.20	-10.0	30.0

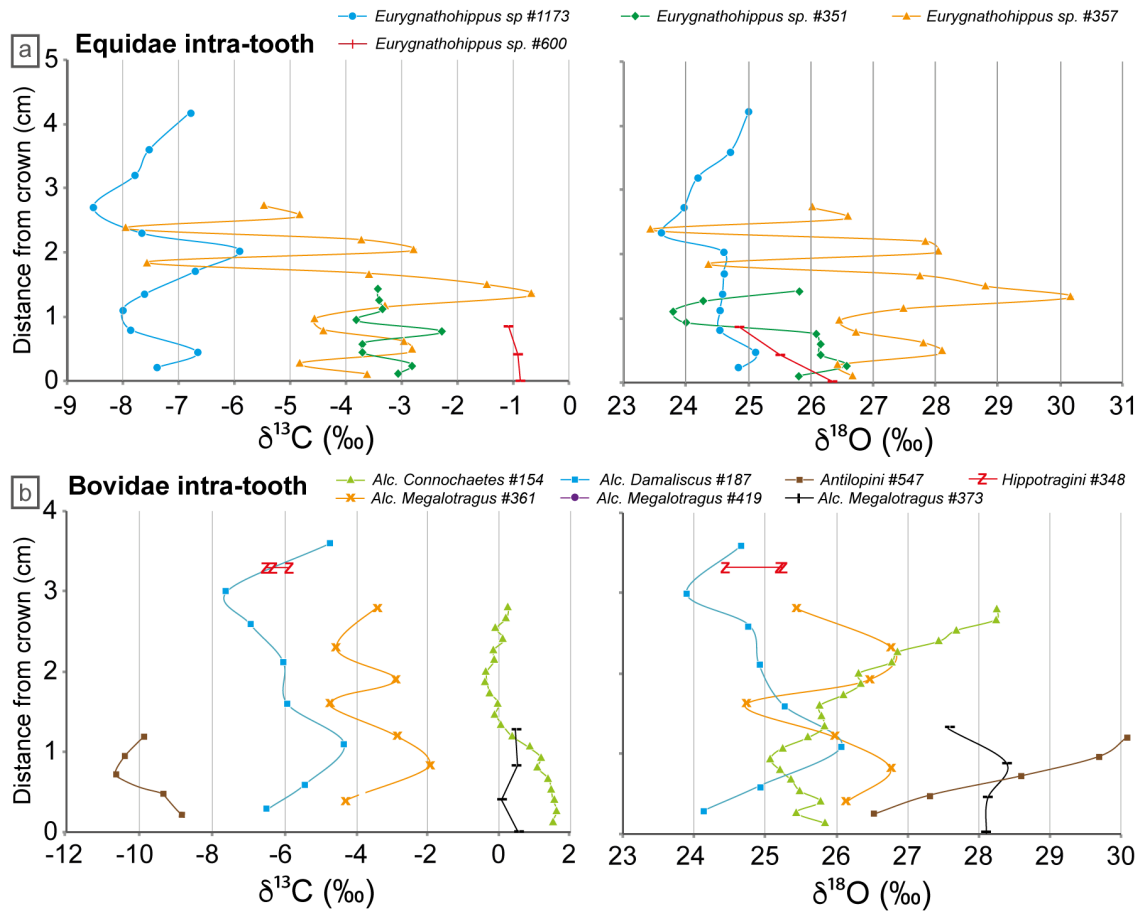


Figure 5.8: Intra-tooth $\delta^{13}\text{C}$ and $\delta^{18}\text{O}$ variations of all equids (a) and bovids (b) analyzed for this paper. 5.8.5d $\delta^{18}\text{O}$ values of analyzed meteoric waters

5.8.5 $\delta^{18}\text{O}$ values of analyzed meteoric waters

List of modern meteoric waters $\delta^{18}\text{O}$ (lake, river groundwater and rainwater) from northern Malawi with sample ID, GPS latitude and longitude, altitude above mean sea level and date sampled.

Table 5.7: Rainwater (Karonga: S9°55.887'; E33°56.570' and Malema: S10°01.199'; E33°55.639')

Sample ID	Location	Date installed	Date removed	$\delta^{18}\text{O}$ VSMOW (‰)
12MRW01	Malema	01-Nov-2012	14-Nov-2012	-1.9
12KRW01	Karonga	01-Nov-2012	15-Nov-2012	-2.9
13KRW01	Karonga	10-Oct-2013	07-Dec-2013	-1.7
13MRW04	Malema	19-Nov-2013	02-Dec-2013	-3.6
12MRW03	Malema	29-Nov-2012	12-Dec-2012	-4.4
12KRW03	Karonga	29-Nov-2012	13-Dec-2012	-6.3
12MRW04	Malema	13-Dec-2012	26-Dec-2012	-5.8
12KRW04	Karonga	13-Dec-2012	27-Dec-2012	-6.7
13MRW05	Malema	03-Dec-2013	16-Dec-2013	-4.5
13KRW02	Karonga	07-Dec-2013	21-Dec-2013	-0.3
13MRW06	Malema	17-Dec-2013	30-Dec-2013	-7.9
13KRW03	Karonga	21-Dec-2013	03-Jan-2014	-3.0
12MRW05	Malema	27-Dec-2012	09-Jan-2013	-5.0
12KRW05	Karonga	27-Dec-2012	10-Jan-2013	-3.3
12MRW06	Malema	10-Jan-2013	23-Jan-2013	-2.5
12MRW07	Malema	24-Jan-2013	06-Feb-2013	-2.7
12KRW07	Karonga	24-Jan-2013	07-Feb-2013	-3.0
13MRW07	Malema	31-Dec-2013	13-Jan-2014	0.7
13KRW04	Karonga	03-Jan-2014	16-Jan-2014	-7.1
13MRW08	Malema	14-Jan-2014	27-Jan-2014	-5.8
13KRW05	Karonga	16-Jan-2014	29-Jan-2014	-5.2
12MRW08	Malema	7-Feb-2013	20-Feb-2013	-2.8
12KRW08	Karonga	7-Feb-2013	21-Feb-2013	-2.5
12MRW09	Malema	21-Feb-2013	06-Mar-2013	-6.1
12KRW09	Karonga	21-Feb-2013	07-Mar-2013	-2.0
13MRW09	Malema	28-Jan-2014	10-Feb-2014	-1.3
13KRW06	Karonga	29-Jan-2014	11-Feb-2014	-5.9
13KRW07	Karonga	11-Feb-2014	24-Feb-2014	-6.5
12MRW10	Malema	07-Mar-2013	20-Mar-2013	-3.0
12KRW10	Karonga	07-Mar-2013	21-Mar-2013	-5.7
12MRW11	Malema	21-Mar-2013	03-Apr-2013	-2.9
12KRW11	Karonga	21-Mar-2013	04-Apr-2013	-2.8
13KRW08	Karonga	24-Feb-2014	09-Mar-2014	-7.3
13MRW11	Malema	25-Feb-2014	09-Mar-2014	-4.0
13KRW09	Karonga	9-Mar-2014	22-Mar-2014	-4.9
13KRW10	Karonga	22-Mar-2014	04-Apr-2014	-5.1
13MRW13	Malema	24-Mar-2014	07-Apr-2014	-2.6
12MRW12	Malema	04-Apr-2013	17-Apr-2013	-2.4
12KRW12	Karonga	04-Apr-2013	18-Apr-2013	-2.6
12MRW13	Malema	18-Apr-2013	01-May-2013	-0.7
12KRW13	Karonga	18-Apr-2013	02-May-2013	-0.5
13KRW12	Karonga	17-Apr-2014	30-Apr-2014	-1.9
13MRW15	Malema	22-Apr-2014	05-May-2014	-2.3
12KRW14	Karonga	2-May-2013	10-May-2013	0.3

Table 5.8: Rivers

Sample ID	Position	Altitude (m asl)	Date sampled	$\delta^{18}\text{O}_{\text{VSMOW}}$ (‰)
11MW146	S9°35.272'; E33°44.601'	516	10-Nov-2011	-3.4
11MW159	S10°45.746'; E34°07.390'	848	12-Nov-2011	-4.8
12MW021	S9°56.763'; E33°50.491'	518	24-Sep-2012	-4.9
12MW022	S9°56.624'; E33°46.500'	541	24-Sep-2012	-5.8
12MW030	S10°05.822'; E33°33.466'	1336	24-Sep-2012	-5.8
12MW033	S10°31.021'; E33°43.532'	2047	24-Sep-2012	-7.0
12MW036	S10°43.809'; E33°40.942'	1789	25-Sep-2012	-6.5
12MW067	S10°37.910'; E34°05.012'	1028	04-Oct-2012	-5.8
13MW084	S10°49.686'; E34°05.629'	949	29-Sep-2013	-5.3

Table 5.9: Groundwater

Sample ID	Position	Altitude (m asl)	Date sampled	$\delta^{18}\text{O}_{\text{VSMOW}}$ (‰)
11MW038	S10°00.106'; E33°55.460'	542	26-Oct-2011	-4.7
11MW039	S10°01.023'; E33°56.510'	500	26-Oct-2011	-5.0
11MW040	S10°01.235'; E33°55.595'	510	26-Oct-2011	-5.0
11MW067	S10°19.063'; E34°08.314'	509	31-Oct-2011	-4.9
11MW068	S10°20.312'; E34°08.213'	523	31-Oct-2011	-4.8
11MW130	S10°18.106'; E34°02.595'	548	06-Nov-2011	-4.5
11MW136	S10°17.448'; E34°01.913'	575	06-Nov-2011	-4.7
11MW149	S9°36.330'; E33°42.810'	521	10-Nov-2011	-4.3
11MW150	S9°35.272'; E33°44.519'	519	10-Nov-2011	-4.4
11MW151	S9°41.568'; E33°51.120'	495	10-Nov-2011	-3.6
11MW153	S9°59.464'; E33°55.548'	498	10-Nov-2011	-5.2
11MW154	S10°05.066'; E33°58.939'	500	12-Nov-2011	-5.1
11MW155	S10°16.591'; E34°06.418'	508	12-Nov-2011	-5.4
11MW156	S10°31.609'; E34°12.261'	545	12-Nov-2011	-4.6
11MW157	S10°39.493'; E34°11.567'	485	12-Nov-2011	-4.2
11MW158	S10°44.267'; E34°09.046'	971	12-Nov-2011	-5.4
11MW160	S10°53.074'; E34°02.767'	1005	12-Nov-2011	-5.5
11MW161	S11°04.205'; E33°54.772'	1040	12-Nov-2011	-6.8
11MW162	S11°00.979'; E33°46.534'	1076	12-Nov-2011	-5.5
11MW163	S11°08.053'; E33°39.280'	1091	12-Nov-2011	-5.7
11MW165	S11°14.508'; E33°52.196'	1115	13-Nov-2011	-6.0
11MW166	S11°24.636'; E33°59.036'	1310	13-Nov-2011	-6.0
11MW167	S11°32.315'; E34°09.911'	611	13-Nov-2011	-4.9
11MW168	S11°45.387'; E34°12.874'	521	13-Nov-2011	-4.5
11MW169	S11°57.204'; E34°05.012'	484	13-Nov-2011	-4.8
11MW170	S12°21.148'; E34°03.100'	468	13-Nov-2011	-5.5
11MW171	S12°37.157'; E34°09.986'	487	13-Nov-2011	-5.6
11MW172	S12°48.079'; E34°12.988'	491	13-Nov-2011	-5.4
12MW023	S9°56.605'; E33°46.542'	542	24-Sep-2012	-5.5
12MW024	S9°55.167'; E33°39.530'	1013	24-Sep-2012	-5.6

Table 5.9 (continued)

Sample ID	Position	Altitude (m asl)	Date sampled	$\delta^{18}\text{O}_{\text{VSMOW}}$ (‰)
12MW025	S9°54.206'; E33°36.099'	1149	24-Sep-2012	-5.5
12MW026	S9°49.080'; E33°28.585'	1301	24-Sep-2012	-5.9
12MW027	S9°49.655'; E33°25.146'	1325	24-Sep-2012	-6.0
12MW028	S9°58.512'; E33°23.552'	1538	24-Sep-2012	-6.8
12MW029	S10°02.335'; E33°28.468'	1513	24-Sep-2012	-6.3
12MW031	S10°20.952'; E33°38.308'	1289	24-Sep-2012	-6.3
12MW037	S10°54.940'; E33°35.041'	1395	25-Sep-2012	-6.7
12MW046	S10°24.292'; E34°11.149'	601	27-Sep-2012	-4.2
12MW049	S10°25.774'; E34°10.484'	541	27-Sep-2012	-4.5
12MW051	S10°25.496'; E34°11.438'	530	27-Sep-2012	-4.5
12MW061	S10°01.554'; E33°55.338'	546	01-Oct-2012	-4.8
12MW066	S10°36.700'; E34°06.786'	1375	04-Oct-2012	-5.7
12MW068	S10°38.202'; E34°04.893'	1033	04-Oct-2012	-5.1
12MW069	S10°40.734'; E34°04.052'	1174	04-Oct-2012	-5.4
13MW082	S12°38.309'; E33°29.871'	1195	28-Oct-2013	-6.8
13MW096	S10°20.523'; E34°11.409'	542	04-Oct-2012	-5.4
13MW098	S10°21.258'; E34°09.130'	546	04-Oct-2012	-5.1
13MW099	S10°12.612'; E34°05.647'	501	04-Oct-2012	-4.9
13MW109	S10°01.234'; E33°55.602'	527	08-Oct-2013	-5.0
13MW114	S10°02.047'; E33°55.860'	564	09-Oct-2013	-5.2
13MW124	S11°07.390'; E33°43.141'	1105	13-Oct-2013	-6.4

Table 5.10: Lakes

Sample ID	Position	Lake	Altitude (m asl)	Date sampled	$\delta^{18}\text{O}_{\text{VSMOW}}$ (‰)
11MW174	S13°02.776';; E34°19.671'	Lake Malawi	489	13-Nov-2011	2.1
12MW034	S10°35.763'; E33°48.429'	Dam Nyika	2277	25-Sep-2012	-5.7
12MW035	S10°36.527'; E33°48.276'	Dam Nyika	2267	25-Sep-2012	-5.4
12MW065	S10°00.760'; E33°57.409'	Lake Malawi	489	02-Oct-2012	2.4
13MW135	S13°42.535'; E34°37.298'	Lake Malawi	490	17-Oct-2012	2.0

5.9 References

- Aronson, J.L., Hailemichael, M., Savin, S.M., 2008. Hominid Environments at Hadar from Paleosol Studies in a Framework of Ethiopian Climate Change. *Journal of Human Evolution* 55, 532-550.
- Ayliffe, L.K., Chivas, A.R., 1990. Oxygen Isotope Composition of the Bone Phosphate of Australian Kangaroos: Potential as a Palaeoenvironmental Recorder. *Geochimica et Cosmochimica Acta* 54, 2603-2609.
- Bedaso, Z.K., Wynn, J.G., Alemseged, Z., Geraads, D., 2013. Dietary and Palaeoenvironmental Reconstruction Using Stable Isotopes of Herbivore Tooth Enamel from Middle Pliocene Dikika, Ethiopia: Implication for Australopithecus Afarensis Habitat and Food Resources. *Journal of Human Evolution* 64, 21-38.
- Behrensmeyer, A.K., Todd, N.E., Potts, R., McBrinn, G.E., 1997. Late Pliocene Faunal Turnover in the Turkana Basin, Kenya and Ethiopia. *Science* 278, 1589-1594.
- Betzler, C., Ring, U., 1995. Sedimentology of the Malawi Rift: Facies and Stratigraphy of the Chiwondo Beds, Northern Malawi. *Journal of Human Evolution* 28, 13.
- Bibi, F., Kiessling, W., 2015. Continuous Evolutionary Change in Plio-Pleistocene Mammals of Eastern Africa. *Proceedings of the National Academy of Sciences* 112, 10623-10628.
- Bibi, F., Souron, A., Bocherens, H., Uno, K., Boisserie, J.-R., 2013. Ecological Change in the Lower Omo Valley around 2.8 Ma. *Biology Letters* 9, 20120890.
- Birkeland, P.W., 1984. *Soils and Geomorphology*. Oxford University Press, Oxford.
- Bishop, L.C., Hill, A., Kingston, J.D., 1999. *Paleoecology of Suidae from the Tugen Hills, Baringo, Kenya*. In: Andrew, A.E., Banham, P. (Eds.), Late Cenozoic Environments and Hominid Evolution: A Tribute to Bill Bishop. Geological Society of London, London, pp. 399-420.
- Bocherens, H., Koch, P.L., Mariotti, A., Geraads, D., Jaeger, J.J., 1996. Isotopic Biogeochemistry (^{13}C , ^{18}O) of Mammalian Enamel from African Pleistocene Hominid Sites. *Palaios* 11, 306-318.
- Boisserie, J.-R., Zazzo, A., Merceron, G., Blondel, C., Vignaud, P., Likius, A., Mackaye, H.T., Brunet, M., 2005. Diets of Modern and Late Miocene *Hippopotamids*: Evidence from Carbon Isotope Composition and Micro-Wear of Tooth Enamel. *Palaeogeography, Palaeoclimatology, Palaeoecology* 221, 153-174.
- Brachert, T.C., Brüggmann, G.B., Mertz, D.F., Kullmer, O., Schrenk, F., Jacob, D.E., Ssemmanda, I., Taubald, H., 2010. Stable Isotope Variation in Tooth Enamel from Neogene *Hippopotamids*: Monitor of Meso and Global Climate and Rift Dynamics on the Albertine Rift, Uganda. *International Journal of Earth Sciences* 99, 1663-1675.
- Bromage, T.G., Schrenk, F., Zonneveld, F.W., 1995. Paleoanthropology of the Malawi Rift: An Early Hominid Mandible from the Chiwondo Beds, Northern Malawi. *Journal of Human Evolution* 28, 71-108.
- Bryant, D.J., Froelich, P.N., 1995. A Model of Oxygen Isotope Fractionation in Body Water of Large Mammals. *Geochimica et Cosmochimica Acta* 59, 4523-4537.
- Bryant, D.J., Koch, P.L., Froelich, P.N., Showers, W.J., Genna, B.J., 1996. Oxygen Isotope Partitioning between Phosphate and Carbonate in Mammalian Apatite. *Geochimica et Cosmochimica Acta* 60, 5145-5148.
- Cerling, Harris, J.M., Passey, B.H., 2003. Diets of East African Bovidae Based on Stable Isotope Analysis. *Journal of Mammalogy* 84, 456-470.
- Cerling, T.E., 1992. Use of Carbon Isotopes in Paleosols as an Indicator of the $p(\text{CO}_2)$ of the Paleatmosphere. *Global Biogeochemical Cycles* 6, 8.
- Cerling, T.E., Andanje, S.A., Blumenthal, S.A., Brown, F.H., Chritz, K.L., Harris, J.M., Hart, J.A., Kirera, F.M., Kaleme, P., Leakey, L.N., Leakey, M.G., Levin, N.E., Manthi, F.K., Passey, B.H., Uno, K.T., 2015. Dietary Changes of Large Herbivores in the Turkana Basin, Kenya from 4 to 1 Ma. *Proceedings of the National Academy of Sciences* 37, 11467-11472.

- Cerling, T.E., Bowman, J.R., O'Neil, J.R., 1988. An Isotopic Study of a Fluvial-Lacustrine Sequence: The Plio-Pleistocene Koobi Fora Sequence, East Africa. *Palaeogeography, Palaeoclimatology, Palaeoecology* 63, 22.
- Cerling, T.E., Chritz, K.L., Jablonski, N.G., Leakey, M.G., Kyalo Manthi, F., 2013. Diet of *Theropithecus* from 4 to 1 Ma in Kenya. *Proceedings of the National Academy of Sciences* 110, 10507–10512.
- Cerling, T.E., Harris, J.M., 1999. Carbon Isotope Fractionation between Diet and Bioapatite in Ungulate Mammals and Implications for Ecological and Paleocological Studies. *Oecologia* 120, 347-363.
- Cerling, T.E., Harris, J.M., Hart, J.A., Kaleme, P., Klingel, H., Leakey, M.G., Levin, N.E., Lewison, R.L., Passey, B.H., 2008. Stable Isotope Ecology of the Common *Hippopotamus*. *Journal of Zoology* 276, 204-212.
- Cerling, T.E., Harris, J.M., Leakey, M.G., 1999. Browsing and Grazing in Elephants: The Isotope Record of Modern and Fossil Proboscideans. *Oecologia* 120, 364-374.
- Cerling, T.E., Harris, J.M., Leakey, M.G., 2003. *Isotope Paleocology of the Nawata and Nachukui Formations at Lothagam, Turkana Basin, Kenya*. In: Leakey, M.G., Harris, J.M. (Eds.), *Lothagam: The Dawn of Humanity in Eastern Africa*. Columbia University Press, New York, pp. 583-604.
- Cerling, T.E., Harris, J.M., Leakey, N., 2003. *Stable Isotope Ecology of Northern Kenya, with Emphasis on the Turkana Basin*. In: Leakey, M.G., Harris, J.M. (Eds.), *Lothagam: The Dawn of Humanity in Eastern Africa*. Columbia University Press, New York, pp. 583-603.
- Cerling, T.E., Harris, J.M., MacFadden, B.J., Leakey, M.G., Quade, J., Eisenmann, V., Ehleringer, J.R., 1997. Global Vegetation Change through the Miocene/Pliocene Boundary. *Nature* 389, 153-158.
- Cerling, T.E., Hay, R.L., 1986. An Isotopic Study of Paleosol Carbonates from Olduvai Gorge. *Quaternary Research* 25, 63-78.
- Cerling, T.E., Levin, N.E., Passey, B.H., 2011a. Stable Isotope Ecology in the Omo-Turkana Basin. *Evolutionary Anthropology* 20, 228-237.
- Cerling, T.E., Wynn, J.G., Andanje, S.A., Bird, M.I., Korir, D.K., Levin, N.E., Mace, W., Macharia, A.N., Quade, J., Remien, C.H., 2011b. Woody Cover and Hominin Environments in the Past 6 Million Years. *Nature* 476, 51-56.
- Codron, D., Codron, J., Lee-Thorp, J.A., Sponheimer, M., De Ruiter, D., Sealy, J., Grant, R., Fourie, N., 2007. Diets of Savanna Ungulates from Stable Carbon Isotope Composition of Faeces. *Journal of Zoology* 273, 21-29.
- Cooke, H.B.S., Wilkinson, Q.F., 1978. *Suidae and Tayassuidae*. In: Coppens, Y. (Ed.), *Evolution of African Mammals*. Harvard University Press, Cambridge, MA, pp. 435-482.
- DeBusk, G.H., 1994. *Transport and Stratigraphy of Pollen in Lake Malawi, Africa*. PhD Thesis, Duke University.
- Delvaux, D., 1995. Age of Lake Malawi (Nyasa) and Water Level Fluctuations. *Annual Rapports of the Royal Museum of Central Africa. Department of geology and Mineralolgy 1993-1994*, 99-108.
- deMenocal, P.B., 1995. Plio-Pleistocene African Climate. *Science* 270, 53-59.
- deMenocal, P.B., 2004. African Climate Change and Faunal Evolution During the Pliocene-Pleistocene. *Earth and Planetary Science Letters* 220, 3-24.
- DeNiro, M.J., Epstein, S., 1978. Influence of Diet on the Distribution of Carbon Isotopes in Animals. *Geochimica et Cosmochimica Acta* 42, 495-506.
- Drapeau, M.S.M., Bobe, R., Wynn, J.G., Campisano, C.J., Dumouchel, L., Geraads, D., 2014. The Omo Mursi Formation: A Window into the East African Pliocene. *Journal of Human Evolution* 75, 64-79.
- Drayton, R.S., 1984. Variations in the Level of Lake Malawi. *Hydrological Sciences Journal* 29, 1-12.

- Ehleringer, J.R., Monson, R.K., 1993. Evolutionary and Ecological Aspects of Photosynthetic Pathway Variation. *Annual Review of Ecology and Systematics* 24, 411-439.
- Estes, R.D., 2012. *The Behavior Guide to African Mammals, Including Hoofed Mammals, Carnivores, Primates. Including Hoofed Mammals, Carnivores, Primates, 20th Anniversary Edition.* University of California Press.
- Farquhar, G.D., Ehleringer, J.R., Hubick, K.T., 1989. Carbon Isotope Discrimination and Photosynthesis. *Annual Review of Plant Physiology and Plant Molecular Biology* 40, 503-537.
- Feakins, S.J., Levin, N.E., Liddy, H.M., Sieracki, A., Eglinton, T.I., Bonnefille, R., 2013. Northeast African Vegetation Change over 12 M.Y. *Geology* 41, 295-298.
- Feranec, R.S., 2003. Stable Isotopes, Hypsodonty, and the Paleodiet of *Hemiauchenia* (Mammalia: Camelidae): A Morphological Specialization Creating Ecological Generalization. *Paleobiology* 29, 230-242.
- Finney, B.P., Scholz, C.A., Johnson, T.C., 1996. *Late-Quaternary Lake Level Fluctuations in Lake Malawi, Africa, in Phase with Southern Hemisphere Insolation Variations.* In: Johnson, T.C., Odata, E. (Eds.), *Limnology, Climatology and Paleoclimatology of the East African Lakes.* Taylor & Francis, pp. 495-508.
- Fisher, D.C., Fox, D.L., 1998. Oxygen Isotopes in Mammoth Teeth: Sample Design, Mineralization Patterns, and Enamel–Dentin Comparisons. *Journal of Vertebrate Paleontology* 18, 41A-42A.
- Franz-Odenaal, T.A., Lee-Thorp, J.A., Chinsamy, A., 2002. New Evidence for the Lack of C₄ Grassland Expansions During the Early Pliocene at Langebaanweg, South Africa. *Paleobiology* 28, 378-388.
- Gagnon, M., Chew, A.E., 2000. Dietary Preferences in Extant African Bovidae. *Journal of Mammalogy* 81, 490-511.
- Gajewski, K., Lézine, A.-M., Vincens, A., Delestan, A., Sawada, M., 2002. Modern Climate–Vegetation–Pollen Relations in Africa and Adjacent Areas. *Quaternary Science Reviews* 21, 1611-1631.
- Gasse, F., Chalié, F., Vincens, A., Williams, M.A.J., Williamson, D., 2008. Climatic Patterns in Equatorial and Southern Africa from 30,000 to 10,000 Years Ago Reconstructed from Terrestrial and near-Shore Proxy Data. *Quaternary Science Reviews* 27, 2316-2340.
- Gentry, A.W., 1992. The Subfamilies and Tribes of the Family Bovidae. *Mammal Review* 22, 1-32.
- Goddard, L., Graham, N.E., 1999. Importance of the Indian Ocean for Simulating Rainfall Anomalies over Eastern and Southern Africa. *Journal of Geophysical Research: Atmospheres* 104, 19099-19116.
- Hamiel, Y., Baer, G., Kalindekaffe, L., Dombola, K., Chindandali, P., 2012. Seismic and Aseismic Slip Evolution and Deformation Associated with the 2009-2010 Northern Malawi Earthquake Swarm, East African Rift. *Geophysical Journal International*, 898-908.
- Harris, J.M., 1983. *Family Suidae.* In: Harris, J.M. (Ed.), *Koobi Fora Research Project. The Fossil Ungulates: Proboscidea, Perissodactyla, and Suidae.* Clarendon Press, Oxford, pp. 215-302.
- Harris, J.M., Cerling, T.E., 2002. Dietary Adaptations of Extant and Neogene African Suids. *Journal of Zoology* 256, 45-54.
- Harris, J.M., Cerling, T.E., Leakey, M.G., Passey, B.H., 2008. Stable Isotope Ecology of Fossil *Hippopotamids* from the Lake Turkana Basin of East Africa. *Journal of Zoology* 275, 323-331.
- Harrison, T., 2011. *Paleontology and Geology of Laetoli: Human Evolution in Context.* Volume 1: Geology, Geochronology, Paleoecology and Paleoenvironment. Springer.
- Heinzelin, J.d., Clark, J.D., White, T., Hart, W., Renne, P., WoldeGabriel, G., Beyene, Y., Vrba, E., 1999. Environment and Behavior of 2.5-Million-Year-Old Bouri Hominids. *Science* 284, 625-629.

- Hély, C., Bremond, L., Alleaume, S., Smith, B., Sykes, M.T., Guiot, J., 2006. Sensitivity of African Biomes to Changes in the Precipitation Regime. *Global Ecology and Biogeography* 15, 258-270.
- Hillson, S., 2005. *Teeth*. Cambridge University Press, pp388.
- Hoppe, K.A., Stover, S.M., Pascoe, J.R., Amundson, R., 2004. Tooth Enamel Biomineralization in Extant Horses: Implications for Isotopic Microsampling. *Palaeogeography, Palaeoclimatology, Palaeoecology* 206, 355-365.
- Iacumin, P., Bocherens, H., Mariotti, A., Longinelli, A., 1996. Oxygen Isotope Analyses of Co-Existing Carbonate and Phosphate in Biogenic Apatite: A Way to Monitor Diagenetic Alteration of Bone Phosphate? *Earth and Planetary Science Letters* 142, 1-6.
- IAEA/WMO (2015). *Global Network of Isotopes in Precipitation*. The GNIP Database. Accessible at: <http://www.iaea.org/water>.
- Ivory, S.J., Lézine, A.-M., Vincens, A., Cohen, A.S., 2012. Effect of Aridity and Rainfall Seasonality on Vegetation in the Southern Tropics of East Africa During the Pleistocene/Holocene Transition. *Quaternary Research* 77, 77-86.
- Kappelman, J., Plummer, T., Bishop, L., Duncan, A., Appleton, S., 1997. Bovids as Indicators of Plio-Pleistocene Paleoenvironments in East Africa. *Journal of Human Evolution* 32, 229-256.
- Kaufulu, Z.M., Stern, N., 1987. The first stone artefacts to be found in situ within the Plio-Pleistocene Chiwondo Beds in Northern Malawi. *Journal of Human Evolution* 16, 729-740.
- Kingdon, J., 1982. *East African Mammals. An Atlas of Evolution in Africa III. Parts C and D (Bovids)*. Academic Press, London.
- Kingdon, J.D., 2015. *The Kingdon Field Guide to African Mammals, 2nd edition*. University Press Group, Princeton, NJ.
- Kingston, J.D., 1999. *Environmental Determinants in Early Hominid Evolution: Issues and Evidence from the Tugen Hills, Kenya*. In: Andrews, P., Banham, P. (Eds.), Late Cenozoic Environments and Hominid Evolution: A Tribute to Bill Bishop. Geological Society, London, pp. 69-84.
- Kingston, J.D., 2011. *Stable Isotopic Analyses of Laetoli Fossil Herbivores*. In: Harrison, T. (Ed.), Paleontology and Geology of Laetoli: Human Evolution in Context. Volume 1: Geology, Geochronology. Springer, Berlin, pp. 293-328.
- Kingston, J.D., Harrison, T., 2007. Isotopic Dietary Reconstructions of Pliocene Herbivores at Laetoli: Implications for Early Hominin Paleocology. *Palaeogeography, Palaeoclimatology, Palaeoecology* 243, 272-306.
- Kingston, J.D., Marino, B.D., Hill, A., 1994. Isotopic Evidence for Neogene Hominid Paleoenvironments in the Kenya Rift Valley. *Science* 264, 955-959.
- Koch, P.L., Tuross, N., Fogel, M.L., 1997. The Effects of Sample Treatment and Diagenesis on the Isotopic Integrity of Carbonate in Biogenic Hydroxylapatite. *Journal of Archaeological Science* 24, 417-429.
- Kohn, M.J., Cerling, T.E., 2002. *Stable Isotope Compositions of Biological Apatite*. In: Kohn, M.J., Rakovan, J., Hughes, J.M. (Eds.), Phosphates. Geochemical, Geobiological, and Materials Importance. Mineralogical Society of America, Washington, D.C., pp. 455-488.
- Kohn, M.J., Schoeninger, M.J., Barker, W.W., 1999. Altered States: Effects of Diagenesis on Fossil Tooth Chemistry. *Geochimica et Cosmochimica Acta* 63, 2737-2747.
- Kohn, M.J., Schoeninger, M.J., Valley, J.W., 1996. Herbivore Tooth Oxygen Isotope Compositions: Effects of Diet and Physiology. *Geochimica et Cosmochimica Acta* 60, 3889-3896.
- Kolodny, Y., Luz, B., Navon, O., 1983. Oxygen Isotope Variations in Phosphate of Biogenic Apatites, I. Fish Bone Apatite - Rechecking the Rules of the Game. *Earth and Planetary Science Letters* 64, 398-404.
- Kullmer, O., 2008. The Fossil Suidae from the Plio-Pleistocene Chiwondo Beds of Northern Malawi, Africa. *Journal of Vertebrate Paleontology* 28, 208-216.

- Kullmer, O., Sandrock, O., Abel, R., Schrenk, F., Bromage, T.G., Juwayeyi, Y.M., 1999. The first Paranthropus from the Malawi Rift. *Journal of Human Evolution* 37, 121-127.
- Kullmer, O., Sandrock, O., Kupczik, K., Frost, S.R., Volpato, V., Bromage, T.G., Schrenk, F., 2011. New primate remains from Mwenirondo, Chiwondo Beds in northern Malawi. *Journal of Human Evolution* 61, 617-623.
- Lee-Thorp, J., Van der Merwe, N.J., 1987. Carbon Isotope Analysis of Fossil Bone Apatite. *South African Journal of Science* 83, 712-715.
- Lee-Thorp, J.A., Sealy, J.C., van der Merwe, N.J., 1989. Stable Carbon Isotope Ratio Differences between Bone Collagen and Bone Apatite, and Their Relationship to Diet. *Journal of Archaeological Science* 16, 585-599.
- Leroux, M., 2001. *The Meteorology and Climate of Tropical Africa*. Springer, Praxis Publishing, London.
- Levin, N.E., Brown, F.H., Behrensmeyer, A.K., Bobe, R., Cerling, T.E., 2011. Paleosol Carbonates from the Omo Group: Isotopic Records of Local and Regional Environmental Change in East Africa. *Palaeogeography, Palaeoclimatology, Palaeoecology* 307, 75-89.
- Levin, N.E., Cerling, T.E., Passey, B.H., Harris, J.M., Ehleringer, J.R., 2006. A Stable Isotope Aridity Index for Terrestrial Environments. *Proceedings of the National Academy of Sciences* 103, 11201-11205.
- Levin, N.E., Quade, J., Simpson, S.W., Semaw, S., Rogers, M., 2004. Isotopic Evidence for Plio-Pleistocene Environmental Change at Gona, Ethiopia. *Earth and Planetary Science Letters* 219, 93-110.
- Longinelli, A., 1984. Oxygen Isotopes in Mammal Bone Phosphate: A New Tool for Paleohydrological and Paleoclimatological Research? *Geochimica et Cosmochimica Acta* 48, 385-390.
- Lüdecke, T., Schrenk, F., Thiemeyer, H., Kullmer, O., Bromage, T.G., Sandrock, O., Fiebig, J., Mulch, A., 2016. Persistent C₃ Vegetation Accompanied Plio-Pleistocene Hominin Evolution in the Malawi Rift (Chiwondo Beds, Malawi). *Journal of Human Evolution* 90, 163-175.
- Lüdecke, T., Thiemeyer, H., 2013. *Paleoenvironmental Characteristics of the Plio-Pleistocene Chiwondo and Chitimwe Beds (N-Malawi)*. In: Runge, J. (Ed.), *Journal of Palaeoecology of Africa*. CRC Press, London, pp. 143-161.
- Luz, B., Kolodny, Y., 1985. Oxygen Isotope Variations in Phosphate of Biogenic Apatites, IV. Mammal Teeth and Bones. *Earth and Planetary Science Letters* 75, 29-36.
- Luz, B., Kolodny, Y., Horowitz, M., 1984. Fractionation of Oxygen Isotopes between Mammalian Bone-Phosphate and Environmental Drinking Water. *Geochimica et Cosmochimica Acta* 48, 1689-1693.
- Magill, C.R., Ashley, G.M., Freeman, K.H., 2013a. Ecosystem Variability and Early Human Habitats in Eastern Africa. *Proceedings of the National Academy of Sciences* 110, 1167-1174.
- Magill, C.R., Ashley, G.M., Freeman, K.H., 2013b. Water, Plants, and Early Human Habitats in Eastern Africa. *Proceedings of the National Academy of Sciences* 110, 1175-1180.
- Malawi Government, 1983. *The National Atlas of Malawi*. Government Malawi, Department of Surveys.
- Marchant, R., Mumbi, C., Behera, S., Yamagata, T., 2007. The Indian Ocean Dipole - the Unsung Driver of Climatic Variability in East Africa. *African Journal of Ecology* 45, 4-16.
- Medina, E., Minchin, P., 1980. Stratification of $\delta^{13}\text{C}$ Values of Leaves in Amazonian Rain Forests. *Oecologia* 45, 377-378.
- Medina, E., Montes, G., Guevas, E., Rokzandic, Z., 1986. Profiles of CO₂ Concentration and $\delta^{13}\text{C}$ Values in Tropical Rain Forests of the Upper Rio Negro Basin, Venezuela. *Journal of Tropical Ecology* 2, 207-217.
- Morgan, M.E., Kingston, J.D., Marino, B.D., 1994. Carbon Isotopic Evidence for the Emergence of C₄ Plants in the Neogene from Pakistan and Kenya. *Nature* 367, 162-165.

- National Oceanic and Atmospheric Administration (NOAA). *Karonga Climate Normals 1961-1990*. Retrieved July 23, 2015.
- Nicholson, S.E., 1996. *A Review of Climate Dynamics and Climate Variability in Eastern Africa*. In: Johnson, T.C., Odada, E.O. (Eds.), *The Limnology, Climatology and Paleoclimatology of the East African Lakes*. Gordon and Breach, Amsterdam, pp. 22-56.
- Nicholson, S.E., 2000. The Nature of Rainfall Variability over Africa on Time Scales of Decades to Millennia. *Global and Planetary Change* 26, 137-158.
- Nicholson, S.E., Klotter, D., Chavula, G., 2014. A Detailed Rainfall Climatology for Malawi, Southern Africa. *International Journal of Climatology* 34, 315-325.
- Passey, B.H., Cerling, T.E., 2002. Tooth Enamel Mineralization in Ungulates: Implications for Recovering a Primary Isotopic Time-Series. *Geochimica et Cosmochimica Acta* 66, 3225-3234
- Passey, B.H., Robinson, T.F., Ayliffe, L.K., Cerling, T.E., Sponheimer, M., Dearing, M.D., Roeder, B.L., Ehleringer, J.R., 2005. Carbon Isotope Fractionation between Diet, Breath CO₂, and Bioapatite in Different Mammals. *Journal of Archaeological Science* 32, 1459-1470.
- Pearcy, R.W., Ehleringer, J., 1984. Comparative Ecophysiology of C₃ and C₄ Plants. *Plant, Cell & Environment* 7, 1-13.
- Pérez-Barbeña, F.J., Gordon, I.J., Nores, C., 2001. Evolutionary Transitions among Feeding Styles and Habitats in Ungulates. *Evolutionary Ecology Research* 3, 221-230.
- Pickford, M., 1986. *A Revision of the Miocene Suidae and Tayassuidae, (Artiodactyla, Mammalia) of Africa*. Tertiary Research Group, London.
- Plummer, T.W., Bishop, L.C., 1994. Hominid Paleoecology at Olduvai Gorge, Tanzania as Indicated by Antelope Remains. *Journal of Human Evolution* 27, 47-75.
- Plummer, T.W., Bishop, L.C., Ditchfield, P., Hicks, J., 1999. Research on Alte Pliocene Oldowan Sites at Kanjera South, Kenya. *Journal of Human Evolution* 36, 20.
- Pustovoytov, K., 2003. Growth Rates of Pedogenic Carbonate Coatings on Coarse Clasts. *Quaternary International* 106-107, 131-140.
- Quinn, R.L., Lepre, C.J., Wright, J.D., Feibel, C.S., 2007. Paleogeographic Variations of Pedogenic Carbonate $\delta^{13}\text{C}$ Values from Koobi Fora, Kenya: Implications for Floral Compositions of Plio-Pleistocene Hominin Environments. *Journal of Human Evolution* 53, 560-573.
- Ring, U., Betzler, C., 1995. Geology of the Malawi Rift: Kinematic and Tectonosedimentary Background to the Chiwondo Beds, Northern Malawi. *Journal of Human Evolution* 28, 7-21.
- Roche, D., Ségalen, L., Senut, B., Pickford, M., 2013. Stable Isotope Analyses of Tooth Enamel Carbonate of Large Herbivores from the Tugen Hills Deposits: Palaeoenvironmental Context of the Earliest Kenyan Hominids. *Earth and Planetary Science Letters* 381, 39-51.
- Sage, R.F., Sage, T.L., 2013. *C₄ Plants*. In: Levin, S.A. (Ed.), *Encyclopedia of Biodiversity* (2nd Edition). Academic Press, Waltham, pp. 361-381.
- Sandrock, O., Dauphin, Y., Kullmer, O., Abel, R., Schrenk, F., Denys, C., 1999. Malema: Preliminary Taphonomic Analysis of an African Hominid Locality. *Earth and Planetary Sciences* 328, 133-139.
- Sandrock, O., Kullmer, O., Schrenk, F., Juwayeyi, Y.M., Bromage, T.G., 2007. *Fauna, Taphonomy, and Ecology of the Plio-Pleistocene Chiwondo Beds, Northern Malawi*. In: Bobe, R., Alemseged, Z., Behrensmeyer, A. (Eds.), *Hominin Environments in the East African Pliocene: An Assessment of the Faunal Evidence*. Springer Netherlands, pp. 315-332.
- Sankaran, M., Hanan, N.P., Scholes, R.J., Ratnam, J., Augustine, D.J., Cade, B.S., Gignoux, J., Higgins, S.I., Le Roux, X., Ludwig, F., Ardo, J., Banyikwa, F., Bronn, A., Bucini, G., Caylor, K.K., Coughenour, M.B., Diouf, A., Ekaya, W., Feral, C.J., February, E.C., Frost, P.G.H., Hiernaux, P., Hrabar, H., Metzger, K.L., Prins, H.H.T., Ringrose, S., Sea, W., Tews, J., Worden, J., Zambatis, N., 2005. Determinants of Woody Cover in African Savannas. *Nature* 438, 846-849.

- Schemmel, F., Mikes, T., Rojay, B., Mulch, A., 2013. The Impact of Topography on Isotopes in Precipitation across the Central Anatolian Plateau (Turkey). *American Journal of Science* 313, 61-80.
- Schrenk, F., Bromage, T.G., Betzler, C.G., Ring, U., Juwayeyi, Y.M., 1993. Oldest Homo and Pliocene Biogeography of the Malawi Rift. *Nature* 365, 833-836.
- Ségalen, L., Lee-Thorp, J.A., Cerling, T., 2007. Timing of C₄ Grass Expansion across Sub-Saharan Africa. *Journal of Human Evolution* 53, 549-559.
- Semaw, S., Simpson, S.W., Quade, J., Renne, P.R., Butler, R.F., McIntosh, W.C., Levin, N., Dominguez-Rodrigo, M., Rogers, M.J., 2005. Early Pliocene Hominids from Gona, Ethiopia. *Nature* 433, 301-305.
- Shemesh, A., 1990. Crystallinity and Diagenesis of Sedimentary Apatites. *Geochimica et Cosmochimica Acta* 54, 2433-2438.
- Sikes, N.E., 1994. Early Hominid Habitat Preferences in East Africa: Paleosol Carbon Isotopic Evidence. *Journal of Human Evolution* 27, 25-45.
- Sikes, N.E., Ashley, G.M., 2007. Stable Isotopes of Pedogenic Carbonates as Indicators of Paleocology in the Plio-Pleistocene (Upper Bed I), Western Margin of the Olduvai Basin, Tanzania. *Journal of Human Evolution* 53, 574-594.
- Sikes, N.E., Potts, R., Behrensmeyer, A.K., 1999. Early Pleistocene Habitat in Member 1 Olorgesailie Based on Paleosol Stable Isotopes. *Journal of Human Evolution* 37, 721-746.
- Sponheimer, M., Lee-Thorp, J.A., 1999. Oxygen Isotopes in Enamel Carbonate and Their Ecological Significance. *Journal of Archaeological Science* 26, 723-728.
- Spötl, C., Vennemann, T.W., 2003. Continuous-Flow Isotope Ratio Mass Spectrometric Analysis of Carbonate Minerals. *Rapid communications in mass spectrometry* 17, 1004-1006.
- Sternberg, L.O., Deniro, M.J., Johnson, H.B., 1984. Isotope Ratios of Cellulose from Plants Having Different Photosynthetic Pathways. *Plant Physiology* 74, 557-561.
- Trauth, M.H., Deino, A.L., Bergner, A.G.N., Strecker, M.R., 2003. East African Climate Change and Orbital Forcing During the Last 175 Kyr Bp. *Earth and Planetary Science Letters* 206, 297-313.
- Trauth, M.H., Maslin, M.A., Deino, A., Strecker, M.R., 2005. Late Cenozoic Moisture History of East Africa. *Science* 309, 2051-2053.
- Uno, K.T., Cerling, T.E., Harris, J.M., Kunimatsu, Y., Leakey, M.G., Nakatsukasa, M., Nakaya, H., 2011. Late Miocene to Pliocene Carbon Isotope Record of Differential Diet Change among East African Herbivores. *Proceedings of the National Academy of Sciences* 108, 6509-6514.
- van der Merwe, N.J., Thackeray, J.F., Lee-Thorp, J.A., Luyt, J., 2003. The Carbon Isotope Ecology and Diet of Australopithecus Africanus at Sterkfontein, South Africa. *Journal of Human Evolution* 44, 581-597.
- Van Wilgen, B.W., 1997. *Fire in Southern African Savannas: Ecological and Atmospheric Perspectives*. Witwatersrand University Press.
- Wang, Y., Cerling, T.E., 1994. A Model of Fossil Tooth and Bone Diagenesis: Implications for Paleodiet Reconstruction from Stable Isotopes. *Palaeogeography, Palaeoclimatology, Palaeoecology* 107, 281-289.
- Wesselmann, H.B., 1985. Fossil Micromammals as Indicators of Climatic Change About 2.4 Myr Ago in the Omo Valley, Ethiopia. *South African Journal of Science* 81, 260-261.
- White, F., Unesco, Office, U.N.S.-S., 1983. *The Vegetation of Africa: A Descriptive Memoir to Accompany the Unesco/Aetfat/Unso Vegetation Map of Africa*. Unesco.
- White, T.D., WoldeGabriel, G., Asfaw, B., Ambrose, S., Beyene, Y., Bernor, R.L., Boisserie, J.R., Currie, B., Gilbert, H., Haile-Selassie, Y., Hart, W.K., Hlusko, L.J., Howell, F.C., Kono, R.T., Lehmann, T., Louchart, A., Lovejoy, C.O., Renne, P.R., Saegusa, H., Vrba, E.S., Wesselman, H., Suwa, G., 2006. Asa Issie, Aramis and the Origin of Australopithecus. *Nature* 440, 883-889.

- Wilson, K.E., Maslin, M.A., Leng, M.J., Kingston, J.D., Deino, A.L., Edgar, R.K., Mackay, A.W., 2014. East African Lake Evidence for Pliocene Millennial-Scale Climate Variability. *Geology* 41, 955-958.
- WoldeGabriel, G., Ambrose, S.H., Barboni, D., Bonnefille, R., Bremond, L., Currie, B., DeGusta, D., Hart, W.K., Murray, A.M., Renne, P.R., Jolly-Saad, M.C., Stewart, K.M., White, T.D., 2009. The Geological, Isotopic, Botanical, Invertebrate, and Lower Vertebrate Surroundings of *Ardipithecus Ramidus*. *Science* 326, 65-65, 65e61-65e65.
- Wynn, J.G., 2000. Paleosols, Stable Carbon Isotopes, and Paleoenvironmental Interpretation of Kanapoi, Northern Kenya. *Journal of Human Evolution* 39, 411-432.
- Zazzo, A., Balasse, M., Patterson, W.P., 2005. High-Resolution $\delta^{13}\text{C}$ Intratooth Profiles in Bovine Enamel: Implications for Mineralization Pattern and Isotopic Attenuation. *Geochimica et Cosmochimica Acta* 69, 3631-3642.
- Zazzo, A., Bocherens, H., Brunet, M., Beuvilain, A., Billiou, D., Mackaye, H.T., Vignaud, P., Mariotti, A., 2000. Herbivore Paleodiet and Paleoenvironmental Changes in Chad During the Pliocene Using Stable Isotope Ratios of Tooth Enamel Carbonate. *Paleobiology* 26, 294-309.

Chapter 6

Stable isotope-based reconstruction of Oligo-Miocene paleoenvironment and paleohydrology of Central Anatolian lake basins (Turkey)

Tina Lüdecke^{1,2,*}, Tamás Mikes^{2,6}, F. Bora Rojay³, Michael A. Cosca⁴,
Andreas Mulch^{1,2,5}

¹Senckenberg Biodiversity and Climate Research Centre, Frankfurt, Germany

²Institute of Geosciences, Goethe University Frankfurt, Germany

³Department of Geological Engineering, Faculty of Engineering, Middle East Technical University, Ankara, Turkey

⁴US Geological Survey, Denver Federal Center, Denver, Colorado, USA

⁵Senckenberg Research Institute and Natural History Museum, Frankfurt, Germany

⁶Eriksfiord AS, Stavanger, Norway

Published in *Turkish Journal of Earth Sciences* (2013), 22: 793-819.

doi: 10.3906/yer-1207-11

Abstract Isotope geochemistry of lacustrine carbonate represents a powerful tool to reconstruct paleoclimatic and paleoenvironmental conditions. Here, we present a comprehensive set of long-term oxygen ($\delta^{18}\text{O}$) and carbon ($\delta^{13}\text{C}$) stable isotope records from five Chattian to Burdigalian lacustrine sequences distributed over the Central Anatolian Plateau. Field relationships combined with stable isotope geochemistry indicate a relatively humid subtropic Late Oligocene climate with an environment characterized by large, temporally open freshwater lakes. Approximately during the middle Aquitanian, a 4‰-5‰ increase in lake $\delta^{18}\text{O}$ values indicates changes in regional climate including more arid conditions and an increasing dominance of closed saline lake conditions in the central plateau region. This time period was also characterized by frequent climatic fluctuations such as short-lived humid periods, possibly recording the influence of seasonality, topography, and the waxing and waning of aridity. In general, relatively high Oligo-Miocene $\delta^{18}\text{O}$ lake water values within the modern plateau interior, even for the least evaporative sequences, suggest the absence of significant orographic barriers at both the northern and southern plateau margins prior to 20-16 Ma.

Keywords Cenozoic, lacustrine carbonates, stable isotopes, $^{40}\text{Ar}/^{39}\text{Ar}$ geochronology, Central Anatolian Plateau, Turkey

6.1 Introduction

The Oligocene/Miocene represents a critical interval with respect to the tectonic, geologic, and climatic history of the Central Anatolian Plateau (CAP) prior to and during the uplift of the plateau margins. Fission-track evidence points to an initial phase of Late Oligocene to Middle Miocene uplift of the Western Pontides in the northwest of the plateau (Zattin et al. 2005; Okay et al. 2008; Cavazza et al. 2012), whereas the still ongoing differential surface uplift of the Central Pontides, which is mainly driven by the North Anatolian Fault Zone, started in the Late Miocene to Early Pliocene (Yildirim et al. 2011). Equally important is the multiphased surface uplift history of the Central Taurides that border the CAP from the south, for which Mediterranean slab dynamics appear to have played a fundamental driving role in triggering a rapid phase of surface uplift post-8 Ma (Cosentino et al. 2012; Schildgen et al. 2012a, 2012b).

Oligo-Miocene continental basins cover a remarkably large area of the CAP (Fig. 6.1). Numerous studies were carried out to reconstruct Middle Cenozoic paleoenvironments in the Eastern Mediterranean to better understand the vegetation and climate history of the region. However, most of these studies are based on micro- and macrofloral records, either addressing spatially extensive coverage (e.g., Ivanov et al. 2002; Kovar-Eder et al. 2006; Akgün et al. 2007; Bruch et al. 2007; Fauquette et al. 2007; Ivanov et al. 2007a, 2007b; Strömberg et al. 2007; Ivanov et al. 2008; Yavuz-Işık and Toprak 2010; Bruch et al. 2011; Ivanov et al. 2011; Utescher et al. 2011) or focusing on more local records (e.g., Akgün 1993; Whateley and Tuncali 1995; Akgün and Sözbilir 1999; Karayığit et al. 1999; Akgün et al. 2002; Akkiraz and Akgün 2005; Kayseri et al. 2006). Other approaches use mammal fossils as climatic proxies (e.g., Böhme 2003; Fortelius et al. 2006; Eronen et al. 2009) or are based on sedimentologic analysis, such as tracing the presence of lignite as an indicator of a warm and wet climate (e.g., Yağmurlu et al. 1988; İnci 1990).

This work presents the first comprehensive long-term oxygen ($\delta^{18}\text{O}$) and carbon ($\delta^{13}\text{C}$) stable isotope analysis carried out on Middle Cenozoic continental successions on the CAP. Lacustrine and pedogenic continental carbonate deposits are ubiquitous on the modern plateau and represent a premier framework for reconstructing Late Oligocene and Early Miocene paleoenvironments of the region. One of the main obstacles in reconstructing past environmental conditions on the CAP, however, is the scarcity of high-precision chronological constraints. Ages of the sequences documented here are therefore based in part on published biostratigraphic and magnetostratigraphic data as well as new $^{40}\text{Ar}/^{39}\text{Ar}$ geochronology of intercalated ash layers.

$\delta^{18}\text{O}$ and $\delta^{13}\text{C}$ data from Chattian to Burdigalian paleolakes of the CAP indicate a long-term overall increase in lacustrine oxygen and carbon isotopic ratios over time, with younger successions displaying an increased positive covariance between $\delta^{13}\text{C}$ and $\delta^{18}\text{O}$. Together with field indicators of aridity (e.g., desiccation cracks) such a $\delta^{18}\text{O}$ - $\delta^{13}\text{C}$ covariance suggests a shift towards

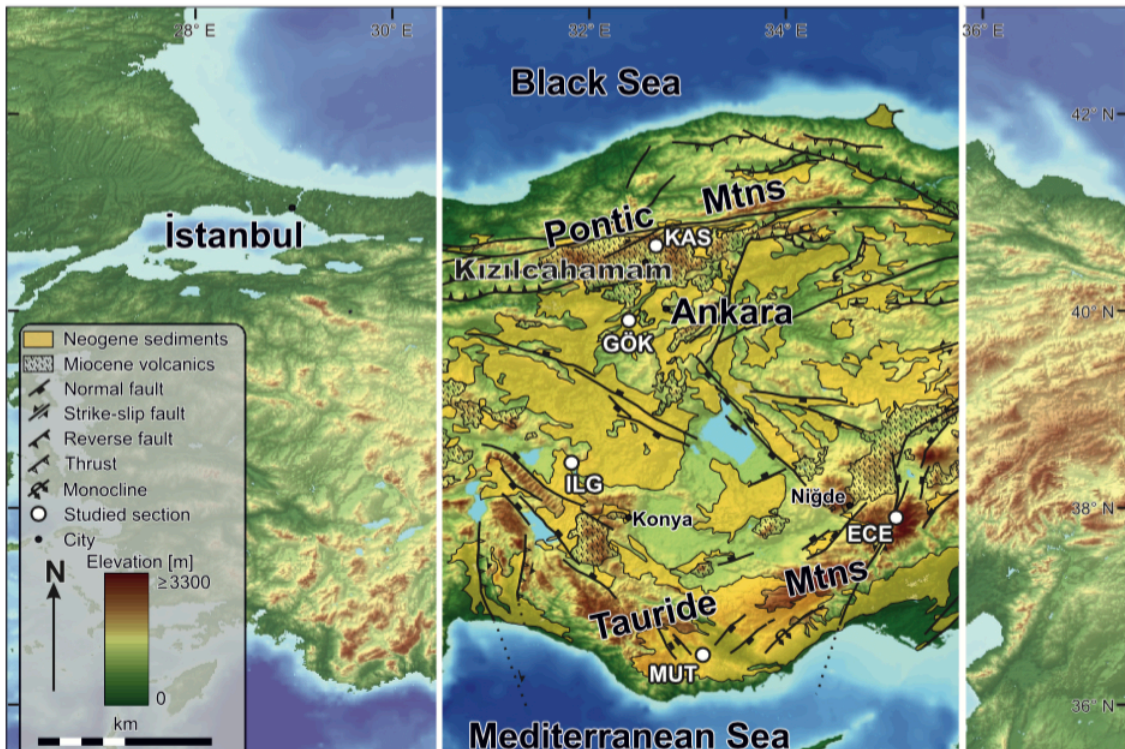


Figure 6.1: Digital elevation map of Turkey with relevant geological and tectonic features and location of the studied sedimentary sequences. ECE: Ececiği Basin, MUT: Mut Basin, ILG: Ilgın Basin, GÖK: Gökler Locality (Ankara region), KAS: Kasımlar Locality (Ankara region). For geographic coordinates of the sampled sections see Tab. 6.1, for field photographs Fig. 6.2, 6.3 and 6.4.

more arid conditions during the Early Miocene. This trend may be episodically interrupted by phases of increased humidity, especially during the Aquitanian when frequent climatic (rainfall) fluctuations seem to have been common.

6.2 Isotopic compositions of lake sediments

6.2.1 Stable oxygen isotope geochemistry

In contrast to marine environments, which are buffered physically and chemically against minor environmental changes, lakes represent highly sensitive and dynamic systems, with the potential to record changes in hydrology such as water residence time, water balance, origin and composition of meteoric waters, sediment input, and climate changes such as fluctuations in precipitation (e.g., Tucker and Wright 1990; Leng and Marshall 2004; Gierlowski-Kordesch 2010). Provided that adequate age control is available, lacustrine carbonate deposited in such environments is capable of tracking some of this information and hence represents a valuable paleoenvironmental record.

Lake waters are part of the meteoric water cycle. The oxygen isotopic composition of meteoric waters ($\delta^{18}\text{O}_{\text{mw}}$) is affected by many factors, with the most important fractionation mechanisms for water being evaporation and condensation at the hydrosphere-atmosphere interface (Horita and Wesolowski 1994). The $\delta^{18}\text{O}$ of lake water ($\delta^{18}\text{O}_{\text{lw}}$) is influenced by the oxygen isotopic composition of meteoric waters supplied to the lake, such as precipitation, surface runoff, and groundwater inflow. Evaporation, itself governed by

temperature and relative humidity, strongly controls the depletion in the light oxygen isotope ^{16}O in the water phase. Changes in temperature, rainfall sources, riverine influx, and groundwater input are retained in the oxygen isotope ratios of carbonates ($\delta^{18}\text{O}_{\text{carb}}$) which precipitate from lake water (e.g., Turner et al. 1983; Talbot 1990; Teranes et al. 1999; Lamb et al. 2000; Schwab and Dean 2002; Leng and Marshall 2004; Yansa et al. 2007; Davis et al. 2009; Deocampo 2010; Kent-Corson et al. 2010). Stratigraphic changes in $\delta^{18}\text{O}_{\text{carb}}$ values of lacustrine sections can therefore be attributed to changes in temperature or $\delta^{18}\text{O}_{\text{lw}}$ (Leng and Marshall 2004). Lacustrine carbonate oxygen isotope records have been also used in isotope-based paleoelevation models exploiting the systematic relationship between oxygen isotopes in precipitation and surface elevation (e.g., Currie et al. 2005; Garzzone et al. 2008; Mix et al. 2011; Campani et al. 2012).

A common obstacle in assessing all such paleoenvironmental conditions is that $\delta^{18}\text{O}_{\text{lw}}$ does not necessarily reflect the primary composition of $\delta^{18}\text{O}_{\text{mw}}$; it is therefore important to account for evaporation, the residence time of the lake water, and biogeochemical processes in the lake that potentially affect $\delta^{18}\text{O}_{\text{lw}}$ (and $\delta^{13}\text{C}$) (Fronval et al. 1995; Cyr et al. 2005). Likewise, size and hydrology of a lake strongly control its ability to buffer short-term (seasonal to decennial) hydrometeorologic variations in $\delta^{18}\text{O}_{\text{mw}}$ that affect $\delta^{18}\text{O}_{\text{lw}}$. Finally, it should be noted that $\delta^{18}\text{O}$ values of the global oceans (and hence meteoric water) change over time. An increase of about 1.2‰ in marine $\delta^{18}\text{O}$ is estimated from the Early to Late Miocene; the difference between Late Miocene and recent marine $\delta^{18}\text{O}$ is about an additional 1‰ (Friedman and Hardcastle 1988; Zachos et al. 2001).

6.2.2 Stable carbon isotope geochemistry

The total dissolved inorganic carbon (TDIC) concentration in lacustrine environments is governed by changes in carbon and nutrient cycling, as well as by productivity within the lake and its catchment, which are often climatically induced (Leng and Marshall 2004). Carbon isotopes are fractionated during various carbon-cycle transitions and eventually get incorporated into authigenic and biogenic carbonates. The HCO_3^- is derived from the interaction of groundwater with rocks and soils in the catchment and the dissociation of CO_2 dissolved in the lake water. The temperature effect on $\delta^{13}\text{C}$ is relatively small during carbonate precipitation (Kelts and Talbot 1990). In general, $\delta^{13}\text{C}$ in lacustrine environments is controlled by 3 predominant processes: (1) $\delta^{13}\text{C}$ of inflowing waters, (2) CO_2 exchange between atmosphere and TDIC, and (3) photosynthesis/respiration of aquatic plants within the lake (Leng and Marshall 2004).

Because closed-basin lakes generally experience stronger perturbations in their physical and chemical parameters, larger isotopic variations accompany their hydrological balance as compared to open lakes and strong $\delta^{13}\text{C}_{\text{carb}}-\delta^{18}\text{O}_{\text{carb}}$ covariance is typically indicative of closed lake hydrology. In contrast, an absence of such covariation is often displayed in lakes with stable water level,

where the effect of vapor exchange with the atmosphere has a strong influence of the stable isotopic compositions (Li and Ku 1997).

6.3 Analytical techniques

6.3.1 Stable carbon and oxygen isotope geochemistry

Whole-rock samples were digested in orthophosphoric acid and analyzed as CO₂ in continuous flow mode using a Thermo Delta V mass spectrometer at the Institute of Geology, University of Hannover, as well as a Thermo MAT 253 mass spectrometer at the Institute of Geosciences, University of Frankfurt. Both instruments were interfaced to a Thermo GasBench II. Analytical procedures followed those of Spötl and Vennemann (2003). Raw isotopic ratios were calibrated against a Carrara marble in-house standard as well as against NBS18 and NBS19 carbonate reference materials. Final isotopic ratios are reported against VSMOW ($\delta^{18}\text{O}$) and VPDB ($\delta^{13}\text{C}$). Overall analytical uncertainties on the isotopic ratios are better than 0.07‰ absolute ($\delta^{18}\text{O}$) and 0.04‰ absolute ($\delta^{13}\text{C}$). Carbonate contents were derived from standard-sample total peak area ratios and are precise to within 5% absolute. Isotopic compositions of samples with less than 10 wt.% carbonate were not considered in this work. Accepted results from 230 samples are given in the Supplementary Material 6.11.

6.3.2 $^{40}\text{Ar}/^{39}\text{Ar}$ geochronology

Hornblende and biotite from tephra intercalations in the lacustrine sequences were dated by the $^{40}\text{Ar}/^{39}\text{Ar}$ method at the US Geological Survey (USGS) in Denver, Colorado. High-purity mineral separates of one sample of hornblende and two samples of biotite were irradiated together with mineral standards for 2 MWh in the central thimble position of the USGS TRIGA reactor using cadmium lining to prevent nucleogenic production of ^{40}Ar . The neutron flux was monitored using Fish Canyon Tuff sanidine, applying an age of 28.20 ± 0.08 Ma (Kuiper et al. 2008), and isotopic production ratios were determined from irradiated CaF and KCl salts. For this irradiation, the following production values were measured: $^{36}\text{Ca}/^{37}\text{Ca} = 2.447 \times 10^{-4} \pm 0.47 \times 10^{-4}$; $^{39}\text{Ca}/^{37}\text{Ca} = 6.5 \times 10^{-4} \pm 0.13 \times 10^{-4}$; and $^{38}\text{K}/^{39}\text{K} = 1.29 \times 10^{-2} \pm 0.01 \times 10^{-2}$. Several irradiated mineral grains from the samples and individual mineral grains from the standards were loaded into 3-mm wells within a stainless steel planchette attached to a fully automated ultrahigh vacuum extraction line constructed of stainless steel. Samples were incrementally degassed and eventually fused using a 20 W CO₂ laser equipped with a beam-homogenizing lens. The gas was expanded and purified by exposure to a cold finger maintained at -140 °C and two hot SAES GP50 getters. Following purification, the gas was expanded into a Mass Analyser Products 215-50 mass spectrometer and argon isotopes were measured by peak jumping using an electron multiplier operated in analog mode. Data were acquired during 10 cycles, and time-zero intercepts were determined by best-fit regressions to the data. Ages were calculated from data that were corrected for mass discrimination, blanks, radioactive decay subsequent to irradiation, and interfering nucleogenic reactions. Results are summarized in Table 6.1.

Table 6.1: Results of $^{40}\text{Ar}/^{39}\text{Ar}$ geochronology, along with sample ID, basin name and lithostratigraphy, geographic coordinates, dated mineral phase and plateau age.

Sample ID	Basin (section)	Latitude (N)	Longitude (E)	Phase dated	Plateau age with 1σ error [Ma]
10-GK-04	Ankara (Gökler)	39°57'12.9"	32°25'22.4"	Hornblende	20.7 ± 0.2
09-GK-13	Ankara (Gökler)			Biotite	22.2 ± 0.2
V-01-05	Mut (Fakırca)	36°30'24.1"	33°9'19.9"	Biotite	25.5 ± 0.2

6.4 Geologic and tectonic framework

The Cenozoic geodynamic history of the Eastern Mediterranean region was characterized by the interactions of several microcontinents, including the opening and closure of oceanic basins and parts of the Paratethys (e.g., Şengör and Yılmaz 1981; Şengör 1984, 1987; Stampfli 2000; Robertson et al. 2004). Post-Late Eocene closure of the Tethyan Ocean resulted in the development of the Pontides in the north and Taurides in the south. Parts of the Western Pontides were exhumed along a pre-Miocene ductile shear zone (Okay et al. 2008), while the active uplift of the Central Pontides at the northern plateau margin is attributed to stress across the restraining bend of the North Anatolian Fault since the Late Miocene (Yildirim et al. 2011). Multiphase post-8 Ma surface uplift of the Central Taurides at the southern margin is associated with slab break-off, which likely also influenced the evolution of the CAP as a whole (Cosentino et al. 2012; Schildgen et al. 2012a, 2012b). In the plateau interior of Anatolia Oligo-Miocene basin development was accompanied by intense Miocene volcanism in the Galatian Province (e.g., Wilson et al. 1997). At the same time, the last marine deposits record Tethyan regression through SE Anatolia towards the SE (Şengör and Yılmaz 1981; Mazzini et al. 2013).

In Central Anatolia northward-dipping tilted basins developed initially under a compressional regime as a result of intracontinental convergence. These basins experienced episodic marine incursions (particularly in the east; e.g., Lüttig and Steffens 1975). Arc- and collision-related basins developed in the Late Cretaceous to Oligocene, filled by marine turbidites and in turn by shelf to nonmarine successions (Görür et al. 1998). Widespread calc-alkaline magmatism, extension, and strike-slip faulting all had a profound effect on the depositional architecture of the Neogene basins of Central Anatolia (Okay 2008).

6.5 Paleoenvironment

6.5.1 Oligo-Miocene climatic development

Oligo-Miocene lakes of Central Anatolia developed under a pattern of global climate change that involved the waxing and waning of Antarctic continental ice sheets (Zachos et al. 2001, 2008). Late Oligocene warming reduced the extent of Antarctic ice and until the Middle Miocene, global ice volumes remained (relatively) low. With the exception of several brief periods of glaciation, oceanic

bottom water temperatures slightly increased over time (Wright et al. 1992) and this warm phase peaked from 17 until 15 Ma (Middle Miocene Climatic Optimum, Flower and Kennett 1994). Numerical simulations indicate global mean annual temperatures of about 3 °C higher than today, and northern hemisphere meridional temperature gradients being less pronounced than today. Climate proxy data from Central Europe indicate terrestrial temperatures that may have been 9 to 12 °C warmer during this time (Böhme 2003; Mosbrugger et al. 2005; You et al. 2009; Ivanov and Böhme 2011; Knorr et al. 2011). This mid-Miocene warm phase was followed by long-term gradual cooling and reestablishment of a major ice sheet on Antarctica by 10 Ma (Zachos et al. 2001).

6.5.2 Eastern Mediterranean

The climate history of Anatolia and its surrounding regions is not only influenced by global climate changes, but also by more regional events, such as regional-scale tectonic uplift, which affects paleotopography, land-sea distributions, and, as a consequence, local climatic response. Semiquantitative Miocene paleotemperature and paleoprecipitation reconstructions in Western and Central Anatolia were established from the paleobotanical record (e.g., Akgün et al. 2007; Akkiraz et al. 2011; Utescher et al. 2011). These results indicate a warm subtropical climate in Central Anatolia during the latest Chattian (ca. 24 Ma), with mean annual temperature between 16.5 and 21.1 °C, coldest month temperature (CMT) between 5.5 and 13.3 °C, warmest month temperature (WMT) between 27.3 to 28.2 °C, and mean annual precipitation that reached 1100-1400 mm/ year. Subsequently, early Aquitanian (23-22 Ma) CMT and WMT remained largely constant with the potential presence of slightly lower (cold season?) temperatures. These results are in agreement with the palynological record (Nagy 1990; Planderová 1991; Yavuz-Işık and Demirci 2009) and the widespread occurrence of reefal limestones in Turkey and neighboring regions that also indicate warm conditions (Görür et al. 1995). During the latest Burdigalian (ca. 16 Ma), palynomorph data still suggest warm subtropical conditions, yet with lower temperatures than during the Chattian and Aquitanian periods. Even cooler but still subtropical conditions persisted during the Langhian (16-14 Ma), yet the impact of the Middle Miocene Climatic Optimum on CAP temperature and rainfall patterns is still largely elusive. Collectively, these data suggest a persistent subtropical climate with alternating warmer and cooler periods in Central Anatolia. Starting in the middle to late Serravallian (12-11 Ma), the climate changed from subtropical to warm temperate. This cooling trend continued in the Tortonian, where a warm temperate climate dominated with seasonally dry conditions (Görür and Tüysüz 2001). Mediterranean coral records indicate the presence of seasonal climate variability as reflected by changes in temperature and composition of Eastern Mediterranean seawater during the Tortonian (ca. 10-8 Ma) when North Atlantic atmospheric circulation dynamics may have had similar impact on temperature and rainfall seasonality as today (Brachert et al. 2006). For the Late Miocene and Early Pliocene, interpretation of palynological proxy data is still

controversial, including warm and dry, warm and humid, or cold and humid conditions (Bertini 2006; Yavuz-Işık and Toprak 2010). Mammal chronofauna data indicate a decrease in precipitation starting in the latest Middle Miocene with a climax in the middle Late Miocene (Eronen et al. 2009). Thus, Messinian climate conditions in the Eastern Mediterranean are far from being understood, yet significant changes in temperature and aridity compared to the Tortonian are likely (Schneck et al. 2010).

6.5.3 Paleogeography of Turkey

Many aspects of the paleotopographic history of Anatolia are still elusive. There is limited evidence for the presence of significant relief already during the Oligocene and Miocene, such as apatite fission-track data reflecting Late Paleogene exhumation in the Pontides (Zattin et al. 2005; Okay et al. 2008; Cavazza et al. 2011) or the presence of palynofloral elements that prefer higher altitudes such as pines (Akkiraz and Akgün 2005). In addition, the widespread occurrence of thick, coarse-grained red continental clastic sediments of Oligocene age as well as the mere presence of lakes, which require a topographic isolation from the Paratethyan and Mediterranean seaways, strongly suggest that some paleorelief was present within Anatolia. Along the SE margin of the plateau, marine sediments overlapping the Tauride basement units (Cosentino et al. 2012) and coarse Oligocene postalpidic conglomerates along the northern flank of the margin (Clark and Robertson 2002, 2005) imply pre-Late Miocene paleorelief. Rich species diversification in mountainous forests in Central Anatolia suggests that its paleotopography was higher compared to that of western Anatolia (Akgün et al. 2007). A potential scenario depicts central Turkey as an erosional highland in the Miocene, which decreased in elevation towards the surrounding shallow seas in the north, east, and south (Görür and Tüysüz 2001). The Bitlis Ocean still existed in the Early Miocene between the Anatolian highland and the Arabian platform, although it might have been reduced to a narrow seaway (Görür and Tüysüz 2001). Sedimentary evidence implies the existence of the Kırkkavak ridge along the southwest plateau margin since at least the Middle Miocene (Deynoux et al. 2005; Çiner et al. 2008).

The onset of uplift of the Taurides bordering the present-day CAP to the south is dated at post-8 Ma (Cosentino et al. 2012); the northern Pontide orogenic belt was uplifted largely synchronously in the Late Miocene (Yıldırım et al. 2011). It is very likely that much of the Central Taurides did not yet exist as a prominent topographic entity during the evolution of the paleolakes studied here, although some paleorelief was present pre-Late Miocene in the area (Clark and Robertson 2002, 2005; Cosentino et al. 2012; Schildgen et al. 2012b). Marine sediments uplifted 1.5 to 2 km on the southern margin together with regional lithostratigraphic correlations indicate an important period of surface uplift between ca. 7 and 5.45 Ma, most likely due to the dynamics of the subducting African slab and upper mantle upwelling beneath Central Anatolia (Cosentino et al. 2012; Schildgen et al. 2012b).

6.6 Geologic setting of the studied sections and sampling strategy

This study focuses on Upper Oligocene to Early Miocene lacustrine sequences and examines how combined climatic and lake fill histories are recorded in their $\delta^{13}\text{C}_{\text{carb}}$ and $\delta^{18}\text{O}_{\text{carb}}$ records. Stratigraphic sections presented here cover a large portion of the present-day CAP, including the Iğın Basin near Konya, the Ecemiş Corridor, and Mut Basin in the south, as well as the Gökler and Kasımlar (sub)basins in the north, near Ankara (Fig. 6.1).

Table 6.2: List of each sampled formation in the studied basins showing age, time span covered by the sampled section with an assumed sedimentation rate ¹⁾ of 100 m/Ma (Einsele 2000); ²⁾ of 11.7m/Ma, as derived from two geochronological tie-points in the section; and ³⁾ of 50 m/Ma, as derived from magnetostratigraphic data (Krijgsman et al. 1996). The most probable age range is provided by ^{a)} Fortelius (2012); ^{b)} this work; ^{c)} Krijgsman et al. (1996); ^{d)} Blumenthal (1956); Yetis (1968); Nazik and Göken (1992); Ünlügenç et al. (1993).

Basin (section)	Ankara (Kasımlar)	Ankara (Gökler)	Iğın	Mut	Ecemiş
Latitude [N]	40°39'46.8"	39°57'12.9"	38°27'37.2"	36°30'24.1"	37°54'4.4"
Longitude [E]	32°40'48.6"	32°25'22.4"	31°49'19.7"	33°9'19.9"	35°7'14.9"
Age	Burdigalian	Aquitanian	Aquitanian	Chattian	Oligocene to Early Miocene
Age constrained by	Mammals ^a	Geo-chronology ^b	Magneto-stratigraphy ^c	Geo-chronology ^b	Non-marine fossils ^d
Thickness of sampled carbonates [m]	6.0	17.5	38.5	8.9	44.0
Timespan covered [Ma]	0.06 ¹	1.5 ²	0.77 ³	0.09 ¹	0.44 ¹
Age range covered [Ma]	20.0-18.0	23.0-16.0	22.3-20.7	28.4-23.0	33.9-16.0

6.6.1 Timing of deposition and sedimentation rates

To better evaluate the paleoenvironmental proxy data, it is important to estimate the amount of time represented by each sedimentary section studied by means of sedimentation rates. Based on the high carbonate proportion of the mainly fine-grained sediments, we uniformly assume a sedimentation rate of ca. 100 m/Ma (Einsele 2000) for all sections where stratigraphic tie-points are lacking. We are fully aware that such an approach is likely to be compromised by discontinuous sedimentation histories, change in basin subsidence, or sediment delivery and compaction, but given the overall limited age constraints currently represents a first-order framework within which we correlate our $\delta^{18}\text{O}$ and $\delta^{13}\text{C}$ lake records.

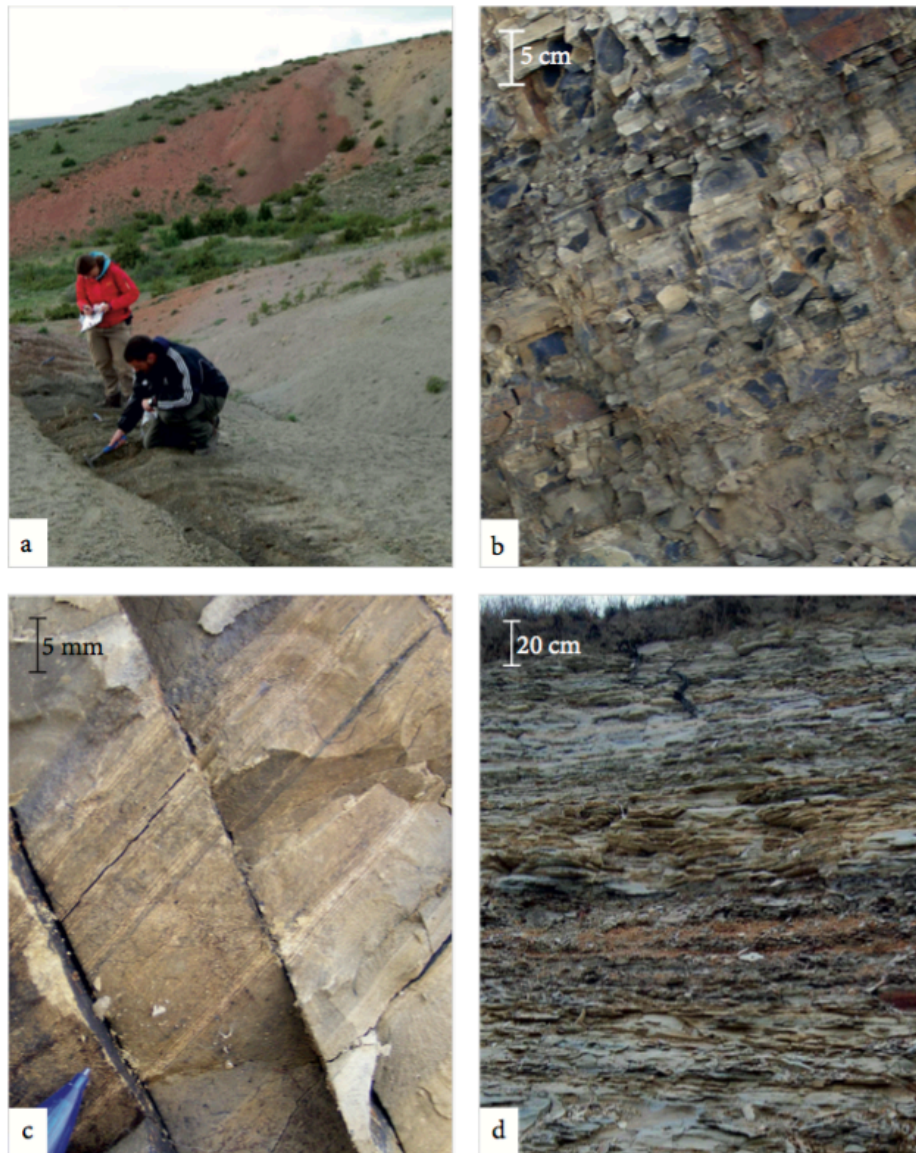


Figure 6.2: Field characteristics of the studied Oligocene to Lower Miocene sediments. a) Dense sampling of the Çukurbağ Formation in the Ecemiş Corridor near Pınarbaşı. b) Laminated silty marls of the Fakırca Formation in the Mut Basin near Gezende. c) Close-up view of the Fakırca marls showing well-developed lamination. d) Organic-bearing marls in the Ankara region near Kasımlar.

In the Gökler section, our new argon geochronological data derive from the basal and the topmost beds of the sampled interval, which therefore precisely bracket a time span of 1.5 ± 0.4 Ma covered by the section. Here, the possibly fastest calculated sedimentation rate is 15.9 m/Ma (Tab. 6.2). Krijgsman et al. (1996) suggested a sedimentation rate of 50 m/Ma for the lacustrine sediments in the Ilgın Basin, derived from magnetostratigraphic and radiometric data. Therefore, the 38.5-m-thick succession could cover a time span of ca. 0.8 Ma, which is in good agreement with the relatively low sedimentation rates of <100 m/Ma for large, long-lived, carbonate-dominated lakes (Einsele 2000. pp. 92 and 389).

Lignite beds occur in some of the examined sections. Their accumulation and preservation depend on the depositional environment and on the maintenance

of a sufficiently high groundwater level (Bohacs 1999). Due to the sum of uncertainties, all sedimentation rates are only considered to be first-order estimates.

6.6.2 Ecemiş Corridor

In the south of the CAP, the Ecemiş Fault Zone developed in concert with Neogene-to-recent regional exhumation and surface uplift of the Central Taurides (Jaffey and Robertson 2001, 2005). Oligocene to Miocene nonmarine sedimentary environments were dominated by braided rivers flowing from the Niğde metamorphic massif in the N feeding large inward draining lakes; the clastic fluvial deposits (Çukurbağ Formation) unconformably overlie Upper Eocene shallow marine carbonates (Yetiş 1968). Age constraints on the timing and rates of sedimentation are rather poor. For the sampled Çukurbağ Formation we rely on published nonmarine fossil assemblages such as gastropods and ostracods that were correlated in the Ecemiş Corridor with adjacent nonmarine basins (Blumenthal 1955; Yetiş 1968; Nazik and Gökçen 1992). Early Oligocene planktic foraminifera (Ünlügenç *et al.* 1993) are indicative for marine conditions during deposition of the lower part of the Çukurbağ Formation (Karsantı Basin), which places the overlying continental deposits into the Oligocene (Yetiş 1968) or Oligocene to Early Miocene (Jaffey and Robertson 2001). Sedimentological characteristics, such as horizontally or trough-cross bedded sandstones with poorly sorted rounded grains, suggest that some of the coarser-grained parts of the Çukurbağ Formation must have been reworked material deposited in both alluvial fan and braided river environments, whereas the gray-green massive silty mud units are considered to have formed in lacustrine and flood-plain environments (Gürel *et al.* 2007). About 40 km east of Niğde, and ca. 2.5 km north of the village of Pınarbaşı (37°54'4.4"N, 35°7'14.9"E), we sampled subvertically dipping NNE-SSW striking strata (Fig. 6.2a). The logged profile has a thickness of 44.4 m, and we analyzed 40 gray-to-green and red-to-black marls collected from an alternating sequence of coarsening-upward silty marls with rare intercalations of thin-bedded, medium to very coarse grained sandstones and pebble horizons.

6.6.3 Mut Basin

The Mut Basin at the southern margin of the CAP is situated in the central part of the Taurides. A mixed siliciclastic- carbonate succession of up to 1600 m thick makes up the Oligocene and Miocene basin fill, which overlies deformed Paleozoic and Mesozoic marine platform carbonates and dismembered ophiolites (Şafak *et al.* 2005). The lithologically diverse succession of the Mut Basin is divided into 5 main lithostratigraphic units: (1) the deep- water, deltaic to lacustrine Yenimahalle Formation; (2) lacustrine siltstones and marls of the Fakırca Formation, overlain by (3) red beds of the Derinçay Formation and (4) upper Burdigalian-upper Tortonian marls and limestones of the Köşelerli Formation that already form part of a marine transgressive succession, mainly represented by (5) the Mut Formation (upper Serravallian-upper Tortonian), that completely overlies the continental series (Gedik *et al.* 1979; Tanar and Gökçen 1990; Şafak and Gökçen 1991; Ilgar and Nemeç 2005; Şafak *et al.* 2005;

Cosentino et al. 2012; Cipollari et al. 2013). We sampled laminated silty marls of the Fakırca Formation (Fig. 2b and 6.2c). Ostracod microfaunas from various levels define an age range that encompasses the Late Oligocene to basal Miocene (Tanar and Gökçen 1990), which is in very good agreement with an $^{40}\text{Ar}/^{39}\text{Ar}$ age of 25.5 ± 0.2 Ma obtained from an approximately 5-mm-thin biotite-rich ash intercalated within the sampled section (sample V-01-05; see below).

Ostracod and foraminiferal assemblages as identified in the topmost Fakırca Formation range from Aquitanian to mid-Burdigalian and indicate a transition from Chattian freshwater conditions to a lagoonal to marine littoral setting (Şafak et al. 2005).

The logged profile has a thickness of 8.9 m; 57 fine-grained, laminated marl samples and one sample from the ash layer were taken from a road cut ca. 0.5 km south of the village of Gezende ($36^{\circ}30'24.1''\text{N}$; $33^{\circ}9'19.9''\text{E}$), about 70 km northwest of Silifke.

6.6.4 Ilgın Basin

In the Ilgın Basin, in the western part of the CAP, a Neogene succession of conglomerates, sandstones, marls, mudstones, limestones, and lignites (Ilgın Formation) unconformably overlies Paleozoic metamorphic schists and Mesozoic crystalline limestones (Canik 1981; Karayiğit et al. 1999; Koçyiğit 2000; Inaner 2005; Özdemir and İnce 2005). The Ilgın Formation has been subdivided into 3 members: the oldest, fluvial Tekeler Member is overlain by the lacustrine Harmanyazı Member, itself overlain by fluvial sediments of the Sebiller Member (Karayiğit et al. 1999). The studied Harmanyazı Member consists of light gray marls; partly laminated yellow, gray, and white siltstones; claystones; and limestones that collectively attain up to 180 m of thickness (Fig. 6.3).

The age assignment for the Ilgın lignites and the associated sediments is controversial. Based on limited ostracod fauna and palynological data, a Late Miocene age was proposed (Çağlar and Ayhan 1991) but later revised to Early Miocene according to ostracod faunal assemblages (Tunoğlu and Celik 1995). Rodent assemblages identified in the section directly above the lignite were attributed to the mammal zone MN1 or MN2 (Aquitanian; de Bruijn and Saraç 1991) and correlation with paleomagnetic data placed the succession at ca. 22.3 to 20.7 Ma (Krijgsman et al. 1996; using calibration of Gradstein et al. 2005). Oligocene $^{40}\text{Ar}/^{39}\text{Ar}$ ages of 30.5 Ma in a volcanic horizon on the top of the section are in conflict with the magnetostratigraphic results and suggest that these biotite-bearing sediments are in fact reworked (Krijgsman et al. 1996). Subsequently, a Middle Miocene age was suggested for the Ilgın section on the basis of spores and pollen data (Karayiğit et al. 1999). $^{40}\text{Ar}/^{39}\text{Ar}$ ages of volcaniclastic horizons in the Upper Altınapa Group in the adjacent Altınapa Basin provide an age of 11.9 to 11.6 Ma (Koç et al. 2012). Field relations suggest that the Upper Altınapa Group is younger than the sampled Harmanyazı Member, yet to an unknown extent. Because of the excellent

correlation of the micromammal and paleomagnetic data, we consider an Aquitanian age (Krijgsman et al. 1996) to be most reliable for the sampled Ilgin section.

We collected 67 carbonate samples from a 40-m-thick outcrop at the northern flank of an abandoned lignite quarry about 21 km north of Ilgin and ca. 2.6 km west of the village of Gölyaka (38°27'37.2"N, 31°49'19.7"E).

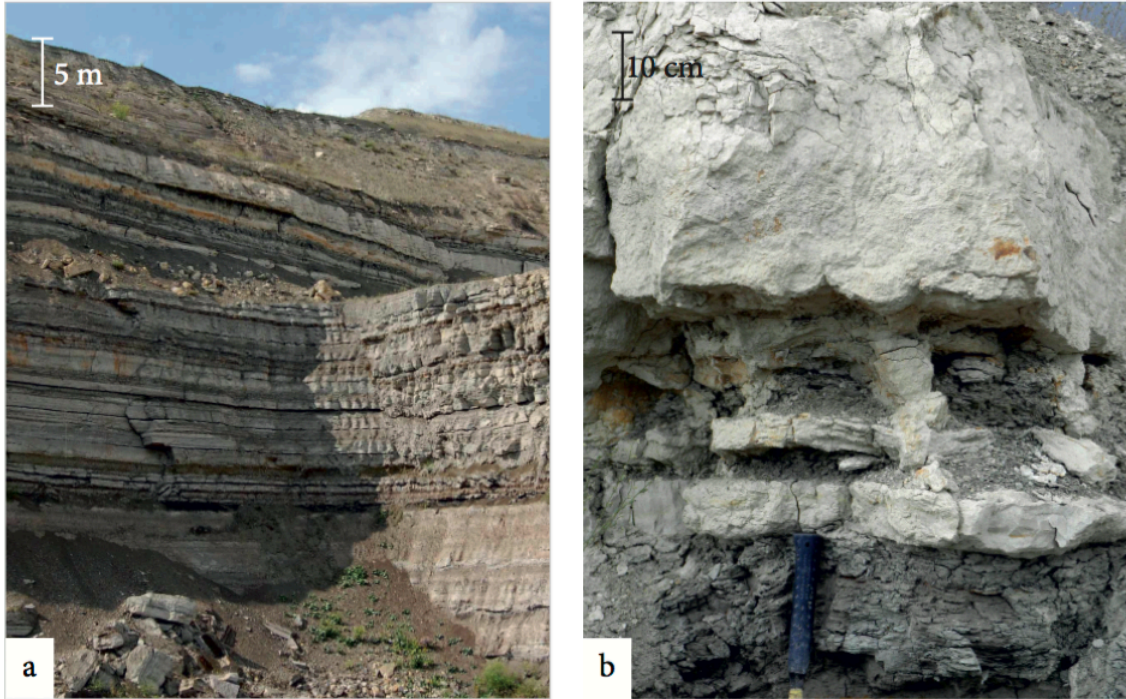


Figure 6.3: a) Excellent outcrop conditions of the Aquitanian Ilgin Formation in an abandoned coal quarry near Gölyaka. b) Dewatering structures in mudrocks and overlying marls of the Ilgin Formation.

6.6.5 Ankara region

In the Ankara region we focused on two sections close to the villages of Gökler (SW of Kazan) and Kasımlar (N of Kızılcahamam).

Here, an iron oxide hardground surface that developed on top of Middle Eocene (Lutetian) marine carbonates (Orhaniye, NW of Ankara) is overlain by Miocene red clastic sediment. These are overlain by light gray-green-beige mudrock successions, which consist of an alternation of clayey limestone, siltstone, sandstone, and marls with tuff and tuffite interbeds and lignite layers.

6.6.5.1 Gökler section

An abandoned quarry, formerly exploited for lignite, ca. 40 km west of Ankara and ca. 0.8 km south of the village of Gökler (39°57'12.9"N, 32°25'22.4"E) exposes an alternation of partly laminated light gray to green silty mudrocks, a few lignite horizons, and tuffite beds, overlain by white diatomites (Fig. 6.4). Fifty-three carbonate samples were analyzed from a section of ca. 17.5 m thick. In addition, two volcanic layers (samples 09-GK-13 and 10-GK-04) were sampled for $^{40}\text{Ar}/^{39}\text{Ar}$ geochronology and place the section within the Aquitanian (see below).

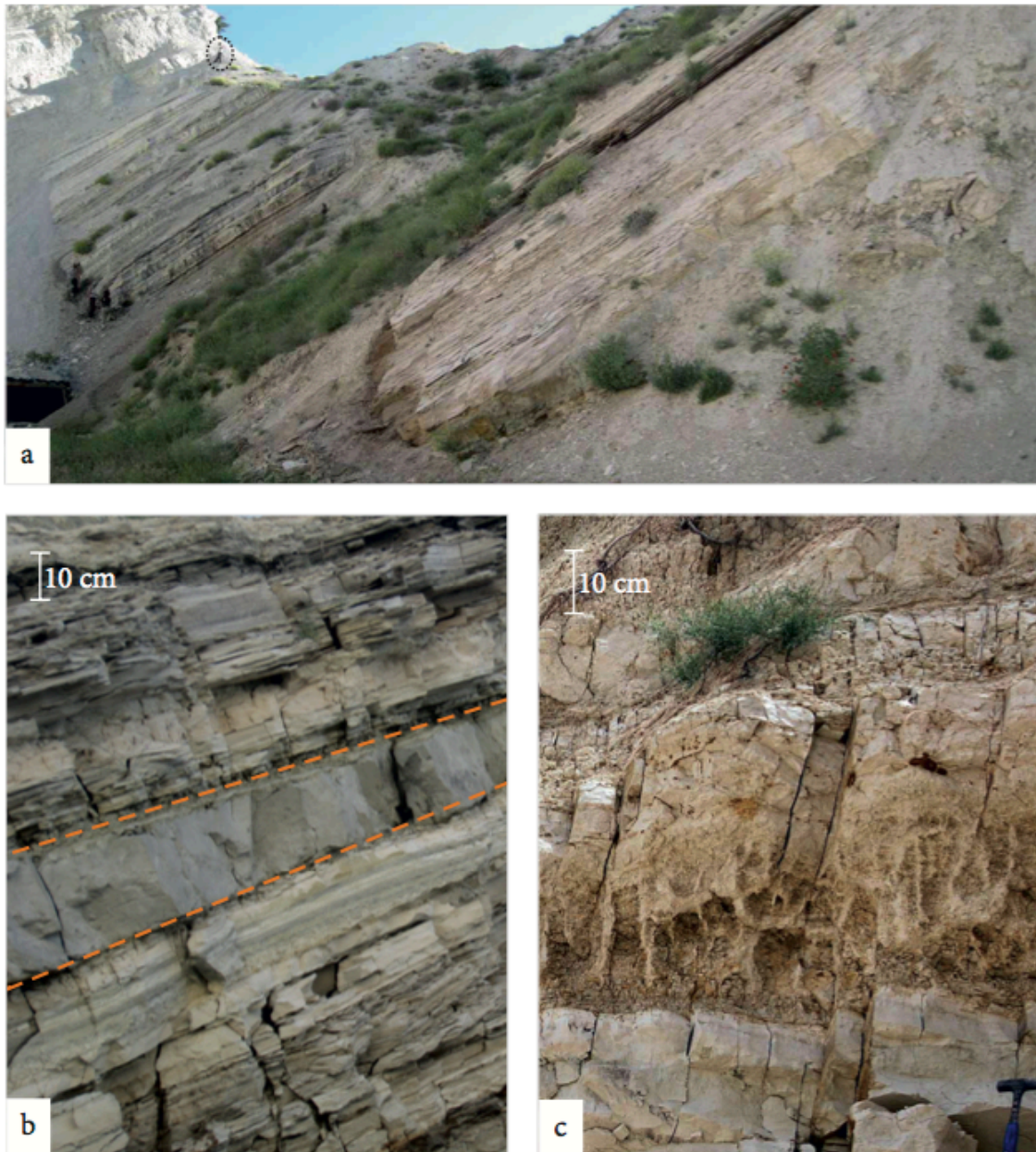


Figure 6.4: Outcrop conditions of the Lower Miocene Gökler sequence in the Ankara region. a) Overview of the sampled succession with laminated marls at the base, overlain by lignite (dark unit), volcanic intercalation and diatom rich sediments. Person (circle) for scale. b) Laminated marls and ca. 20 cm of ash layer (indicated with orange lines). c) Large shrinkage cracks in the upper part of the quarry indicate desiccation of wet sediment. Note that the shrinkage cracks occur slightly above the logged portion of the succession.

6.6.5.2 Kasımlar section

The Kasımlar section consists exclusively of monotonous, very finely laminated, dark gray organic-bearing marls (or “paper shales”; Fig. 6.2d). Thirteen marl samples were taken from a 6-m-thick section, exposed in an outcrop 85 km north of Ankara, ca. 0.8 km east of the village of Kasımlar (40°39’46.8”N, 32°40’48.6”E). The Kasımlar marl succession is listed in the “Neogene of the Old World Database of Fossil Mammals” (NOW) with an age of 20 to 18 Ma (Fortelius 2012) based on micromammal chronology indicating mammal zone MN3 (de Bruijn and Saraç 1991; Rummel 1999; Saraç 2003; López-Antoñanzas et al. 2004).

6.7 Results

Table 6.1 summarizes the new $^{40}\text{Ar}/^{39}\text{Ar}$ geochronological data. ^{39}Ar release spectra as derived from multigrain step-heating experiments are presented in Figure 6.5. A list of each sampled section with the most probable age range and time span is given in Table 6.2. Table 6.3 provides an overview of the $\delta^{18}\text{O}$ and $\delta^{13}\text{C}$ data. Isotopic data of the individual samples are listed in the Supplementary Material 6.11.

6.7.1 Ecemiş Corridor

Oxygen isotope ratios of lacustrine carbonates ($\delta^{18}\text{O}_{\text{carb}}$) in the Çukurbağ Formation vary between 22.1‰ and 25.6‰ with a median value of 24.7‰, whereas carbon isotope ratios ($\delta^{13}\text{C}_{\text{carb}}$) range between -6.0‰ and -0.8‰ with a median value of -3.6‰ (n = 40; Fig. 6.6a; Tab. 6.3). $\delta^{18}\text{O}_{\text{carb}}$ values decrease by about 1‰ in the lower 10 m from 25.5‰ to 24.5‰, and then increase upsection to about 25.0‰ at around 20 m. The upper half of the section (20 to 40 m) is characterized by a larger (up to ca. 3‰) variability in the oxygen isotope data with $\delta^{18}\text{O}_{\text{carb}}$ values between 22.1‰ and 25.2‰.

Generally, $\delta^{13}\text{C}_{\text{carb}}$ values show an inverse trend when compared to the $\delta^{18}\text{O}_{\text{carb}}$ values. In the lower 20 m of the section, $\delta^{13}\text{C}_{\text{carb}}$ increases from ca. -5.5‰ to -2.5‰. Upsection the $\delta^{13}\text{C}_{\text{carb}}$ values average at ca. -3.0‰, yet with an increased intrasample variability (up to 4.1‰). Most of the marl samples from the Ecemiş Corridor have carbonate contents between 30% and 60%; however, there is no significant correlation between the carbonate content and $\delta^{18}\text{O}$ and $\delta^{13}\text{C}$ values.

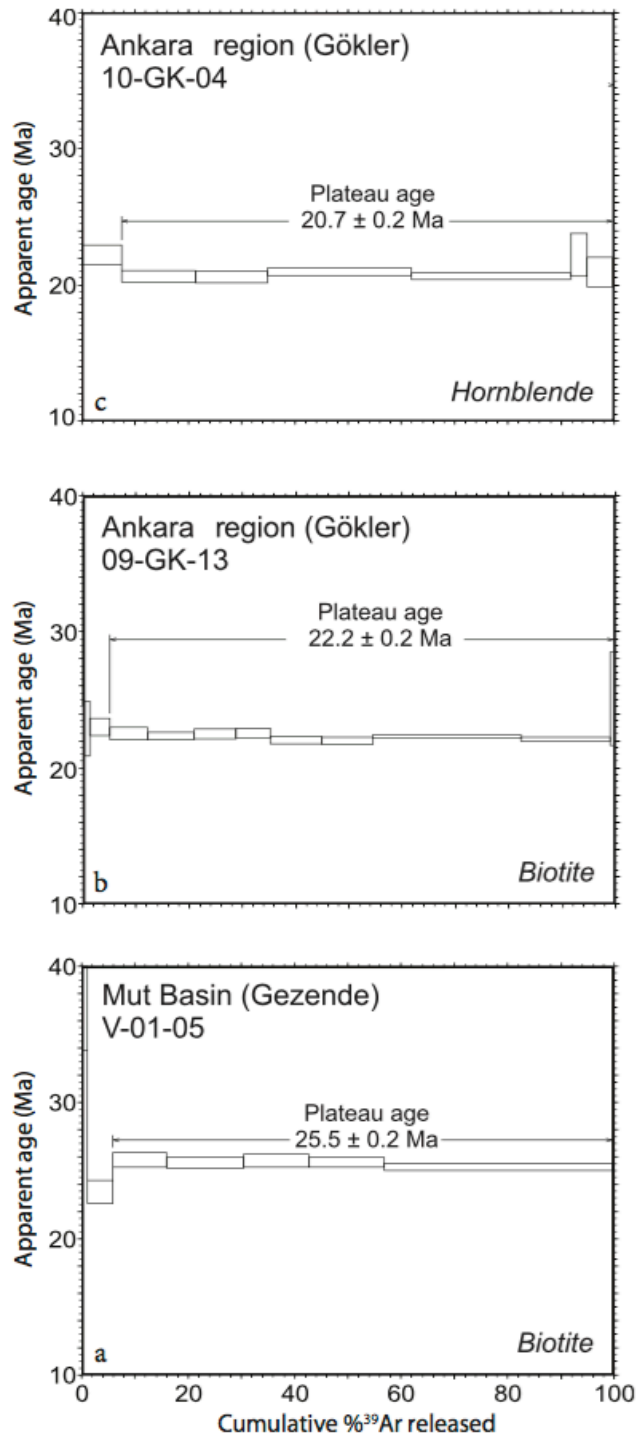


Figure 6.5: Stepwise-heating $^{40}\text{Ar}/^{39}\text{Ar}$ degassing spectra with the derived plateau ages from a) a ca. 5 mm thick, biotite-rich, moderately altered ash layer at 7.0 m of the Fakırca Formation in the Mut Basin (sample V-01-05), b) a tuffite bed at the base of the Gökler profile (sample 09-GK-13), c) an ash layer (crystal tuff) at 7.4 m of the Gökler profile (sample 10-GK-04).

Table 6.3: List of the stable isotope results for each sampled unit, sorted by age, with $\delta^{18}\text{O}_{\text{carb}}$ and $\delta^{13}\text{C}_{\text{carb}}$ ranges, their average and 2σ standard deviation, number of analyzed carbonate samples, median $\delta^{18}\text{O}_{\text{mw,rec}}$ values of recent meteoric waters in the vicinity of the examined sections with the 2σ standard deviation and number of samples (Schemmel et al. 2013), calculated fossil meteoric water $\delta^{18}\text{O}$ values for lake temperature of 20°C using the fractionation equation of Kim and O'Neil (1997), and the average difference between fossil and modern meteoric water $\delta^{18}\text{O}$.

Basin (section)	Median $\delta^{18}\text{O}_{\text{carb}}$ [‰]	Median $\delta^{13}\text{C}_{\text{carb}}$ [‰]	Nr. of carbonate samples	$\delta^{18}\text{O}_{\text{mw,rec}}$ [‰] (Schemmel et al. 2013)	Fossil $\delta^{18}\text{O}_{\text{mw,cal}}$ [‰]	Mean Δ $\delta^{18}\text{O}_{\text{mw,rec}} -$ $\delta^{18}\text{O}_{\text{mw,cal}}$ [‰]
Ankara (Kasımlar)	27.9 ± 3.0	7.7 ± 4.9	13	$(-10.7) \pm 1.2$ $n = 9$	(-1.2)	9.5
Ankara (Gökler)	29.2 ± 3.9	4.9 ± 3.4	53	$(-9.0) \pm 0.8$ $n = 5$	0.1	9.1
Ilgın (Ilgın)	30.0 ± 6.4	7.6 ± 12.5	67	$(-9.6) \pm 1.0$ $n = 7$	0.9	10.5
Mut (Fakırca)	24.2 ± 0.7	(-132) ± 0.5	57	$(-9.8) \pm 0.6$ $n = 4$	(-4.9)	4.9
Ecemiş (Çukurbağ)	24.7 ± 1.6	(-3.6) ± 2.0	40	$(-11.7) \pm 1.3$ $n=15$	(-4.4)	7.3

6.7.2 Mut Basin

Lithologically monotonous marls of the Fakırca Formation show very little variation in $\delta^{18}\text{O}_{\text{carb}}$ and $\delta^{13}\text{C}_{\text{carb}}$ values (Fig. 6.6b; Tab. 6.3). $\delta^{18}\text{O}_{\text{carb}}$ values vary between 23.8‰ and 25.1‰ with a median value of 24.2‰, whereas $\delta^{13}\text{C}_{\text{carb}}$ values range from -1.6‰ to -0.8‰ with a median of -1.3‰ ($n = 57$) and one outlier of -2.6‰ at around 4 m of the section. At the base of the section, $\delta^{18}\text{O}_{\text{carb}}$ values are generally uniform around 24.0‰, with a slight increase upsection, yet with a notably smaller variability than that observed in the older Çukurbağ Formation (Ecemiş Corridor). The $\delta^{18}\text{O}_{\text{carb}}$ values fall within the same range as those of these older sediments, but when compared to the Çukurbağ Formation, the $\delta^{13}\text{C}_{\text{carb}}$ values of the Fakırca Formation are about 2‰ less negative (Fig. 6.6).

Radiometric dating of biotites from a thin ash layer in the upper part of the section yielded a $^{40}\text{Ar}/^{39}\text{Ar}$ plateau age of 25.5 ± 0.2 Ma (Tab. 6.1; Fig. 6.5a).

6.7.3 Ilgın Basin

$\delta^{18}\text{O}_{\text{carb}}$ values of lacustrine marls in the Ilgın Basin vary between 20.9‰ and 34.5‰ with a median value of 30.0‰, whereas $\delta^{13}\text{C}_{\text{carb}}$ values are characterized by a remarkably large variability ranging from -7.9‰ to 26.1‰ with a median value of 7.6‰ (Fig. 6.7a). Overall, isotopic values in the Ilgın Basin display the most extreme variability of all analyzed sections ($n = 67$; Fig. 6.7 and 9; Tab. 6.3). Between 10 and 22 m in the section, $\delta^{18}\text{O}_{\text{carb}}$ values increase from 22‰ to more than 31‰. Upsection $\delta^{18}\text{O}_{\text{carb}}$ values remain stable before they decrease again at the top of the section (44 to 48 m) to ca. 22‰.

$\delta^{13}\text{C}_{\text{carb}}$ values co-vary with $\delta^{18}\text{O}_{\text{carb}}$. Between 10 and 22 m in the section,

$\delta^{13}\text{C}_{\text{carb}}$ values increase from -7‰ to 10‰ and remain stable around 9‰ to 10‰ before they decrease again to values around 1‰ at the top of the section. We adopted the Aquitanian age of Krijgsman et al. (1996) of ca. 22.3 to 20.7 Ma for the succession.

6.7.4 Ankara region

6.7.4.1 Gökler section

$\delta^{18}\text{O}_{\text{carb}}$ values range between 24.3‰ and 30.9‰ with a median value of 29.4‰; values range from 3.5‰ to 7.7‰ with a median value of 4.9‰ for $\delta^{13}\text{C}_{\text{carb}}$ ($n = 53$; Fig. 6.8a; Tab. 6.3). From 0 to 5 m, $\delta^{18}\text{O}_{\text{carb}}$ values scatter around ca. 27‰ and then decrease to values of ca. 25‰ at ca. 7 m, yet with large variability in both $\delta^{18}\text{O}_{\text{carb}}$ and $\delta^{13}\text{C}_{\text{carb}}$. At 8 m, a very distinct shift of ca. 4‰ occurs and $\delta^{18}\text{O}_{\text{carb}}$ values attain ca. 30‰, and then remain relatively uniform with a variability of mostly less than $\pm 1\%$. Between 0 and 3 m, $\delta^{13}\text{C}_{\text{carb}}$ values average at ca. 4.5‰ and show a positive correlation with $\delta^{18}\text{O}_{\text{carb}}$. In a similar fashion to $\delta^{18}\text{O}_{\text{carb}}$, the $\delta^{13}\text{C}_{\text{carb}}$ values also increase between 8 and 11 m before a good positive correlation between oxygen and carbon isotope ratios is observed again. Within the Gökler section, we dated two volcanic ashes: at the base of the succession biotites from a biotite-rich tuffite yielded a $^{40}\text{Ar}/^{39}\text{Ar}$ plateau age of 22.2 ± 0.2 Ma, whereas amphibole from a crystal tuff bed at the top of the section yielded a $^{40}\text{Ar}/^{39}\text{Ar}$ plateau age of 20.7 ± 0.2 Ma (Tab. 6.1; Fig. 6.5b, 6.5c, and 6.7a). Therefore, the timing of the deposition of the Gökler succession would largely overlap with that of the Ilgın succession.

6.7.4.2 Kasımlar section

Monotonous laminated marls in the northern Ankara region show $\delta^{18}\text{O}_{\text{carb}}$ values between 26.3‰ and 31.3‰ with a median value of 27.9‰, whereas $\delta^{13}\text{C}_{\text{carb}}$ values plot between 3.8‰ and 12.3‰ with a median value of 7.7‰ ($n = 13$; Fig. 6.8b). An overall trend in either isotopic composition in this short section is not evident. A covariation of the oxygen and carbon isotopic values is, however, rather apparent. Oxygen isotope ratios tend to increase with decreasing carbonate content, which mostly ranges between 20% and 50%. Absence of volcanic interbeds prevents radiometric dating of this part of the section, but seven rodent and eight insectivore species place the sampled section within mammal zone MN3, corresponding to an early Burdigalian age (ca. 20–18 Ma; de Bruijn and Saraç 1991; Rummel 1999; Saraç 2003; López-Antoñanzas et al. 2004; Fortelius 2012).

6.8 Discussion

Oxygen and carbon isotope data of six paleolakes distributed over large distances on the CAP offer valuable insights into the hydrological and paleoenvironmental conditions in Central Anatolia during the Oligo-Miocene. Collectively, the data show an increase in aridity over time, interrupted by intervals of higher humidity.

6.8.1 Fossil and recent $\delta^{18}\text{O}_{\text{mw}}$

The oxygen isotopic composition of lacustrine carbonates reflects the composition of lake water ($\delta^{18}\text{O}_{\text{lw}}$) during carbonate formation (e.g., Leng and Marshall 2004). $\delta^{18}\text{O}_{\text{lw}}$ can be reconstructed using carbonate-water fractionation equations (e.g., Kim and O'Neil 1997) and assuming lake water temperatures. Temperature is probably not the only important parameter, since a 20 °C change of lake water temperature changes $\delta^{18}\text{O}_{\text{carb}}$ values by only 4‰ to 5‰ (Kim and O'Neil 1997). For simplicity, only the values corresponding to a lake water temperature of 20 °C are given hereafter.

The reconstructed oxygen isotope ratios for Oligo-Miocene lake waters plot between -4.9‰ and 0.9‰ (Tab. 6.3). Depending on the geographic position with respect to the modern orography of the CAP and its margins, oxygen isotope ratios of present-day meteoric waters ($\delta^{18}\text{O}_{\text{mw}}$) on the plateau range from -12‰ to -8‰ with an isotopic lapse rate of ca. -3‰/km across the Taurides and Pontides (Schemmel et al. 2013). Hence, modern $\delta^{18}\text{O}_{\text{mw}}$ values are significantly more negative than the calculated fossil lake water oxygen isotope ratios (Tab. 6.3). This difference might arise from 2 scenarios: (1) protracted evaporation of Oligo-Miocene lake waters, and/or (2) an essentially flat topographic structure of Central Anatolia, which was fundamentally different from that of the present-day CAP, with no major orographic barriers developed at either margin.

Indeed, all studied successions were deposited prior to the onset of Late Neogene major surface uplift of the southern and northern plateau margins (Yildirim et al. 2011; Cosentino et al. 2012; Schildgen et al. 2012a, 2012b) apart from parts of the Western Pontides, which were exhumed along a pre-Miocene ductile shear zone (Okay et al. 2008). Based on our data, however, this relatively small topographic relief had no large effect on oxygen isotopes in precipitation on the plateau. The Oligo-Miocene oxygen isotopic data presented here are, therefore, consistent with the lack of a marked orographic rainout at the margins of the CAP (and associated decrease in $\delta^{18}\text{O}$ of precipitation within the plateau interior).

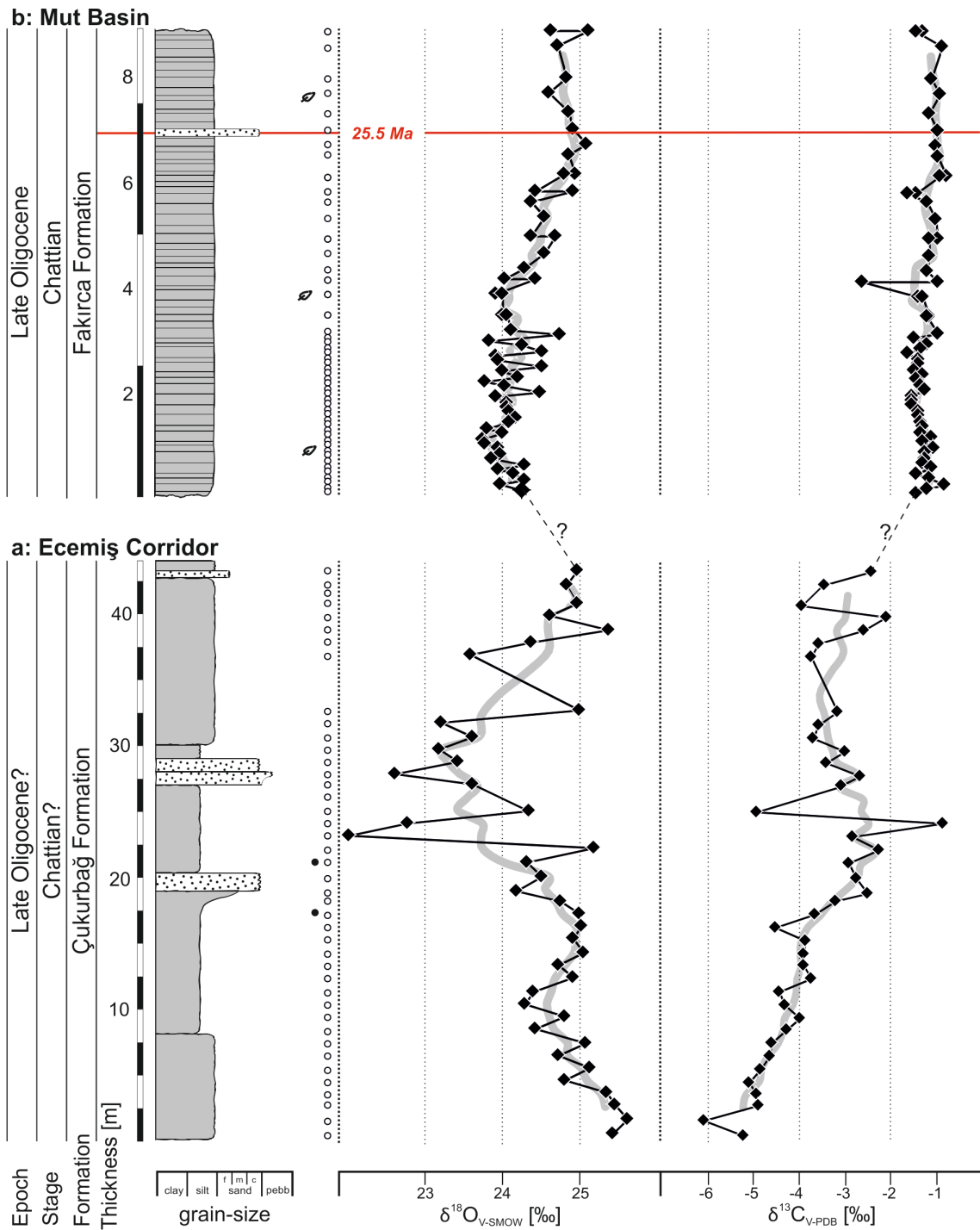


Figure 6.6: Stratigraphic columns of the sampled sediments of the Ecemiş a) and Mut b) Basins showing main sedimentological features, the position of the samples (open circles) as well as the oxygen and carbon stable isotopic ratios. For legend see Fig. 6.7b. a) Stratigraphic column of the Ecemiş sediments near Pınarbaşı. b) Stratigraphic column of the Mut sediments near Gezende. Red line indicates position of the $^{40}\text{Ar}/^{39}\text{Ar}$ -dated sample. Displayed thickness of the ash layer is not to scale, real thickness is 5 mm.

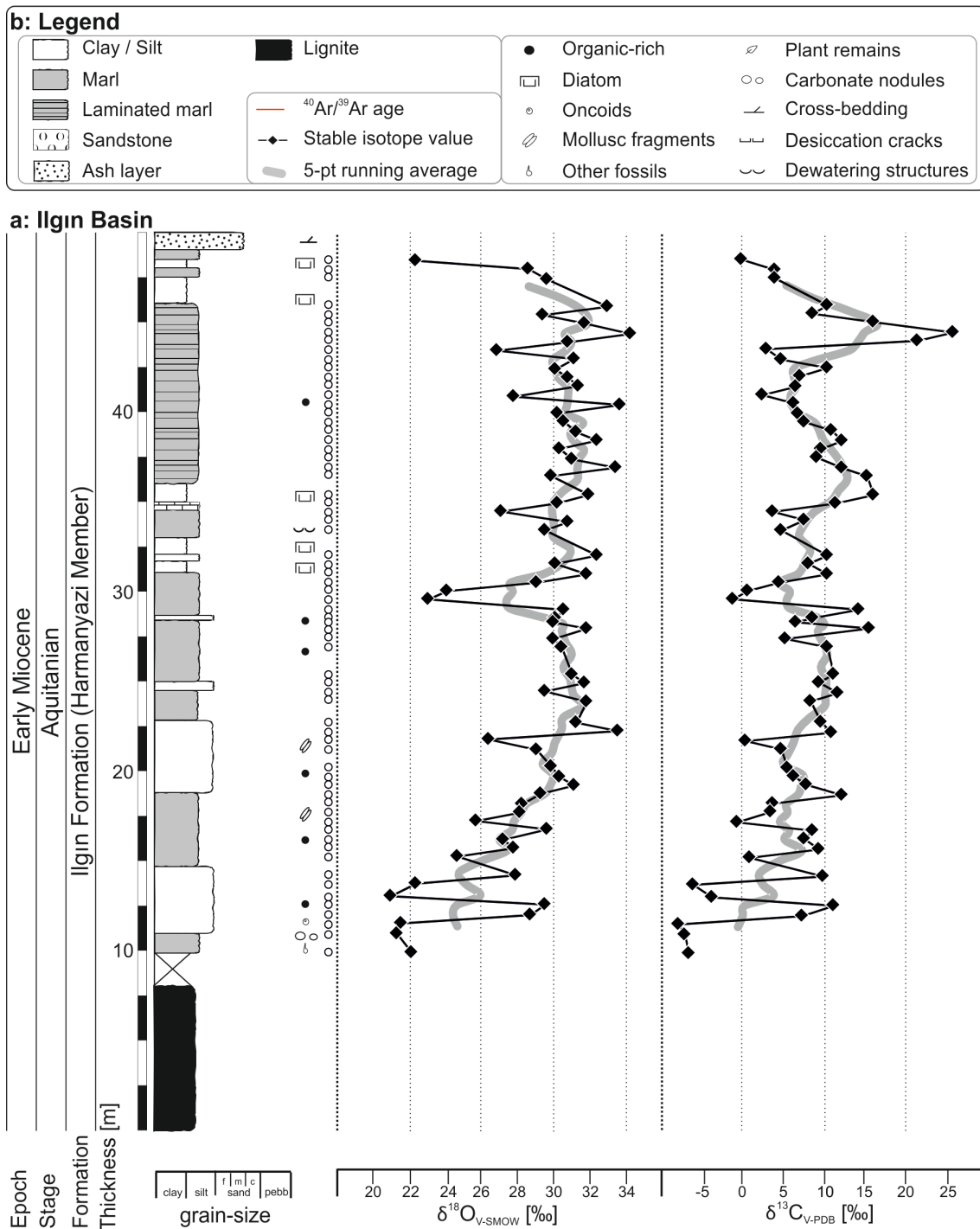


Figure 6.7: a) Stratigraphic column of the sampled sediments of the Ilgın Basin showing main sedimentological features, the position of the samples (open circles) as well as the oxygen and carbon stable isotopic compositions. b) legend for lithology, isotope plots, structures and fossils as shown in Fig. 6.6, 6.7 and 6.8.

Lacustrine carbonates of the Chattian Ecemiş Corridor and Mut Basin show 5‰ to 7‰ less negative values in fossil $\delta^{18}\text{O}_{\text{mw}}$ than recent meteoric waters in this area (Tab. 6.3). This difference is in line with the magnitude of oxygen isotope fractionation related to present-day orographic rainout along the Pontide (ca. 4‰ to 5‰) and Tauride (ca. 7‰ to 8‰) margins (Schemmel et al. 2013). We therefore tentatively attribute the fossil $\delta^{18}\text{O}_{\text{mw}}$ values to a paleotopography devoid of high-relief margins and hence predating the surface uplift of the

Taurides and Pontides. This interpretation is supported by the stable isotope geochemical features of the paleolakes close to the southern margin, which indicate humid subtropical conditions with extensive, hydrologically open basins. A rather flat topography is further indicated by marine sediments directly overlying the sampled section in the Mut Basin (Ilgar and Nemeč 2005).

Fossil $\delta^{18}\text{O}_{\text{mw,cal}}$ values from the Aquitanian to Burdigalian Ilgın and Ankara sections are about 4‰ to 6‰ more positive than those from the Oligocene sections (Tab. 6.3). We attribute this difference to a shift towards more arid climatic conditions, as well as changes in lake hydrology, which will be discussed below.

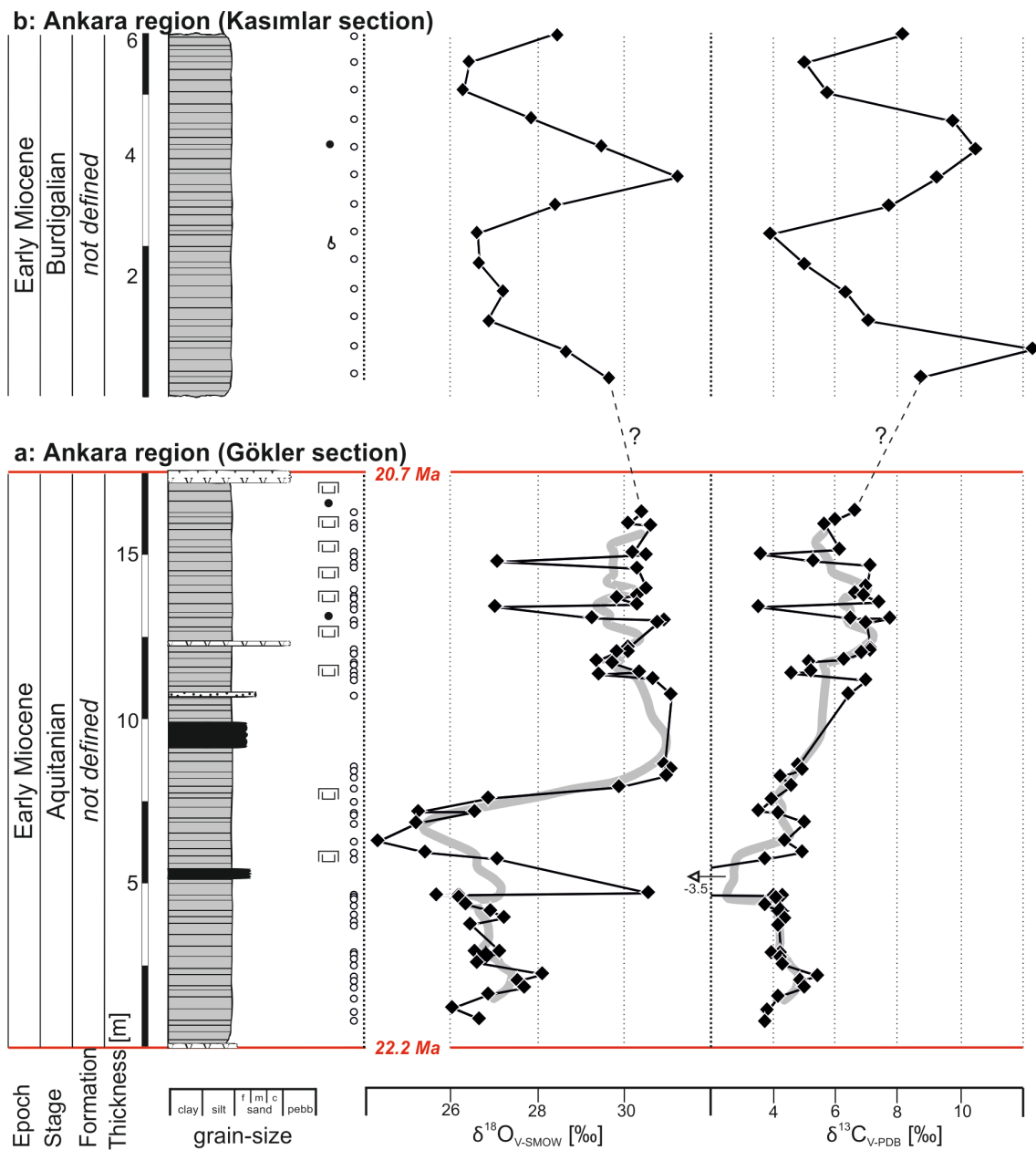


Figure 6. 8: Stratigraphic columns of the sampled sediments within two successions of the Ankara region showing main sedimentological features, the position of the samples (open circles) as well as the oxygen and carbon stable isotopic compositions. For legend see Fig. 6.7b. a) Stratigraphic column of the Gökler locality. Red line indicates position of the $^{40}\text{Ar}/^{39}\text{Ar}$ -dated sample. b) Stratigraphic column of the sediments of the Kasımlar locality.

6.8.2 Oligo-Miocene paleoenvironmental conditions of the CAP

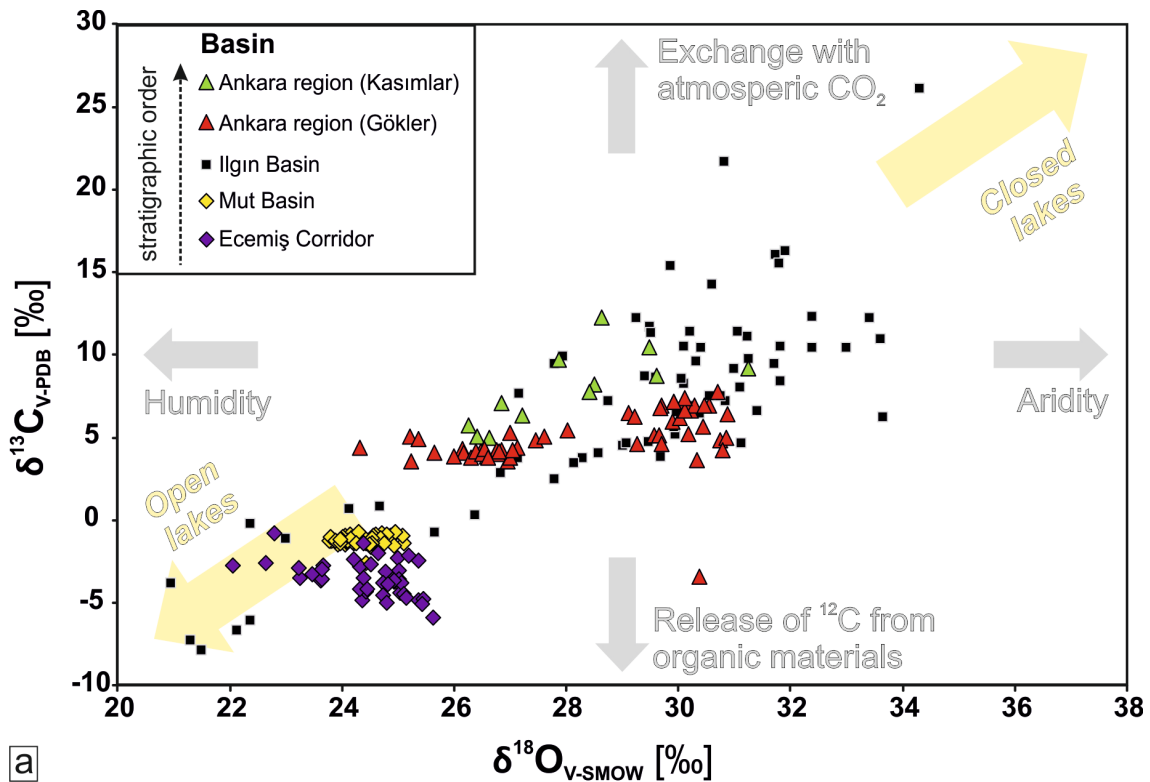
Based on five detailed lacustrine $\delta^{18}\text{O}$ and $\delta^{13}\text{C}$ records that cover the precursor region of the CAP, we establish a first-order paleoenvironmental framework of Central Anatolia during the Late Oligocene and Early Miocene.

6.8.2.1 Chattian (Ecemiş Corridor and Mut Basin)

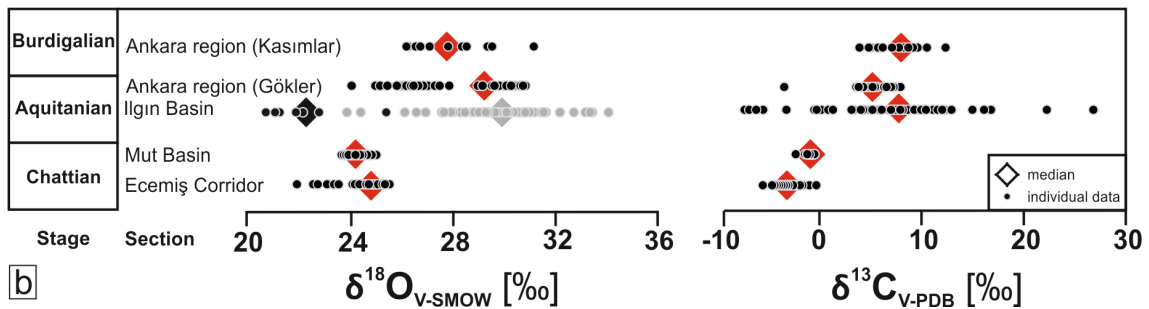
Field and stable isotope geochemical data of the Çukurbağ Formation in the Ecemiş Corridor indicate broadly similar paleoenvironmental conditions when compared to deposition of lacustrine marls of the Fakırca Formation in the neighboring Mut Basin (Fig. 6.6). It is therefore likely that the two basins share broadly similar paleoenvironmental histories. Such an interpretation is consistent with previous sedimentological studies (Şafak et al. 2005) and suggests a similar (Chattian) age for the Fakırca Formation and the analyzed part of the Çukurbağ Formation, and may hence refine previous age assignments that included a broader, Oligocene to Early Miocene time interval (Blumenthal 1955; Yetiş 1968; Nazik and Gökçen 1992; Ünlügenç et al. 1993; Jaffey and Robertson 2005). Palynological data indicate Early Oligocene humid subtropical conditions in southwest Anatolia with lowland slope, swamp, and freshwater aquatic elements (Akkiraz and Akgün 2005). Previous sedimentological studies describe Late Oligocene deposition in southern Anatolia as dominated by alluvial fans and large lakes, consistent with regional evidence for a (periodically?) humid climate during this time (İlgar and Nemeç 2005; Jaffey and Robertson 2005), which agrees well with the observed $\delta^{18}\text{O}$ lake water records in this study. Oligocene palynological data of the CAP also indicate humid subtropical climatic conditions and suggest a paleoenvironment with montane, lowland, slope swamp and water-edge palynofloral elements as well as freshwater lakes in the western part of the CAP during this time (Akkiraz and Akgün 2005; Akgün et al. 2007; Akkiraz et al. 2011; Utescher et al. 2011). Furthermore, our results agree with those of Şafak et al. (2005), who suggested that the lacustrine depositional environment of the Fakırca Formation was tranquil, with a very restricted supply of terrigenous detritus and with little evidence of sustained wave or current activity. The $\delta^{18}\text{O}_{\text{carb}}$ values from both the Mut and Ecemiş sections are relatively low (22‰ to 25‰). Together with the low $\delta^{13}\text{C}_{\text{carb}}$ values (−6‰ to −1‰), the overall restricted oxygen and carbon isotope variability, the published palynological data, and the lack of aridity indicators in the sedimentary facies, the combined Mut/Ecemiş record most likely reflects a hydrologically open lake system with large water volumes and stable lake levels developed under a relatively humid climate with a positive precipitation-evaporation balance (Fig. 6.9a; Leng and Marshall 2004; Deocampo 2010).

6.8.2.2 Aquitanian to Burdigalian (İlgin Basin and Ankara region)

Sediments of the Gökler section have been precisely dated herein; deposition of the sampled interval took place between 22.2 ± 0.2 and 20.7 ± 0.2 Ma, corresponding to an Aquitanian age (Fig. 6.8a) and therefore possibly largely overlapping with the age of the İlgin section. The overlying Kasımlar section has



a



b

Figure 6.9: Results of the stable oxygen and carbon isotope analysis. a) Plot of $\delta^{18}O_{carb}$ versus $\delta^{13}C_{carb}$ values of all 230 carbonate samples considered in this study. Hydrologically closed lakes often show $\delta^{18}O_{carb}$ vs. $\delta^{13}C_{carb}$ covariance, the high values reflect different degrees of equilibration of the TDIC with atmospheric CO_2 and preferential evaporative loss of the light oxygen isotope (after Leng and Marshall 2004). b) Dot-chart of oxygen (left) and carbon (right) isotopic values of each sample site stratigraphically sorted by the most probable age. Red diamond indicates median of all individual sample values for each section. The spread of the data from the Ilgın section is extremely large. The median of all values is therefore displayed as a grey diamond. The black diamond indicates the median of $\delta^{18}O$ median of samples with a negative $\delta^{13}C$ (black circles) as the best estimate for least evaporative lake water conditions. Note that the timing of the deposition of the Ilgın and Gökler (Ankara region) sediments possibly largely overlap.

been dated by micromammals (de Bruijn and Saraç 1991; Rummel 1999; Saraç 2003; López- Antoñazas et al. 2004) and is listed in the NOW Database with an assigned age of 20 to 18 Ma (Fortelius 2012). Based on the above age constraints, we place the Kasımlar section stratigraphically above the Gökler section. The age control on the Ilgın section is provided by biostratigraphical and paleomagnetic data, which places the formation into the middle Aquitanian (22.3 to 20.7 Ma; Krijgsman et al. 1996). Collectively, these three sections cover parts of the Early Miocene time interval.

The relatively sharp contact between the lignite seam at the base of the Ilgın section and the overlying sediments of the Ilgın Formation may reflect a

relatively rapid change in paleoenvironmental conditions from a (sub)humid climate that favored development and preservation of the lignite seam (Karayığit et al. 1999) to a more arid, subtropical environment as indicated by increasing $\delta^{18}\text{O}$ ratios from below 22‰ to ca. 30‰ in the lowermost 10 m of carbonates above the lignite.

The fossil spore-pollen assemblages of the Iğın lignite indicate a warm and humid climate with lakes and extensive wetlands (Karayığit et al. 1999). The relatively low $\delta^{18}\text{O}_{\text{carb}}$ values (22‰ to 24‰) of the sediments immediately overlying the lignite are in agreement with the inferred subtropical conditions; mean $\delta^{18}\text{O}_{\text{carb}}$ values, however, rapidly increase by ca. 8‰ (from 22‰ to 30‰) between 10 and 20 m of the sampled section. Similarly, we observe an increase in $\delta^{13}\text{C}$ from ca. -5‰ to 4‰. Taken together, these data indicate a transition towards more arid conditions and the development of an increasingly closed lake system. This interpretation is supported by a decreasing grain-size trend and a statistically significant positive covariance of the oxygen and carbon isotopic ratios. Upsection (20 to 56 m) $\delta^{18}\text{O}$ and $\delta^{13}\text{C}$ values remain high and display a remarkable high-frequency variability.

The extremely large but (quasi-)periodic fluctuations in $\delta^{18}\text{O}$ and $\delta^{13}\text{C}$ values of the Iğın lacustrine carbonates indicate that the lake environment reacted rapidly to changing paleoenvironmental conditions including lake level, freshwater input, and biological productivity. Whereas the overall extremely high $\delta^{18}\text{O}$ and $\delta^{13}\text{C}$ values appear to be climatically controlled, their well-documented high-frequency, high-amplitude fluctuations are likely connected to local environmental factors.

$\delta^{18}\text{O}$ and $\delta^{13}\text{C}$ data in the Gökler section suggest a shift in lake hydrology towards more restricted lake conditions at approximately around 21 Ma (4–6 m of section; Fig. 6.8a). At this time (middle Aquitanian) carbonate precipitation took place in a humid environment with a positive precipitation-to-evaporation ratio. This interpretation is supported by comparatively low $\delta^{18}\text{O}_{\text{carb}}$ values of ca. 26‰ to 27‰ at the base of the section, which increase rapidly by about 5‰ (from ca. 25.5‰ to ca. 30.5‰) over the course of 1 to 2 m in the section. $\delta^{13}\text{C}_{\text{carb}}$ values are not as negative as in the Chattian (28.4 to 23 Ma) Ecemiş and Mut sections described above, but they do not attain such extremely positive values as those in the section in the stratigraphically similar Iğın Basin (Fig. 6.7). The $\delta^{18}\text{O}_{\text{carb}}$ shift in Gökler section occurs roughly coeval to the deposition of the ca. 1-m-thick lignite deposits and is accompanied by a slightly sluggish shift in the $\delta^{13}\text{C}_{\text{carb}}$ values, amounting to about 2‰. Storm deposits, the presence of lignite, and desiccation cracks (ca. 5 m above the logged portion of the section) all indicate a relatively shallow littoral environment, with the stable isotope data strongly suggesting a changeover from hydrologically open to more restricted conditions shortly before the Aquitanian/Burdigalian transition. Whereas the elevated oxygen and carbon isotopic ratios most likely reflect a more arid climate compared to the Chattian, the fact that the major isotopic shift occurs coeval to lignite deposition (itself typically requiring humid conditions)

calls for additional processes affecting the hydrologic balance of the lake, such as, e.g., the separation of an ephemeral lagoon or regional forest-wetland environments.

The Burdigalian Kasımlar sediments in the Ankara region show an increased variability in $\delta^{18}\text{O}$ and $\delta^{13}\text{C}$ values (Fig. 6.8b). First-order covariance between $\delta^{18}\text{O}$ and $\delta^{13}\text{C}$ values is consistent with fluctuating lake level, biological productivity in the lake, and a relatively low precipitation-to-evaporation ratio. Nevertheless, the homogeneous, laminated, organic-rich character of the marls suggests a relatively distal depositional environment. Paleovegetational climatic proxy data for the late Aquitanian to Burdigalian are in excellent agreement with our findings (Akgün et al. 2007). The taxonomic composition of middle Burdigalian silicified fossil wood from the Ankara region bears good resemblance with its present-day counterparts (Akkemik et al. 2009). Hypsodonty-based interpretation of precipitation rates indicates an east-west (continental-marine) humidity gradient, i.e. a shift of semiarid conditions in Europe from the east to the west, between ca. 11 and 7 Ma (Fortelius et al. 2006).

To complement the stable isotope records presented here, it would be beneficial to further distinguish the effects of regional and temporal climatic and hydrological variations and evaluate their influence on the stable isotopic compositions in lacustrine carbonates. In addition, further work should concentrate on determining the timing and rates of sedimentation in lacustrine environments covering the modern CAP.

6.9 Conclusion

We present a comprehensive long-term oxygen and carbon stable isotope study from five dated sedimentary sequences distributed over the CAP, ranging in age from Chattian to Burdigalian and encompassing 230 lacustrine carbonate samples. In addition to existing biostratigraphic and paleomagnetic data, we use new $^{40}\text{Ar}/^{39}\text{Ar}$ geochronological data from volcanic ashes to add new age constraints to the depositional ages of the individual basin successions.

Field relationships and stable isotope geochemistry are consistent with a relatively humid climate in the Late Oligocene with landscapes characterized by large, hydrologically open freshwater lakes. In the Aquitanian, a phase of generally more arid conditions with frequent climatic fluctuations such as short-lived humid periods, possibly recording the influence of seasonality, topography, and the waxing and waning of aridity, is reported. Roughly around 21 Ma, the climatic evolution of the CAP led to increasingly arid conditions with a dominance of closed, freshwater to mildly saline lakes. The absence of significant orographic barriers along the plateau margin prior to 20 to 16 Ma, such as the Taurides and Pontides today, is consistent with the generally high fossil $\delta^{18}\text{O}$ lake water values sampled within the modern plateau interior. Altogether, the paleoenvironment and paleohydrology of Central Anatolian lake basins was spatially and temporally highly variable in the Late Oligocene and Early Miocene.

6.10 Acknowledgments

This is a VAMP contribution to the ESF Eurocores TopoEurope project (DFG Mu-2845/1-1 to A.M. and TÜBİTAK Project 107Y333 to B.R.). A.M. acknowledges additional support through the LOEWE funding program (Landes Offensive zur Entwicklung Wissenschaftlich ökonomischer Exzellenz) of Hesse's Ministry of Higher Education, Research, and the Arts. The manuscript benefited from helpful reviews by D. Cosentino and C.S. Bayarı. We acknowledge discussion about the interpretation of NOW data with J. Eronen.

6.11 Supplementary Material

Table 6.4: List of all carbonate samples sorted according to sections, with sample ID, stratigraphic position within the section, isotopic values, and carbonate proportion

Section	Sample ID	Depth [m]	$\delta^{18}\text{O}_{\text{VSMOW}}$ [‰]	$\delta^{13}\text{C}_{\text{VPDB}}$ [‰]	Carbonate [%]
Kasımlar	10-KR-13	6.0	28.5	8.1	15
Kasımlar	10-KR-12	5.5	26.4	5.0	47
Kasımlar	10-KR-11	5.0	26.3	5.7	44
Kasımlar	10-KR-10	4.5	27.9	9.7	44
Kasımlar	10-KR-09	4.0	29.5	10.4	38
Kasımlar	10-KR-08	3.5	31.3	9.2	32
Kasımlar	10-KR-07	3.0	28.4	7.7	33
Kasımlar	10-KR-06	2.5	26.6	3.8	52
Kasımlar	10-KR-05	2.0	26.6	4.9	64
Kasımlar	10-KR-04	1.5	27.2	6.3	26
Kasımlar	10-KR-03	1.0	26.8	7.0	49
Kasımlar	10-KR-02	0.5	28.6	12.3	40
Kasımlar	10-KR-01	0.0	29.6	8.7	25
Gökler	09-GK-50	16.2	30.2	6.6	37
Gökler	09-GK-49	15.9	29.9	5.9	15
Gökler	09-GK-48	15.8	30.4	5.6	32
Gökler	09-GK-47	15.0	30.0	6.1	28
Gökler	09-GK-46	14.9	30.3	3.6	32
Gökler	09-GK-44	14.7	27.0	5.2	16
Gökler	09-GK-43	14.5	30.1	7.1	35
Gökler	09-GK-42	13.9	30.3	6.9	18
Gökler	09-GK-41	13.7	30.1	6.6	23
Gökler	09-GK-40	13.6	29.7	6.9	24
Gökler	09-GK-39	13.4	30.1	7.3	31
Gökler	09-GK-38	13.3	26.9	3.5	17
Gökler	09-GK-37	13.0	29.1	6.5	24
Gökler	09-GK-53	12.9	30.7	7.7	43
Gökler	09-GK-36	12.8	30.6	6.9	21
Gökler	09-GK-31	12.1	29.9	7.1	38
Gökler	09-GK-30	12.0	29.9	7.1	34
Gökler	09-GK-29	12.0	29.7	6.8	29
Gökler	09-GK-28	11.7	29.2	6.2	32
Gökler	09-GK-27	11.6	29.7	5.1	22
Gökler	09-GK-26	11.4	30.2	5.2	26

Table 6.4 (continued)

Section	Sample ID	Depth [m]	$\delta^{18}\text{O}_{\text{VSMOW}}$ [‰]	$\delta^{13}\text{C}_{\text{VPDB}}$ [‰]	Carbonate [%]
Gökler	09-GK-25	11.3	29.3	4.6	38
Gökler	09-GK-55	11.1	30.5	6.9	35
Gökler	09-GK-54	10.7	30.9	6.3	23
Gökler	09-GK-38	8.5	30.7	4.8	44
Gökler	09-GK-37	8.4	30.9	4.9	47
Gökler	09-GK-36	8.2	30.8	4.2	48
Gökler	09-GK-35	7.9	29.7	4.5	39
Gökler	09-GK-34	7.5	26.8	4.0	37
Gökler	09-GK-12B	7.1	25.2	3.5	40
Gökler	09-GK-12A	7.1	26.5	4.1	34
Gökler	09-GK-11	6.8	25.2	5.0	24
Gökler	09-GK-10	6.3	24.3	4.4	28
Gökler	09-GK-09	5.9	25.4	4.9	35
Gökler	09-GK-08	5.7	27.0	3.7	48
Gökler	09-GK-07B	4.6	30.4	-3.5	47
Gökler	09-GK-07A	4.6	25.6	4.0	38
Gökler	09-GK-06	4.6	26.2	4.3	54
Gökler	09-GK-05	4.5	26.2	4.1	50
Gökler	09-GK-04	4.3	26.3	3.7	54
Gökler	09-GK-03	4.1	26.8	4.2	53
Gökler	09-GK-02	3.9	27.1	4.4	50
Gökler	09-GK-01	3.7	26.4	4.1	48
Gökler	09-GK-24B	2.9	27.0	4.2	24
Gökler	09-GK-24A	2.9	26.5	4.0	43
Gökler	09-GK-23	2.7	26.8	4.2	51
Gökler	09-GK-22	2.5	26.6	4.3	50
Gökler	09-GK-21	2.2	28.0	5.4	52
Gökler	09-GK-20	2.0	27.5	4.8	48
Gökler	09-GK-19	1.8	27.6	5.0	38
Gökler	09-GK-18	1.5	26.8	4.1	41
Gökler	09-GK-16	1.1	26.0	3.8	49
Gökler	09-GK-15	0.8	26.6	3.7	47
Ilgın	11-CS-98	38.5	22.4	-0.3	100
Ilgın	11-CS-97	38.0	28.6	4.0	52
Ilgın	11-CS-96	37.5	29.7	3.8	67
Ilgın	11-CS-93	36.0	33.0	10.4	98
Ilgın	11-CS-92	35.5	29.4	8.7	89
Ilgın	11-CS-91	35.0	31.7	16.1	100
Ilgın	11-CS-90	34.5	34.3	26.1	100
Ilgın	11-CS-89	34.0	30.8	21.7	87
Ilgın	11-CS-88	33.5	26.8	2.8	67
Ilgın	11-CS-87	33.0	31.1	4.7	75
Ilgın	11-CS-86	32.5	30.1	10.5	73
Ilgın	11-CS-85	32.0	30.8	7.2	59
Ilgın	11-CS-84	31.5	31.4	6.6	32

Table 6.4 (continued)

Section	Sample ID	Depth [m]	$\delta^{18}\text{O}_{\text{VSMOW}}$ [‰]	$\delta^{13}\text{C}_{\text{VPDB}}$ [‰]	Carbonate [%]
Ilgın	11-CS-83	31.0	27.8	2.5	45
Ilgın	11-CS-82	30.5	33.6	6.2	72
Ilgın	11-CS-81	30.0	30.2	6.9	53
Ilgın	11-CS-80	29.5	30.6	7.5	44
Ilgın	11-CS-79	29.0	31.2	11.1	68
Ilgın	11-CS-78	28.5	32.4	12.3	91
Ilgın	11-CS-77	28.0	30.3	9.6	78
Ilgın	11-CS-76	27.5	31.0	9.1	86
Ilgın	11-CS-75	27.0	33.4	12.2	88
Ilgın	11-CS-74	26.5	29.9	15.4	58
Ilgın	11-CS-72	25.5	31.9	16.2	93
Ilgın	11-CS-71	25.0	30.2	11.4	84
Ilgın	11-CS-70	24.5	27.1	3.7	93
Ilgın	11-CS-69	24.0	30.8	7.5	98
Ilgın	11-CS-68	23.5	29.5	4.7	53
Ilgın	11-CS-67	22.1	32.4	10.4	96
Ilgın	11-CS-66	21.6	30.1	8.2	62
Ilgın	11-CS-65	21.1	31.8	10.5	81
Ilgın	11-CS-64	20.6	29.0	4.5	56
Ilgın	11-CS-63	20.1	24.1	0.7	88
Ilgın	11-CS-62	19.6	23.0	-1.1	98
Ilgın	11-CS-61	19.1	30.6	14.3	78
Ilgın	11-CS-60	18.6	30.1	8.5	64
Ilgın	11-CS-36	18.4	30.0	6.5	41
Ilgın	11-CS-35	18.0	31.8	15.5	95
Ilgın	11-CS-34	17.5	29.9	5.2	36
Ilgın	11-CS-33	17.0	30.4	10.4	44
Ilgın	11-CS-30	15.5	31.0	11.4	87
Ilgın	11-CS-29	15.0	31.7	9.5	82
Ilgın	11-CS-28	14.5	29.5	11.7	77
Ilgın	11-CS-27	14.0	31.8	8.4	86
Ilgın	11-CS-26	12.8	31.3	9.7	75
Ilgın	11-CS-25	12.3	33.6	10.9	84
Ilgın	11-CS-24	11.8	26.4	0.3	64
Ilgın	11-CS-23	11.3	29.1	4.6	61
Ilgın	11-CS-21	10.3	29.9	5.6	13
Ilgın	11-CS-20	9.8	30.4	6.4	55
Ilgın	11-CS-19	9.3	31.1	8.0	47
Ilgın	11-CS-18	8.8	29.2	12.2	63
Ilgın	11-CS-17	8.3	28.3	3.7	59
Ilgın	11-CS-16	7.8	28.1	3.5	76
Ilgın	11-CS-15	7.3	25.7	-0.7	50
Ilgın	11-CS-14	6.8	29.6	8.6	68
Ilgın	11-CS-13	6.3	27.1	7.6	86
Ilgın	11-CS-12	5.8	27.8	9.4	83

Table 6.4 (continued)

Section	Sample ID	Depth [m]	$\delta^{18}\text{O}_{\text{VSMOW}}$ [‰]	$\delta^{13}\text{C}_{\text{VPDB}}$ [‰]	Carbonate [%]
Ilgın	11-CS-11	5.3	24.7	0.8	63
Ilgın	11-CS-09	4.3	27.9	9.9	81
Ilgın	11-CS-08	3.8	22.4	-6.1	81
Ilgın	11-CS-07	3.1	20.9	-3.9	80
Ilgın	11-CS-06	2.6	29.5	11.3	49
Ilgın	11-CS-05	2.1	28.8	7.2	91
Ilgın	11-CS-04	1.6	21.5	-7.9	88
Ilgın	11-CS-02	1.0	21.3	-7.3	33
Ilgın	11-CS-01	0.0	22.1	-6.7	64
Mut	V-01-126B	8.9	24.6	-1.3	34
Mut	V-01-126A	8.9	25.1	-1.4	40
Mut	V-01-125	8.6	24.7	-0.8	58
Mut	V-01-124	8.0	24.8	-1.1	50
Mut	V-01-123	7.7	24.6	-0.9	60
Mut	V-01-122	7.3	24.9	-1.1	62
Mut	V-01-121	7.0	24.9	-0.9	67
Mut	V-01-120	6.7	25.1	-1.0	70
Mut	V-01-119	6.5	24.9	-1.0	65
Mut	V-01-118B	6.1	24.9	-0.8	71
Mut	V-01-118A	6.1	24.8	-0.9	64
Mut	V-01-117B	5.8	24.4	-1.4	35
Mut	V-01-117A	5.8	24.9	-1.6	30
Mut	V-01-116	5.6	24.4	-1.2	60
Mut	V-01-115	5.3	24.6	-1.0	67
Mut	V-01-114B	4.9	24.4	-1.0	62
Mut	V-01-114A	4.9	24.7	-1.2	52
Mut	V-01-113	4.6	24.5	-1.1	55
Mut	V-01-112	4.3	24.3	-1.2	56
Mut	V-01-111B	4.1	24.1	-1.0	60
Mut	V-01-111A	4.1	24.4	-2.6	19
Mut	V-01-110B	3.8	23.9	-1.4	51
Mut	V-01-110A	3.8	24.0	-1.3	52
Mut	V-01-109B	3.4	24.0	-1.1	56
Mut	V-01-109A	3.4	24.1	-1.2	60
Mut	V-01-108	3.1	24.1	-0.9	60
Mut	V-01-107	3.0	24.8	-1.5	42
Mut	V-01-106	2.9	23.9	-1.2	58
Mut	V-01-105B	2.8	24.3	-1.3	48
Mut	V-01-105A	2.7	24.5	-1.6	33
Mut	V-01-104	2.6	23.9	-1.4	56
Mut	V-01-103	2.5	24.0	-1.4	53
Mut	V-01-102	2.4	24.5	-1.5	48
Mut	V-01-101	2.3	24.0	-1.3	58
Mut	V-01-100	2.2	24.2	-1.4	47
Mut	V-01-99	2.1	23.8	-1.3	52

Table 6.4 (continued)

Section	Sample ID	Depth [m]	$\delta^{18}\text{O}_{\text{VSMOW}}$ [‰]	$\delta^{13}\text{C}_{\text{VPDB}}$ [‰]	Carbonate [%]
Mut	V-01-98	2.0	24.0	-1.2	53
Mut	V-01-97	1.9	24.5	-1.5	35
Mut	V-01-96B	1.8	23.9	-1.5	42
Mut	V-01-96A	1.7	24.1	-1.5	30
Mut	V-01-95	1.6	24.1	-1.4	46
Mut	V-01-94	1.5	24.1	-1.4	40
Mut	V-01-93	1.4	24.2	-1.4	50
Mut	V-01-92	1.3	24.1	-1.3	36
Mut	V-01-91	1.2	23.8	-1.3	57
Mut	V-01-90B	1.1	24.0	-1.1	53
Mut	V-01-90A	1.0	23.8	-1.3	53
Mut	V-01-89B	0.9	23.8	-1.1	56
Mut	V-01-89A	0.8	24.0	-1.3	48
Mut	V-01-88B	0.7	24.0	-1.2	52
Mut	V-01-88A	0.6	23.9	-1.3	52
Mut	V-01-87B	0.5	24.3	-1.1	52
Mut	V-01-87A	0.4	24.0	-1.4	48
Mut	V-01-86	0.3	24.2	-1.2	39
Mut	V-01-85B	0.2	24.3	-0.8	64
Mut	V-01-85A	0.1	24.0	-1.2	53
Mut	V-01-84	0.0	24.3	-1.4	44
Ecemiş	10-BM-42	44.0	25.0	-2.4	41
Ecemiş	10-BM-41	43.0	24.8	-3.4	43
Ecemiş	10-BM-39	41.5	25.0	-3.9	44
Ecemiş	10-BM-38	40.5	24.6	-2.1	52
Ecemiş	10-BM-37	39.5	25.4	-2.5	40
Ecemiş	10-BM-36	38.5	24.4	-3.5	40
Ecemiş	10-BM-35	37.5	23.6	-3.7	41
Ecemiş	10-BM-34	33.2	25.0	-3.1	37
Ecemiş	10-BM-33	32.2	23.3	-3.5	63
Ecemiş	10-BM-32	31.2	23.6	-3.6	45
Ecemiş	10-BM-31	30.2	23.2	-2.9	54
Ecemiş	10-BM-30	29.2	23.5	-3.4	53
Ecemiş	10-BM-29	28.3	22.7	-2.6	49
Ecemiş	10-BM-28	27.5	23.6	-3.0	56
Ecemiş	10-BM-26	25.5	24.4	-4.9	42
Ecemiş	10-BM-25	24.5	22.8	-0.8	67
Ecemiş	10-BM-24	23.5	22.1	-2.8	54
Ecemiş	10-BM-23	22.5	25.2	-2.2	37
Ecemiş	10-BM-22	21.5	24.3	-2.8	36
Ecemiş	10-BM-21	20.3	24.5	-2.7	41
Ecemiş	10-BM-20	19.2	24.2	-2.5	44
Ecemiş	10-BM-19	18.5	24.8	-3.1	37
Ecemiş	10-BM-18	17.5	25.0	-3.6	31
Ecemiş	10-BM-17	16.5	25.0	-4.5	35

Table 6.4 (continued)

Section	Sample ID	Depth [m]	$\delta^{18}\text{O}_{\text{VSMOW}}$ [‰]	$\delta^{13}\text{C}_{\text{VPDB}}$ [‰]	Carbonate [%]
Ecemiş	10-BM-16	15.5	24.9	-3.8	30
Ecemiş	10-BM-15	14.5	25.1	-3.8	35
Ecemiş	10-BM-14	13.5	24.7	-3.8	37
Ecemiş	10-BM-13	12.5	24.9	-3.7	39
Ecemiş	10-BM-12	11.5	24.4	-4.4	40
Ecemiş	10-BM-11	10.5	24.3	-4.2	43
Ecemiş	10-BM-10	9.5	24.8	-3.9	36
Ecemiş	10-BM-09	8.5	24.5	-4.2	41
Ecemiş	10-BM-08	7.5	25.1	-4.5	46
Ecemiş	10-BM-07	6.5	24.7	-4.6	38
Ecemiş	10-BM-06	5.5	25.2	-4.8	45
Ecemiş	10-BM-05	4.5	24.8	-5.0	47
Ecemiş	10-BM-04	3.6	25.4	-4.9	37
Ecemiş	10-BM-03	2.7	25.5	-4.8	34
Ecemiş	10-BM-02	1.5	25.6	-6.0	54
Ecemiş	10-BM-01	0.4	25.4	-5.1	48

6.12 References

- Akgün, F. 1993. Palynological age revision of the Neogene Soma coal basin. *Bulletin of the Geological Society of Greece* 28, 151–170.
- Akgün, F., Akay, E. and Erdoğan, B. 2002. Terrestrial to shallow marine deposition in Central Anatolia: a palynological approach. *Turkish Journal of Earth Sciences* 11, 11–27.
- Akgün, F., Kayseri M.S. and Akkiraz M.S. 2007. Paleoclimatic evolution and vegetational changes during the late Oligocene- Miocene period in Western and Central Anatolia (Turkey). *Palaeogeography, Palaeoclimatology, Palaeoecology* 253, 56–106.
- Akgün, F. and Sözbilir, H. 1999. A palynostratigraphic approach to the SW Anatolian molasse basin: Kale-Tavas molasse and Denizli molasse. *Geodinamica Acta* 14, 71–93.
- Akkemik, Ü., Türkoğlu, N., Poole, I., Çiçek, İ., Köse, N. and Gürgen, G. 2009. Woods of a Miocene petrified forest near Ankara, Turkey. *Turkish Journal of Agriculture and Forestry* 33, 89–97.
- Akkiraz, M.S. and Akgün, F. 2005. Palynology and age of the Early Oligocene units in Çardak-Tokça Basin, Southwest Anatolia: paleoecological implications. *Geobios* 38, 283–299.
- Akkiraz, M.S., Akgün, F., Utescher, T., Bruch, A.A. and Mosbrugger, V., 2011. Precipitation gradients during the Miocene in Western and Central Turkey as quantified from pollen data. *Palaeogeography, Palaeoclimatology, Palaeoecology* 304, 276–290.
- Bertini, A. 2006. The Northern Apennines palynological record as a contribute for the reconstruction of the Messinian paleoenvironments. *Sedimentary Geology* 188–189, 235–258.
- Blumenthal, M.M. 1955. Yüksek Bolkardağı'nın kuzey kenar bölgelerinin ve batı uzantılarının jeolojisi. *MTA Enstitüsü Yayın Serisi, Series D 7*, 1–153 (in Turkish).
- Bohacs, K.M. 1999. Sequence stratigraphy of lake basins: unraveling the influence of climate and tectonics. *American Association of Petroleum Geologists Bulletin* 83, 11.
- Böhme, M. 2003. Miocene climatic optimum: evidence from lower vertebrates of central Europe. *Palaeogeography, Palaeoclimatology, Palaeoecology* 195, 389–401.
- Brachert, T.C., Reuter, M., Felis, T., Kroeger, K.F., Lohmann, G., Micheels, A. and Fassoulas, C. 2006. Porites corals from Crete (Greece) open a window into Late Miocene (10 Ma) seasonal and interannual climate variability. *Earth and Planetary Science Letters* 245, 81–94.
- Bruch, A.A., Uhl, D. and Mosbrugger, V. 2007. Miocene climate in Europe – Patterns and evolution: A first synthesis of NECLIME. *Palaeogeography, Palaeoclimatology, Palaeoecology* 253, 1–7.
- Bruch, A.A., Utescher, T., Mosbrugger, V. and NECLIME members 2011. Precipitation patterns in the Miocene of Central Europe and the development of continentality. *Palaeogeography, Palaeoclimatology, Palaeoecology* 304, 202–211.
- de Bruijn, H.D. and Saraç, G. 1991. Early Miocene rodent faunas from the eastern Mediterranean area. Part II. Mirabella (Paracricetodontinae, Muroidea). *Proceedings of the Koninklijke Nederlandse Akademie van Wetenschappen - Series B - Physical Sciences* 95, 25–40.
- Çağlar, A.T. and Ayhan, A. 1991. Geological features of the Haremikoy Ilgın–Konya region and lignite deposits (in Turkish, English Abstr.). *Journal of Engineering and Architecture Faculty of Selçuk University* 2, 20–35.
- Campani, M., Mulch, A., Kempf, O., Schlunegger, F. and Mancktelow, N. 2012. Miocene paleotopography of the Central Alps. *Earth and Planetary Science Letters* 337–338, 174–185.
- Canik, B. 1981. Ilgın sıcak su kaynaklarının hidrojeoloji incelemesi. *Selçuk University, Bulletin of Science Faculty* 1, 1–18 (in Turkish).
- Cavazza, W., Federici, I., Okay, A.I. and Zattin, M. 2012. Apatite fission-track thermochronology of the Western Pontides (NW Turkey). *Geological Magazine* 149, 133–140.

- Çiner, A., Karabıyıköğlü, M., Monod, O., Deynoux, M. and Tuzcu, S. 2008. Late Cenozoic sedimentary evolution of the Antalya Basin, southern Turkey. *Turkish Journal of Earth Science* 17, 1–41.
- Cipollari, P., Halássová, E., Gürbüz, K. and Cosentino, D. 2013. Middle- Upper Miocene paleogeography of southern Turkey: insights from stratigraphy and calcareous nannofossil biochronology of the Olukpinar and Başyayla sections (Mut-Ermenek Basin). *Turkish Journal of Earth Sciences* [this issue].
- Clark, M.S. and Robertson, A.H.F. 2002. The role of the Early Tertiary Ulukışla Basin, southern Turkey, in suturing of the Mesozoic Tethys Ocean. *Journal of the Geological Society* 159, 673–690.
- Clark, M.S. and Robertson, A.H.F. 2005. Uppermost Cretaceous-Lower Tertiary Ulukışla Basin, south-central Turkey: sedimentary evolution of part of a unified basin complex with an evolving Neotethyan suture zone. *Sedimentary Geology* 173, 15–51.
- Cosentino, D., Schildgen, T.F., Cipollari, P., Faranda, C., Gliozzi, E. Hudáčková, N., Lucifora, S. and Strecker, M.R. 2012. Late Miocene surface uplift of the southern margin of the Central Anatolian Plateau, Central Taurides, Turkey. *Geological Society of America Bulletin* 124, 133–145.
- Currie, B.S., Rowley, D.B. and Tabor, N.J. 2005. Middle Miocene paleoaltimetry of southern Tibet: implications for the role of mantle thickening and delamination in the Himalayan orogen. *Geology* 33, 181–184.
- Cyr, A.J., Currie, B.S. and Rowley, D.B. 2005. Geochemical evolution of Fenghuoshan Group lacustrine carbonates, North-Central Tibet: implications for the paleoaltimetry of the Eocene Tibetan Plateau. *The Journal of Geology* 113, 517–533.
- Davis, S.J., Mulch, A., Carroll, A.R., Horton, T.W. and Chamberlain, C.P. 2009. Paleogene landscape evolution of the central North American Cordillera: developing topography and hydrology in the Laramide foreland. *Geological Society of America Bulletin* 121, 100–116.
- Deocampo, D.M. 2010. The geochemistry of continental carbonates. In: Alonso-Zarza, A.M. and Tanner, L.H. (eds), *Carbonates in Continental Settings: Geochemistry, Diagenesis and Applications*. Elsevier, Amsterdam, 1–59.
- Deynoux, M., Çiner, A., Monod, O., Karabıyıköğlü, M., Manatschal, G. and Tuzcu, S. 2005. Facies architecture and depositional evolution of alluvial fan to fan-delta complexes in the tectonically active Miocene Köprüçay Basin, Isparta Angle, Turkey. *Sedimentary Geology* 173, 315–343.
- Einsele, G. 2000. *Sedimentary Basins: Evolution, Facies and Sediment Budget*. 2nd ed. Springer, Berlin-Heidelberg.
- Eronen, J.T., Mirzaie Atabadi, M., Micheels, A., Karme, A., Bernor, R.L. and Fortelius, M. 2009. Distribution history and climatic controls of the Late Miocene Pikermian chronofauna. *Proceedings of the National Academy of Sciences* 106, 11867– 11871.
- Fauquette, S., Suc, J.P., Jiménez-Moreno, G., Micheels, A., Jost, A., Favre, E., Bachiri-Taoufiq, N., Bertini, A., Clet-Pellerin, M., Diniz, F., Farjanel, G., Feddi, N. and Zheng, Z. 2007. Latitudinal climatic gradients in the Western European and Mediterranean regions from the Mid-Miocene (c. 15 Ma) to the Mid- Pleistocene (c. 3.5 Ma) as quantified from pollen data. In: Williams, M., Haywood, A.M., Gregory, F.J. and Schmidt, D.N. (eds), *Deep-Time Perspectives on Climate Change: Marrying the Signal from Computer Models and Biological Proxies*. The Micropalaeontological Society, Special Publication 2, 481–502.
- Flower, B.P. and Kennett, J.P. 1994. The middle climatic transition: East Antarctic ice sheet development, deep ocean circulation and global carbon cycling. *Palaeogeography, Palaeoclimatology, Palaeoecology* 108, 537–555.
- Fortelius, M. (coordinator) 2012. Neogene of the Old World Database of Fossil Mammals (NOW). University of Helsinki. Available at <http://www.helsinki.fi/science/now/>.
- Fortelius, M., Eronen, J., Liping, L., Pushkina, D., Tesakov, A., Vislobokova, I. and Zhang, Z. 2006. Late Miocene and Pliocene large land mammals and climatic changes in Eurasia. *Palaeogeography, Palaeoclimatology, Palaeoecology* 238, 219– 227.
- Friedman, I. and Hardcastle, K. 1988. Deuterium in interstitial water from deep-sea cores. *Journal of Geophysical Research* 93, 8249– 8263.

- Fronval, T., Jensen, N.B. and Buchardt, B. 1995. Oxygen isotope disequilibrium precipitation of calcite in Lake Arresø, Denmark. *Geology* 23, 463–466.
- Garziona, C.N., Hoke, G.D., Libarkin, J.C., Withers, S., MacFadden, B., Eiler, J., Ghosh, P. and Mulch, A. 2008. Rise of the Andes. *Science* 320, 1304–1307.
- Gedik, A., Bilgili, Ş., Yılmaz, H. and Yoldaş, R. 1979. Mut-Ermenek- Silifke yöresinin jeolojisi ve petrol olonakları. *Türkiye Jeoloji Kurumu Bülteni* 22, 7–26 (in Turkish).
- Gierlowski-Kordesch, E.H. 2010. Lacustrine carbonates. In: Alonso- Zarza, A.M. and Tanner, L.H. (eds), *Carbonates in Continental Settings: Facies, Environments and Progresses*. Elsevier, Amsterdam, 1–101.
- Görür, N., Sakıncı, M., Barka, A., Akkök, A. and Ersoy, S. 1995. Miocene to Pliocene Palaeogeographic evolution of Turkey and its surroundings. *Journal of Human Evolution* 28, 309–324.
- Görür, N. and Tüysüz, O. 2001. Cretaceous to Miocene paleogeographic evolution of Turkey: implications for hydrocarbon potential. *Journal of Petroleum Geology* 24, 119–146.
- Görür, N., Tüysüz, O. and Şengör, A.M. 1998. Tectonic evolution of the Central Anatolian Basins. *International Geology Review* 40, 831–850.
- Gradstein, F., Ogg, J., Schmitz, M. and Ogg, G. 2005. *A Geologic Time Scale 2004*. Cambridge University Press, Cambridge, UK.
- Gürel, A., Emin, Ç. and Kerey, E. 2007. Sedimentological characteristics of the Çukurbağ Formation deposited along the Ecemiş Fault Zone, Central Anatolia, Turkey. *Journal Geological Society of India* 70, 59–72.
- Horita, J. and Wesolowski, D.J. 1994. Liquid-vapor fractionation of oxygen and hydrogen isotopes of water from the freezing to the critical temperature. *Geochimica et Cosmochimica Acta* 58, 3425–3437.
- Ilgar, A., and Nemec, W. 2005. Early Miocene lacustrine deposits and sequence stratigraphy of the Ermenek Basin, Central Taurides, Turkey. *Sedimentary Geology* 173, 233–275.
- Inaner, H. 2005. Properties of lignite from the Konya-Ilgın-Çavuşçu deposit and its potential use in a future power plant (Turkey). *Bulletin of Geoscience* 80, 19–22.
- İnci, U. 1991. Miocene alluvial fan – alkaline playa lignite- trona bearing deposits from an inverted basin in Anatolia: sedimentology and tectonic controls on deposition. *Sedimentary Geology* 71, 73–97.
- Ivanov, D., Ashraf, A.R., Mosbrugger, V. and Palamarev, E. 2002. Palynological evidence for Miocene climate change in the Forecarpathian Basin (Central Paratethys, NW Bulgaria). *Palaeogeography, Palaeoclimatology, Palaeoecology* 178, 19–37.
- Ivanov, D., Ashraf, A.R., Utescher, T., Mosbrugger, V. and Slavomirova, E. 2007a. Late Miocene vegetation and climate of the Balkan region: palynology of the Beli Breg Coal Basin sediments. *Geologica Carpathica* 58, 367–381.
- Ivanov, M. and Böhme, M. 2011. Snakes from Griesbeckerzell (Langhian, Early Badenian), North Alpine Foreland Basin (Germany), with comments on the evolution of snake faunas in Central Europe during the Miocene Climate Optimum. *Geodiversitas* 33, 411–449.
- Ivanov, D., Bozukov, V. and Koleva-Rekalova, E. 2007b. Late Miocene flora from SE Bulgaria: vegetation, landscape, and climate reconstruction. *Phytologia Balcanica* 13, 281–292.
- Ivanov, D., Utescher, T., Ashraf, A.R., Mosbrugger, V., Slavomirova, E., Djorgova, N. and Bozukov, V. 2008. Vegetation structure and dynamics in the late Miocene of Staniantsi Basin (West Bulgaria). First results. *Comptes rendus de L'Academie bulgare des Sciences* 61, 223–232.
- Ivanov, D., Utescher, T., Mosbrugger, V., Syabryaj, S., Djordjević- Milutinović, D. and Molchanoff, S. 2011. Miocene vegetation and climate dynamics in Eastern and Central Paratethys (Southeast Europe). *Palaeogeography, Palaeoclimatology, Palaeoecology* 304, 262–275.
- Jaffey, N. and Robertson, A.H.F. 2001. New sedimentological and structural data from the Ecemiş Fault Zone, southern Turkey: implications for its timing and offset and the Cenozoic tectonic escape of Anatolia. *Journal of the Geological Society, London* 158, 367–378.

- Jaffey, N. and Robertson, A.H.F. 2005. Non-marine sedimentation associated with Oligocene-Recent exhumation and uplift of the Central Taurus Mountains, Turkey. *Sedimentary Geology* 173, 53–89.
- Karayiğit, A.İ., Akgün, F., Gayer, R.A. and Temel, A. 1999. Quality, palynology, and paleoenvironmental interpretation of the Iğın lignite, Turkey. *International Journal of Coal Geology* 38, 219–236.
- Kayseri, M.S. and Akgün, F. 2002. Palynostratigraphic correlation of the Miocene sediments with lignites and their depositional environments in the Central Anatolia, Turkey. *Proceedings of the 6th European Paleobotany-Palynology Conference*, Greece, 217–218.
- Kayseri, M.S., Akgün, F., Ilgar, A. and Derman, S. 2006. Palynostratigraphy and palaeoclimatology of the Ermenek and Mut regions (Southern Turkey) in the earliest Oligocene period. *7th European Paleobotany-Palynology Conference: Program and Abstracts*, Prague, 63.
- Kelts, K. and Talbot, M. 1990. Lacustrine carbonates as geochemical archives of environmental change and biotic/abiotic interactions. In: Tilzer, M. and Serruya, C. (eds), *Large Lakes – Ecological Structures and Function*. Springer, Berlin-Heidelberg, 288–315.
- Kent-Corson, M.L., Mulch, A., Graham, S.A., Carroll, A.C., Ritts, B.D. and Chamberlain, C.P. 2010. Diachronous isotopic and sedimentary responses to topographic change as indicators of mid-Eocene hydrologic reorganization in the western United States. *Basin Research* 22, 6, 829–845.
- Kim, S.T. and O’Neil, J.R. 1997. Equilibrium and nonequilibrium oxygen isotopic effects in synthetic carbonates. *Geochimica et Cosmochimica Acta* 61, 3461–3475.
- Knorr, G., Butzin, M., Micheels, A. and Lohmann, G. 2011. A warm Miocene climate at low atmospheric CO₂ levels. *Geophysical Research Letters* 38, L20701.
- Koç, A., Kaymakci, N., van Hinsbergen, D.J.J., Kuiper, K.F. and Vissers, R.L.M. 2012. Tectono-sedimentary evolution and geochronology of the Middle Miocene Altınapa Basin, and implications for the Late Cenozoic uplift history of the Taurides, southern Turkey. *Tectonophysics* 532–535, 134–155.
- Koçyiğit, A. 2000. Orta Anadolu’nun genel tektonik özellikleri ve yeni tektonik gelişim. *Bulletin of the Geological Society of Turkey* 27, 1–16 (in Turkish).
- Kovar-Eder, J., Kvacek, Z., Martinetto, E. and Roiron, P. 2006. Late Miocene to Early Pliocene vegetation of southern Europe (7–4 Ma) as reflected in the megafossil plant record. *Palaeogeography, Palaeoclimatology, Palaeoecology* 238, 321–339.
- Krijgsman, W., Duermeijer, C.E., Langreis, C.G., de Bruijn, H., Saraç, G. and Andriessen, P.A.M. 1996. Magnetic polarity stratigraphy of late Oligocene to middle Miocene mammal-bearing continental deposits in Central Anatolia (Turkey). *Newsletters on Stratigraphy* 34, 13–29.
- Kuiper, K.F., Deino, A., Hilgen, F.J., Krijgsman, W., Renne, P.R. and Wijbrans, J.R. 2008. Synchronizing rock clocks on Earth history. *Science* 320, 500–504.
- Lamb, A.L., Leng, M.J., Lamb, H.F. and Mohammed, M.U. 2000. A 9000- year oxygen and carbon isotope record of hydrological change in small Ethiopian Crater Lake. *The Holocene* 10, 167–177.
- Leng, M.J. and Marshall, J.D. 2004. Paleoclimatic interpretation of stable isotope data from lake sediment archives. *Quaternary Science Reviews* 23, 811–831.
- Li, H.C. and Ku, T.L. 1997. $\delta^{18}\text{O}$ - $\delta^{13}\text{C}$ covariance as a paleohydrological indicator for closed-basin lakes. *Palaeogeography, Palaeoclimatology, Palaeoecology* 133, 69–80.
- López-Antoñanzas, R., Sen, S. and Saraç, G. 2004. A new large ctenodactylid species from the Lower Miocene of Turkey. *Journal of Vertebrate Paleontology* 24, 676–688.
- Lüttig, G. and Steffens, P. 1975. *Paleogeographic Atlas of Turkey from the Oligocene to the Pleistocene*. Bundesanstalt für Geowissenschaften und Rohstoffe, Hannover, Germany.

- Mazzini, I., Hudáčková, N., Joniak, P., Kováčová, M., Mikes, T., Mulch, A., Rojay, B., Lucifora, S., Esu, D., and Soulié-Märsche, I. 2013. Paleoenvironmental and chronological constraints on the Tuğlu Formation (Çankırı Basin, Central Anatolia, Turkey). "Late Cenozoic Evolution of the Central Anatolia Plateau" In: Çiner, A., Strecker, M. and Bertotti, G. (eds), *Turkish Journal of Earth Sciences* 22, 747–777.
- Mix, H.T., Mulch, A., Kent-Corson, M.L and Chamberlain, C.P. 2011. Cenozoic migration of topography in the North American Cordillera. *Geology* 39, 87–90.
- Mosbrugger, V., Utescher, T. and Dilcher, D.L. 2005. Cenozoic continental climatic evolution of Central Europe. *Proceedings of the National Academy of Sciences* 102, 14964–14969.
- Nagy, E. 1990. *Palynological Correlation of the Neogene of the Central Paratethys*. Geological Institute of Hungary, Budapest, 1–126.
- Nazik, A. and Gökçen, N. 1992. Ostracoda genus *Zonocypris* and its species in Kurtulmus Formation of Ulukışla Basin (Turkey). *Revista Española de Micropaleontología* 24, 63–69.
- Okay, A.I. 2008. Geology of Turkey: a synopsis. *Anschnitt* 21, 19–42.
- Okay, A.I., Satır, M., Zattin, M., Cavazza, W. and Topuz, G. 2008. An Oligocene strike-slip shear zone: The Uludağ Massif, northwest Turkey – Implications for the westward translation of Anatolia. *Geological Society of America Bulletin* 120, 893–911.
- Özdemir, A. and İnce, İ. 2005. Geology seismotectonics and soil liquefaction susceptibility of Ilgın (west-central part of Turkey) residential area. *Engineering Geology* 77, 169–188.
- Planderová, E. 1991. *Miocene Microflora of Slovak Central Paratethys and Its Biostratigraphical Significance*. Geologický ústav Dionýza Štúra, Bratislava, 1–144.
- Robertson, A.H.F., Ustaömer, T., Pickett, E., Collins, A., Andrew, T. and Dixon, J.E. 2004. Testing models of the Late Palaeozoic-Early Mesozoic orogeny in Western Turkey: support for an evolving open Tethys model. *Journal of the Geological Society, London* 161, 501–511.
- Rummel, M. 1999. Tribe Cricetodontini. In: Rössner, G. and Heissig, K. (eds), *The Miocene Land Mammals of Europe*. Verlag Dr. Friedrich Pfeil, Munich, 359–364.
- Şafak, Ü. and Gökçen, N. 1991. Planktik foraminifer zonlamasına Doğu Akdeniz provensinden. Bir örnek: Mut Havzası Tersiyer istifi. *Türkiye Jeoloji Bülteni* 34, 27–35 (in Turkish).
- Şafak, Ü., Kelling, G., Gökçen, N.S. and Gürbüz, K. 2005. The mid- Cenozoic succession and evolution of the Mut basin, southern Turkey, and its regional significance. *Sedimentary Geology* 173, 121–150.
- Saraç, G. 2003. Türkiye omurgalı fosil yatakları. Maden Tetkik ve Arama Genel Müdürlüğü Derleme Rapor. Jeoloji Kütüphanesi No. 637, Jeoloji Etütleri Dairesi 2003 (in Turkish).
- Schemmel, F., Mikes, T., Rojay, B. and Mulch, A. 2013. The impact of topography on isotopes in precipitation across the Central Anatolian Plateau (Turkey). *American Journal of Science* 313, 61–80.
- Schildgen, T.F., Cosentino, D., Bookhagen, B., Niedermann, S., Yıldırım, C., Echtler, H., Wittmann, H. and Strecker, M.R. 2012a. Multi-phased uplift of the southern margin of the Central Anatolian Plateau, Turkey: a record of tectonic and upper mantle processes. *Earth and Planetary Science Letters* 317–318, 85–95.
- Schildgen, T.F., Cosentino, D., Caruso, A., Buchwaldt, R., Yıldırım, C., Bowring, S.A., Rojay, B., Echtler, H. and Strecker, M.R. 2012b. Surface expression of eastern Mediterranean slab dynamics: Neogene topographic and structural evolution of the southwest margin of the Central Anatolian Plateau, Turkey. *Tectonics* 31, TC2005.
- Schneck, R., Micheels, A. and Mosbrugger, V. 2010. Climate modelling sensitivity experiments for the Messinian Salinity Crisis. *Palaeogeography, Palaeoclimatology, Palaeoecology* 286, 149–163.
- Schwab, A. and Dean, W.E. 2002. Reconstruction of hydrological changes and response to effective moisture variations from north-central USA lake sediments. *Quaternary Science Reviews* 21, 1541–1554.
- Şengör, A.M.C. 1984. The Cimmeride Orogenic System and the Tectonics of Eurasia. *Geological Society of America, Special Paper* 195, 1–82.

- Şengör, A.M.C. 1987. Tectonics of the Tethysides: orogenic collage development in a collisional setting. *Annual Reviews of Earth and Planetary Sciences* 15, 213–244.
- Şengör, A.M.C. and Yılmaz, Y. 1981. Tethyan evolution of Turkey: a plate tectonic approach. *Tectonophysics* 75, 181–241.
- Spötl, C. and Vennemann, T.W. 2003. Continuous-flow isotope ratio mass spectroscopic analysis of carbon minerals. *Rapid Communications in Mass Spectrometry* 17, 1004–1006.
- Stampfli, G.M. 2000. Tethyan oceans. In: Bozkurt, E., Winchester, J.A. and Piper, J.D.A. (eds), *Tectonics and Magmatism in Turkey and the Surrounding Area*. Geological Society of London, Special Publication 173, 1–23.
- Strömberg, C.A.E., Werdelin, L., Friis, E.M. and Saraç, G. 2007. The spread of grass-dominated habitats in Turkey and surrounding areas during the Cenozoic: phytolith evidence. *Palaeogeography, Palaeoclimatology, Palaeoecology* 250, 18–49.
- Talbot, M.R. 1990. A review of the palaeohydrological interpretation of carbon and oxygen isotope ratios in primary lacustrine carbonates. *Chemical Geology* 80, 261–279.
- Tanar, Ü. and Gökçen, N. 1990. Mut-Ermenek Tersiyer istifinin stratigrafisi ve mikropaleontolojisi. *Bulletin of the Mineral Research and Exploration Directorate (MTA)* 110, 175–180 (in Turkish).
- Teranes, J.N., McKenzie, J.A., Bernasconi, S.M., Lotter, A.F. and Sturm, M. 1999. A study of oxygen isotopic fractionation during bio-induced calcite precipitation in eutrophic Baldeggersee, Switzerland. *Geochimica et Cosmochimica Acta* 63, 1981–1999.
- Tucker, M.E. and Wright, V.P. 1990. *Carbonate Sedimentology*. Blackwell Scientific Publications, Oxford, UK.
- Tunoğlu, C. and Celik, M., 1995. The Ostracoda association and environmental characteristics of Lower Miocene sequence of Iğın Konya district, Central Anatolia, Turkey. In: Riha, J. (ed.), *Ostracoda and Biostratigraphy*. Balkema, Rotterdam, 229–235.
- Turner, J.V., Fritz, P., Karrow, P.F. and Warner, B.G. 1983. Isotopic and geochemical compositions of marl lake waters and implications for radiocarbon dating of marl lake sediments. *Canadian Journal of Earth Sciences* 20, 599–615.
- Ünlügenç, U., Demirkol, C. and Şafak, U. 1993. Stratigraphical and sedimentological characteristics of the Karsanti Basin fill to the N–NE of the Adana Basin. In: Suat, A. (ed), *Erk Jeoloji Simpozyumu, Bildirileri*, 215–227 (in Turkish with English abstract).
- Utescher, T., Böhme, M. and Mosbrugger, V. 2011. The Neogene of Eurasia: spatial gradients and temporal trends – the second synthesis of NECLIME. *Palaeogeography, Palaeoclimatology, Palaeoecology* 304, 196–201.
- Whateley, M.K.G. and Tuncali, E. 1995. Origin and distribution of sulphur in the Neogene Beypazari Lignite Basin, Central Anatolia, Turkey. In: Whateley, M.K.G. and Spears, D.A. (eds), *European Coal Geology*. Geological Society of London, Special Publication 82, 307–323.
- Wilson, M., Tankut, A. and Guleç, N. 1997. Tertiary volcanism of the Galatia province, north-west Central Anatolia, Turkey. *Lithos* 42, 105–121.
- Wright, J.D., Miller K.G. and Fairbanks R.G. 1992. Early and Middle Miocene stable isotopes: implications for deepwater circulation and climate. *Paleoceanography* 7, 357–389.
- Yağmurlu, F., Helvacı, C. and İnci, U. 1988. Depositional setting and geometric structure of the Beypazari lignite deposits, Central Anatolia. *International Journal of Coal Geology* 10, 337–360.
- Yansa, C.H., Dean, W.E. and Murphy, E.C. 2007. Late Quaternary paleoenvironments of an ephemeral wetland in North Dakota, USA: relative interactions of groundwater hydrology and climate change. *Journal of Paleolimnology* 38, 441–457.
- Yavuz-Işık, N. and Demirci, C. 2009. Miocene spores and pollen from Pelitçik Basin, Turkey – environmental and climatic implications. *Comptes Rendus Palevol* 8, 437–446.
- Yavuz-Işık, N. and Toprak, V. 2010. Palynostratigraphy and vegetation characteristics of Neogene continental deposits interbedded with the Cappadocia ignimbrites (Central Anatolia, Turkey). *International Journal of Earth Sciences* 99, 1887–1897.

- Yetiş, C. 1968. Geology of the Çamardı (Niğde) region and the characteristics of the Ecemiş Fault Zone between Maden Boğazi and Kanişlıç. *Istanbul Üniversitesi Fen Fakültesi Mecmuası, Seri B* 43, 41–61.
- Yildirim, C., Schildgen, T.F., Echtler, H., Melnick, D. and Strecker, M.R. 2011. Late Neogene and active orogenic uplift in the Central Pontides associated with the North Anatolian Fault: implications for the northern margin of the Central Anatolian Plateau, Turkey. *Tectonics* 30, TC5005.
- You, Y., Huber, M., Müller, R.D., Poulsen, C.J. and Ribbe, J. 2009. Simulation of the Middle Miocene Climate optimum. *Geophysical Research Letters* 36, L04702.
- Zachos, J., Dickens, G.R. and Zeebe, R.E. 2008. An early Cenozoic perspective on greenhouse warming and carbon-cycle dynamics. *Nature* 451, 279–283.
- Zachos, J., Pagani, M., Sloan, L., Thomas, E. and Billups, K. 2001. Trends, rhythms, and aberrations in Global Climate 65 Ma to Present. *Science* 292, 686–693.
- Zattin, M., Okay, A.I. and Cavazza, W. 2005. Fission-track evidence for late Oligocene and mid-Miocene activity along the North Anatolian Fault in southwestern Thrace. *Terra Nova* 17, 95–101.

Chapter 7

Summary and Outlook

7.1 Summary

7.1.1 Karonga Basin

The development of East African savannas is crucial for the evolution, migration and foraging strategies of early hominins. These ecosystems range from closed woodland to open grassland savannas and vary widely in fraction of woody cover, providing a large variation in the supply of food, water and shelter for their associated fauna.

This thesis focuses on Plio-Pleistocene terrestrial deposits in the Karonga Basin (Malawi Rift), which are exposed along the northwestern shore of Lake Malawi in the southern part of the East African Rift (EAR). The sediments generally show pedogenic overprint and contain abundant soil carbonate nodules. Vertebrate fossils (ca. 4.3 Ma to 0.6 Ma) include some of the earliest remains (2.4 Ma) of the genera *Homo* (Schrenk et al., 1993; Bromage et al., 1995; Kullmer et al., 2011) and *Paranthropus* (Kullmer et al., 1999). The Uraha and Malema localities are situated between the well-studied early hominin bearing sites of what today is Somali-Masai savanna in the Eastern Rift, and the Highveld Grassland in southern Africa. These sites fill therefore an important geographical gap for hominin research in Africa. Data presented in this thesis represent the first long-term (4.3 Ma to today) southern hemisphere stable isotope record in the EAR, a region particularly interesting for reconstructing ecosystem patterns and correlating them across the Intertropical Convergence Zone (ITCZ) with data on the evolution and migration of early hominins.

This thesis documents stable carbon and oxygen isotope analyses of 321 paleosol carbonate samples spanning all five units, including several modern pedogenic nodules. These records provide the basis for reconstructions of the paleoenvironment in the vicinity of paleolake Malawi with emphasis of patterns in C₃- and C₄-vegetation regimes. Additionally, analyzes of $\delta^{13}\text{C}$ and $\delta^{18}\text{O}$ values of 122 fossil tooth enamel samples from 14 different large-bodied herbivores (suid, equid, bovid, elephant and hippopotamid) were performed to extend our understanding of the habitat with respect to migration ranges and dietary preferences of individual taxa. Finally, this thesis presents a correlation of $\delta^{18}\text{O}$ values from these fossil proxies to modern meteoric water by analyzing a total of 111 samples of precipitation, river, lake and groundwater, to relate Plio-Pleistocene paleohydrological parameters with today's conditions. For summary of the stable isotope data see Fig. 7.1.

Average $\delta^{13}\text{C}$ values of pedogenic carbonate plot persistently around -9‰ while their $\delta^{18}\text{O}$ values are <26‰, both records experience no significant short-term excursions or long-term trends throughout the analyzed time intervals (Fig. 7.1a, b). The very negative carbon isotope values indicate a C₃-dominated

environment with a high fraction of woody cover (60% to 70%) near paleolake Malawi throughout the last ca. 4.3 Ma (Fig. 7.1a). The oxygen isotopic signatures of paleosol carbonate are low (compared to other subtropical African ecosystems) and therefore reflect only minor influences of evaporation on soils during time of carbonate formation (Fig. 7.1b). While overall low $\delta^{18}\text{O}$ values of pedogenic nodules correspond to generally low $\delta^{13}\text{C}$ values, the small variation within the two datasets do not exhibit a co-variance, which supports the theory of persistent climate settings.

Stable isotope data from herbivore enamel show more complex habitat patterns. While stable isotope values of suid (*Notochoerus*, *Metridiochoerus*, *Phacochoerus*), elephant (*Elephantidae*) and hippo (*Hippopotamus amphibius*) enamel show very similar values to the pedogenic carbonate (indicating browsing on woodland structures near freshwater sources, Fig. 7.1c, d), some equids and bovids show more complex patterns. Karonga Basin equids (*Eurygnathohippus* sp.) - usually (C_4 -)grazers since 7 Ma in Eastern Africa - show a large range in $\delta^{13}\text{C}$ (-9‰ to +1‰) and $\delta^{18}\text{O}$ (23‰ to 31‰) values, indicating an extensive variation in foraging strategies. While some analyzed individuals reflect either a C_3 - or C_4 -dominated diet, the majority reflects mixed-feeding with varying portions of C_3 - and C_4 -biomass intake. The water-source for equids was influenced by evaporation in variable degrees. The stable carbon isotope record of bovid tooth enamel displays similar complex patterns. While *Antilopini* had a pure C_3 -diet and *Hippotragini* mostly browsed, the $\delta^{13}\text{C}$ values of *Alcelaphini* reflect diverse feeding behaviors with a preference for grazing, peaking in *Alc. Connochates*, which had a pure C_4 diet.

Generally, herbivore $\delta^{13}\text{C}$ and $\delta^{18}\text{O}$ values show a positive co-variance, indicating an enhancement in C_4 -biomass consumption accompanied by water intake from sources that experienced an increasing degree of evaporation. An exception is *Antilopini*, a browsing individual that obtained its drinking water from a highly evaporated source; this probably reflects foraging in the woodlands near evaporated lakes/paleolake Malawi as ^{18}O -enriched drinking sources.

To conclude, these results reconstruct a Plio-Pleistocene paleoenvironment in the Karonga Basin that is similar to the habitat today. Wooded savannas with a large portion of C_3 biomes - the preferred habitat for omnivores and water dependent animals - were dominant near freshwater sources such as rivers along the rift flanks and paleolake Malawi. At drier locations, vegetation included a higher fraction of (C_4 -)grasslands, here specialized grazers were foraging in an ecosystem where (drinking) water was more evaporative.

Complementing this interpretation, similar $\delta^{18}\text{O}$ values of modern meteoric water and reconstructed fossil herbivore drinking water indicates Plio-Pleistocene paleoclimatic patterns comparable to today, regarding especially seasonality and evaporation.

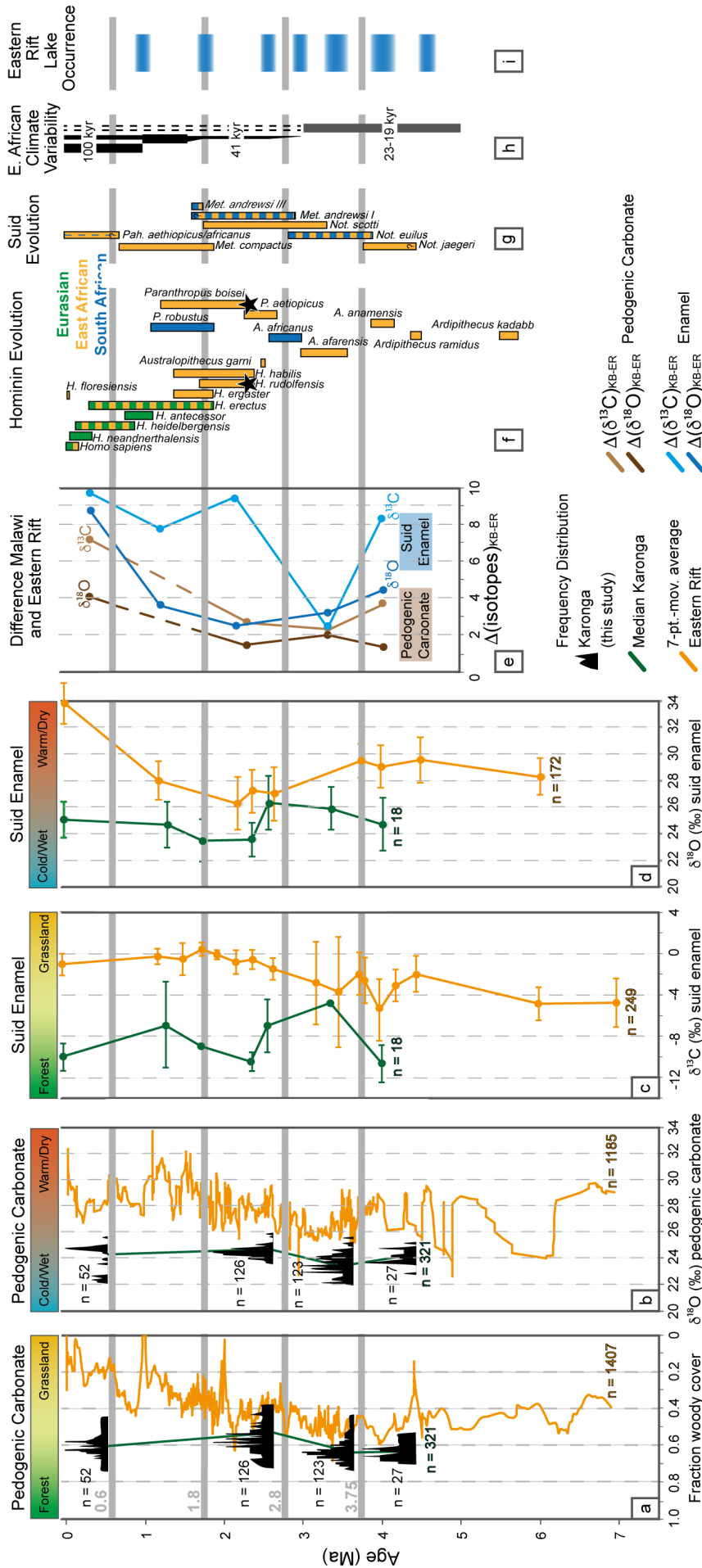


Figure 7.1: Summary of pedogenic carbonate and suid enamel $\delta^{13}\text{C}$ and $\delta^{18}\text{O}$ analyses performed for this thesis. Composite record of paleosol $\delta^{13}\text{C}$ (a) and $\delta^{18}\text{O}$ (b) values from the Karonga Basin (marked in black) presented as normalized probability density function ($\delta^{13}\text{C}$ values are presented in predicted woody cover). Lines present the overall median of stable isotope values of Malawi Rift samples per unit (green) and the 7-point moving average for pedogenic carbonate from the Eastern Rift (orange). Median $\delta^{13}\text{C}$ (c) and $\delta^{18}\text{O}$ (d) values for suid data of the Malawi Rift (green) and the Eastern Rift (orange) with 1 σ standard deviation. Note that the sample density for other mammal taxa is not sufficient for plots across the time intervals. e) Differences of average $\delta^{13}\text{C}$ and $\delta^{18}\text{O}$ values between Karonga Basin and Eastern Rift for pedogenic carbonate (brown) and suid enamel (blue). Although absolute stable isotope values cover a large range especially in the Eastern Rift, the difference in stable isotope values between the Eastern Rift and the Malawi Rift is distinct throughout time and becomes more pronounced during the last ca. 2.5 Ma in both proxy materials. f) Hominin evolution transitions after Shultz et al. (2012) and references therein. Stars indicate Karonga Basin hominins. g) Suidae genera age distribution after White (1995), Kullmer (2010) and Bishop (2010). h) Step-like increases in East African aridity and variability around 2.8, 1.8 and 1 Ma (deMenocal, 1995 and 2004). i) East African Lake occurrences do not include data from the Malawi Rift and show an increase in aridity in the Eastern Rift Valley (Trauth et al., 2005, 2007, Shultz and Maslin, 2013). (Paleo-)Lake Malawi was continuously present since 4.5 Ma (Ring and Betzler, 1995).

The absence of long-term trends towards more positive $\delta^{13}\text{C}$ values contrasts with the increasing role of C_4 -grasslands in the southern EAR valley, which is well documented for hominin localities in the Eastern Rift. Analyzed Karonga Basin herbivore enamel and soil carbonate $\delta^{13}\text{C}$ and $\delta^{18}\text{O}$ values are generally consistently lower than the ones recorded further north, with an increasing difference since 2.5 Ma, resulting in the largest discrepancy in modern samples (Fig. 7.1). My data hence point to regional divergence in climate and vegetation dynamics during the Plio-Pleistocene across the ITCZ in eastern Africa, in a similar manner to the difference between the ecosystems of the Zambezian Savanna (Malawi Rift) and Somali-Masai Endemic Zone (Eastern Rift) today. The boundary between these savanna types therefore did not move as far south as the northern shore of Lake Malawi since the Early Pliocene.

The results of this thesis conclusively document persistence of paleoenvironmental dynamics in the southern branch of the EAR at times of early hominin evolution. This suggests that hominin adaptations are not necessarily directly linked to the emergence of open landscapes and indicates habitat versatility in the co-existing *H. rudolfensis* and *P. boisei*, as both were able to exist in predominantly closed (Malawi Rift) and open (Eastern Rift) savanna settings. This challenges current climate-evolution hypotheses, which are based on Eastern Rift data and generally link hominin evolution to variable patterns (e.g., ‘variability selection hypothesis’) or permanent changes (e.g., ‘savanna hypothesis’) of ecosystems.

7.1.2 Central Anatolian Plateau

Another comprehensive long-term oxygen and carbon stable isotope study for this thesis was performed on Oligo-Miocene sedimentary sequences distributed over the Central Anatolian Plateau, which encompasses 230 lacustrine carbonate samples from five lake basins. Also, in addition to existing biostratigraphic and paleomagnetic data, this study presents new $^{40}\text{Ar}/^{39}\text{Ar}$ geochronological data from volcanic ashes to add new age constraints to the depositional ages of the individual basin successions.

The reconstruction documents spatially and temporally highly variable paleoenvironmental and paleohydrological conditions of Central Anatolian lake basins in the Oligo-Miocene. In the Late Oligocene, large hydrologically open freshwater lakes were dominant in a preponderant humid climate. This setting became more arid during the Aquitanian (ca. 23 Ma to 20.4 Ma), a time of frequent climatic fluctuation and only short-lived humid periods, probably recording the influence of seasonality, topography, and the waxing and waning of aridity. At ca. 21 Ma, the aridity peaked, resulting in closed, freshwater to mildly saline lakes dominating the ecosystem of the CAP.

The documented fossil $\delta^{18}\text{O}$ values determined from lacustrine successions within the modern CAP interior are generally high and therefore support the proposed absence of significant orographic barriers along the plateau margins before at least 21 Ma.

7.2 Outlook

Further (geochemical) analyses of materials implemented in this thesis, as well as and other proxies can be applied to amplify the reconstruction of the landscape early hominins thrived in.

7.2.1 *Clumped isotope paleothermometry of pedogenic carbonate*

Temperature is one of the biggest influences on climatic patterns. Although $\delta^{18}\text{O}$ values are temperature-dependent, many other factors such as source water isotopic composition or evaporation influence the stable oxygen isotope values of carbonate. Δ_{47} measurements provide an estimation of the temperature at which carbonate formed, resulting in an independent paleothermometer. Clumped isotope fossil soil temperature from the Turkana Basin (Eastern Rift) shows the region was - similar to today - continually hot during the past 4 Ma, with soil temperatures during carbonate formation often exceeding 35°C (Passey et al., 2010). Compared to the Turkana Basin, the Karonga Basin Plio-Pleistocene vegetation has a higher fraction of woody cover due to C_3 -plants thriving in a more humid environment. Contrasting soil temperatures of these different savanna biomes provides further insights in the paleohabitat in which early hominins evolved.

7.2.2 *Stable isotope data of fossil hominin enamel*

Some of the earliest remains (ca. 2.4 Ma) of the genera *Paranthropus* and *Homo* were collected from the Chiwondo sediments. To further reconstruct the environmental features and behavior of these early hominins, it is essential to analyze stable isotopes of their enamel, which is preserved on teeth of the mandible (*Homo rudolfensis*) as well as the maxilla fragment (*Paranthropus boisei*). $\delta^{13}\text{C}$ and $\delta^{18}\text{O}$ data of different hominin species from well-studied fossil sites in the Eastern Rift have already been analyzed (e.g., Sponheimer et al., 2013 and references therein), allowing interpretations of early hominin foraging strategies. While the earliest species, *Australopithecus anamensis* (~4.2 Ma to 4.0 Ma) rarely consumed C_4 foods (Wynn et al., 2013), results indicate that *Australopithecus africanus* (~2.8 Ma to 2.1 Ma), *Paranthropus robustus* (~2 Ma to 2.1 Ma) and early *Homo* (~2 Ma) are to about the same extent enriched in ^{13}C , reflecting 30% to 35% C_4 food intake, even if the primary diet is obtained from berries, nut, leaves or other C_3 items (Cerling et al., 2013). However, $\delta^{13}\text{C}$ values of enamel from *P. boisei* are much higher, indicating it obtained 75% to 80% of its diet from C_4 resources (Cerling et al., 2011). The large difference in *P. boisei* and *P. robustus* dietary behavior is unexpected, because the species are remarkably similar in skull and tooth morphology (Klein, 2013). It would be very revealing to a) evaluate the foraging patterns of the two Karonga Basin individuals, b) compare the diet of Malawi Rift hominins to taxa from the Eastern Rift which inhabited a much more open environment and were therefore exposed to a different variety in food supplies and c) gain information about the diets of these early hominin taxa in an early evolutionary stage.

7.2.3 High-resolution and continuous stable isotope analyses

The more than 300 analyzed pedogenic carbonates cover almost 100 m of sediment, spanning over 4 Ma. For this thesis produced geochemical records give a general overview of medium- to large-scale paleoenvironmental fluctuations. High-resolution sampling (~2 cm) of soil carbonate within selected profiles of the Chiwondo Beds could deepen our understanding of the fluctuations of environmental parameters in the region.

Additionally, if possible, continuous sampling throughout all subunits within the Chiwondo Beds should be performed to eliminate the gap in the pedogenic carbonate record of this thesis. Subunit 3B (~1.8 to 0.6 Ma) has not been sampled so far due to poor outcrop conditions. Prospective future fieldwork could therefore focus on exposed sediments of Subunit 3B at “Hut Hill” in the Uraha region.

7.2.4 Stable isotope data from Lake Malawi drill core material

The Lake Malawi Drilling Project (<http://malawidrilling.syr.edu/>) completed a scientific drilling campaign on Lake Malawi in 2005, and the two recovered sediment cores are broadly used for paleoclimatic studies (e.g., Reinthal et al., 2011; Scholz et al., 2011). Pedogenic carbonate is present in the sediments that are today in >350 m water depth, and stable isotope analyses would allow insights of climate patterns at lake level low stands during megadroughts. The maximum age of the retrieved material is 1.5 Ma and therefore roughly covers the timespan of Unit 3B and younger.

7.2.5 Tooth morphology of Karonga Basin herbivores

By combining isotope data with ecomorphological data, such as mesowear and hypsodonty, an estimation of local and regional environmental conditions can be made. With a focus on the fossil-rich (including *P. boisei*) Malema locality and further expansion of the temporal and spatial sequences, a reconstruction of ecological patterns through space and time is possible. Therefore, insights in the links between diets and environmental conditions can be gained. Again, a comparison to existing data from southern and eastern Africa would broaden the knowledge on the evolution of the different ecosystems of our early ancestors.

7.3 References

- Bishop, L.C., 2010. *Suoidea*. In: Werdelin, L., Sanders, W.J. (Eds.), *Cenozoic mammals of Africa*. University of California Press, Berkeley, pp. 821-842.
- Bromage, T.G., Schrenk, F., Zonneveld, F.W., 1995. Paleoanthropology of the Malawi Rift: An Early Hominid Mandible from the Chiwondo Beds, Northern Malawi. *Journal of Human Evolution* 28, 71-108.
- Cerling, T.E., Mbua, E., Kirera, F.M., Manthi, F.K., Grine, F.E., Leakey, M.G., Sponheimer, M., Uno, K.T., 2011. Diet of *Paranthropus beisei* in the early Pleistocene of East Africa. *Proceedings of the National Academy of Sciences USA* 108, 9337-9341.
- Cerling, T.E., Manthi, F.K., Mbua, E.N., Leakey, L.N., Leakey, M.G., Leakey, R.E., Brown, F.H., Grine, F.E., Hart, J.A., Kalembe, P., Roche, H., Uno, K.T., Wood, B.A., 2013. Stable isotope-based diet reconstructions of Turkana Basin hominins. *Proceedings of the National Academy of Sciences USA* 110, 10501-10506.
- deMenocal, P.B., 1995. Plio-Pleistocene African climate. *Science* 270, 53-59.
- deMenocal, P.B., 2004. African climate change and faunal evolution during the Pliocene-Pleistocene. *Earth and Planetary Science Letters* 220, 3-24.
- Klein, R.G., 2013. Stable carbon isotopes and human evolution. *Proceedings of the National Academy of Sciences USA* 110, 10470-10472.
- Kullmer, O., 2008. The fossil *Suoidea* from the Plio-Pleistocene Chiwondo Beds of Northern Malawi, Africa. *Journal of Vertebrate Paleontology* 28, 208-216.
- Kullmer, O., Sandrock, O., Abel, R., Schrenk, F., Bromage, T.G., Juwayeyi, Y.M., 1999. The first *Paranthropus* from the Malawi Rift. *Journal of Human Evolution* 37, 121-127.
- Kullmer, O., Sandrock, O., Kupczik, K., Frost, S.R., Volpato, V., Bromage, T.G., Schrenk, F., 2011. New primate remains from Mwenirondo, Chiwondo Beds in northern Malawi. *Journal of Human Evolution* 61, 617-623.
- Maslin, M.A., Brierley, C.M., Milner, A.M., Shultz, S., Trauth, M., Wilson, K.E., 2014. East African climate pulses and early human evolution. *Quaternary Science Reviews* 101, 1-17.
- Passey, B.H., Levin, N.E., Cerling, T.E., Brown, F.H., Eiler, J.M., 2010. High-temperature environments of human evolution in East Africa based on bond ordering in paleosol carbonates. *Proceedings of the National Academy of Sciences USA* 107, 11245-11249.
- Reinthal, P.N., Cohen, A.S., Dettman, D.L., 2011. Fish fossils as paleo-indicators of ichthyofauna composition and climatic change in Lake Malawi, Africa. *Palaeogeography, Palaeoclimatology, Palaeoecology* 202, 126-132.
- Ring, U., Betzler, C., 1995. Geology of the Malawi Rift: Kinematic and Tectonosedimentary Background to the Chiwondo Beds, Northern Malawi. *Journal of Human Evolution* 28, 15.
- Schrenk, F., Bromage, T.G., Betzler, C.G., Ring, U., Juwayeyi, Y.M., 1993. Oldest *Homo* and Pliocene Biogeography of the Malawi Rift. *Nature* 365, 833-836.
- Scholz, C.A., Cohen, A.S., Johnson, T.C., King, J., Talbot, M.R. and Brown, E.T., 2011. Scientific Drilling in the Great Rift Valley: The 2005 Lake Malawi Scientific Drilling Hemisphere East Africa. *Palaeogeography, Palaeoclimatology, Palaeoecology* 303, 3-19.
- Shultz, S., Maslin, M.A., 2013. Early human specification brain expansion and dispersal influenced by African climate pulses. *PLoS ONE* 8, e76750
- Shultz, S., Nelson, E., Dunbar, R.I.M., 2012. Hominin cognitive evolution: identifying patterns and processes in the fossil and archaeological record. *Philosophical transactions of the Royal Society of London. Series B, Biological sciences Royal Society*. 367, 2130-2140.
- Sponheimer, M., Alemseged, Zeresenay, Cerling, T.E., Grine, F.E., Kimbel, W.H., Leakey, M.G., Lee-Thorp J.A., Manthi, F.K., Reed, K.E., Wood, B.A., Wynn, J.G., 2013. Isotopic evidence of early hominin diets. *Proceedings of the National Academy of Sciences USA* 110, 10513-10518.
- Trauth, M.H., Maslin, M.A., Deino, A.L., Strecker, M.R., 2005. Late Cenozoic moisture history of East Africa. *Science* 309, 2051-2053.

- Trauth, M.H., Maslin, M.A., Deino, A.L., Bergner, M.L., Strecker, M.R., Bergner, A.G.N., Dünforth, M., 2007. High- and low-latitude controls and East African forcing of Plio-Pleistocene African climate and early hominid evolution. *Journal of Human Evolution* 53, 475-486.
- White, T.D., 1995. *African omnivores: global climatic change and Plio-Pleistocene hominids and suids*. In: Vrba, E.S., Denton, G.H., Partridge, T.C., Burchle, L.H. (Eds.), *Paleoclimate and Evolution, with Emphasis on Human Origins*. Yale University Press, New Haven, pp. 369-384.

Zusammenfassung

Kohlenstoff- ($\delta^{13}\text{C}$) und Sauerstoff- ($\delta^{18}\text{O}$) Isotopengeochemie verschiedener terrestrischer Materialien ist ein aussagekräftiges Werkzeug um paläoklimatische und paläoökologische Bedingungen zu rekonstruieren, insbesondere wenn Saisonalität eine wichtige Rolle in der Evolution von Ökosystemen spielt. Unser Verständnis von Landschaften und deren Bezug zu Klima, Vegetationsmustern, Evolution und Veränderung des Nahrungsbedarfs von Tieren, Geologie und Tektonik sind maßgeblich für die Rekonstruktion von fossilen Ökosystemen. Diese Arbeit besteht aus zwei umfangreichen Isotopenstudien im Karonga Becken (Malawi, Südafrika) und im Zentralanatolischen Plateau (Türkei).

Karonga Becken

Geochemiker, Anthropologen, Paläontologen und Archäologen sind ebenso wie die breite Öffentlichkeit seit jeher fasziniert Einblicke in die Entwicklung unserer Vorfahren zu erhalten. Diese Dissertation studiert daher fossile afrikanische Savannen-Biome um die „Wiege der Menschheit“ zu rekonstruieren.

Hauptfragen dieser Arbeit sind:

- Wie haben sich die Paläoumwelt der Savannen des Karonga Beckens - insbesondere in Bezug auf Paläovegetation und Paläoklima - während der Evolution früher Hominini entwickelt?
- Wie unterschiedlich entwickelten sich die fossilen Lebensräume der heutigen Sambesischen Savanne (Malawi) zu dem Ökosystem der Somali-Masai Endemischen Zone (Tansania, Kenia, Äthiopien) in den letzten ca. 4.3 Ma?

Die Entwicklung der ostafrikanischen Savannen ist entscheidend für die Evolution, Migration und Ernährung von frühen Hominiden. Diese weitläufigen Ökosysteme reichen von bewaldeten Flächen zu offenen Grassavannen und variieren stark im Anteil der holzigen Bedeckung, wodurch unterschiedliche Angebote an Nahrung, Trinkwasser und Schutz für die dort lebende Fauna, einschließlich der Hominiden, existieren. Als Schlüsselement zum Verständnis der menschlichen Evolution gilt die Entwicklung von offenen Grassavannen im subtropischen Afrika. Daher ist der Zeitpunkt des Auftretens von C_4 -Gräsern besonders wichtig, um großflächige Vegetationsveränderungen zu erfassen und den Einfluss auf die Evolution von Menschen nachzuvollziehen.

Der Fokus dieser Dissertation liegt auf den am nordwestlichem Ufer des Lake Malawi aufgeschlossenen Plio-Pleistozänen Chiwondo- und Chitimwe-Sedimenten im Karonga Becken, Malawi Rift. Das ermittelte Alter dieser terrestrischen Ablagerungen beruht auf einer Korrelation von radiometrisch datierten Faunen (besonders Suiden) aus Formationen vom östlichen Bereich des Großen Afrikanischen Grabenbruchs. So sind die fluvialen, sumpfigen,

Delta- und Seeablagerungen in fünf stratigraphische Bereiche (Units) unterteilt (die anthropologisch wichtige Unit 3 hat ein Alter von ca. 3.75 bis 0.6 Ma und wird noch weiter in die Zonen 3A-I, 3A-II und 3B unterteilt).

Im Allgemeinen beinhalten die Sedimente durch sekundäre Überprägung entstandenes pedogenes Karbonat in einer karbonatfreien Matrix. Unit 2 und 3 sind fossilienführend und beherbergen unter anderem Fossilien von *Homo rudolfensis* und *Paranthropus boisei*. Diese Fundstellen (Uraha und Malema) der ungefähr 2.4 Ma alten Hominini dokumentieren die früheste Koexistenz der beiden Gattungen. Sie liegen zwischen den intensiv untersuchten Ausgrabungsorten früher Hominini im östlichen Teil des Großen Afrikanischen Grabenbruchs in der heutigen Somali-Masai Endemischen Zone und Fundstellen in dem Highveld Grasland im südlichen Afrika und füllen daher eine wichtige geographische Lücke im Bereich der Hominiden Forschung. Unsere Daten repräsentieren die erste langfristige stabile Isotopenanalyse zu dem sich auf der Südhalbkugel befindlichen Bereich des Grabensystems. Diese Region ist besonders interessant um Vegetationsmuster über die Innertropische Konvergenzzone (ITCZ) hinaus mit der Evolution und Migration der frühen Hominini zu korrelieren.

Wir führen stabile Kohlenstoff- und Sauerstoffisotopenanalysen an 321 pedogenen Karbonaten aus 14 Profilen durch, welche alle fünf Units der Plio-Pleistozänen Sedimente umfassen und zusätzlich mehrere rezente Karbonatknollen beinhalten. Die Ergebnisse liefern eine Basis für Rekonstruktionen der Paläoumwelt in Ufernähe des Malawisees, mit dem Fokus auf das Verhältnis von C₃- und C₄-Pflanzen.

Außerdem haben wir $\delta^{13}\text{C}$ und $\delta^{18}\text{O}$ Werte von 122 fossilen Zahnschmelzproben 14 verschiedener pflanzenfressender Großsäuger (Suiden, Equiden, Boviden, Flusspferden und Elefanten) gemessen, um die Rekonstruktionen der komplexen Umweltbedingungen auf den Migrationsradius der verschiedenen Taxa auszudehnen und ihr Nahrungsangebot zu ermitteln.

Zusätzlich korrelieren wir die Sauerstoffisotopie dieser fossilen organischen und anorganischen Materialien mit der von rezentem meteorischen Wasser, indem wir insgesamt 111 Proben aus Seen und Flüssen sowie Grundwasser und Niederschlag analysieren. So können wir heutige hydrologische Bedingungen im Karonga Becken mit fossilen Parametern vergleichen.

Die ermittelten $\delta^{13}\text{C}$ Werte der pedogenen Karbonaten schwanken nur gering um einen Durchschnittswert von ca. -9‰, während die $\delta^{18}\text{O}$ Werte um 24‰ ebenfalls kaum fluktuieren. Die Ergebnisse beider Isotopenanalysen weisen seit dem frühen Pliozän weder kurz- noch langfristige Veränderungen auf. Die niedrigen Kohlenstoffisotopenwerte reflektieren eine von C₃-Pflanzen dominierte Vegetation in den letzten ca. 4.3 Ma. Die Sauerstoffisotopensignatur deutet auf einen Lebensraum mit einem relativ ausgeglichenen Wasserhaushalt mit nur geringem Einfluss von Evaporation hin und ergänzt daher diese Interpretation. Obwohl niedrige $\delta^{18}\text{O}$ Werte generell mit sehr negativen $\delta^{13}\text{C}$

Werten korrelieren, zeigen die relativ kleinen Fluktuationen innerhalb der beiden Datensätze nur eine sehr geringe Kovarianz. Dies unterstützt die Theorie von weitgehend gleichbleibenden Klimabedingungen.

Stabile Isotope aus Zahnschmelzproben von pflanzenfressenden Säugetieren ergänzen diese Interpretation mit komplexen Paläohabitatmustern. Kohlenstoff- und Sauerstoffisotopendaten von Suiden (*Notochoerus*, *Metridiochoerus*, *Phacochoerus*), Elefanten (*Elephantidae*) und Flusspferden (*Hippopotamus amphibius*) zeigen vergleichbare Werte zu denen pedogener Karbonate. Dies deutet auf eine Ernährung in einer von C₃-Pflanzen dominierten, relativ feuchten Savanne mit Frischwasserreservoir, die kaum von Verdunstung beeinflusst sind, hin. Einige Equiden und Boviden reflektieren ein vielseitigeres Muster. Ostafrikanische Pferde (*Eurygnathohippus sp.*) gelten seit ca. 7 Ma als spezialisierte C₄-Grassfresser. Die im Karonga Becken lebenden Individuen weisen allerdings eine große Fluktuation in $\delta^{13}\text{C}$ (-9‰ bis +1‰) und $\delta^{18}\text{O}$ (23‰ bis 31‰) Werten auf, was auf eine Variabilität in der Nahrungsaufnahme hindeutet. Während sich einige Pflanzenfresser fast ausschließlich entweder von C₄- oder C₃-Pflanzen ernährten, nahmen die meisten Equiden beide Pflanzentypen und unterschiedlich stark von Evaporation beeinflusstes Wasser auf. Die stabilen Isotopenwerte im Zahnschmelz von Boviden (*Alcelaphinae*, *Hippotragini*, *Antilopini*) zeigen ein ähnlich breites Spektrum. Während *Antilopini* und *Hippotragini* hauptsächlich C₃-Pflanzen aufnahmen, zeigen verschiedenen Arten von *Alcelaphinae* ein diverses Fressverhalten, das stark von C₄-Pflanzen beeinflusst wird. *Alc. Connochaetes* ernährte sich sogar fast ausschließlich von C₄-Gräsern.

Generell zeigen $\delta^{13}\text{C}$ und $\delta^{18}\text{O}$ Werte von Zahnschmelz eine positive Kovarianz, dies deutet auf das Einhergehen von erhöhter C₄-Pflanzenaufnahme mit stärker von Evaporation beeinflusstem Trinkwasser hin. Eine Ausnahme bildet hier *Antilopini*, dessen Nahrung fast ausschließlich aus C₃-Pflanzen besteht aber dessen Trinkwasser stark evaporativ beeinflusst ist. Dies deutet auf eine Existenz in den bewaldeten Gebieten in der Nähe von Seen hin, die wie der heutige Malawisee eine hohe Verdunstungsrate besitzen.

Zusammenfassend rekonstruieren diese Ergebnisse ein Plio-Pleistozänes Ökosystem welches ähnlich zum heutigen Lebensraum im Karonga Becken ist. Dominant sind Gebiete mit Baumsavannen (Feuchtere Sambesische Savanne), die sich großflächig um Frischwasserreservoir bilden und Nahrung und Schutz für omnivore und stark wasserabhängige Tiere bieten. In trockeneren und höher gelegenen Regionen entstehen offene (C₄-)Savannen (Trockenere Sambesische Savanne), in der spezialisierte Herbivoren grasen. Die $\delta^{18}\text{O}$ Werte von heutigen meteorischen Wässern bekräftigen diese Rekonstruktion und weisen auf ein beständiges hydrologisches Milieu seit dem Plio-Pleistozän hin.

Die Werte der Kohlenstoff- und Sauerstoffanalysen des fossilen Zahnschmelzes, wie auch die der Bodenkarbonate aus dem Karonga Becken sind in der Regel kontinuierlich niedriger als die Werte aus den vergleichbaren

Plio-Pleistozänen Proxys von Hominini Fundstellen im östlichen Teil des Großen Grabenbruchs (Tansania, Kenia, Äthiopien). Die Werte nehmen hier seit ca. 2.5 Ma stetig zu und kulminieren in der größten Abweichung zwischen den beiden Habitaten in rezenten Proben. Die Abwesenheit von langfristigen Trends zu positiveren $\delta^{13}\text{C}$ Werten in den analysierten Materialien aus dem Karonga Becken steht demnach im Kontrast zu dem zunehmenden Einfluss von C_4 -Gräsern im nördlichen Teil des Grabens; dieser wurde für Hominini Fundstellen mehrfach dokumentiert. Unsere Daten weisen also auf regionale Unterschiede zwischen den Gebieten nördlich und südlich der ITCZ, in Bezug auf Klima- und Vegetationsdynamik während des Plio-Pleistozäns, hin. Diese Differenzen sind vermutlich vergleichbar mit denen der Somali-Masai Savanne im Norden und der Sambesischen Savanne im Süden heute. Die Grenzen zwischen diesen beiden Ökosystemen haben sich daher seit dem frühen Pliozän nie weiter südlich als das nördliche Ufer des Lake Malawis bewegt.

Unsere Ergebnisse dokumentieren dadurch beständige paläoökologische Bedingungen mit einer bewaldeten Savanne im südlichen Teil des Ostafrikanischen Grabenbruchs während der Zeit der Evolution des frühen Menschen. Dies suggeriert, dass die Anpassung der Hominiden nicht zwangsläufig an die Entstehung von offenen Grassavannenlandschaften gekoppelt ist. Demnach waren die koexistierenden *H. rudolfensis* und *P. boisei* jeweils anpassungsfähiger an unterschiedliche Habitate als bisher angenommen.

Zentralanatolisches Plateau

Diese Dissertation beinhaltet eine weitere umfassende Studie, um anhand von Sauerstoff- und Kohlenstoffisotopenanalysen eine zusätzliche Frage zu beantworten:

- Wie haben sich die Paläoumweltfaktoren im späten Oligozän und frühen Miozän im Zentralanatolischen Plateau in Hinsicht auf Klima und der Abwesenheit orographischer Barrieren entwickelt?

Hierzu wurden über das Zentralanatolische Plateau (CAP) verteilte Oligo-Miozäne sedimentäre Abfolgen beprobt und über 200 Seekarbonate aus fünf verschiedenen datierten Lokalitäten geochemisch untersucht. Zusätzlich wurden geochronologische $^{40}\text{Ar}/^{39}\text{Ar}$ Alter vulkanischer Aschen gemessen um erstmals direkte Datierungen der Ablagerungsfolgen der individuellen Becken zu ermitteln.

Meine Rekonstruktionen deuten auf eine sowohl räumlich als auch zeitlich variable Paläoumwelt und Paläohydrologie der zentralanatolischen Becken im Oligo-Miozän hin. Im späten Oligozän dominierten große exorheische Frischwasserseen in einem überwiegend feuchten Klima. Dieses Milieu wird im Aquitanium, einer Zeitspanne die von häufigen klimatischen Schwankungen beherrscht wurde, zunehmend arid. Kurzweilige feuchtere Perioden weisen vermutlich auf den Einfluss von Saisonalität, Topographie und der Ab- und

Zunahme von Aridität hin. Vor ca. 21 Ma nahm die Trockenheit weiter zu und führte auf dem Zentralanatolischen Plateau zu meist endorheischen Seen, welche zum Teil leicht salin waren.

Die fossilen $\delta^{18}\text{O}$ Werte der limnischen Becken die sich heute im inneren Teil des Plateaus befinden sind im Allgemeinen hoch und bestätigen daher die Abwesenheit von signifikanten orographischen Barrieren entlang der Plateaugrenzen während des Oligo-Miozäns.

Acknowledgments

First of all I would like to thank my two supervisors, Andreas Mulch and Friedemann Schrenk. They made it possible to accomplish this work from beginning to end, including extensive fieldwork, laboratory analyses, manuscript writing and conference attendance. Friedemann introduced me to his world of early hominin evolution and made me see problems from a very different perspective. I owe my stable isotope knowledge to Andreas, who is always incredibly supportive and full of exciting new ideas.

Special thanks goes to Heinrich Thiemeyer for joining me on all my trips to Malawi and completing three seasons of successful fieldwork with many fruitful discussions and unforgettable birthday celebrations! I also thank Nicolas Thiemeyer for his assistance in the field.

I am deeply indebted to Ottmar Kullmer who always took the time to answer my many questions about mammalian teeth and human evolution. His thoughtful input improved the quality of this thesis a lot.

I am also grateful to our local Malawian field crew in Karonga, the Cultural Museum Centre Karonga, and the Malawi Government. I want to thank in particular Harrison Simfukwe for assistance and hospitality.

I thank Ulrike Wacker and Jens Fiebig who greatly supported me in the lab and patiently helping me to comprehend complex laboratory equipment.

I received lot of help from Sven Hoffmann, Ulrich Treffert and Christine Wenske in the lab, even if it sometimes meant to quickly fix things I broke. Thank you!

Insightful discussions with my colleagues Angela Bruch, Christine Hertler, Jussi Eronen, Timothy G. Bromage, Oliver Sandrock, Tamás Mikes, Marion Campani, Bora Rojaj and Susanne Haupt greatly inspired my work.

Thanks also to my colleagues at the Stanford School of Earth, Energy and Environmental Sciences, namely Page Chamberlain, Jeremy Caves, Dan Ibarra, Matt Winnick and Annie Ritch.

Thank you, Iryna Yashchenko for answering not only my administrative related questions.

Special thanks goes to my lunch group Sijo Mampilli, Matthew Forrest, Vanesa Nieto-Moreano, Katharina Methner, Camille Gaillard, Liam Langan and Nicolò Ardenghi for talking about stuff, often enough non-work related. I totally needed these breaks in the middle of the day!

I would also like to thank my office mates Fabian Schemmel and Emilija Krsnik for putting up with me every day and fueling my candy-addiction.

Thanks to all my friends, especially Erik, Karo, Stephan, Hannes, Jüli, Dani and Kathy!

Ein ganz besonderer Dank gilt meiner Familie, vor allem meinen Eltern, Peter und Biene, die mich mein gesamtes Studium hindurch unterstützt haben.

Appendix

This Appendix lists all stable isotope data* from pedogenic carbonate (Tab. Appendix 1) and fossil herbivore tooth enamel (Tab. Appendix 2) analyzed for this thesis with standard deviation, (sub-)unit, amount of sample material reacted with H_3PO_4 , position within the profile (pedogenic material) or distance to the crown (tooth enamel), carbonate content (linear correlation of the IRMS signal intensity (2nd peak) and sample weight; normalized with Carrara; error ca. 2%), year sampled (pedogenic material) and number of GasBench run for this thesis. Also, the taxa, locality, body part as well as the first and last appearance date are given for the tooth enamel samples.

Additionally, a “calculated age” is given for paleosol samples. This is not a precise age assignment. Biostratigraphic age constraints (based mostly on surface finds) were established for sediments with an age range of ca. 4.3 Ma (Not. jaegeri) to 0.7 Ma (Met. compactus). Correlation of the fluvial, lacustrine and swamp successions is based on field relationships established during three field campaigns in 2011, 2012 and 2013, structural mapping, mammal fossil occurrence and the pattern of $\delta^{13}C$ and $\delta^{18}O$ values within individual sections. It is not possible to assign an absolute age for each profile and nodule, but the Plio-Pleistocene deposits were divided into five intervals used in this thesis: ca. 4.3 to 3.75 Ma (Unit 1 & 2), 3.75 to 2.8 Ma (Unit 3A-1), 2.8 to 1.8 Ma (Unit 3A-2), 1.8 to 0.6 Ma (Unit 3B) and <0.6 Ma (Unit 4 & 5). The stratigraphic order of each sampling profile within these intervals is accurate, however it is difficult to ascertain sediment accumulation rates in these erosional, mostly high-energy deposits that usually stretch only over a small lateral distance, rarely up to a few hundreds of meters. When compared to the total stratigraphic thickness of each unit, the data presented here commonly covers the entire unit and I tentatively assign the oldest (and youngest) age of the unit to the stratigraphically lowest (and highest) sample. Within each unit I assume constant accumulation rates (that range from 60 and 26 m/Ma), however, the overall results of this thesis are largely independent of this assumption.

*Note that all information on meteoric water data is given in Chapter 5, on CAP data in Chapter 6.

Table Appendix 1: List of all Karonga Basin paleosol carbonate samples with Sample ID, stable carbon and oxygen isotope values with standard error (s.e.), (sub-) unit, profile meter, calculated age, sample weight, carbonate content, year of sampling, and number of run for the analysis.

Sample ID	$\delta^{13}\text{C}_{\text{PDB}}$ [‰]	$\delta^{18}\text{O}_{\text{SMOW}}$ [‰]	$\delta^{13}\text{C}$ s.e [‰]	$\delta^{18}\text{O}$ s.e [‰]	(sub-) Unit	Profile meter	Calculated Age [Ma]	Sample weight [µg]	Carbonate content [%]	Field campaign [year]	Run
MR-13-02	-9.1	24.0	0.01	0.02	modern	0.40	0	2008	12	2012	14
MR-13-01	-11.2	24.6	0.01	0.01	modern	0.00	0	116	86	2012	10
MR-15-01	-9.6	22.6	0.01	0.01	modern	3.00	0	120	82	2012	10
MR-14-01	-6.8	22.7	0.01	0.01	modern	2.00	0	124	73	2012	10
MR-66-01	-8.2	24.2	0.02	0.01	5	1.00	0.1	119	96	2011	3
U-55-22	-8.5	24.8	0.02	0.02	4	4.30	0.24	124	99	2012	13
U-55-21	-7.9	23.9	0.02	0.02	4	4.00	0.25	100	71	2012	13
U-53-20	-9.4	24.9	0.02	0.02	4	3.80	0.26	125	86	2012	13
U-53-19	-8.9	24.8	0.02	0.02	4	3.60	0.27	121	74	2012	13
U-53-18	-8.8	24.7	0.02	0.02	4	3.40	0.28	119	80	2012	13
U-53-17	-9.2	24.7	0.02	0.02	4	3.20	0.28	125	62	2012	13
U-53-16	-9.5	24.6	0.02	0.02	4	3.00	0.29	124	75	2012	13
U-53-15	-10.2	24.8	0.02	0.02	4	2.80	0.30	114	71	2012	13
U-53-14	-8.7	24.8	0.02	0.02	4	2.60	0.31	116	79	2012	13
U-53-13	-10.3	24.8	0.02	0.02	4	2.40	0.32	121	82	2012	13
U-53-12	-9.2	24.7	0.02	0.02	4	2.20	0.32	125	77	2012	13
U-53-11	-8.9	24.7	0.02	0.02	4	2.00	0.33	110	85	2012	13
U-53-10	-9.8	24.9	0.02	0.02	4	1.80	0.34	116	82	2012	13
U-53-09	-9.1	25.0	0.02	0.02	4	1.60	0.35	112	80	2012	13
U-53-08	-8.7	24.9	0.02	0.02	4	1.40	0.35	120	76	2012	13
U-53-07	-8.7	24.7	0.02	0.02	4	1.20	0.36	122	81	2012	13
U-53-06	-8.9	24.8	0.02	0.02	4	1.00	0.37	119	80	2012	13
U-53-05	-10.7	25.0	0.02	0.02	4	0.80	0.38	124	89	2012	13
U-53-04	-8.5	24.6	0.02	0.02	4	0.60	0.38	111	99	2012	13
U-53-03	-8.8	24.7	0.02	0.02	4	0.40	0.39	112	93	2012	13
U-53-02	-9.5	24.8	0.02	0.02	4	0.20	0.40	116	82	2012	13
U-53-01	-8.8	24.8	0.02	0.02	4	0.00	0.41	117	77	2012	13
U-47-18	-9.9	25.6	0.02	0.02	4	3.60	0.46	116	100	2012	12
U-47-17	-10.2	24.4	0.02	0.02	4	3.40	0.47	126	100	2012	12
U-47-16	-9.5	24.9	0.02	0.02	4	3.20	0.48	125	98	2012	12
U-47-15	-9.6	23.6	0.02	0.02	4	3.00	0.48	116	84	2012	12
U-47-14	-8.8	24.5	0.02	0.02	4	2.80	0.49	115	89	2012	12

Table Appendix 1 (continued)

Sample ID	$\delta^{13}\text{C}_{\text{PDB}}$ [‰]	$\delta^{18}\text{O}_{\text{SMOW}}$ [‰]	s.e. $\delta^{13}\text{C}$ [‰]	s.e. $\delta^{18}\text{O}$ [‰]	(sub-) Unit	Profile meter	Calculated Age [Ma]	Sample weight [µg]	Carbonate content [%]	Field campaign [year]	Run
U-47-13	-9.2	23.6	0.02	0.02	4	2.60	0.50	110	80	2012	12
U-47-12	-9.8	22.7	0.02	0.02	4	2.45	0.51	114	88	2012	12
U-47-11	-10.0	24.7	0.02	0.02	4	2.30	0.51	119	93	2012	12
U-47-10	-9.6	24.6	0.02	0.02	4	2.10	0.52	116	93	2012	12
U-47-09	-9.6	22.5	0.02	0.02	4	1.90	0.53	116	49	2012	12
U-47-08	-9.7	22.7	0.02	0.02	4	1.70	0.53	117	82	2012	12
U-47-07	-9.7	22.3	0.02	0.02	4	1.50	0.54	116	69	2012	12
U-47-06	-9.8	22.6	0.02	0.02	4	1.30	0.55	124	88	2012	12
U-47-05	-10.4	22.4	0.02	0.02	4	0.80	0.57	118	82	2012	12
U-47-04	-10.1	22.2	0.02	0.02	4	0.60	0.58	126	76	2012	12
U-47-03	-10.0	22.2	0.02	0.02	4	0.40	0.58	121	81	2012	12
U-47-02	-9.5	22.4	0.02	0.02	4	0.20	0.59	125	95	2012	12
U-47-01	-9.7	22.3	0.02	0.02	4	0.00	0.60	116	84	2012	12
MR-19-01	-7.3	24.5	0.01	0.01	3A	7.50	1.80	118	100	2012	10
MR-19-03	-8.8	24.2	0.01	0.01	3A	7.30	1.81	112	81	2012	10
MR-19-05	-8.6	24.4	0.01	0.01	3A	7.20	1.81	112	75	2012	10
MR-19-07	-8.5	24.6	0.01	0.01	3A	7.10	1.81	118	78	2012	10
MR-19-09	-7.9	24.5	0.01	0.01	3A	7.00	1.81	123	78	2012	10
MR-19-11	-8.9	24.1	0.01	0.01	3A	6.90	1.82	125	74	2012	10
MR-19-13	-7.4	24.5	0.01	0.01	3A	6.80	1.82	122	50	2012	10
MR-19-15	-8.6	24.3	0.01	0.02	3A	6.70	1.82	337	16	2012	15
MR-19-19	-8.7	24.4	0.01	0.01	3A	6.50	1.83	116	90	2012	10
MR-19-21	-9.0	24.5	0.01	0.01	3A	6.40	1.83	124	68	2012	10
MR-19-23	-9.3	24.2	0.02	0.02	3A	6.30	1.83	112	95	2012	11
MR-19-25	-9.3	24.4	0.02	0.02	3A	5.90	1.84	120	76	2012	11
MR-19-26	-9.3	24.2	0.02	0.02	3A	5.70	1.85	118	85	2012	11
MR-19-37	-9.4	24.2	0.02	0.02	3A	2.70	1.93	114	83	2012	11
MR-19-38	-9.8	23.9	0.02	0.02	3A	2.60	1.93	122	95	2012	11
MR-19-39	-8.9	24.4	0.02	0.02	3A	2.50	1.94	110	86	2012	11
MR-19-40	-9.7	23.9	0.02	0.02	3A	2.40	1.94	117	75	2012	11
MR-19-41	-9.0	24.2	0.02	0.02	3A	2.30	1.94	119	80	2012	11
MR-19-42	-8.7	24.3	0.02	0.02	3A	2.20	1.94	120	89	2012	11
MR-19-43	-9.7	24.2	0.02	0.02	3A	2.10	1.95	115	89	2012	11
MR-19-44	-9.0	24.7	0.02	0.02	3A	2.00	1.95	110	100	2012	11

Table Appendix 1 (continued)

Sample ID	$\delta^{13}\text{C}_{\text{PDB}}$ [‰]	$\delta^{18}\text{O}_{\text{SMOW}}$ [‰]	s.e. $\delta^{13}\text{C}$ [‰]	s.e. $\delta^{18}\text{O}$ [‰]	(sub-) Unit	Profile meter	Calculated Age [Ma]	Sample weight [µg]	Carbonate content [%]	Field campaign [year]	Run
MR-19-45	-8.2	24.6	0.02	0.02	3A	1.90	1.95	116	100	2012	11
MR-19-46	-8.7	24.6	0.02	0.02	3A	1.80	1.95	110	80	2012	11
MR-19-47	-8.8	24.5	0.02	0.02	3A	1.70	1.96	122	90	2012	11
MR-19-48	-9.8	24.2	0.02	0.02	3A	1.60	1.96	110	84	2012	11
MR-19-49	-9.4	24.3	0.02	0.02	3A	1.50	1.96	120	82	2012	11
MR-19-50	-10.3	23.7	0.02	0.02	3A	1.40	1.96	118	70	2012	11
MR-19-51	-10.2	24.0	0.02	0.02	3A	1.30	1.97	115	95	2012	11
MR-19-52	-9.1	24.2	0.02	0.02	3A	1.20	1.97	113	85	2012	11
MR-19-53	-8.9	24.3	0.02	0.02	3A	1.10	1.97	119	59	2012	11
MR-19-54	-10.0	23.8	0.02	0.02	3A	1.00	1.98	114	45	2012	11
MR-19-55	-11.0	23.6	0.02	0.02	3A	0.90	1.98	125	88	2012	11
MR-19-56	-10.3	24.0	0.02	0.02	3A	0.50	1.99	112	82	2012	11
MR-19-57	-9.9	23.7	0.02	0.02	3A	0.00	2.00	113	86	2012	11
MR-04-96	-6.6	25.0	0.01	0.02	3A	8.85	2.01	120	67	2011	1
MR-04-95	-7.8	24.7	0.01	0.02	3A	8.55	2.01	116	95	2011	1
MR-04-94	-6.6	24.4	0.01	0.02	3A	8.40	2.02	116	89	2011	1
MR-04-93	-6.4	25.8	0.01	0.02	3A	8.25	2.02	119	45	2011	1
MR-04-92	-7.1	24.6	0.03	0.02	3A	7.90	2.03	118	85	2011	5
MR-04-91	-6.3	25.1	0.01	0.02	3A	7.70	2.04	110	82	2011	1
MR-04-90	-8.0	24.5	0.01	0.02	3A	7.50	2.04	116	80	2011	1
MR-04-89	-7.6	24.5	0.01	0.02	3A	7.20	2.05	116	71	2011	1
MR-04-88	-5.9	24.8	0.01	0.02	3A	7.10	2.05	113	75	2011	1
MR-04-87	-6.2	25.1	0.01	0.02	3A	6.85	2.06	131	79	2011	1
MR-04-86	-7.9	24.7	0.01	0.02	3A	6.75	2.06	120	67	2011	1
MR-04-85	-8.4	24.2	0.01	0.02	3A	6.50	2.07	113	73	2011	1
MR-04-84	-8.6	24.1	0.01	0.02	3A	6.40	2.07	111	99	2011	1
MR-04-83	-7.6	24.6	0.01	0.02	3A	6.20	2.08	111	33	2011	1
MR-04-82	-7.2	25.0	0.01	0.02	3A	5.95	2.09	112	43	2011	1
MR-04-81	-8.0	24.4	0.01	0.02	3A	5.60	2.09	115	65	2011	1
MR-04-80	-8.4	24.5	0.01	0.02	3A	5.40	2.10	111	22	2011	1
MR-04-79	-8.9	24.1	0.03	0.02	3A	5.05	2.11	114	89	2011	5
MR-04-77	-8.1	24.7	0.01	0.02	3A	4.30	2.13	120	54	2011	1
MR-04-76	-8.3	24.6	0.01	0.02	3A	3.80	2.14	111	75	2011	1
MR-04-75	-8.9	24.3	0.01	0.02	3A	3.55	2.15	123	85	2011	1

Table Appendix 1 (continued)

Sample ID	$\delta^{13}\text{C}_{\text{PDB}}$ [‰]	$\delta^{18}\text{O}_{\text{SMOW}}$ [‰]	s.e. $\delta^{13}\text{C}$ [‰]	s.e. $\delta^{18}\text{O}$ [‰]	(sub-) Unit	Profile meter	Calculated Age [Ma]	Sample weight [µg]	Carbonate content [%]	Field campaign [year]	Run
MR-04-74	-9.3	24.2	0.01	0.02	3A	3.10	2.16	110	70	2011	1
MR-04-72	-8.1	24.7	0.01	0.02	3A	2.65	2.30	120	71	2011	1
MR-04-71	-8.2	24.7	0.01	0.02	3A	2.10	2.33	117	39	2011	1
MR-04-70	-8.6	24.1	0.01	0.02	3A	1.60	2.35	120	53	2011	1
U-84-14	-7.8	24.8	0.03	0.02	3A	2.70	2.30	119	82	2011	4
U-84-13	-7.8	24.9	0.03	0.02	3A	2.60	2.31	116	88	2011	4
U-84-12	-10.0	24.3	0.03	0.02	3A	2.30	2.33	110	92	2011	4
U-84-11	-9.7	24.5	0.03	0.02	3A	2.10	2.34	120	95	2011	4
U-84-10	-10.3	24.3	0.03	0.02	3A	1.90	2.36	114	49	2011	4
U-84-09	-9.1	24.5	0.03	0.02	3A	1.70	2.37	117	53	2011	4
U-84-08	-9.3	24.2	0.03	0.02	3A	1.50	2.39	117	23	2011	4
U-84-07	-8.3	24.4	0.03	0.02	3A	1.30	2.40	121	54	2011	4
U-84-06	-8.7	24.3	0.03	0.02	3A	1.10	2.42	114	45	2011	4
U-84-05	-8.5	24.1	0.03	0.02	3A	0.85	2.44	111	48	2011	4
U-84-04	-8.7	24.3	0.03	0.02	3A	0.55	2.46	120	89	2011	4
U-84-03	-8.8	24.0	0.03	0.02	3A	0.40	2.47	114	42	2011	4
U-84-02	-5.9	25.6	0.03	0.02	3A	0.25	2.48	111	56	2011	4
U-84-01	-8.3	24.8	0.03	0.02	3A	0.10	2.49	117	78	2011	4
RC-08-51	-9.5	24.4	0.02	0.03	3A	0.00	2.50	125	92	2012	9
RC-08-50	-9.0	24.5	0.02	0.03	3A	0.05	2.50	112	92	2012	9
RC-08-49	-9.3	24.3	0.02	0.03	3A	0.10	2.49	123	68	2012	9
RC-08-48	-8.2	24.7	0.02	0.03	3A	0.15	2.49	115	87	2012	9
RC-08-47	-7.9	24.4	0.02	0.02	3A	0.20	2.49	112	77	2012	8
RC-08-46	-8.7	24.2	0.02	0.02	3A	0.25	2.48	112	83	2012	8
RC-08-45	-6.6	24.7	0.02	0.02	3A	0.30	2.48	117	98	2012	8
RC-08-44	-9.4	23.8	0.02	0.02	3A	0.35	2.47	121	89	2012	8
RC-08-43	-8.1	24.3	0.02	0.02	3A	0.40	2.47	109	91	2012	8
RC-08-42	-8.2	24.4	0.02	0.02	3A	0.45	2.47	125	95	2012	8
RC-08-41	-9.3	24.0	0.02	0.02	3A	0.50	2.46	120	100	2012	8
RC-08-40	-7.1	24.5	0.02	0.02	3A	0.55	2.46	127	86	2012	8
RC-08-39	-6.8	24.7	0.02	0.02	3A	0.60	2.46	120	99	2012	8
RC-08-36	-7.1	24.4	0.02	0.02	3A	0.75	2.44	113	84	2012	8
RC-08-35	-6.2	24.7	0.02	0.02	3A	0.80	2.44	113	59	2012	8
RC-08-34	-9.4	23.9	0.02	0.02	3A	0.85	2.44	114	90	2012	8

Table Appendix 1 (continued)

Sample ID	$\delta^{13}\text{C}_{\text{PDB}}$ [‰]	$\delta^{18}\text{O}_{\text{SMOW}}$ [‰]	s.e. $\delta^{13}\text{C}$ [‰]	s.e. $\delta^{18}\text{O}$ [‰]	(sub-) Unit	Profile meter	Calculated Age [Ma]	Sample weight [µg]	Carbonate content [%]	Field campaign [year]	Run
RC-08-33	-6.6	24.9	0.02	0.02	3A	0.90	2.43	110	84	2012	8
RC-08-32	-10.0	24.0	0.02	0.02	3A	0.95	2.43	117	88	2012	8
RC-08-31	-6.9	24.7	0.02	0.02	3A	1.25	2.41	109	92	2012	8
RC-08-30	-7.1	24.4	0.02	0.02	3A	1.30	2.40	118	46	2012	8
RC-08-29	-8.0	24.1	0.02	0.02	3A	1.35	2.40	113	83	2012	8
RC-08-28	-10.3	23.9	0.02	0.02	3A	1.40	2.40	113	93	2012	8
RC-08-27	-9.9	24.4	0.02	0.02	3A	1.45	2.39	120	88	2012	8
RC-08-26	-6.6	25.0	0.02	0.02	3A	1.50	2.39	126	86	2012	8
RC-08-24	-7.9	24.4	0.02	0.02	3A	1.60	2.38	125	74	2012	8
RC-08-23	-6.9	24.4	0.02	0.02	3A	1.65	2.38	118	79	2012	8
RC-08-22	-9.4	23.9	0.02	0.02	3A	1.70	2.37	112	81	2012	8
RC-08-20	-9.2	23.9	0.02	0.02	3A	1.80	2.37	118	61	2012	8
RC-08-19	-9.0	24.1	0.02	0.02	3A	1.85	2.36	124	81	2012	8
RC-08-18	-7.7	24.2	0.02	0.02	3A	1.90	2.36	109	83	2012	8
RC-08-17	-7.3	24.8	0.02	0.02	3A	1.95	2.36	126	97	2012	8
RC-08-16	-8.0	24.3	0.02	0.02	3A	2.00	2.35	122	66	2012	8
RC-08-15	-8.8	24.0	0.02	0.02	3A	2.05	2.35	115	91	2012	8
RC-08-14	-9.4	23.8	0.02	0.02	3A	2.10	2.34	123	92	2012	8
RC-08-13	-9.9	23.6	0.02	0.02	3A	2.15	2.34	110	94	2012	8
RC-08-12	-7.6	24.5	0.02	0.03	3A	2.20	2.34	121	91	2012	9
RC-08-11	-7.7	24.3	0.02	0.02	3A	2.25	2.33	124	98	2012	8
RC-08-10	-7.6	24.5	0.02	0.02	3A	2.30	2.33	110	88	2012	8
RC-08-09	-7.8	24.3	0.02	0.02	3A	2.35	2.33	110	86	2012	8
RC-08-08	-7.7	24.4	0.02	0.02	3A	2.40	2.32	116	84	2012	8
RC-08-07	-7.4	24.8	0.02	0.02	3A	2.45	2.32	113	92	2012	8
RC-08-06	-7.6	24.5	0.02	0.02	3A	2.50	2.31	111	71	2012	8
RC-08-05	-9.1	24.2	0.02	0.02	3A	2.55	2.31	114	92	2012	8
RC-08-04	-7.4	24.7	0.02	0.02	3A	2.60	2.31	118	75	2012	8
RC-08-03	-9.1	24.0	0.02	0.02	3A	2.65	2.30	109	85	2012	8
RC-08-02	-7.2	24.4	0.02	0.02	3A	2.68	2.30	127	91	2012	8
RC-08-01	-7.4	24.5	0.02	0.02	3A	2.70	2.30	113	86	2012	8
MR-06-01	-6.7	24.6	0.02	0.03	3A	1.90	2.42	191	23	2012	9
MR-06-02	-7.3	23.9	0.02	0.03	3A	1.60	2.44	186	34	2012	9
MR-06-04	-8.2	25.0	0.02	0.03	3A	1.00	2.46	112	92	2012	9

Table Appendix 1 (continued)

Sample ID	$\delta^{13}\text{C}_{\text{PDB}}$ [‰]	$\delta^{18}\text{O}_{\text{SMOW}}$ [‰]	s.e. $\delta^{13}\text{C}$ [‰]	s.e. $\delta^{18}\text{O}$ [‰]	(sub-) Unit	Profile meter	Calculated Age [Ma]	Sample weight [µg]	Carbonate content [%]	Field campaign [year]	Run
MR-06-05	-8.2	25.8	0.02	0.03	3A	0.60	2.48	110	85	2012	9
MR-06-06	-5.8	24.8	0.02	0.03	3A	0.30	2.49	110	95	2012	9
MR-06-07	-7.6	25.0	0.02	0.02	3A	0.00	2.30	118	90	2012	11
MR-50-29	-8.5	24.7	0.01	0.03	2	9.25	2.95	113	91	2011	2
MR-50-28	-9.2	22.9	0.01	0.03	2	9.75	2.97	109	86	2011	2
MR-50-26	-9.8	23.9	0.01	0.03	2	8.85	2.97	116	95	2011	2
MR-50-25	-9.1	24.2	0.01	0.03	2	8.50	2.98	112	95	2011	2
MR-50-24	-8.7	23.6	0.01	0.03	2	8.20	2.99	119	34	2011	2
MR-50-23	-9.0	23.7	0.01	0.03	2	7.90	3.00	120	79	2011	2
MR-50-17	-9.9	23.9	0.01	0.03	2	4.70	3.07	117	37	2011	2
MR-50-15	-9.4	23.1	0.01	0.03	2	4.10	3.08	113	66	2011	2
MR-50-14	-10.0	23.6	0.02	0.01	2	3.80	3.09	110	62	2011	3
MR-50-13	-10.2	23.1	0.02	0.01	2	3.50	3.09	110	67	2011	3
MR-50-12	-8.6	23.2	0.02	0.01	2	3.30	3.10	113	33	2011	3
MR-50-11	-9.1	23.1	0.02	0.01	2	2.90	3.11	120	54	2011	3
MR-50-10	-9.6	23.3	0.02	0.01	2	2.75	3.11	111	69	2011	3
MR-50-09	-9.0	23.3	0.02	0.01	2	2.55	3.12	112	44	2011	3
MR-50-08	-9.7	23.4	0.02	0.01	2	1.30	3.14	110	76	2011	3
MR-50-07	-9.8	23.2	0.02	0.01	2	1.90	3.13	115	72	2011	3
MR-50-04	-10.3	23.4	0.02	0.01	2	1.10	3.15	110	89	2011	3
MR-50-03	-10.3	23.6	0.02	0.01	2	0.80	3.16	113	62	2011	3
MR-50-02	-10.0	23.1	0.02	0.01	2	0.40	3.16	112	76	2011	3
MR-50-01	-10.2	23.4	0.02	0.01	2	0.10	3.17	110	73	2011	3
MR-58-31	-9.9	24.0	0.01	0.01	2	12.15	3.48	110	40	2012	10
MR-58-30	-9.5	24.1	0.01	0.01	2	12.05	3.48	119	65	2012	10
MR-58-29	-8.9	23.8	0.01	0.01	2	11.50	3.49	118	50	2012	10
MR-58-28	-9.8	25.5	0.01	0.01	2	11.00	3.50	124	90	2012	10
MR-58-27	-9.3	23.2	0.01	0.01	2	9.95	3.53	121	87	2012	10
MR-58-26	-10.1	24.5	0.01	0.01	2	9.85	3.53	113	80	2012	10
MR-58-25	-10.2	24.7	0.01	0.01	2	9.50	3.54	112	80	2012	10
MR-58-24	-9.9	23.3	0.01	0.01	2	9.10	3.55	115	85	2012	10
MR-58-23	-9.3	23.2	0.01	0.01	2	8.90	3.55	124	77	2012	10
MR-58-22	-9.5	23.3	0.01	0.01	2	8.70	3.55	116	82	2012	10
MR-58-21	-10.2	23.3	0.01	0.01	2	8.50	3.56	122	87	2012	10

Table Appendix 1 (continued)

Sample ID	$\delta^{13}\text{C}_{\text{PDB}}$ [‰]	$\delta^{18}\text{O}_{\text{SMOW}}$ [‰]	s.e. $\delta^{13}\text{C}$ [‰]	s.e. $\delta^{18}\text{O}$ [‰]	(sub-) Unit	Profile meter	Calculated Age [Ma]	Sample weight [µg]	Carbonate content [%]	Field campaign [year]	Run
MR-58-20	-9.7	23.4	0.01	0.01	2	8.20	3.57	117	82	2012	10
MR-58-19	-10.6	25.5	0.01	0.01	2	7.40	3.58	125	94	2012	10
MR-58-18	-10.5	25.1	0.01	0.01	2	6.90	3.59	116	89	2012	10
MR-58-17	-10.9	25.1	0.01	0.01	2	6.40	3.61	116	84	2012	10
MR-58-16	-11.2	25.0	0.01	0.01	2	5.60	3.62	124	73	2012	10
MR-58-15	-10.1	23.2	0.01	0.01	2	4.60	3.65	113	93	2012	10
MR-58-14	-11.1	24.7	0.01	0.01	2	4.39	3.65	117	85	2012	10
MR-58-13	-10.8	24.1	0.01	0.01	2	4.20	3.66	125	75	2012	10
MR-58-12	-10.8	23.0	0.01	0.01	2	4.00	3.66	118	79	2012	10
MR-58-11	-10.7	23.9	0.01	0.01	2	3.80	3.66	118	78	2012	10
MR-58-10	-10.6	24.0	0.02	0.03	2	3.60	3.67	110	73	2012	9
MR-58-09	-10.9	23.1	0.02	0.03	2	3.20	3.68	119	85	2012	9
MR-58-08	-10.7	24.3	0.02	0.03	2	2.80	3.69	117	86	2012	9
MR-58-07	-11.1	24.4	0.02	0.02	2	2.40	3.70	112	98	2012	11
MR-58-06	-10.6	24.1	0.02	0.03	2	2.10	3.70	126	73	2012	9
MR-58-05	-10.6	23.8	0.02	0.03	2	1.90	3.71	117	88	2012	9
MR-58-04	-11.0	23.7	0.02	0.03	2	1.35	3.72	114	93	2012	9
MR-58-03	-10.4	24.0	0.02	0.03	2	1.20	3.72	124	77	2012	9
MR-58-02	-10.4	23.7	0.02	0.03	2	1.05	3.73	115	57	2012	9
MR-58-01	-10.7	24.5	0.02	0.03	2	0.40	3.74	124	80	2012	9
MR-115-12	-10.4	24.2	0.02	0.02	2	4.00	3.33	24	51	2013	24
MR-115-11	-10.2	23.8	0.02	0.02	2	3.70	3.32	24	74	2013	24
MR-115-10	-9.6	24.4	0.02	0.02	2	3.50	3.31	24	89	2013	24
MR-115-09	-9.4	24.3	0.02	0.02	2	2.00	3.30	24	32	2013	24
MR-115-08	-9.8	24.3	0.02	0.02	2	1.40	3.30	24	79	2013	24
MR-115-07	-10.0	24.1	0.02	0.02	2	1.30	3.29	24	48	2013	24
MR-115-06	-9.8	23.9	0.02	0.02	2	1.10	3.28	24	49	2013	24
MR-115-05	-9.7	23.5	0.02	0.02	2	1.00	3.27	24	72	2013	24
MR-115-04	-10.1	24.1	0.02	0.02	2	0.90	3.26	24	76	2013	24
MR-115-03	-10.2	23.4	0.02	0.02	2	0.80	3.25	24	65	2013	24
MR-115-02	-9.5	24.0	0.02	0.02	2	0.40	3.24	24	67	2013	24
MR-115-01	-10.1	23.9	0.02	0.02	2	0.00	3.23	24	46	2013	24
MR-117-12	-10.0	23.4	0.02	0.02	2	5.50	3.46	24	63	2013	24
MR-117-11	-10.1	23.2	0.02	0.02	2	5.00	3.45	24	44	2013	24

Table Appendix 1 (continued)

Sample ID	$\delta^{13}\text{C}_{\text{PDB}}$ [‰]	$\delta^{18}\text{O}_{\text{SMOW}}$ [‰]	s.e. $\delta^{13}\text{C}$ [‰]	s.e. $\delta^{18}\text{O}$ [‰]	(sub-) Unit	Profile meter	Calculated Age [Ma]	Sample weight [μg]	Carbonate content [%]	Field campaign [year]	Run
MR-117-10	-10.2	23.4	0.02	0.02	2	4.50	3.44	24	56	2013	24
MR-117-09	-8.8	24.3	0.02	0.02	2	4.00	3.44	24	36	2013	24
MR-117-07	-9.7	23.8	0.02	0.02	2	3.00	3.42	24	33	2013	24
MR-117-05	-9.6	24.1	0.02	0.02	2	2.00	3.41	24	74	2013	24
MR-117-03	-9.5	23.7	0.02	0.02	2	1.00	3.40	24	73	2013	24
MR-117-02	-9.5	24.2	0.02	0.02	2	0.50	3.39	24	87	2013	24
MR-117-01	-9.1	23.9	0.02	0.02	2	0.00	3.38	24	88	2013	24
WK-106-71	-8.4	23.2	0.02	0.02	2	33.80	2.81	24	61	2013	24
WK-106-68	-9.0	23.6	0.02	0.02	2	31.50	2.86	24	90	2013	24
WK-106-67	-9.1	23.4	0.02	0.02	2	30.60	2.88	24	46	2013	24
WK-106-66	-8.4	23.1	0.02	0.02	2	30.40	2.89	24	49	2013	24
WK-106-65	-9.3	23.0	0.02	0.02	2	30.20	2.89	24	55	2013	24
WK-106-64	-9.4	23.9	0.02	0.02	2	29.80	2.90	24	56	2013	24
WK-106-63	-8.9	22.3	0.02	0.02	2	29.70	2.90	24	63	2013	24
WK-106-60	-8.8	23.7	0.02	0.02	2	25.40	3.00	24	43	2013	24
WK-106-59	-8.5	24.7	0.02	0.02	2	25.30	3.00	24	81	2013	24
WK-106-58	-9.5	23.5	0.02	0.02	2	24.80	3.01	24	30	2013	24
WK-106-57	-9.5	24.1	0.02	0.02	2	24.50	3.02	24	61	2013	24
WK-106-56	-9.7	23.4	0.02	0.02	2	23.70	3.04	24	60	2013	24
WK-106-54	-9.4	23.5	0.02	0.02	2	21.40	3.09	24	72	2013	24
WK-106-53	-9.9	22.6	0.02	0.02	2	20.80	3.10	24	56	2013	24
WK-106-52	-10.8	24.9	0.01	0.01	2	20.00	3.12	23	81	2013	23
WK-106-51	-10.9	24.6	0.01	0.01	2	19.60	3.13	23	100	2013	23
WK-106-50	-9.8	22.4	0.01	0.01	2	18.40	3.16	23	72	2013	23
WK-106-47	-10.0	22.6	0.01	0.01	2	17.20	3.18	23	50	2013	23
WK-106-43	-10.1	22.1	0.01	0.01	2	16.40	3.20	23	39	2013	23
WK-106-41	-9.7	22.4	0.01	0.01	2	16.20	3.21	23	74	2013	23
WK-106-40	-8.1	24.0	0.01	0.01	2	16.10	3.21	23	79	2013	23
WK-106-37	-9.2	23.2	0.01	0.01	2	13.05	3.28	23	77	2013	23
WK-106-36	-9.8	22.1	0.01	0.01	2	12.90	3.28	23	31	2013	23
WK-106-35	-10.7	23.6	0.01	0.01	2	12.70	3.28	23	72	2013	23
WK-106-34	-9.7	22.3	0.01	0.01	2	12.50	3.29	23	41	2013	23
WK-106-33	-9.6	22.3	0.01	0.02	2	12.20	3.30	25	24	2013	25
WK-106-32	-10.3	22.7	0.01	0.01	2	11.80	3.30	23	89	2013	23

Table Appendix 1 (continued)

Sample ID	$\delta^{13}\text{C}_{\text{PDB}}$ [‰]	$\delta^{18}\text{O}_{\text{SMOW}}$ [‰]	s.e. $\delta^{13}\text{C}$ [‰]	s.e. $\delta^{18}\text{O}$ [‰]	(sub-) Unit	Profile meter	Calculated Age [Ma]	Sample weight [μg]	Carbonate content [%]	Field campaign [year]	Run
WK-106-31	-9.7	22.2	0.01	0.01	2	11.40	3.31	23	36	2013	23
WK-106-30	-9.7	22.4	0.01	0.01	2	11.10	3.32	23	42	2013	23
WK-106-29	-9.5	22.3	0.01	0.01	2	10.90	3.32	23	95	2013	23
WK-106-28	-9.8	22.0	0.01	0.01	2	10.75	3.33	23	88	2013	23
WK-106-27	-8.1	23.7	0.01	0.02	2	10.50	3.33	25	22	2013	25
WK-106-26	-8.8	22.8	0.01	0.01	2	10.50	3.33	23	84	2013	23
WK-106-25	-8.9	23.1	0.01	0.01	2	10.20	3.34	23	88	2013	23
WK-106-23	-8.7	23.4	0.01	0.01	2	9.70	3.35	23	29	2013	23
WK-106-22	-9.6	22.7	0.01	0.02	2	9.30	3.36	25	6	2013	25
WK-106-21	-9.4	22.1	0.01	0.01	2	9.00	3.37	23	78	2013	23
WK-106-20	-9.7	22.1	0.01	0.01	2	8.90	3.37	23	85	2013	23
WK-106-19	-10.2	22.0	0.01	0.01	2	8.80	3.37	23	100	2013	23
WK-106-18	-9.6	22.2	0.03	0.02	2	8.00	3.39	27	20	2013	27
WK-106-17	-10.0	22.1	0.01	0.01	2	8.10	3.39	23	39	2013	23
WK-106-16	-9.6	22.5	0.01	0.01	2	7.90	3.39	23	66	2013	23
WK-106-15	-9.8	22.5	0.01	0.01	2	7.50	3.40	23	99	2013	23
WK-106-14	-9.7	22.4	0.01	0.01	2	6.30	3.43	23	91	2013	23
WK-106-13	-10.1	22.1	0.01	0.01	2	5.50	3.45	23	96	2013	23
WK-106-12	-10.1	22.9	0.01	0.01	2	5.00	3.46	23	75	2013	23
WK-106-11	-9.1	22.8	0.01	0.01	2	3.80	3.48	23	65	2013	23
WK-106-10	-9.3	22.5	0.01	0.01	2	3.80	3.48	23	48	2013	23
WK-106-03	-10.4	24.2	0.01	0.01	2	1.10	3.55	23	88	2013	23
WK-106-02	-10.4	24.5	0.01	0.01	2	0.50	3.56	23	60	2013	23
WK-106-01	-10.5	24.0	0.01	0.01	2	0.10	3.57	23	53	2013	23
U-99-23	-10.0	24.0	0.03	0.02	1	24.00	3.75	121	71	2011	4
U-99-21	-9.4	24.2	0.03	0.02	1	22.00	3.78	120	87	2011	4
U-99-20	-9.4	24.4	0.03	0.02	1	19.00	3.83	120	86	2011	4
U-99-15	-9.3	24.1	0.03	0.02	1	14.00	3.92	113	76	2011	5
U-99-14	-8.7	23.8	0.03	0.02	1	13.00	3.93	120	57	2011	5
U-99-13	-9.3	23.8	0.03	0.02	1	12.00	3.95	111	84	2011	5
U-99-12	-9.6	23.7	0.03	0.02	1	11.00	3.97	112	97	2011	5
U-99-11	-10.5	23.6	0.03	0.02	1	10.00	3.98	112	74	2011	5
U-99-09	-10.0	24.2	0.03	0.02	1	8.00	4.02	114	74	2011	5
U-99-08	-10.4	24.0	0.03	0.02	1	7.00	4.03	115	79	2011	5
U-99-03	-9.5	24.5	0.03	0.02	1	2.00	4.11	116	71	2011	5

Table Appendix 1 (continued)

Sample ID	$\delta^{13}\text{C}_{\text{PDB}}$ [‰]	$\delta^{18}\text{O}_{\text{SMOW}}$ [‰]	s.e. $\delta^{13}\text{C}$ [‰]	s.e. $\delta^{18}\text{O}$ [‰]	(sub-) Unit	Profile meter	Calculated Age [Ma]	Sample weight [μg]	Carbonate content [%]	Field campaign [year]	Run
U-86-18	-10.1	24.7	0.03	0.02	1	9.20	4.15	119	59	2011	4
U-86-17	-10.1	23.5	0.03	0.02	1	8.70	4.16	111	56	2011	4
U-86-15	-8.4	24.8	0.03	0.02	1	7.75	4.17	115	99	2011	4
U-86-14	-9.1	24.7	0.03	0.02	1	7.35	4.18	117	85	2011	4
U-86-13	-9.4	24.1	0.03	0.02	1	6.80	4.19	112	71	2011	4
U-86-12	-10.0	23.7	0.03	0.02	1	6.00	4.20	116	88	2011	4
U-86-11	-9.7	24.3	0.03	0.02	1	4.80	4.22	118	77	2011	4
U-86-10	-9.5	23.9	0.03	0.02	1	3.90	4.24	112	66	2011	4
U-86-09	-9.9	24.7	0.03	0.02	1	3.70	4.24	117	35	2011	4
U-86-08	-8.1	24.6	0.03	0.02	1	3.50	4.24	113	80	2011	4
U-86-07	-8.8	22.8	0.03	0.02	1	3.00	4.25	117	98	2011	4
U-86-05	-8.5	23.7	0.03	0.02	1	1.20	4.28	112	98	2011	4
U-86-04	-9.9	23.6	0.03	0.02	1	1.00	4.28	121	80	2011	4
U-86-03	-10.4	23.6	0.03	0.02	1	0.80	4.29	115	65	2011	4
U-86-02	-9.6	23.6	0.03	0.02	1	0.60	4.29	115	77	2011	4
U-86-01	-10.6	25.1	0.03	0.02	1	0.15	4.30	118	62	2011	4

Table Appendix 2: List of all herbivore enamel samples with ID (first number = Hominid Corridor Research Project ID, second number = individual sample ID), taxa, stable carbon and oxygen isotope values with standard error (s.e.), first and last appearance date, locality, body-part, sample weight, carbonate content, and number of run for the analysis.

HCRP Sample ID	Taxa	$\delta^{13}\text{C}_{\text{PDB}}$ [‰]	$\delta^{18}\text{O}_{\text{SMOW}}$ [‰]	s.e. $\delta^{13}\text{C}$ [‰]	s.e. $\delta^{18}\text{O}$ [‰]	FAD [Ma]	LAD [Ma]	Locality	Tooth	Weight [μg]	Carb. content [%]	Run
187-01	Bovidae Alc. Damaliscus sp.	-6.4	24.1	0.02	0.03	3.75	1.8	WK11	IM3	930	4	36
187-02	Bovidae Alc. Damaliscus sp.	-5.4	24.9	0.02	0.03	3.75	1.8	WK11	IM3	848	4	36
187-03	Bovidae Alc. Damaliscus sp.	-4.3	26.1	0.02	0.02	3.75	1.8	WK11	IM3	714	5	37
187-04	Bovidae Alc. Damaliscus sp.	-5.9	25.3	0.02	0.02	3.75	1.8	WK11	IM3	736	5	37
187-05	Bovidae Alc. Damaliscus sp.	-6.0	24.9	0.02	0.03	3.75	1.8	WK11	IM3	941	4	36
187-06	Bovidae Alc. Damaliscus sp.	-6.8	24.8	0.02	0.02	3.75	1.8	WK11	IM3	1009	4	37
187-07	Bovidae Alc. Damaliscus sp.	-7.6	23.9	0.02	0.02	3.75	1.8	WK11	IM3	483	8	38
187-08	Bovidae Alc. Damaliscus sp.	-4.7	24.7	0.02	0.03	3.75	1.8	WK11	IM3	729	5	36
361-02	Bovidae Alc. Megalotragus sp.	-4.3	26.1	0.02	0.03	1.8	0.6	U11	IM	825	4	36
361-03	Bovidae Alc. Megalotragus sp.	-2.0	26.7	0.02	0.02	1.8	0.6	U11	IM	828	4	37
361-04	Bovidae Alc. Megalotragus sp.	-2.8	25.9	0.02	0.03	1.8	0.6	U11	IM	894	4	36
361-06	Bovidae Alc. Megalotragus sp.	-4.7	24.7	0.02	0.03	1.8	0.6	U11	IM	896	4	36
361-07	Bovidae Alc. Megalotragus sp.	-2.9	26.4	0.02	0.03	1.8	0.6	U11	IM	808	4	36
361-08	Bovidae Alc. Megalotragus sp.	-4.6	26.8	0.02	0.03	1.8	0.6	U11	IM	989	4	36
361-08	Bovidae Alc. Megalotragus sp.	-3.4	25.4	0.02	0.03	1.8	0.6	U11	IM	853	4	36
419-01	Bovidae Alc. Megalotragus sp.	-1.9	24.2	0.02	0.03	1.8	0.6	U21	LIM3	950	4	36
419-02	Bovidae Alc. Megalotragus sp.	-1.6	24.3	0.02	0.03	1.8	0.6	U21	LIM4	765	5	36
419-03	Bovidae Alc. Megalotragus sp.	-2.1	24.8	0.02	0.03	1.8	0.6	U21	LIM5	977	4	36
419-04	Bovidae Alc. Megalotragus sp.	-4.1	24.5	0.02	0.03	1.8	0.6	U21	LIM6	784	5	36
373-01	Bovidae Alc. Megalotragus sp.	0.5	28.0	0.01	0.02	2.8	1.8	U13	u M	1201	2	21
373-02	Bovidae Alc. Megalotragus sp.	0.1	28.1	0.01	0.02	2.8	1.8	U13	u M	916	2	21
373-03	Bovidae Alc. Megalotragus sp.	0.5	28.3	0.01	0.02	2.8	1.8	U13	u M	962	2	21
373-04	Bovidae Alc. Megalotragus sp.	0.5	27.5	0.02	0.01	2.8	1.8	U13	u M	1236	2	20
154-01	Bovidae Alc. Connochaetes	1.5	25.8	0.01	0.02	2.8	1.8	RC1	Lu M3	976	2	21
154-02	Bovidae Alc. Connochaetes	1.6	25.4	0.01	0.02	2.8	1.8	RC1	Lu M3	1029	2	22
154-03	Bovidae Alc. Connochaetes	1.5	25.8	0.01	0.02	2.8	1.8	RC1	Lu M3	926	2	22
154-04	Bovidae Alc. Connochaetes	1.4	25.5	0.01	0.02	2.8	1.8	RC1	Lu M3	944	2	21
154-05	Bovidae Alc. Connochaetes	1.4	25.4	0.01	0.02	2.8	1.8	RC1	Lu M3	1206	2	22
154-06	Bovidae Alc. Connochaetes	1.1	25.2	0.01	0.02	2.8	1.8	RC1	Lu M3	1026	2	21

Table Appendix 2 (continued)

HCRP Sample ID	Taxa	$\delta^{13}\text{C}_{\text{PDB}}$ [‰]	$\delta^{18}\text{O}_{\text{SMOW}}$ [‰]	s.e. $\delta^{13}\text{C}$ [‰]	s.e. $\delta^{18}\text{O}$ [‰]	FAD [Ma]	LAD [Ma]	Locality	Tooth	Weight [μg]	Carb. content [%]	Run
154-07	Bovidae Alc. Connochaetes	1.1	25.1	0.01	0.02	2.8	1.8	RC1	Lu M3	1130	2	22
154-08	Bovidae Alc. Connochaetes	0.8	25.2	0.01	0.02	2.8	1.8	RC1	Lu M3	1086	2	21
154-09	Bovidae Alc. Connochaetes	0.3	25.6	0.01	0.02	2.8	1.8	RC1	Lu M3	992	2	22
154-10	Bovidae Alc. Connochaetes	0.1	25.8	0.01	0.02	2.8	1.8	RC1	Lu M3	960	2	22
154-11	Bovidae Alc. Connochaetes	-0.1	25.8	0.01	0.02	2.8	1.8	RC1	Lu M3	1150	2	22
154-12	Bovidae Alc. Connochaetes	0.0	25.8	0.01	0.02	2.8	1.8	RC1	Lu M3	1044	2	21
154-13	Bovidae Alc. Connochaetes	-0.3	26.1	0.01	0.02	2.8	1.8	RC1	Lu M3	1005	2	21
154-14	Bovidae Alc. Connochaetes	-0.4	26.3	0.01	0.02	2.8	1.8	RC1	Lu M3	1022	2	21
154-15	Bovidae Alc. Connochaetes	-0.3	26.3	0.01	0.02	2.8	1.8	RC1	Lu M3	1033	2	21
154-16	Bovidae Alc. Connochaetes	-0.1	26.8	0.01	0.02	2.8	1.8	RC1	Lu M3	964	2	22
154-17	Bovidae Alc. Connochaetes	-0.2	26.9	0.01	0.02	2.8	1.8	RC1	Lu M3	912	2	21
154-18	Bovidae Alc. Connochaetes	0.1	27.4	0.01	0.02	2.8	1.8	RC1	Lu M3	907	2	22
154-19	Bovidae Alc. Connochaetes	-0.1	27.7	0.01	0.02	2.8	1.8	RC1	Lu M3	1009	2	21
154-20	Bovidae Alc. Connochaetes	0.2	28.2	0.01	0.02	2.8	1.8	RC1	Lu M3	901	2	21
154-21	Bovidae Alc. Connochaetes	0.3	28.3	0.01	0.02	2.8	1.8	RC1	Lu M3	907	2	22
348-01	Bovidae Hippotraginae gen. & sp.	-6.2	25.1	0.02	0.03	4.3	3.75	U6	u M	745	5	36
348-02	Bovidae Hippotraginae gen. & sp.	-6.4	25.1	0.02	0.03	4.3	3.75	U6	u M	778	5	36
348-03	Bovidae Hippotraginae gen. & sp.	-5.9	24.4	0.02	0.03	4.3	3.75	U6	u M	842	4	36
547-01	Bovidae Antilopinae gen. & sp. indet.	-8.9	26.5	0.02	0.03	4.3	3.75	WK38	l M frag.	857	4	36
547-02	Bovidae Antilopinae gen. & sp. indet.	-9.4	27.3	0.02	0.03	4.3	3.75	WK38	l M frag.	788	5	36
547-03	Bovidae Antilopinae gen. & sp. indet.	-10.7	28.6	0.02	0.03	4.3	3.75	WK38	l M frag.	872	4	36
547-04	Bovidae Antilopinae gen. & sp. indet.	-10.5	29.6	0.02	0.02	4.3	3.75	WK38	l M frag.	716	5	37
547-05	Bovidae Antilopinae gen. & sp. indet.	-10.0	30.0	0.02	0.03	4.3	3.75	WK38	l M frag.	844	4	36
1173-01	Equidae Eurygnathohippus sp.	-7.4	24.9	0.02	0.04	4.3	3.75	MR/RC	l left M	1000	3	34
1173-02	Equidae Eurygnathohippus sp.	-6.7	25.1	0.02	0.04	4.3	3.75	MR/RC	l left M	1279	3	34
1173-03	Equidae Eurygnathohippus sp.	-7.9	24.6	0.02	0.04	4.3	3.75	MR/RC	l left M	1141	3	34
1173-04	Equidae Eurygnathohippus sp.	-8.0	24.5	0.02	0.04	4.3	3.75	MR/RC	l left M	1222	3	34
1173-05	Equidae Eurygnathohippus sp.	-7.6	24.6	0.02	0.04	4.3	3.75	MR/RC	l left M	1123	3	34
1173-06	Equidae Eurygnathohippus sp.	-6.7	24.6	0.02	0.04	4.3	3.75	MR/RC	l left M	1075	3	34
1173-07	Equidae Eurygnathohippus sp.	-5.9	24.6	0.02	0.04	4.3	3.75	MR/RC	l left M	1057	3	34
1173-08	Equidae Eurygnathohippus sp.	-7.7	23.6	0.02	0.04	4.3	3.75	MR/RC	l left M	1041	3	34

Table Appendix 2 (continued)

HCRP Sample ID	Taxa	$\delta^{13}\text{C}_{\text{PDB}}$ [‰]	$\delta^{18}\text{O}_{\text{SMOW}}$ [‰]	s.e. $\delta^{13}\text{C}$ [‰]	s.e. $\delta^{18}\text{O}$ [‰]	FAD [Ma]	LAD [Ma]	Locality	Tooth	Weight [μg]	Carb. content [%]	Run
1173-09	Equidae Eurygnathohippus sp.	-8.5	24.0	0.02	0.04	4.3	3.75	MR/RC	L I left M	1168	3	34
1173-10	Equidae Eurygnathohippus sp.	-7.8	24.2	0.02	0.04	4.3	3.75	MR/RC	L I left M	1339	3	34
1173-11	Equidae Eurygnathohippus sp.	-7.5	24.7	0.02	0.04	4.3	3.75	MR/RC	L I left M	506	7	34
1173-12	Equidae Eurygnathohippus sp.	-6.8	25.0	0.02	0.04	4.3	3.75	MR/RC	L I left M	1119	3	34
600-01	Equidae Eurygnathohippus sp.	-0.8	26.4	0.01	0.02	2.8	1.8	WK	PreM	859	2	21
600-02	Equidae Eurygnathohippus sp.	-0.9	25.5	0.02	0.01	2.8	1.8	WK	PreM	886	2	20
600-03	Equidae Eurygnathohippus sp.	-1.1	24.8	0.01	0.02	2.8	1.8	WK	PreM	1011	2	21
351-01	Equidae Eurygnathohippus sp.	-3.1	25.8	0.02	0.02	4.3	3.75	U8	R I M1	660	6	37
351-02	Equidae Eurygnathohippus sp.	-2.8	26.6	0.02	0.03	4.3	3.75	U8	R I M2	974	4	36
351-03	Equidae Eurygnathohippus sp.	-3.7	26.2	0.02	0.03	4.3	3.75	U8	R I M3	1010	4	36
351-04	Equidae Eurygnathohippus sp.	-3.7	26.1	0.02	0.03	4.3	3.75	U8	R I M4	751	5	36
351-05	Equidae Eurygnathohippus sp.	-2.3	26.1	0.02	0.03	4.3	3.75	U8	R I M5	906	4	36
351-06	Equidae Eurygnathohippus sp.	-3.8	24.0	0.02	0.02	4.3	3.75	U8	R I M6	787	5	37
351-07	Equidae Eurygnathohippus sp.	-3.4	23.8	0.02	0.02	4.3	3.75	U8	R I M7	941	4	37
351-08	Equidae Eurygnathohippus sp.	-3.4	24.3	0.02	0.03	4.3	3.75	U8	R I M8	913	4	36
351-09	Equidae Eurygnathohippus sp.	-3.4	25.8	0.02	0.02	4.3	3.75	U8	R I M9	780	5	37
357-01	Equidae Eurygnathohippus sp.	-3.6	26.7	0.02	0.03	4.3	3.75	U8	R u M1 frag	754	5	36
357-02	Equidae Eurygnathohippus sp.	-4.8	26.4	0.02	0.02	4.3	3.75	U8	R u M1 frag	783	5	37
357-03	Equidae Eurygnathohippus sp.	-2.8	28.1	0.02	0.02	4.3	3.75	U8	R u M1 frag	809	5	37
357-04	Equidae Eurygnathohippus sp.	-3.0	27.8	0.02	0.03	4.3	3.75	U8	R u M1 frag	756	5	36
357-05	Equidae Eurygnathohippus sp.	-4.4	26.7	0.02	0.03	4.3	3.75	U8	R u M1 frag	865	4	36
357-06	Equidae Eurygnathohippus sp.	-4.6	26.5	0.02	0.03	4.3	3.75	U8	R u M1 frag	979	4	36
357-07	Equidae Eurygnathohippus sp.	-3.3	27.5	0.02	0.03	4.3	3.75	U8	R u M1 frag	874	4	36
357-08	Equidae Eurygnathohippus sp.	-0.7	30.2	0.02	0.03	4.3	3.75	U8	R u M1 frag	770	5	36
357-09	Equidae Eurygnathohippus sp.	-1.5	28.8	0.02	0.03	4.3	3.75	U8	R u M1 frag	816	4	36
357-10	Equidae Eurygnathohippus sp.	-3.6	27.7	0.02	0.03	4.3	3.75	U8	R u M1 frag	1016	4	36
357-11	Equidae Eurygnathohippus sp.	-7.6	24.4	0.02	0.02	4.3	3.75	U8	R u M1 frag	502	7	37
357-12	Equidae Eurygnathohippus sp.	-2.8	28.0	0.02	0.03	4.3	3.75	U8	R u M1 frag	1018	4	36
357-13	Equidae Eurygnathohippus sp.	-3.7	27.9	0.02	0.02	4.3	3.75	U8	R u M1 frag	683	5	37
357-14	Equidae Eurygnathohippus sp.	-8.0	23.4	0.02	0.02	4.3	3.75	U8	R u M1 frag	556	7	37
357-15	Equidae Eurygnathohippus sp.	-4.9	26.6	0.02	0.02	4.3	3.75	U8	R u M1 frag	563	7	37

Table Appendix 2 (continued)

HCRP Sample ID	Taxa	$\delta^{13}\text{C}_{\text{PDB}}$ [‰]	$\delta^{18}\text{O}_{\text{SMOW}}$ [‰]	s.e. $\delta^{13}\text{C}$ [‰]	s.e. $\delta^{18}\text{O}$ [‰]	FAD [Ma]	LAD [Ma]	Locality	Tooth	Weight [μg]	Carb. content [%]	Run
357-16	Equidae	-5.4	26.0	0.02	0.03	4.3	3.75	U8	R u M1 frag	877	4	36
1175-01	Elephantidae	-6.0	23.5	0.02	0.04	2.8	1.8	U	?	1125	3	34
1175-02	Elephantidae	-5.4	23.3	0.02	0.04	2.8	1.8	U	?	1121	3	34
1175-03	Elephantidae	-5.5	23.6	0.02	0.04	2.8	1.8	U	?	1155	3	34
1175-04	Elephantidae	-6.4	23.0	0.02	0.04	2.8	1.8	U	?	1097	3	34
1175-05	Elephantidae	-6.5	22.4	0.02	0.04	2.8	1.8	U	?	1106	3	34
1175-06	Elephantidae	-5.1	23.4	0.02	0.04	2.8	1.8	U	?	1312	3	34
1175-07	Elephantidae	-5.5	23.4	0.02	0.04	2.8	1.8	U	?	1337	3	34
1175-08	Elephantidae	-5.6	23.5	0.02	0.04	2.8	1.8	U	?	1202	3	34
1175-09	Elephantidae	-6.4	23.2	0.02	0.04	2.8	1.8	U	?	1264	3	34
1174-01	Hippopotamidae	-6.4	24.40	0.02	0.04	2.8	1.8	WK	u l1 or l2 frg	1374	2	34
1174-02	Hippopotamidae	-4.3	24.50	0.02	0.04	2.8	1.8	WK	u l1 or l2 frg	1176	3	34
457-01	Suidea	-9.5	26.0	0.01	0.02	4.3	3.75	U6	M3 frags.	1028	2	21
546-01	Suidea	-13.1	23.3	0.01	0.02	4.3	3.75	WK38	u M3	898	2	21
546-02	Suidea	-10.6	24.8	0.01	0.02	4.3	3.75	WK38	u M3	1089	13	21
498-01	Suidea	-4.8	24.9	0.01	0.02	2.8	1.8	WK 36	M. frag.	1040	2	21
654-01	Suidea	-5.5	26.9	0.01	0.02	2.8	1.8	WK	u M3 frags.	900	2	21
118-01	Suidea	-9.2	25.8	0.01	0.02	2.8	1.8	MP1	u M3	923	2	21
253-01	Suidea	-5.6	26.9	0.01	0.02	2.8	1.8	WK18	M 3	831	3	21
407-05	Suidea	-12.3	22.9	0.01	0.03	2.8	1.8	U19	L I M3	1147	0	17
407-01	Suidea	-10.3	22.4	0.01	0.03	2.8	1.8	U19	L I M3	1209	0	17
407-03	Suidea	-10.2	24.5	0.01	0.03	2.8	1.8	U19	L I M3	996	0	17
407-04	Suidea	-10.6	24.5	0.01	0.03	2.8	1.8	U19	L I M3	1170	0	17
423-01	Suidea	-9.3	23.5	0.01	0.03	1.8	0.6	U23	M3 frag	859	0	17
429-01	Suidea	-10.3	23.1	0.01	0.03	1.8	0.6	U25	M3 frag	1175	0	17
429-02	Suidea	-4.4	26.3	0.01	0.02	1.8	0.6	U25	M3 frag	815	3	21
129-03	Suidea	-9.1	26.4	0.01	0.02	modern	modern	RC1	L I M3	2009	0	16
129-01	Suidea	-12.0	24.3	0.01	0.02	modern	modern	RC1	L I M3	2024	0	16
129-01w	Suidea	-10.9	24.5	0.01	0.03	modern	modern	RC1	L I M3	952	0	17
129-02	Suidea	-9.3	25.1	0.01	0.02	modern	modern	RC1	L I M3	2027	0	16

DIPL.GEOW.**TINA LÜDECKE**

born October 2nd, 1983 in Bremervörde,
Germany

Hanauer Landstraße 12
60314 Frankfurt
Germany

+49 160 98411221

OCCUPATION AND EDUCATION

01/2011 - present
Scientist

**Senckenberg
Biodiversity and
Climate Research
Centre (BiK-F)** in
cooperation with the
Goethe University
Frankfurt

PhD candidate;
advisors:

Prof. Dr. A. **Mulch**
Prof. Dr. F. **Schrenk**

Expected to **graduate**:
Winter 2015/16

- Topic PhD Thesis: *Stable isotopes based paleoenvironmental reconstructions of terrestrial sediments*
- Acquisition of new and intensification of known geochemical and geoscientific analysis methods
 - $\delta^{13}\text{C}$ and $\delta^{18}\text{O}$ analysis on pedogenic carbonates and fossil enamel
 - **Clumped isotope** analysis on pedogenic carbonate
 - **Mesowear** studies on herbivore molars
 - δD and $\delta^{18}\text{O}$ analysis of meteoric water
- Cooperation at the School of Earth, Energy & Environmental Science, **Stanford University**, CA, USA, duration 6 weeks
- Planning and performing **field campaigns**, collecting pedogenic carbonate, fossil herbivore molars, meteoric water and volcanic material
 - Karonga Basin, Northern **Malawi**, total duration ca. 4 months
 - Central Anatolian Plateau, **Turkey**, total duration ca. 2 months
 - Northwestern US, **Montana** and **Idaho**, duration 2 weeks
- Participation at the **Darwin Summer School on Biogeosciences** "Perturbation of the global carbon cycle" in Utrecht and Texel, Netherlands with the visit to **NIOZ**
- **Publication** of papers in high-impact journals
- Presenting research results on national and international **conferences**

10/2004 to 12/2010
Geosciences
Leibniz University
Hannover, Germany

Degree: Dipl.Geow.

Grade: 1.5 (very good)

- Topic Diploma Thesis: *Late Cenozoic **Paleoenvironmental Signatures** of the Central Anatolian Plateau - **Geochemistry** and **Sedimentology** of Lacustrine and Pedogenic Sediments* (grade 1.0. "very good")
- Acquisition of geochemical and geoscientific analytical data
 - $\delta^{13}\text{C}$ and $\delta^{18}\text{O}$ analysis on pedogenic and lacustrine carbonates (IR-MS)
 - δD and $\delta^{18}\text{O}$ analysis of meteoric water (LWIA)
- Planning and performing **field campaigns**, collecting pedogenic and lacustrine carbonate, meteoric water and volcanic material
 - Central Anatolian Plateau, **Turkey**, duration 1 month
- Internships and student assistant jobs
 - Institute of Geology, Leibniz University, Hannover, Germany
 - Geographic Information System (**GIS**) Department at Western Land Services, Ludington, MI, USA
 - Soil Survey Department at the State Authority for Mining, Energy and Geology (LBEG), Hannover, Germany

06/2004

Abitur
Gymnasium
Bremervörde,
Germany

- Advanced courses: **English**, **Geography**, Mathematics and German
- Senior year **Exchange Student** at the Ludington High School, MI, USA, duration 12 months (degree High School Diploma)
- **Languages**
 - German (native)
 - English (full professional proficiency)

Publications and conference abstracts

Publications

- Lüdecke, T.**, Mikes, T., Rojay, B., Cosca, M.A., Mulch, A., (2013). Stable isotope-based reconstruction of Oligo-Miocene paleoenvironment and paleohydrology of Central Anatolian lake basins (Turkey). *Turkish Journal of Earth Sciences*, 22, 793-819.
- Lüdecke, T.**, Thiemeyer, H. (2013). *Palaeoenvironmental Characteristics of the Plio-Pleistocene Chiwondo and Chitimwe Beds (N-Malawi)*. In: Runge, J. Palaeoecology of Africa Vol. 32, 143-161. An International Yearbook of Landscape Evolution and Palaeoenvironments.
- Lüdecke, T.**, Schrenk, F., Thiemeyer, H., Kullmer, O., Bromage, T.G., Sandrock, O., Fiebig, J., Mulch, A., (2016). Persistent C₃ vegetation accompanied Plio-Pleistocene hominin evolution in the Malawi Rift (Chiwondo Beds, Malawi). *Journal of Human Evolution* 90, 163-175.
- Lüdecke, T.**, Mulch, A., Kullmer, O., Sandrock, O., Thiemeyer, H., Fiebig, J., Schrenk, F., Stable isotope dietary reconstructions of herbivore enamel reveal heterogeneous wooded savanna ecosystems in the Plio-Pleistocene Malawi Rift. *Palaeogeography, Palaeoclimatology, Palaeoecology*, submitted.
- Fiebig, J., Hofmann, S., Löffler, N., **Lüdecke, T.**, Methner K., Wacker, U. (2015). Slight pressure imbalances can affect accuracy and precision of dual inlet-based clumped isotope analysis. *Isotopes in Environmental and Health Studies* 16, 1-17.

Conference abstracts as a lead author

Talk:

- Lüdecke, T.**, Schrenk, F., Thiemeyer, H., Kullmer, O., Fiebig, J., Wacker, U., Mulch, A., (2015). Paleoenvironmental reconstruction based on isotopic evidence of early hominin and herbivore diets (Karonga basin, Malawi). Paper No. 102-8. *Geological Society of America, Annual Meeting 2015, Baltimore, MD, USA.*
- Lüdecke, T.**, Schrenk, F., Thiemeyer H., Kullmer, O., Fiebig, J., Wacker, U., Mulch, A., (2015). Stable isotope-based reconstruction of climate and vegetation during hominin evolution in the Malawi Rift. *Abstract SS23b.01, IAS Meeting of Sedimentology, Krakow, Poland.*
- Lüdecke, T.**, Thiemeyer, H., Schrenk, F., Fiebig, J., Wacker, U., Mulch, A. (2015). Climate and Vegetation Patterns in the Malawi Rift During the time of Early Hominin Evolution. *The Role of Culture in Early Expansions of Humans (ROCEEH) – Expansions 2015, Frankfurt, Germany.*
- Lüdecke, T.**, Thiemeyer H., Schrenk, F., Mulch, A., (2014). Stable isotope-based Plio-Pleistocene ecosystem reconstruction of some of the earliest hominid fossil sites in the East African Rift System (Chiwondo Beds, N Malawi). *Geophysical Research Abstracts, EGU2014-12168, EGU General Assembly 2014, Vienna, Austria.*
- Lüdecke, T.**, Thiemeyer, H., Schrenk, F., Fiebig, J., Wacker, U., Mulch, A., (2014). Stable isotope-based Plio-Pleistocene climate and vegetation reconstructions of southeast African savannas (Chiwondo Beds, Northern Malawi). *GeoFrankfurt "Earth System Dynamics", Frankfurt, Germany.*
- Lüdecke, T.**, Mulch, A., Schrenk, F., Thiemeyer, H., Wacker, U., Fiebig, J., (2014). Stable isotope-based Plio-Pleistocene climate and vegetation reconstructions of some of the earliest hominid fossil sites in the East African Rift System (Chiwondo Beds, N Malawi). Paper No. 292-0. *Geological Society of America, Annual Meeting 2014, Vancouver, Canada.*
- Lüdecke, T.**, Thiemeyer, H., Schrenk, F., Mulch, A., (2013). Stable isotope-based Plio-Pleistocene southern hemisphere climate and vegetation reconstructions (Chiwondo Beds, Northern Malawi). *Abstract #PP24A-02, American Geophysical Union, Fall Meeting 2013, San Francisco, CA, USA.*
- Lüdecke, T.**, Thiemeyer, H., Schrenk, F., Mulch, A. (2013). Pedogenic stable isotope records of Plio- Pleistocene southern hemisphere vegetation dynamics (Chiwondo Beds, Northern Malawi). *Geophysical Research Abstracts, EGU2013-4616, EGU General Assembly 2013, Vienna, Austria.*

Poster:

- Lüdecke, T.**, Mulch, A., Mikes, T., Schemmel, F., Rojay, B. (2011). Late Cenozoic Paleoenvironmental Isotope Records of the Central Anatolian Plateau, Turkey. Abstract# 41-6, AGU-GV "FRAGILE EARTH" Meeting Abstracts, Munich, Germany (**Winner of the Student Poster Award - 3rd Prize**).